An investigation into the solubility and stability of amorphous solid dispersions of BCS class II drugs

Submitted to Waterford Institute of Technology for the Degree of Doctor of Philosophy

By Shrawan Baghel

Pharmaceutical and Molecular Biotechnology Research Centre (PMBRC)

Waterford Institute of Technology,

Waterford, Ireland

Under supervision of

Dr. Niall J. O'Reilly and Dr. Helen Cathcart

DECLARATION

I hereby certify that this work, to the best of my knowledge and belief, which I now submit for assessment is the result of my own investigation except where otherwise identified by references

Signed: .....

ID No.: .....

Date: .....

LIST OF OUTPUTS

Publications

Baghel, S., Cathcart, H., O'Reilly, N. J., An investigation into the effect of temperature and moisture on the physical stability and dissolution profile of spray dried amorphous solid dispersions: Phase separation and crystallization. (Manuscript in preparation).

Baghel, S., Cathcart, H., O'Reilly, N. J., An investigation into the solid-state properties and dissolution profile of spray dried ternary amorphous solid dispersions: A rational step towards the design and development of multi-component amorphous system. (Submitted to *Mol. Pharm.* 15 (2018) 3796-3812.

Baghel, S., Cathcart, H., O'Reilly, N. J., Understanding the generation and maintenance of supersaturation during the dissolution of amorphous solid dispersions using modulated DSC and ^{1}H NMR, *Int. J. Pharm. Sci*, 536 (2018) 414-425.

Baghel, S., Cathcart, H., O'Reilly, N. J. Theoretical and experimental investigation of drug-polymer interaction and miscibility and its impact on drug supersaturation in aqueous medium. *Eur. J. Pharm. Biopharm.* 107 (2016) 16-31.

Baghel, S., Cathcart, H., Reddington, W., O'Reilly, N. J. An investigation into the crystallization tendency/kinetics of amorphous active pharmaceutical ingredients: A case study with dipyridamole and cinnarizine. *Eur. J. Pharm. Biopharm.* 104 (2016) 59-71.

Baghel, S., Cathcart, H., O'Reilly, N. J. Polymeric amorphous solid dispersions: A review of amorphization, crystallization, stabilization, solid-state characterization and aqueous solubilisation of biopharmaceutical classification system class II drugs. *J. Pharm. Sci.* 105 (2016) 2527-2544.

International Conferences

Baghel, S. Investigating the dissolution behavior of dipyridamole and cinnarizine spray dried amorphous solid dispersion using proton NMR. Oral presentation at "Formulation 2017" held on August 28-29, 2017 Brussels, Belgium.

Baghel, S. An investigation into the stability and aqueous solubility of amorphous solid dispersions of BCS class II drugs. Oral presentation at "8th International Conference and

Exhibition on Pharmaceutics & Novel Drug Delivery Systems" held on March 07-09, 2016 Madrid, Spain.

Synthesis and Solid State Pharmaceutical Center (SSPC) Oral Presentations

Baghel, S. An investigation into the physical stability and dissolution behavior of ternary amorphous solid dispersions of BCS class II drugs. 22nd Sept, 2017

Baghel, S. An investigation into the physical stability and dissolution behavior of amorphous solid dispersions of BCS class II drugs. 7th June, 2017

Baghel, S. An investigation into the stability and aqueous solubility of amorphous solid dispersions of BCS class II drugs. 30th March, 2016

Baghel, S. An investigation into the stability and aqueous solubility of amorphous solid dispersions of BCS class II drugs. 2nd September, 2015

Baghel, S. Novel Technologies and optimized formulations for delivery of solid dispersions of BCS class II drugs, 8th June, 2015

SSPC Poster Presentations

Baghel, S. An investigation into the stability and aqueous solubility of amorphous solid dispersions of BCS class II drugs. 30th March, 2016

Baghel, S. Novel Technologies and optimized formulations for delivery of solid dispersions of BCS class II drugs, 10-11 December, 2015

Baghel, S. Novel Technologies and optimized formulations for delivery of solid dispersions of BCS class II drugs, 3rd July, 2015

Baghel, S. Novel Technologies and optimized formulations for delivery of solid dispersions of BCS class II drugs, 3rd September, 2014

ACKNOWLEDGEMENTS

My PhD experience over the last four years at Waterford Institute of Technology has been enjoyable, rewarding and challenging. I would like to take this opportunity to express my gratitude to my supervisor Dr. Niall J. O'Reilly and my co-supervisor Dr. Helen Cathcart for their excellent supervision, assistance, motivation and continuous encouragement throughout my PhD study.

I would also like to thank all my fantastic friends, past and present members of the PMBRC and SSPC research groups. In addition, I would like to mention the kindness of the staff and technicians from WIT for all their help and assistance throughout my PhD study. Many thanks to all those who have trained me on instruments and taught me softwares, thereby, making my PhD life easier than it could have been.

I would like to extend my deepest gratitude to my wonderful parents. I would not be able to complete this work without your unconditional love, continuous support and encouragement.

This thesis is dedicated to my supervisor:

Dr. Niall J. O'Reilly

TABLE OF CONTENTS

LIST OF FIGURES

LIST OF TABLES

LIST OF ABBREVIATIONS

AESS	Aerosol supercritical Extraction System
AFM	Atomic Force Microscopy
α	Extent of crystallization
KWW	Kohlrausch-Williams-Watts
API	Active Pharmaceutical Ingredient
ASD	Amorphous Solid Dispersion
BCS	Biopharmaceutical Classification System
χ	Interaction Parameter
CED	Cohesive Energy Density
CNZ	Cinnarizine
CPMAS	Cross-Polarization Magic Angle Spinning
δ	Density
ΔC_p^{conf}	Configurational heat capacity
ΔG	Gibbs Free Energy
D-P	Drug-polymer
DPM	Dipyridamole
DMTA	Dynamic Mechanical Thermal Analysis
DSC	Differential Scanning Calorimetry
DVS	Dynamic Vapor Sorption
E_a	Activation Energy
GAS	Gas Anti-solvent Process
GFA	Glass Forming Ability
GI	Gastro-intestinal
H-bond	Hydrogen bonding
HME	Hot Melt Extrusion
HPMC	Hydroxypropyl methyl cellulose

HPMCAS	Hydroxypropyl methyl cellulose acetate succinate
HSDSC	High Speed Differential Scanning Calorimetry
FDA	Food and Drug Administration
F-H	Flory-Huggins
FTIR	Fourier Transform Infra-red
IGC	Inverse Gas Chromatography
IVIV	*in-vitro in-vivo*
JMA	Johnson-Mehl-Avrami
K	Kelvin
MDSC	Modulated Differential Scanning Calorimetry
MW	Molecular Weight
m_D	Dynamic Fragility
$m_{D_{CE}}$	Dynamic fragility from extrapolation of configurational entropy to zero
$m_{D_{Tg}}$)	Dynamic fragility from heating rate dependence of T_g
m_T	Thermodynamic Fragility
n	Avrami Exponent
NTR	Nitrendipine
Φ	Volume Fraction
PAA	Polyacrylic Acid
PAS	Precipitation with Compressed Anti-solvent
PASD	Polymeric Amorphous Solid Dispersion
PDF	Pair-wise Distribution Function
PEG	Polyethylene glycol
PEO	Polyethylene Oxide
PVP	Polyvinyl pyrrolidone
PVP/PA	Polyvinyl pyrrolidone pthalate acetate
PVP/VA	Polyvinyl pyrrolidone vinyl acetate

R	Universal Gas Constant
RH	Relative Humidity
SAS	Supercritical Anti-solvent Process
SAXS	Small Angle X-ray Scattering
SCF	Super Critical Fluid
SD	Spray Drying
SEDS	Solution Enhanced Dispersion
SMEDDS	Self Micro-Emulsifying Drug Delivery System
SP	Supersaturation Parameter
ssNMR	Solid-state Nuclear Magnetic Resonance
T	Temperature
T_1	Spin-Lattice Relaxation Time
$T_{1\rho}$	Spin-Spin Relaxation Time
TA	Thermal Analysis
Γ	Mean Relaxation Time
TGA	Thermogravimetric Analysis
T_c	Crystallization Temperature
T_m	Melting Temperature
T_g	Glass Transition Temperature
μ	Chemical Potential
VT	Variable Temperature
VTF	Vogel-Tammann-Fulcher
WAXS	Wide Angle X-ray Scattering
w/w	weight/weight
XPS	X-ray Photoelectron Spectroscopy
XRPD	X-ray Powder Diffraction

ABSTRACT

The poor water solubility of many drugs has emerged as one of the major challenges in the pharmaceutical world. Amorphous solid dispersions (ASDs) are one of the most widely used formulation strategies for the enhancement of in-vitro and in-vivo performance of poorly water-soluble drugs. However, because of their meta-stable nature the physical stability of amorphous solid dispersions has been considered to be the main obstacle for their formulation development and commercialization by the pharmaceutical industry. Significant upfront development is therefore required to generate stable amorphous formulations. The aim of this project was to understand, predict and enhance the solubility and physical stability of ASDs. Two model drugs (dipyridamole and cinnarizine) and three polymeric matrices (polyvinyl pyrrolidone, polyacrylic acid and hydroxypropyl methyl cellulose) were formulated by spray drying into binary and ternary solid dispersions. A series of physicochemical characterization techniques including mDSC, PXRD, FTIR, DVS, *in-vitro* dissolution and NMR were used to evaluate the systems. Physicochemical characterization of the various systems including amorphous drug crystallization kinetic studies, prediction of drug-polymer miscibility, *in-vitro* dissolution studies, physical stability studies and investigation into polymer-surfactant combinations of ternary solid dispersions were carried out. Across the project, several key achievements were obtained. It was revealed that the crystallization tendency of the amorphous drugs, drug-polymer miscibility, drug-polymer interaction, robustness of drug-polymer interaction under stress conditions, processing conditions, drug loading and antiplasticization effect are some of the dominant factors controlling the physical stability and solubility of the amorphous systems. The results of the project are expected to contribute to the formulation development of amorphous solid dispersions in terms of screening suitable drug and polymer candidates, selecting "safe" (physically stable) drug loadings and the identification of methodologies to improve the physical stability and solubility of formulations.

CHAPTER 1. INTRODUCTION

1.1. Introduction

Oral drug delivery is the most commonly employed drug delivery route due to its ease of administration, high patient compliance, cost effectiveness, reduced sterility constraints and flexibility of dosage form design.[1] When a drug is administered orally, it has to cross certain checkpoints (varies from drug to drug) within the biological system including dissolution in gastro-intestinal (GI) fluids, permeation across the gut membrane and first pass metabolism to finally reach its site of action *via* systemic circulation. Every checkpoint presents a potential bottleneck, of which dissolution in gastric fluid is of prime importance. Indeed, for the majority of drugs it is the main requirement to enable systemic circulation which determines the bioavailability. Taking into account the conceivable rate-constraining steps, Amidon *et al.* (1995) classified Active Pharmaceutical Ingredients (APIs) into four groups on the basis of their solubility and permeability known as the Biopharmaceutical Classification System (BCS) as shown in Figure 1.1.[2] BCS involves mathematical analysis to experimentally determine solubility and permeability of drugs under specified conditions.[3] According to the US Food and Drug Administration (FDA), a drug is considered to be highly soluble when its highest clinical dose strength is soluble in 250 mL or less of aqueous media over a pH range of 1-7.5 at 37.5°C and it is considered to be highly permeable if the absorption of an orally administered dose in humans is > 90% when determined using mass balance or in comparison to an intravenous reference dose.[4] A biowaver (permission to skip *in-vivo* bioequivalence studies) may be applied for certain drugs that pass specific *in-vitro* solubility and permeability requirements. The following discussion is limited to BCS Class II drugs (low solubility and high permeability).

Poor aqueous solubility is a matter of serious concern if the clinical dose of drug cannot dissolve in the available volume of GI fluids. A well-known example is Danazol which has an aqueous solubility of ~1μg/mL at gastric pH and a dose of 200-600mg/day.[5, 6] To completely dissolve the lowest clinical dose of danazol at gastric pH, approximately 200 L of aqueous media would be required which is obviously impossible *in vivo*. Furthermore, poorly water soluble drugs will typically exhibit dissolution rate limited absorption as they may pass their absorption site before complete dissolution. Therefore, there is great interest amongst formulation scientists to develop reliable, efficient, cost effective and scalable methods to increase the aqueous solubility of BCS Class II drugs. Common formulation strategies to tackle this challenge include pH adjustment, self-emulsifying drug delivery systems (SMEDDS), particle size reduction, super critical fluid (SCF) processing, inclusion

complexes/complexation, co-solvency, micellar solubilization, hydrotrophy, solid dispersions, nano-suspensions, co-crystals and nano-crystallization.[7] [8] [9] The choice of a particular method depends mainly on the physicochemical characteristics of drug, carrier properties and their expected use.[10]

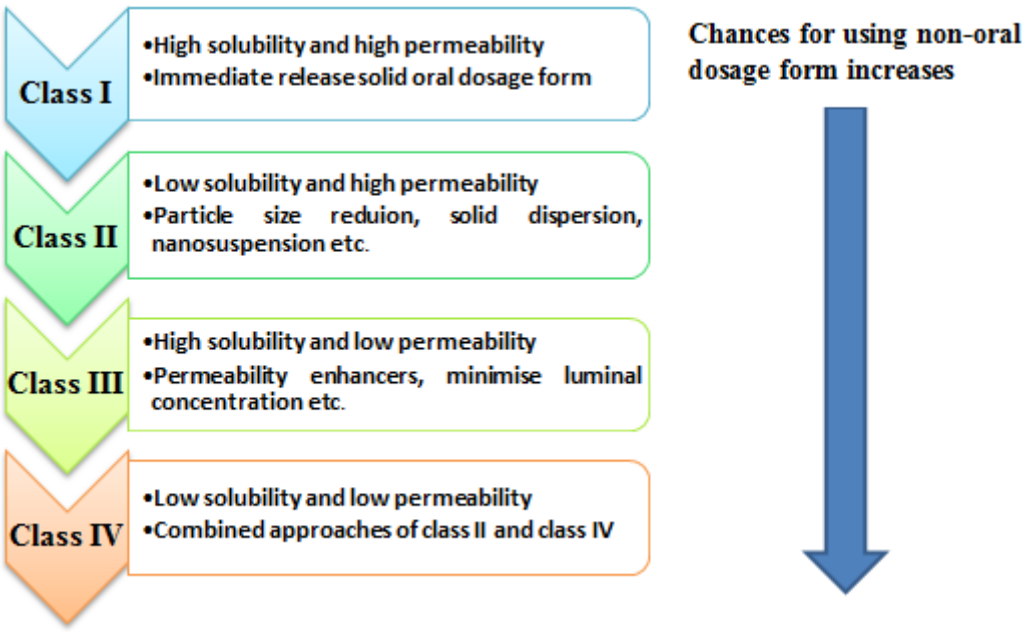

Figure 1.1. Biopharmaceutics classification system and formulation approaches for different classes of drugs

The crystalline form of a drug offers the advantage of high purity and physical/chemical stability. However, the lattice energy barrier is a major constraint in the dissolution of crystalline drug molecules.[11] The amorphous state, on the other hand, exhibits a disordered structure in comparison to crystalline form and possesses higher free energy (thermodynamic driving force) leading to higher apparent water solubility, dissolution rate and oral absorption.[12] Pure amorphous drugs are rarely used in formulation development because of their inherent physical/chemical instability. However, the solubility advantage of these systems can be retained by devising effective strategies to "kinetically stabilize" amorphous APIs. This has encouraged the development of amorphous solid dispersion (ASD) products.

The concept of solid dispersions was first proposed by Sekiguchi and Obi in 1961.[13] On the basis of the distribution of the drug molecules in the carrier matrix, solid dispersions can be divided into three types: (a) Eutectic systems are mixture of two compounds in a specific ratio and have a single melting point which is lower than the melting points of the individual components; (b) Solid solutions which are further divided into substitutional solid solutions (solute molecule replace a solvent molecule), interstitial solid solutions (solute molecule is

present in the interstices) and amorphous solid solution having solute randomly distributed in an amorphous carrier, and; (c) Microfine crystalline dispersions are crystalline dispersions of drugs in the carrier matrix.[14] The concept of a solid dispersion has been successfully applied to oral formulations containing drugs with a high crystallization tendency (such as Ivacaftor in Kalydeco) and also with a high drug loading (375 mg per tablet in Incivek) (Table 1.1).[15] A wide range of pharmaceutical excipients such as carbohydrates, lipids, proteins, sugars (sucrose, xylitol), organic acids (succinic acid), surfactants (Spans®, Renex®), urea, pentaerythritol and polymers have been investigated and employed to kinetically stabilize the amorphous APIs.[16] Taking into consideration its most used form as shown in Table 1.1, solid dispersion can now be more narrowly defined as the dispersion of amorphous drug in a polymeric carrier matrix.[17] The following discussion is limited to a system that fits this more concise definition i.e. polymeric amorphous solid dispersion (PASDs). Information related to eutectic mixture or microfine crystalline dispersion can be found elsewhere.[18]

Table 1.1. FDA approved solid dispersion products

Product Name	Drug	Polymers[a]	PASD preparation method[19]	Maximum drug loading per tablet/capsule (mg)[b]	Dosage form
Kalydeco	Ivacaftor	HPMCAS	Spray Drying	150	Tablet
Zelboraf	Vemurafenib	HPMCAS	Co-precipitation	240	Tablet
Incivek	Telaprevir	HPMCAS	Spray Drying	375	Tablet
Intelence	Etravirine	HPMC	Spray Drying	200	Tablet
Novir	Ritonavir	PVP/PA	Melt Extrusion	100	Tablet
Kaletra	Lopinavir	PVP/VA	Melt Extrusion	200	Tablet

[a]Information obtained from excipients list, patents and other sources.
[b]Drug product label from US Food and Drug Administration (FDA) website
PASD: Polymeric amorphous solid dispersion; HPMCAS: Hydroxypropylmethyl cellulose acetate succinate; HPMC: Hydroxypropylmethyl cellulose; PVP: Polyvinylpyrrolidone; PA: Pthalate acetate; VA: Vinyl acetate

The main focus of the rest of the discussion will be on 1) how to engineer the thermodynamic properties of BCS class II drugs, 2) what are the different factors affecting the stability and physico-chemical properties of amorphous drug in solid dispersion, 3) how different mechanisms are involved in stabilizing the amorphous form in polymer matrices, 4) what should be considered for the rational selection of polymers and preparation techniques and 5) latest characterization methods to develop a multidisciplinary approach towards a molecular level understanding of PASDs.

1.2. The Amorphous State

To have a better understanding of the differences in the thermodynamic properties of crystalline and amorphous forms, consider a crystalline drug which, when heated, undergoes melting at temperature (T_m) as shown in Figure 1.2. As the molten drug is slowly cooled, formation of an orderly system takes place as the molecules have sufficient time to move from their current location to a thermodynamically stable point on crystal lattice.[20] The molecules arrange themselves in a definite order, regenerating a crystalline structure. However, if the molten drug is cooled suddenly, it may attain a super cooled liquid state (without undergoing crystallization), having a temperature lower than its T_m, which is in equilibrium with the molten drug.[21] On further cooling, the system remains in equilibrium until a glass transition temperature (T_g) is reached, below which it enters a non-equilibrium state (super cooled liquid state or lower viscosity rubbery state) and converts into the ‘‘frozen’’ glassy state of the drug.

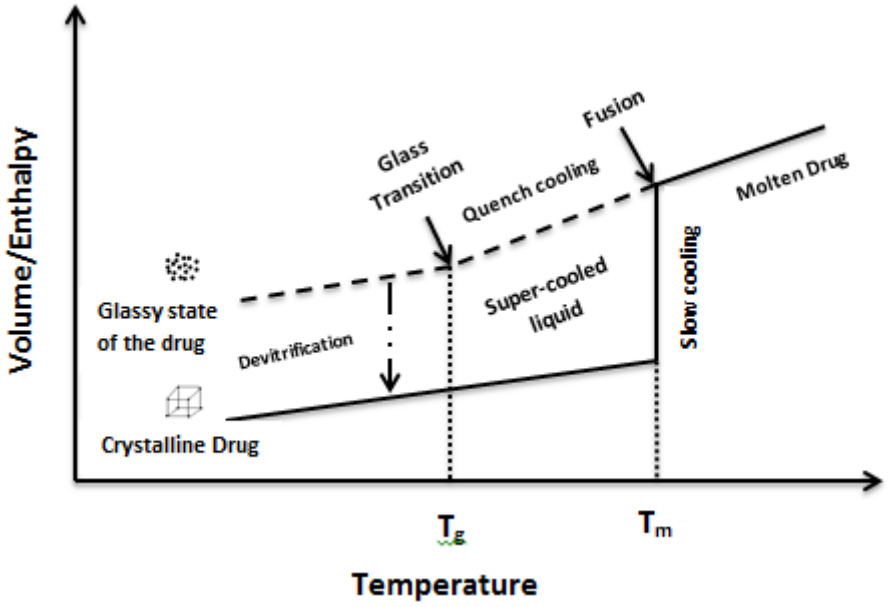

Figure 1.2. Enthalpy and volume of different state of drugs as a function of temperature; Tg and Tm are glass transition and melting temperature respectively; Diagram is not to scale.

A material in a glassy state behaves like a brittle solid, but without crystalline structure and having only short range order.[22] This transition is necessary because if the super-cooled liquid state exists below the glass transition temperature then a point comes whereby the crystals would have higher entropy compared to the super-cooled liquid. The total entropy of the system would become negative before reaching absolute zero temperature; violating the third law of thermodynamics (entropy of perfect crystal is zero at 0 K).[23] The glass transition

is a second order thermodynamic transition characterized by a step change in the heat capacity which is also associated with changes in the derivative of extensive thermodynamic properties such as volume, enthalpy and entropy. The amorphous state of a drug has a higher enthalpy, entropy, free energy and volume compared to the crystalline form which is responsible for its higher apparent solubility (as shown in Figure 1.2). The relative increase in solubility of the amorphous form as compared to the crystalline form can be estimated using the following equations:[25]

$$\Delta G_T^{a,c} = -RT\ln(\sigma_T^a/\sigma_T^c) \quad \ldots\ldots\ldots \quad (1.1)$$

$$\Delta G_T^{a,c} = \Delta H_T^{a,c} - T\Delta S_T^{a,c} \quad \ldots\ldots\ldots \quad (1.2)$$

where (σ_T^a/σ_T^c) is the solubility ratio of the amorphous and crystalline forms, $\Delta G_T^{a,c}$, $\Delta H_T^{a,c}$ and $\Delta S_T^{a,c}$ is the difference in the free energy, enthalpy and entropy, respectively, R is the universal gas constant and T is the absolute temperature. In contrast, the experimentally determined apparent solubility of amorphous APIs remains less than the theoretically predicted values in most cases.[26] On adding an amorphous drug to a media, dissolution occurs rapidly which appears as a peak followed by a decrease in solubility due to devitrification and is known as "spring and parachute effect" (Figure 1.3) which creates considerable challenges during dissolution (discussed later, Chapter 4 and 5).[27, 28, 29, 30]

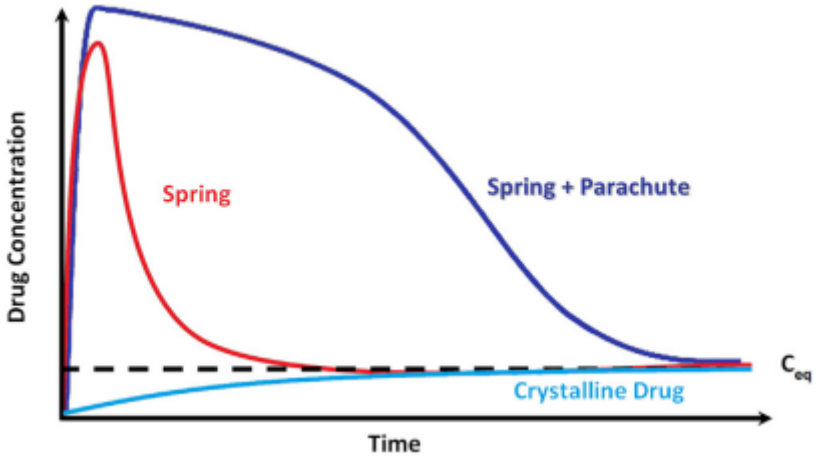

Figure 1.3. Drug profile based on the aqueous solubility of amorphous and crystalline form of the drug; Reproduced with permission from reference 19; Diagram is not to scale.

1.3. Polymers as a Carrier Matrix

Polymers are chemically composed of repetitive structural units known as monomers which are linked with each other forming an extended structural framework. They can be

classified on the basis of their origin as natural (e.g., starch, cellulose and proteins) semi-synthetic (e.g., Hydroxypropyl methyl cellulose) or synthetic polymers (e.g., polyvinylpyrrolidone).[31] From the monomer perspective, they can be classified as homopolymers (one type of monomer) such as methylcellulose or copolymer (two or more monomers) such as crospovidone. Polymers can be amorphous (polyacrylic acid), semi-crystalline (poly L-lactic acid) or crystalline (polyethylene glycol). Due to their complex three dimensional structures with numerous inter- or intra-chain cross links, incorporation of amorphous drugs into these cross-linked networks hinders their molecular mobility. This lowers the chemical potential of the amorphous drug and brings it closer to that of the crystalline form as shown in Figure 1.4.[32, 33] As a result, polymers prevent devitrification thereby preserving the viability (apparent solubility and stability) of the amorphous state over the shelf life of the product.[34] Various polymers have been studied and examined to prepare PASDs and a comprehensive list is given in Table 1.2.

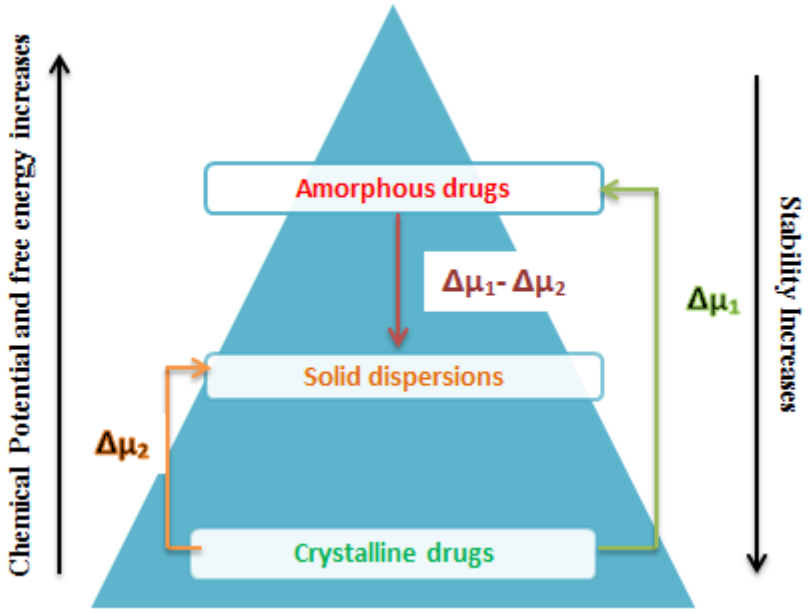

Figure 1.4. Energy pyramid of the crystalline form, amorphous solid dispersion and amorphous form. μ is the chemical potential; Diagram is not to scale.

A number of factors, such as molecular mobility, thermodynamic properties, environmental stress, preparation methods and conditions play a major role in the physical/chemical stability of the amorphous form (as mentioned in Table 1.3.). The following section will briefly review the effect of polymers on these factors along with the different mechanisms of stabilization as shown in Figure 1.5.

Table 1.2. Examples of different polymers used in the formulation of amorphous solid dispersions

Polymers[a]	Drugs stabilized	Preparation method	Comments	References
PVP BASED POLYMERS				
Poly(vinylpyrrolidone) PVP K30 (MW: 40000, T_g 160°C)	**Ezetimibe**	Solvent method	Thermal and spectroscopic analysis revealed that PVP K30 was effective in stabilizing amorphous ezetimibe and also causes faster drug release during *in vitro* dissolution testing, leading to improved oral bioavailability.	35
PVP Vinyl acetate (PVP VA): 60/40 (Plasdone® S630) (MW: 45000-70000, T_g 106°C, T_m 140°C)	**Ketoconazole** (MW: 531.4, T_m 149.85°C, T_g 44.85°C)[b]	Hot Melt Extrusion	Raman mapping demonstrated full homogenous spatial distribution of ketoconazole in PVP VA. Spring and parachute effect was observed during dissolution experiments. The release of drug was carrier controlled initially and then burst release was observed leading to precipitation of amorphous drug.	36
Crospovidone (Polyplasdone® XL) (MW: >10000)	**Glipizide**	Rotary evaporation/Fluid bed drug layering	No sign of phase separation or crystallization was observed. Antiplasticization and drug-polymer miscibility are the key players in stabilizing solid dispersion.	37
PEG BASED POLYMERS				
Polyethylene glycol 4000 (PEG 4000) (MW: 4000, T_g ~45°C)	**Nifedipine** (MW: 346.3, T_m 172.85°C, T_g 46.85°C)[b]	Fusion/solvent method Fusion method	The polymer was capable of prohibiting drug crystallization in solid dispersion. Samples which were prepared at higher temperatures showed better dissolution profiles compared to the samples prepared at nifedipine melting point which may be due to improved drug-polymer mixing at higher temperatures.	38
PEG 8000 (MW: 8000, T_m 62°C)	**Curcumin** (MW: 368.4, T_m 176°C)[c]	Solvent evaporation method	The polymer demonstrated poor capability to disperse the drug in the amorphous form, to inhibit crystal growth and to increase saturation solubility of the drug in water. It may be due to non-surface active property of the polymer.	39
PEG 20,000 (MW: 20000, T_m 60-63°C)	**Carbamazepine** (MW: 236.3, T_m 190°C, T_g 61°C)[d]	Fusion method	Presence of intramolecular H-bonds causes high crystallization tendency of the amorphous drug. No drug-polymer interaction was found in the solid dispersion. Increased dissolution rate was due to the hydrophilic nature of the polymer.	40

Continued

CELLULOSE BASED POLYMERS				
Hydroxypropyl methylcellulose (HPMC) (MW: 10000-1500000, T_g 172°C)	**Tacrolimus** (MW: 804.02, T_m 142°C)	Solvent evaporation method	Drug-polymer interaction and antiplasticization plays a major role in the performance of the amorphous solid dispersion	41
HPMC Acetate succinate (HPMCAS) (MW: 55000-90000, T_g 113°C)	**Itraconazole** (MW: 705.7, T_m 167.85°C, T_g 57.85°C)[b]	Film casting method	Drug loadings as high as 60% was found to be stable for 1 month at 40°C and 75%RH. This may be due to the high solubility of the drug in the polymer.	42
HPMC Pthalate (HPMCP) (MW: 37900, T_g 143°C)	**Dutasteride** (MW: 528.53, T_m 249.7°C)	Spray Drying	Highly effective in stabilizing and maintaining drug supersaturation leading to increased oral absorption of amorphous dutasteride	43
ACRYLATE BASED POLYMERS				
Ammonio methacrylate copolymer (Eudragit® E) (T_g ~55°C)	**Indomethacin** (MW: 356.7, T_m 160.85°C, T_g 44.85°C)[b]	Solvent evaporation	pH dependent solubility was observed. Solubility of polymer in dissolution media has a direct effect on achieving and maintaining drug supersaturation.	44
Polyacrylic acid (Carbomer or Carbopol 940) (MW: 450000, T_g 110°C)	**Carbamazepine** (MW: 236.27, T_m 191.5°C, T_g 53°C)[d]	Hot melt extrusion	High drug loading and better stabilization (12 months at 40°C and 75% RH) due to drug polymer interactions.	45
MISCELLANEOUS POLYMERS				
Kollicoat® IR (MW: 45000, T_g 45°C)	**Fenofibrate** (MW: 360.83, T_m 80.85°C, T_g -17.15°C)[b]	Film freezing	Generated eutectic mixture with intermolecular H-bonding. Low T_g of the polymer causes rapid diffusion of the drug molecules, leading to drug crystallization and lower levels of supersaturation.	46
Soluplus® (MW: 90000-140000, T_g -70°C)	**Carvedilol** (MW: 406.47, T_m 117°C, T_g 42°C)[b]	Solvent evaporation/freeze drying/spray drying	Solid dispersion prepared using freeze drying method showed the highest saturation solubility.	47

[a] Handbook of pharmaceutical excipients, 6th edition, Pharmaceutical press. [b] Data reported in literature.[48] [c] Values obtained from previously published reports.[49] [d] Values taken from literature.[50]; T_g and T_m represent glass transition and melting temperature, respectively; MW and RH represents molecular weight (Da) and relative humidity, respectively.

Table 1.3. Different factors affecting the stability of amorphous drug in solid dispersion

Factors	Impact on the stability of amorphous drugs
Glass transition temperature (T_g)	Stability increases with increasing T_g. Polymers increase the kinetic stability of amorphous drugs (antiplasticization effect)[51]
Structural relaxation/molecular mobility	Responsible for recrystallization. Rate of crystallization is higher at temperatures above T_g. Restriction of molecular mobility improves stability.[52]
Configurational entropy	Low configurational entropy favors crystallization.[53] Lower crystallization tendency of erythromycin free base, for example, can be explained by its lower thermodynamic driving force for crystallization (H_{conf}) [54]
Configurational enthalpy	The greater thermodynamic driving force for crystallization (*i.e.* higher configurational enthalpy) causes increased nucleation rate of nifedipine as compared to felodipine.[55]
Gibbs free energy	Systems having lower Gibbs free energy are generally more stable.[56]
Humidity, mechanical stress and temperature	Temperature significantly affects molecular mobility and moisture may plasticize the material by lowering its T_g near to storage temperature: increases crystallization rate and decreases crystallization temperature.[57] Mechanical stress also causes significant differences in crystallization tendency.[58]
Preparation method (fusion or solvent evaporation method, freeze drying, supercritical fluid technology)	Different preparation methods induce different thermal histories and mechanical stresses leading to different degrees of drug-polymer mixing and drug mobility in the dispersion. Hence variable solid state stability of the solid dispersion can be obtained.[59, 60, 61]
Preparation conditions such as cooling rate, processing temperature and time	Slow cooling of amorphous indomethacin increases its physical stability.[62] Different inlet temperature used in the spray-drying of naproxen led to the difference in dissolution profile and drug stability.[63] Different screw speed (residence time) in hot-melt extrusion effected the stability of fenofibrate formulations in stressed conditions.[64]

1.3.1. Crystallization inhibition

Before developing an ASD based formulation, it is important to estimate the suitability of a compound to form the amorphous phase. Glass forming ability (GFA) and fragility (*m*) can

provide a qualitative estimation of the tendency of a drug candidate to undergo devitrification and may clarify their suitability, on the basis of physical stability, for amorphous dosage forms.

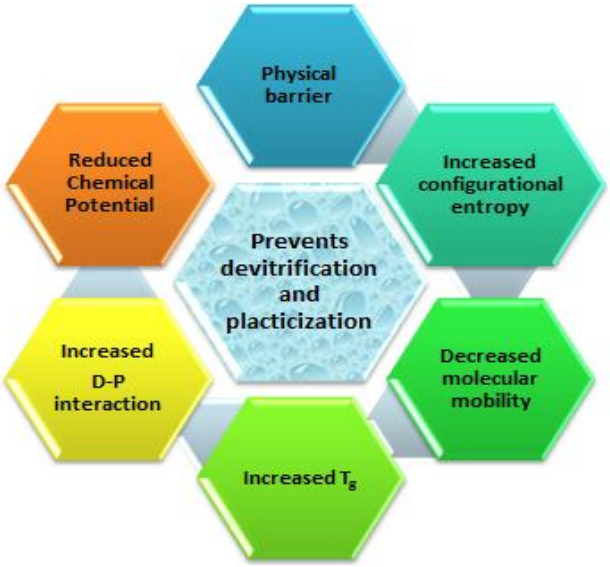

Figure 1.5. Different approaches for stabilizing the amorphous solid dispersion in a polymer matrix; D-P represents drug-polymer and Tg represents glass transition temperature.

GFA and fragility may be considered as an indicator of the life expectancy of an ASD.[65] It has been suggested that crystallization is inversely related to the glass forming ability of amorphous drugs and GFA is defined as the ease with which materials can undergo vitrification upon cooling.[66] Different methods are reported in the literature to measure the GFA of a drug compound such as reduced glass transition temperature (T_{rg}), cooling rate dependence and the crossover-point of the heating/cooling rate dependencies of the crystallization temperature.[67] The kinetic behavior of a supercooled liquid can also be estimated by examining the sensitivity of the liquid structure to temperature change, known as "fragility" of the liquid, which is closely linked to its GFA.[68] It has been observed that strong "liquids" are good glass formers having higher viscosity at T_m and resistant to structural changes. Fragile liquids, on the other hand, are weak glass formers, exhibiting lower viscosity at T_m and allowing larger structural changes with change in temperature.[69] The fragility (*m*) of an amorphous drug can be calculated by measuring the dependence of T_g on the heating rate, q, in differential scanning calorimetry (DSC) measurements.[70] Other methods such as extrapolation of configurational entropy to zero and observation of glass transition width are also mentioned in the literature.[71]

The crystallization of an amorphous drug is a two-step process, although they occur simultaneously. The first step is nucleation which occurs at a lower temperature and second step is crystal growth which requires higher temperature.[72] A supersaturated solution of a drug also favors crystallization. However, these are not the only requirements for the crystallization to start. A certain minimum amount of energy (known as energy of activation) is also required to overcome the high interfacial tension between small particles. Thus, nucleation may not start until a certain degree of supersaturation is reached to overcome the energy barrier. This range of supersaturated concentrations where no nucleation occurs is known as the *metastable zone* and a smart choice of polymeric excipients can expand this region by causing an increase in the degree of supersaturation or decrease in interfacial energy.[72] Polymeric excipients that increase aqueous solubility (by inhibiting precipitation of the dissolved drug) can retard the nucleation rate by decreasing the free drug concentration available for nuclei/seed formation.[73] Polymer also increases the viscosity of the system which may alter the frequency of atomic/molecular transport at the surface of the nucleus.[74] Moreover, polymers have sufficiently high configurational entropy due to their large, complex and flexible structures, their high molecular weights and their ability to exist in many conformations. These significantly reduce the chance of drug recrystallization as it lowers the free energy of the ASD (Figure 1.4).[75]

1.3.2. Anti-Plasticization

Anti-plasticization is the reduction of plasticity or the hardening of a material.[76] In thermodynamics, it is described as a phenomenon which leads to an increase in the T_g of the material which increases the free energy required by the amorphous drug to convert into the crystalline form. When two materials having different T_g's are mixed together, the final T_g of the mixture will be somewhere between the T_g's of both the materials.[77] Mixing a low T_g amorphous drug with a high T_g polymer at the molecular level leads to the formation of PASD with a T_g intermediate of these two components. In other words, the polymer undergoes plasticization whereas the T_g of the drug increases and it undergoes antiplasticization. The resultant T_g of the final mixture can be calculated by using Gordon-Taylor equation:[78]

$$T_g = \frac{W_1 T_{g1} + K_G W_2 T_{g2}}{W_1 + K_G W_2} \qquad \ldots\ldots\ldots \qquad (1.3)$$

where T_g, T_{g1} and T_{g2} are glass transition temperatures of the drug polymer mixture, the amorphous drug and the polymer respectively, w_1 and w_2 are the weight fraction of the drug

and polymer, respectively, and K_G is a constant the value of which depends on the level of interaction between the drug and the polymer and can be calculated using the equation as shown:

$$K_G = \frac{\rho_1 T_{g1}}{\rho_2 T_{g2}} \qquad \ldots\ldots\ldots \qquad (1.4)$$

where ρ_1 and ρ_2 are the densities of amorphous drug and polymer respectively. Other equations such as Fox,[79] Couchman-Karasz[80] or Kwei[81] are also reported in the literature to estimate the resultant T_g of the PASD. Mahmah *et al.* has studied the stabilization of amorphous felodipine and reported that the stability of the amorphous drug in solid dispersion having PVP and HPMC as carrier is due to the anti-plasticizing effect of the polymer, which increases the viscosity of the system and decreases the diffusion of drug molecules (necessary to form crystalline lattice).[82] However, sometimes, experimentally obtained T_g values deviate significantly from the theoretically predicted values as shown in Figure 1.6. This is due to the volume non-additivity resulting from non-ideal mixing of the drug and polymer.[83]

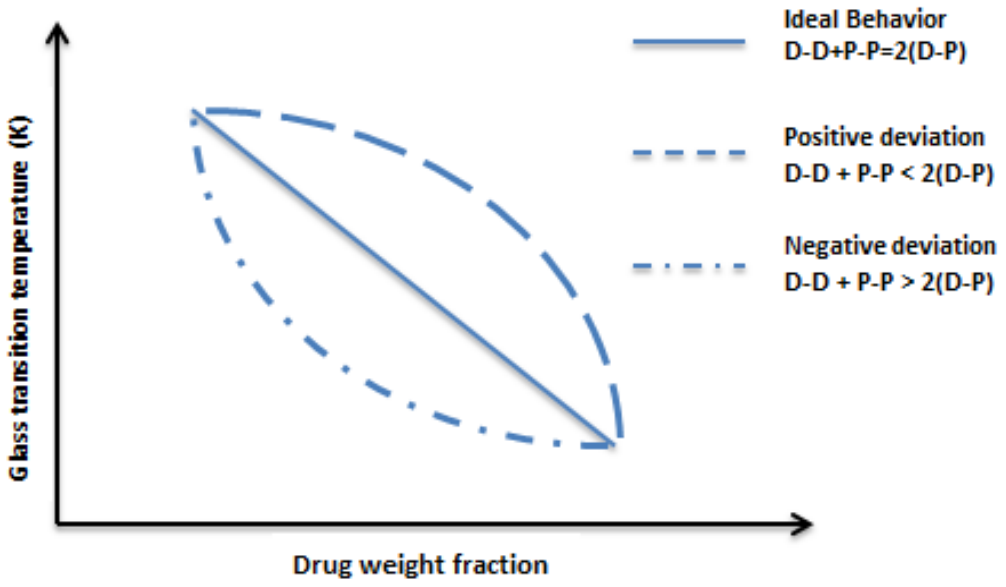

Figure 1.6. Deviation from ideal behavior as predicted by Gordon-Taylor equation; D represents drug and P represents polymer; Diagram is not to scale.

When a drug is dispersed in the polymer matrix, several homo-nuclear and hetero-nuclear interactions come into play. These interactions can be represented as following:

1. D-D + P-P > 2(D-P)

2. D-D + P-P < 2(D-P)
3. D-D + P-P = 2(D-P)

where D and P represent drug and polymer, respectively. It is the relative strength of these interactions which defines the final volume of ASDs. In the first case, the homo-nuclear interactions are stronger than the hetero-nuclear interactions. Thus, when a solid dispersion is formed, there would be a net contraction in the volume. The second case represents stronger hetero-nuclear interactions causing a net expansion of the system. The third case is the ideal condition wherein there is no net increase or decrease in volume and volume additivity is perfect. Ideally, the drug and polymer should be completely miscible with each other and the drug should be evenly dispersed in the polymer carrier. However, in most cases, the drug polymer mixture is not ideal and this non-ideality in mixing causes deviation between experimental and theoretical T_g values. A stronger drug-polymer interaction is generally preferred resulting in favorable exothermic mixing with increased configurational entropy.[84] Crowley *et al.* have studied the non-ideality of mixing and suggested that these deviations from predictions are due to the relative extent of hetero-molecular to homo-molecular interactions.[85] The conclusions were in accordance with the work carried out by Maniruzzaman *et al.* who also concluded that intermolecular interaction between drug and polymer play a great role in non-ideality of mixing.[86]

1.3.3. Intermolecular interaction

The drug molecules may interact with the polymer molecules *via* several weak forces such as H-bonding, van der Waals forces, electrostatic, ionic or hydrophobic forces.[87] These intermolecular bonds restrict the molecular mobility of the drug molecules in the polymer matrix and provide stability to the system. Khougaz *et al.* have reported on the role of specific drug-polymer interaction in stabilizing a solid dispersion.[88] They found that when amorphous MK-0591 was dispersed in different polymers such as PVP K-12 and PVP/VA, the final T_g of the ASD was less than the T_g of the amorphous drug. However, the solid dispersion remained stable after one year of storage. This shows that anti-plasticization is not the only factor responsible for a reduction in devitrification rate. Infrared (IR) spectra confirmed the presence of ion-dipole interactions between the PVP carbonyl group and the MK-0591 carboxylate group (COO^-Na^+) showing that that weak intermolecular forces also play an important role in stabilizing amorphous drugs in polymer matrix. Another interesting study was carried out by Meng *et al.* which highlighted the importance of bond formation or drug-polymer interaction in the stability of amorphous curcumin as a model drug.[89] They

examined the ability of different polymers, such as PVP K90, Eudragit EPO®, HPMC and PEG 8000, to interact with the curcumin, through stable bond formation. It was found that Eudragit® was the only one of the four polymers which stabilized curcumin at the limit of miscibility during stability studies and also improved its dissolution performance. Interaction between curcumin and Eudragit® were verified using IR and Raman spectroscopy. It was concluded that a certain degree of interaction between a drug and a polymer is important for successful formulation of ASDs.

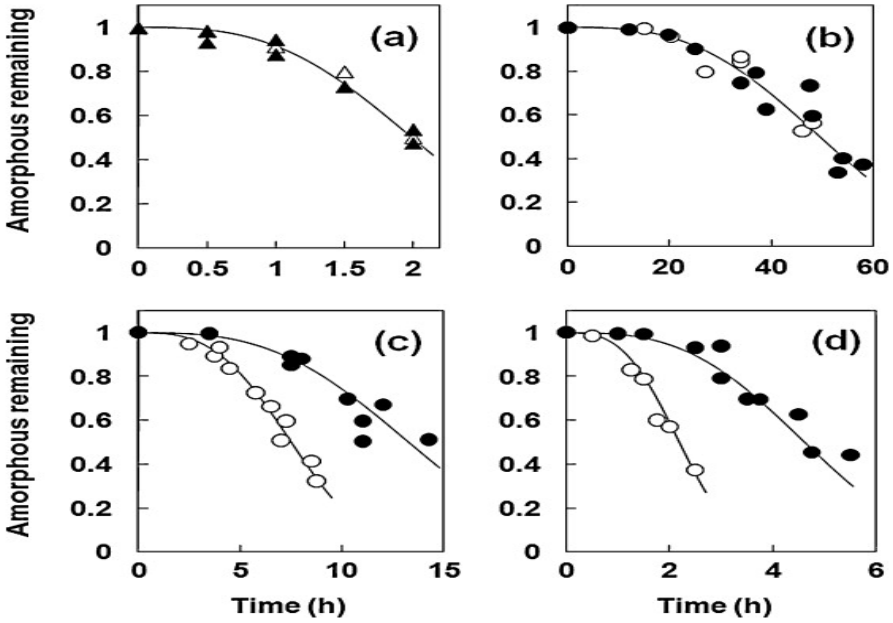

Figure 1.7. Crystallization rate of each nitrendipine enantiomer (a) and the enantiomers in amorphous solid dispersion with 10%PVP (b), 10% HPMC (c) and 10% HPMCP (d) at 60°C; Reproduced with permission from reference 90. (The lines represent the best fit to the Avrami model). (Closed symbols represent (+)-nitrendipine (NTR) and open symbols represent (-)-NTR enantiomer).

A study by Miyazaki *et al.* demonstrated the role of steroeselective interaction in the stability of amorphous nitrendipine (NTR) prepared by the melt quenching method.[90] They elucidated the effect of steroeselective drug-polymer interaction on the crystallization rate of ASD using PVP, HPMC and HPMCP as model chiral polymers. The effect of chiral polymers, HPMC and HPMCP on the crystallization inhibition of (+)-NTR was more effective compared to that of (-)-NTR at 50-70°C as shown in Figure 1.7. PVP, on the other hand, does not preferentially interact with any of the enantiomers and hence has no effect on the crystallization profile of NTR. This difference in crystallization profile or physical stability can be attributed to steroeselective interaction between drug and polymer. However,

due to the weak nature of this interaction, the effect on the physical stability of ASD was minimal at 25°C.

The contribution of drug-polymer interaction in maintaining drug stability, higher drug solubility and degree of supersaturation has further been emphasized by Shah *et al.* using vemurafenib as the model drug and HPMCAS, HPMCP and Eudragit® L as model polymers.[91] Amorphous solid dispersions were prepared by the solvent-controlled co-precipitation method. They demonstrated that HPMCAS can effectively interact with vemurafenib functional groups via H-bonding and other weak interactions in the PASD as compared to other polymers. This leads to a greater stability and a higher level of supersaturation maintenance. Indeed, Maniruzzaman *et al.* further confirmed their role in stabilizing PASDs prepared using hot-melt extrusion process.[92] Research findings showed the presence of H-bonding and intermolecular ionic interaction between polymer carboxylic groups and API amino functional groups which were confirmed by molecular modelling (Figure 1.8) and X-ray photoelectron spectroscopy (XPS). They also demonstrated that the magnitude of the intermolecular interactions were dependent on the drug-polymer ratio and miscibility.

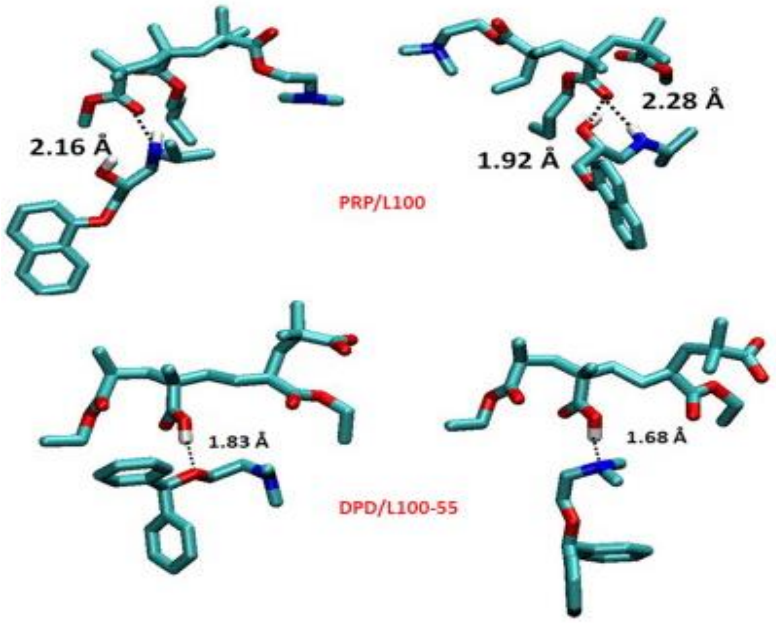

Figure 1.8. Molecular modelling of drug/polymers after energy optimization at the B3LYP 6-31G using Gaussian 09 software; PRP represent propranolol HCl, L100 represents Eudragit L100 and L100-55 represents Eudragit L100-55; Reproduced with permission from reference 92.

1.3.4. Reduction of molecular mobility of amorphous drug in PASD

The increased physical/chemical stability of amorphous drugs in PASD can be explained in terms of molecular mobility. An isolated metastable crystalline state of a drug may behave as if it is not affected by the stable crystalline form, until a polymorphic transition takes place. However, an amorphous drug may behave as if it always "identifies" the presence of the more stable crystalline state and gradually evolves towards it in a certain way which can be predicted from its thermal history and the extent of non-equilibrium. This is known as structural relaxation.[93] The molecular mobility of amorphous materials determines their physical stability and reactivity. Indeed, phase separation and crystallization involves diffusion and nucleation, both of which require sufficient molecular mobility. Different methods such as Kohlrausch-William-Watts method and Adam-Gibbs-Vogel equation are used to measure molecular mobility in terms of structural relaxation.[94, 95] Polymer molecules, when used as a carrier for amorphous drug, have the capacity to restrict the molecular mobility of the amorphous API. Therefore, mechanistic investigation of reduced crystallization tendency due to restricted molecular mobility of amorphous drugs in PASD is essential to assess their stability. DSC,[96] solid-state nuclear magnetic resonance (ssNMR)[97] and dielectric spectroscopy (DS)[98] are commonly used to monitor molecular mobility in glass systems.

Knapik *et al.* have shown that the physical stability and water solubility of the amorphous drug (ezetimibe) was improved over six times when mixed within a PASD using Soluplus® as carrier.[99] DSC and DS analysis of amorphous ezetimibe led to the conclusion that high molecular mobility, reflected in structural relaxation, is mainly responsible for its high crystallization tendency. This indicates that formation of a PASD in the Soluplus® matrix acts as physical barrier to the molecular motions of glass ezetimibe leading to improved stability. Mistry *et al.* have also shown that stronger drug-polymer interactions (ionic or H-bonding) reduces the molecular motion of amorphous ketoconazole which can potentially delay crystallization onset time and reduce crystallization extent.[100] In another interesting study conducted by Kothari *et al.* it has been found that the relaxation time of the drug increases with an increase in polymer concentration.[101] The improved stability results were attributed to the restriction of molecular mobility of amorphous drug.

1.4. Rational Selection of Polymers for PASDs

At an early developmental stage, with a limited drug supply, it is very important to characterize and correlate the physicochemical properties (such as chemical structure,

molecular weight, melting or glass transition temperature, melting enthalpy and entropy, viscosity of drug and polymer below and above T_g, structural flexibility, complexity and symmetry, functional groups contributing to bond formation and so on) of the drug and polymer to design a robust amorphous solid dispersion systems. A number of key parameters must be considered when selecting a polymer. As discussed previously, high T_g polymers at high concentrations are generally chosen to prepare ASDs owing to their antiplasticizing effect on the amorphous drug. However, at lower polymer weight fractions where no T_g differences (between amorphous drug and solid dispersion) are observed, usually drug-polymer interactions will determine the shelf life of the product.[102] Increasing the molecular weight raises the T_g of polymers which favors antiplasticization of amorphous drugs.[103] However, at high molecular weights, the rise in T_g become insignificant as other factors such as viscosity comes into play during the dissolution process. The viscosity of a polymer increases with molecular weight which has a significant effect on the dissolution properties.[104] Also, the polymer should have low melting point and solubility parameters similar to drug. In addition, the extent of miscibility of an amorphous drug in the polymer is also important as highly miscible systems are found to be more resistant to drug recrystallization.[105] The formation of a stable single phase or separate coexisting phases depends on the thermodynamic miscibility of the drug and polymer at the required condition. A change of conditions may cause phase separation of the homogenous single phase system (Table 1.3). Therefore, conflicting requirements have to be met when choosing a suitable polymeric carrier. Different methods such as the solubility parameter approach, Flory-Huggins theory, the melting enthalpy approach and molecular modelling as preformulation tools for the rational selection of polymers are discussed in the following sections.

1.4.1. Solubility parameter approach

The experimental determination of the solubility of a drug in a polymer is challenging. However, a qualitative estimation of drug-polymer miscibility can be achieved using the solubility parameter approach. The solubility parameter is equal to the square root of the cohesive energy density (CED) (total attractive force within a condensed state material) as shown below:[106]

$$\delta = \sqrt{CED} = \sqrt{\Delta E_v / V_m} \qquad \ldots\ldots\ldots \qquad (1.5)$$

where δ is the Fedor solubility parameter, ΔE_v is the energy of vaporization and V_m is the molar volume. Similar values of CED for drug and polymer indicate that lesser energy is

required from external sources to break the interaction between the two similar molecules as the energy required will be compensated from the energy released by the interaction between two dissimilar molecules. It has been found that the cohesive energy also depends on the interactions between polar groups and hydrogen bonding. Better predictions of interaction can, therefore, be made by using Hoftyzer and Van Krevelen Method as shown by the following equations:[107]

$$\delta^2 = \delta_d^2 + \delta_p^2 + \delta_h^2 \quad \text{……..} \quad (1.6)$$

$$\delta_d = \frac{\sum F_{di}}{V}, \delta_p = \frac{\sqrt{\sum F_{pi}^2}}{V} \text{ and } \delta_h = \sqrt{\frac{\sum E_{hi}}{V}} \quad \text{.....} \quad (1.7)$$

where δ_d, δ_p and δ_h are the contributions from the dispersive forces, polar forces and hydrogen bonding respectively; δ is the total solubility parameter; F_{di} is the molar attraction constant due to dispersive component; F_{pi} is the molar attraction constant due to polar component; E_{hi} is the hydrogen bonding energy; and V is the molar volume. Other methods for solubility parameter calculation, such as Hoy, Small, Dunkel, Hayes and Di Benedetto, are also reported in the literature.[108] Generally, drug-polymer systems with lower $\Delta\delta$ values are predicted to be more miscible. Systems with $\Delta\delta$ < 7.0 $MPa^{1/2}$ are found to be miscible whereas with $\Delta\delta$ > 10.0 $MPa^{1/2}$ are likely to be immiscible.[109] Although widely used, this approach has certain limitations as well. The theoretical calculation of this approach is applicable for drug-polymer systems where van der Waal interactions plays a major role, while for drug-polymer mixtures forming highly directional interactions such as H-bonds or long range forces such as ionic interactions, this method can yield erroneous results.[110]

1.4.2. Flory-Huggins Theory

Flory-Huggins (FH) theory is a well-known lattice-based theory which describes polymer-solvent miscibility on the basis of the Gibbs free energy change associated with the mixing of a polymer in a solvent.[111] Recently, this theory has been applied for assessing drug-polymer miscibility using the melting point depression method to obtain FH interaction parameter, χ, and the modified FH equation by Nishi-Wang is shown below:[112]

$$-\left(\frac{1}{T_m} - \frac{1}{T_m^o}\right) * \frac{\Delta H_f}{R} - ln\Phi_d - \left(1 - \frac{1}{m}\right)\Phi_p = \chi\Phi_p^2 \quad \text{……} \quad (1.8)$$

where T_m and T_m^o are the melting points of the drug-polymer physical mixture and pure drug respectively, ΔH_f is the melting enthalpy of pure drug, $\Phi_d$and Φ_p are the volume fraction of

drug and polymer respectively, and m is the ratio of the polymer volume to that of the drug. The slope of the line obtained by plotting left hand side of the equation against Φ_p^2 will give the value of FH interaction parameter, χ. A negative value of χ will indicate stronger drug-polymer interaction than individual drug-drug or polymer-polymer interaction which predicts drug-polymer miscibility whereas a positive value indicates that homo-nuclear interactions are preferred over hetero-nuclear which may lead to phase separation.[113, 1140, 115]

1.4.3. Melting enthalpy method

The physical stability of ASD primarily depends on the drug solubility in the polymer at the storage temperature. Initial determination of drug solubility in a particular polymer can be used as a screening tool *i.e.*, polymer(s) which solubilizes higher drug weight fraction can be used for further downstream processing of ASD. The most widely used method for the estimation of drug solubility in a polymer is the melting enthalpy of the crystalline drug in a drug-polymer system measured by hyper DSC.[116] This method is based on the simple principle that the fraction of drug dissolved in the polymer does not contribute to the melting endotherm. Therefore, by measuring the melting enthalpy of a series of drug concentrations in drug-polymer mixtures and extrapolating the plot to zero enthalpy, the solubility of a given drug in selected polymers could be estimated from the x-intercept of the plotted line as shown in Figure 1.9.

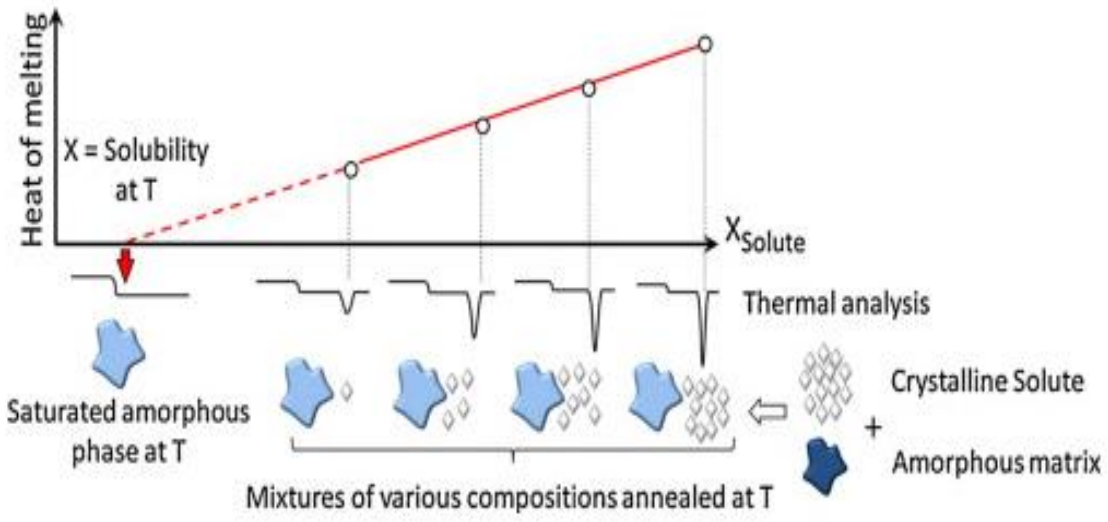

Figure 1.9. Melting enthalpy as a function of different drug loading in the drug-polymer physical mixture showing the fraction of unmixed drug contributing to the melting enthalpy; Reproduced with permission from reference 116

1.4.4. Molecular simulation

Recent computational advances in the area of atomistic and molecular simulation have given us powerful tools to probe the molecular processes of different systems, thus permitting prediction of the thermodynamic behavior of amorphous solid dispersions that are not well characterized experimentally.[117] *In silico* predictive tools such as GROMACS all-atom field package, Monte Carlo simulations, Dreiding 2.21 force field measurement using Cerius 2 software, SYBYL/MMFF94 force field measurement and Gaussian 09 software using density functional theory have been successfully employed to PASD systems to understand glass transition, crystallization tendency, drug-polymer interaction and stability.[118] These simulation tools in combination with Flory-Huggins theory have also been used to estimate the solubility of a drug in a lipid carrier.[119] Furthermore, condensed-phase optimized molecular potentials for atomistic simulation studies (COMPASS) force field can predict the solubility parameter for drug-polymer systems.[120] Moreover, the density functional theory using B3LYP exchange correlation function gives a reasonable estimation of drug-polymer interactions (Figure 1.8).[121] These findings demonstrate that *in silico* based molecular modelling is a powerful preformulation tool that can enable formulation scientists to rationally select polymers to use for PASDs.

1.5. Methods for Dispersing Amorphous Drugs in Polymers

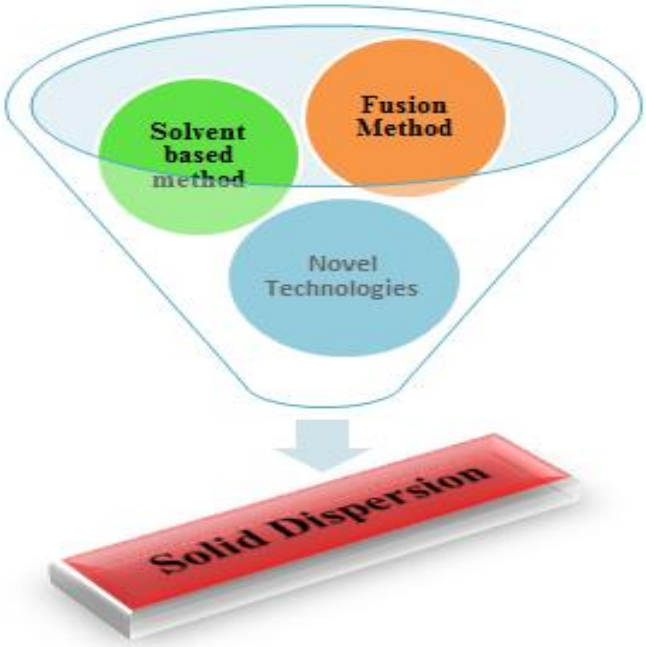

Figure 1.10. Different manufacturing techniques of solid dispersions

Various preparation methods for solid dispersions have been reported in the literature (Table 1.2) including nanosuspension techniques, cryogenic techniques, cyclodextrin based

inclusion complex techniques, electrostatic spinning, electrostatic blowing, electro-spraying film casting, hydrotrophy and mechanical activation method.[122] These techniques rely on a solubilizing mechanism such as micellar solubilization, complexation, increased porosity or decreased particle size and it should be differentiated from polymer based ASD. Binary systems are most commonly used for the preparation of ASDs due to simple formulation strategy, ease of scale up and lower cost of production.[123] Sometimes more complex ternary and quaternary systems have also been produced depending on the requirement of the formulation and the drug stability.[124] Surfactants may increase stability and solubility of ASDs but also increase the complexity of the process. Furthermore, they are not always tolerated well in the body.[125] Requirements such as intimate mixing at the molecular level should also be met while designing a suitable process. Care has to be taken to avoid de-mixing or phase separation while choosing the techniques. Generally, phase separation or recrystallization can be prevented by restricting the molecular mobility of amorphous drugs and polymers during preparation. Three different methods (Figure 1.10) for preparing solid dispersion are discussed in the following sections. More information on preparation techniques can be found in a number of excellent review articles.[126]

1.5.1. Fusion Method

The fusion method, also known as the melt method, was first proposed by Sekiguchi and Obi in 1961.[127] A physical mixture of drug and polymer is heated to form a molten mixture which is then cooled and solidified with rigorous stirring. The resultant solid mass is then crushed, pulverized and sieved to obtain the desired particle size. Although frequently used, there are a number of challenges in preparing solid dispersions using this method such as lack of drug-polymer miscibility at the heating temperature. The use of surfactants may avoid this problem.[128] However, drugs and polymers have to be thermally stable at the melting temperature and consequently, lower processing temperatures are preferred.[129] Also, the fused mixture has to be stable against recrystallization and phase separation upon aging over the shelf life of the products. Sheng *et al.* has reported that the supersaturation of amorphous drug in a felodipine-Eudragit formulation causes phase separation on aging.[130] Similar results have been reported by Save *et al.* upon slowly cooling the melt mixture of nifedipine-polyethylene glycol 6000 formulation.[131]

Hot melt extrusion is the modern version of the fusion method in which intense mixing of the components is induced by the extruder. Compared to the traditional fusion method, melt extrusion offers the potential to shape the molten drug-polymer mixture into

implants, pellets or oral dosage forms.[132] This method requires complete miscibility of the drug and polymer in the molten state. Solubility parameter phase diagrams can be used to predict miscibility and to rationally select a compatible polymer. This technique offers several advantages such as (a) solvent free method (b) fewer processing steps as there is no compression of ingredients and no need to dry products which makes this technique simple, continuous and efficient and (c) thorough mixing at high shear rate and temperature causes the particles to de-aggregate and create a uniform distribution of fine drug particles in the polymer matrix and molecular level dispersion.[133] Furthermore, compared to the traditional fusion method, this technique offers the possibility of continuous manufacture, which makes it suitable for large scale production. Some examples of commonly used polymeric materials which are used in hot-melt extrusion include HPMC, HPMC-AS, PVP, PVP-VA and PEO (Table 1.2).[134]

1.5.2. Solvent Method

The solvent method involves the preparation of a solution of both drug and polymer in a single solvent followed by removal of the solvent to yield a solid dispersion. This technique enables molecular level mixing which is preferred to increase the solubility and stability of the product. The main advantage of this method is that thermal decomposition of the drug and polymer can be prevented as low temperatures are typically required to evaporate organic solvents. However, formulation scientists face two challenges when using this approach. The first challenge is to mix the drug and the polymer in a single solvent which can be difficult if they have significant polarity differences. Sometimes surfactants are used to improve drug or polymer solubility in particular solvents. However, the amount of surfactant remaining in final dosage form is often significant which reduces the drug loading capacity and may also cause problems if they are not well tolerated in the body. Also, the need to evaporate large amount of the solvent makes the process expensive. The second challenge is the phase separation which may occur during removal of the solvent. Vacuum drying is frequently used to dry the solution. Sometimes fast drying is achieved by a rotary evaporator. Higher drying temperatures are preferred which reduces the time available for phase separation. However, the high molecular mobility of drugs and polymers at elevated temperatures may accelerate phase separation.[135]

Spray drying has emerged as a popular processing technology for developing solid dispersions of drugs.[136] It is used to convert a solution or suspension into a dry powder in a single step. This technique provides a better control of process variables, producing powders

with desired size, shape, density and flow properties.[137] Evaporation of solvent occurs at a very fast rate in spray drying, causing a sudden rise in viscosity which leads to the entrapment of drug molecule in the polymer matrix.[138] Drugs with poor aqueous solubility may be spray dried into very small particles provided that they are soluble in certain solvents suitable for spray drying. The nature of the solid particles formed also depends upon chemical properties of the drug, and spray drying may produce amorphous material, crystalline forms, imperfect crystals or metastable crystals.[139] Indeed, Mahlin *et al.*[140] and Baird *et al.*[141] have worked on the different drug compounds and showed that generating an amorphous form depends on the chemical nature of the drugs rather than on the process variables. However, the stability of the amorphous form depends on the process variables.[142] Spray drying offers great control of the powder characteristics and due to cheaper manufacturing costs, ease of scale up and continuous batch manufacture, it has become the most popular solvent based production method.[143]

1.5.3. Supercritical Fluid Method

Supercritical fluids (SCF) possess the properties of both liquid and gas. Under supercritical conditions, materials have liquid-like solvent properties and gas-like viscosity, diffusivity and thermal conductivity. While the solvent properties are beneficial for drug/polymer solubilization, the gas-like properties significantly enhance the mass transport characteristics of the fluids. This method is mostly applied using supercritical carbon dioxide (CO_2) either as a solvent for drug and polymer or as an anti-solvent.[144] The polymer and drug are dissolved in supercritical CO_2 and sprayed through a nozzle into low pressure region causing adiabatic expansion of the CO_2 and rapid cooling. Thus, this technique allows the production of drug particles with a greatly reduced particle size. This technique is known as rapid expansion of supercritical solution (RESS). Current SCF methods have demonstrated the potential to create nano-particulate suspensions of particles with 5-2000 nm diameters.[145] Since this technique is not dependent on the use of organic solvents and the small amount of the residual CO_2 trapped inside the polymer poses no danger to patients, this technique is referred to as environment friendly. Furthermore, the ability of CO_2 to plasticize and swell polymers can also be exploited. However the low solubility of most pharmaceutical compounds in CO_2 limits the practical application of this approach.[146] Several methods of SCF processing have been developed to address individual aspects of these shortcomings and to improve the solubility. These methods includes precipitation with a compressed anti-solvent (PAS),[147] solution enhanced dispersion by SCF (SEDS),[148] supercritical anti-solvent

processes (SAS),[149] gas anti-solvent recrystallization (GAS),[150] and aerosol supercritical extraction system (AESS).[151]

1.6. Characterization of PASDs

The nature of ASDs and the inherent risk of recrystallization requires in depth characterization of these formulations. Quality by Design principles demands a thorough understanding of the processes taking place at a molecular level. A single characterization technique may not give the full picture, and, therefore, a suite of complementary methods is often required (Figure 1.11). A brief selection of the available literature will be discussed here.

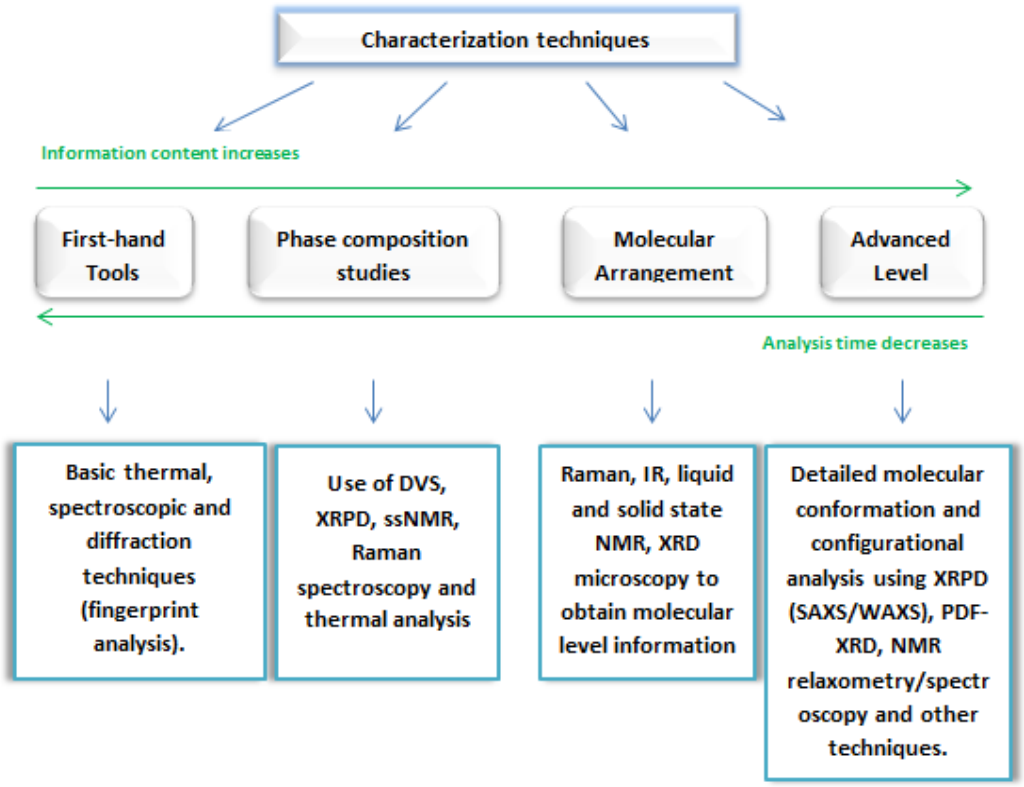

Figure 1.11. Solid-state characterization tools for polymeric amorphous solid dispersions

1.6.1. X-Ray Powder Diffraction (XRPD)

Powder x-ray diffraction is an indispensable tool for the characterization of amorphous solid dispersions. [152] Moes *et al.*[153], Zhao *et al.*[154] and Al-Obaidi *et al.*[155] have reported the use of this technique to confirm the presence of amorphous drug in a solid dispersion. Recent advancements in XRPD instrumentation and software can provide useful information under non-ambient conditions, such as XRPD equipped with variable temperature (VT) or humidity

control which can provide an insight into molecular behavior of amorphous drugs in solid dispersion under stressed conditions.[156] Zhu *et al* have studied the crystallization kinetics of a naproxen solid dispersion at different temperatures by in situ small-angle X-ray scattering/wide-angle scattering (SAXS/WAXS).[157] Furthermore, atomic pair-wise distribution function (PDF) has gained importance to detect the degree of amorphization induced into crystalline drugs.[158] Nollenberger *et al.*, have used PDF analysis to show that subtle changes at the molecular level of polymer structure can have a significant effect on the release characteristics of the final product.[159]

1.6.2. Thermal analysis (TA)

The most widely used thermal analysis methods are differential scanning calorimetry (DSC) and thermogravimetric analysis (TGA). However, other methods such as dynamic mechanical analysis (DMA) and isothermal micro-calorimetry are also used for routine analysis in the pharmaceutical industry. An insight into processes occurring at a molecular level in the solid dispersion such as glass-transition, crystallization, polymorphic transition, molecular mobility, structural relaxation and miscibility between drug and polymer can be obtained using DSC and other emerging thermal analysis techniques.[160] Mahajan *et al.* has applied this technique to quantify the amorphous content in carvedilol tablets by carrying out T_g and heat capacity analyses.[161] Furthermore, the higher sensitivity of Fast-Scan DSC offers the advantage of separating the overlapping thermal events.[162] The information regarding viscoelastic properties of polymers, relaxation transitions and miscibility in binary or ternary systems can be obtained by using differential mechanical thermal analysis (DMTA).[163]

With the advent of more sophisticated instruments in the past few years, it is now possible to perform real-time solid-state characterization as a function of change in temperature. The molecular orientation and structural relaxation of amorphous drugs in solid dispersions and their interaction with polymers can now be studied in greater detail with the use of techniques such as VT molecular spectroscopy, VT-XRPD and VT solid state nuclear magnetic resonance (VT-ssNMR). Nano-thermal analysis, a localized thermal analysis technique, when combined with atomic force microscopy (AFM) can provide high resolution images of the thermal behavior of amorphous drugs. In nano-TA based AFM, a miniature heater having topographic resolution of approximately 5 nm is placed on top of the micro-fabricated silicon based probe enabling the measurement of thermal properties at a nanometer scale.[164]

1.6.3. Spectroscopy

Fourier transformed infrared spectroscopy (FTIR), combined with attenuated total reflectance and/or diffuse reflectance, and Raman Spectroscopy are the two very efficient techniques among the vibrational spectroscopic methods.[165, 166] These techniques have been used for a range of pharmaceutical applications including polymorph identification, phase transition, recrystallization stability, evaluation of different manufacturing methods for solid dispersions, phase separation, nature and extent of drug-polymer interaction. [167, 168] These techniques offer information on structural and molecular conformation in the solid state by probing band vibrations. Furthermore, Raman spectroscopy is a powerful light scattering technique used to diagnose the internal structure of molecules and crystals. Also, an insight into the crystal packing may be obtained by studying low energy lattice vibration associated with different crystal packing arrangements.[169] Furuyama *et al.* have used Raman spectroscopy as a mapping technique to distinguish between the crystalline and the amorphous form of troglitazone in solid dispersions.[170] Sinclaire *et al.* applied FT Raman spectroscopy to measure the recrystallization kinetics of an amorphous solid dispersion of the drug ibipinabant.[171] It is also used to detect the presence of trace crystallinity which would otherwise go undetected by XRPD or high sensitivity DSC (HSDSC).[172]

1.6.4. Water Vapour Sorption

Water vapor sorption has been frequently used to study the behavior of amorphous and crystalline material in the presence of moisture. Theoretical approaches such as by predicting the additivity of the moisture sorption isotherm of the individual components or by using ternary Flory-Huggins interaction theory can be used to interpret the moisture sorption data which may provide an insight into drug-polymer-water interactions.[173] When combined with other techniques such as DSC, FT-IR and NMR, it can provide various information on molecular level attributes such as surface properties, degree of amorphization, phase transitions, critical RH for glass transition and crystallization and physical stability of freshly prepared and aged materials.[174, 175, 176] Dynamic vapor sorption combined with Near infrared spectroscopy can provide an insight into the desorption behavior of amorphous materials before and during crystallization, as a function of temperature and relative humidity (RH).[177]

1.6.5. Solid-state nuclear magnetic resonance (ssNMR)

Solid-state NMR (ssNMR) is non-destructive technique which provides qualitative and quantitative information about amorphous solid dispersions. It provides detailed one-

dimensional and two-dimensional structural information based on NMR relaxometry/spectroscopy/imaging techniques.[178] By correlating the relaxation time with the length scale of the spin diffusion, predictions can be made about drug-polymer domain size in solid dispersions. For example, values of the spin-lattice relaxation time, T_1, ranging between 1-5 seconds correspond to a domain size of approximately 20-50 nm. Additionally, $T_{1\rho}$ (spin-spin relaxation time) values between 5-50 ms will suggest the length scale of approximately 2-5 nm. Reliable predictions can be made based on these relaxation time measurements. A single value of ^1H T_1 and $T_{1\rho}$ obtained from the amorphous solid dispersions will suggest that domain size is smaller than 2-5 nm. Different $T_{1\rho}$ values but the same T_1 value will indicate a domain size of about 5-20 nm. For domain size larger than 20-50 nm will give different values of T_1 and $T_{1\rho}$ for drug and polymer. This method is much more sensitive than DSC which has a sensitivity of about 20-30 nm and domain size smaller than this will give a single T_g values. Thus, ssNMR relaxometry will provide a better understanding of drug-polymer intimacy in the solid dispersion which helps in improving the stability of amorphous solid dispersions and preventing phase separation over the shelf life of the product.[179] Information regarding phase composition and molecular mobility of the polymers in solid dispersions can be obtained by ^1H transverse magnetization relaxation T_2 measurements.[180] ^{13}C cross-polarization magic angle spinning (CP/MAS) NMR experiments were used to probe the recrystallization of amorphous troglitazone in solid dispersion prepared by different methods where no difference was observed in the XRPD pattern.[181] NMR micro-imaging technique is a valuable addition to analytical methods to study water penetration and polymer mobilization kinetics.[182]

1.6.6. Inverse gas chromatography (IGC)

Inverse gas chromatography is still an emerging technology and has been used to analyze surface properties of amorphous solid dispersions.[183] It is used to examine molecular mobility, amorphous transition or recrystallization and molecular relaxation which is especially useful in detecting batch-to-batch variation of amorphous solid dispersions prepared by the same or different methods.[184] Furthermore, the study of higher molecular mobility on the surface of the material than in the bulk will provide an insight into moisture interaction and recrystallization of amorphous drugs.[185] Hasegawa *et al.* has used IGC to study the structural relaxation at the surface of solid dispersions and found that structural relaxation occurs faster at the surface than in the bulk due to higher molecular mobility at the

surface.[186] Predictions regarding physical stability of amorphous products can be made by investigating the crystallization kinetics on the surface of solid dispersions.[187]

1.7. Dissolution Behaviour of PASDs

The most widely employed method to predict *in vivo* performance of a formulation is dissolution. However, it is challenging to establish an accurate *in-vitro/in-vivo* (IVIV) correlation because the dissolution kinetics may not be predictive of the complex nature of supersaturation generation and maintenance (Figure 1.12) or fully consider the driving force for absorption *via* solubilizing power of such drug delivery systems.[188] This holds true for PASDs because several different complex processes occur simultaneously during their dissolution.[189]

Increased efforts from academic and industrial researchers have pushed the understanding of drug-polymer interaction in aqueous media.[190] The general solubilization mechanism of PASDs is the so called "spring and parachute" concept.[191] The drug first dissolves along with the soluble polymer matrix to generate a supersaturated solution ("spring") followed by decline in drug concentration in the media due to either absorption or precipitation ("parachute") as shown in Figure 1.3. Three different scenarios are possible for dissolution behavior of PASD as shown in Figure 1.12.[192] In the first case, PASD particles dissolve rapidly generating a highly supersaturated solution followed by the formation of drug nanoclusters (amorphous or crystalline) within the polymer matrix. The second case represents the gradual release of drug and polymer while drug remains amorphous in the undissolved particles. In the third scenario, the drug and polymer are released gradually; however, the drug may undergo crystallization mainly at the surface of undissolved PASD particles due to plasticizing effect of water. It is important to mention here that the free drug concentration in the dissolution media is dependent on the aqueous solubility of the crystalline or amorphous drug which in turn depends on many factors including, but not limited to, drug crystallization rate, drug-polymer interaction and drug-polymer ratio. The success of the PASD depends on the ability of the polymer to maintain supersaturation without precipitation long enough to facilitate drug absorption. The mechanism of how the polymer delays supersaturation is not completely understood and needs further research. However, as discussed previously, it is generally believed that drug-polymer interactions play a major role in inhibiting crystallization either by interfering with the nucleation process or by inhibiting crystal growth.

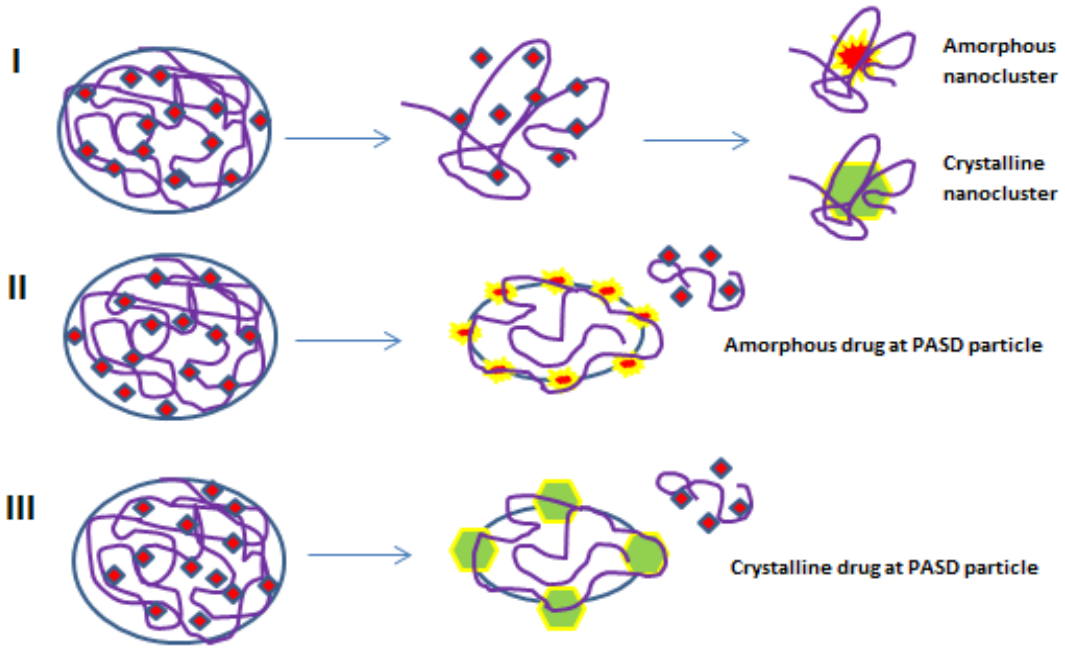

Figure 1.12. Dissolution behavior of polymeric amorphous solid dispersions

1.8. Research Objectives

The project aims to develop and optimize a method for successfully delivering a range of BCS class II drugs utilizing amorphous solid dispersion technology. To develop a stable and highly soluble system, a variety of drugs and polymers will be examined initially including dipyridamole (DPM), cinnarizine (CNZ), polyvinyl pyrrolidone (PVP) and polyacrylic acid (PAA) (Figure 1.13) to determine the optimum formulation for solid dispersions. DPM and CNZ are typical BCS class II drugs with practical poor aqueous solubility (~6.8 µg/mL at pH 6.8 for DPM and ~2 µg/mL at pH 6.5 for CNZ) and high GI membrane permeability (Log P values for DPM and CNZ are 3.71 and 5.71, respectively).[192, 193, 194] The glass transition temperatures of DPM (~40°C) and CNZ (~6°C) reported in literature suggests their fragile nature in the amorphous state.[50, 79] This qualifies them as model compounds for the present investigation. Another interesting feature of DPM and CNZ is the presence of a different number of H-bond donor (DPM – 4 and CNZ – 0) and acceptor groups (DPM – 12 and CNZ – 2). As discussed previously, H-bonding was found to have a significant effect on the physical stability of amorphous drug-polymer systems. Thus, it would be interesting to compare the recrystallization tendency of DPM and CNZ in a polymer matrix since both the drugs have different nature and strength of forming H-bonds. The thermodynamic stability of amorphous drugs can be enhanced by incorporating them into polymeric carrier matrix which prevents conversion of amorphous drug into crystalline form either due to thermodynamic or kinetic factors. The selected carriers for the present project,

PVP and PAA, are amorphous hydrophilic polymers soluble in water, methanol, dichloromethane and other such solvents.[195] The presence of a tertiary amide group in PVP and carboxyl group in PAA gives them H-bond forming ability.[50] Furthermore, the different glass transition temperature of PVP (165°C) and PAA (106°C) may result in different degree of antiplasticization effect on the DPM and CNZ.[197] This will provide a better understanding of the role of H-bonding, antiplasticization and molecular mobility on the recrystallization tendency of amorphous DPM and CNZ within ASD.

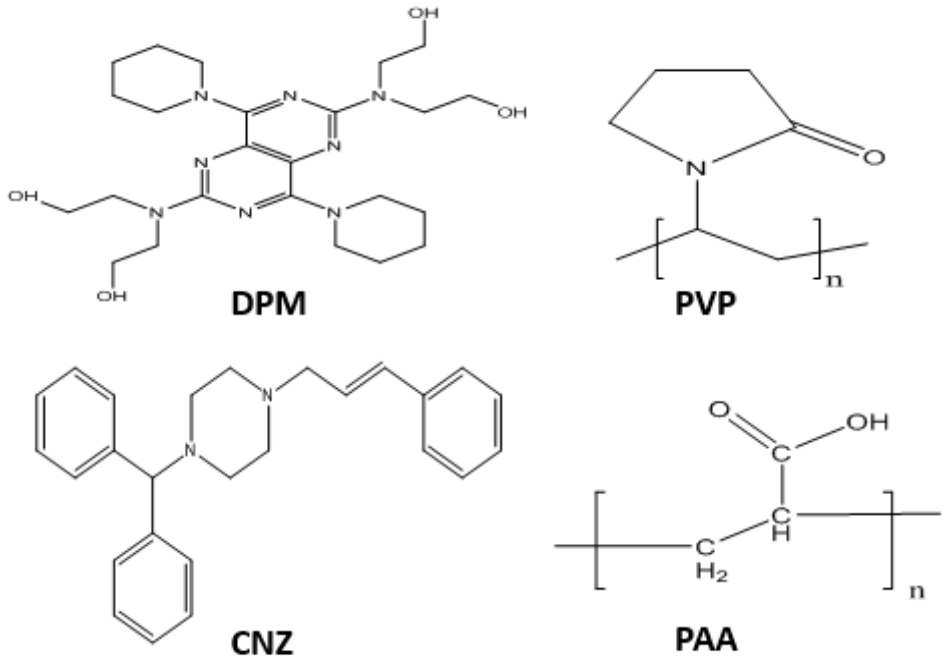

Figure 1.13. Chemical structure of DPM, CNZ, PAA and PVP K30 (clockwise from top)

The research will investigate the crystallization tendency/kinetics of the amorphous drugs, the rational selection of polymers to stabilize the amorphous drugs, *in-vitro* dissolution behaviour of binary ASDs, the effect of temperature and moisture on the solubility and stability of the ASDs and formulation of multi-component ASDs. Crystallization tendency/kinetics studies (Chapter 2) of the amorphous drugs will be carried out using MDSC and XRPD. These analytical techniques will be used to examine the fragility, glass forming ability, isothermal crystallization kinetics and non-isothermal crystallization kinetics. Using the data from these techniques and methods, the tendency of the amorphous drugs to undergo devitrification can be predicted. Once the relative instability of amorphous drugs has been established, further studies will be carried out to rationally select the polymer to stabilize amorphous drugs (Chapter 3). This is achieved by determining the drug-polymer

interaction and miscibility using the solubility parameter approach, melting point depression analysis and phase diagram. Solid dispersions will be prepared and characterized using MDSC, XRPD, FTIR and DVS. Furthermore, the strength of the drug-polymer-water interaction will also be investigated by applying ternary Flory-Huggins theory. This will be followed by *in-vitro* dissolution studies (Chapter 4) of the ASDs to understand the dissolution behaviour and the role of drug-polymer interaction and drug loading on the supersaturation generation and maintenance of spray dried ASDs. Furthermore, an investigation into the effect of temperature and moisture on the solubility and stability of ASDs will be carried out in Chapter 5. Finally, an investigation into the solid-state properties and dissolution profile of spray dried ternary ASDs will be carried out in Chapter 6 to rationally design and develop multi-component amorphous systems.

1.9. References

1. Aulton M. 2008. Aulton's Pharmaceutics; the design and manufacture of medicines. Third edition. Churchill Livingstone Elsevier: 441-482.

2. Amidon GL, Lennarnas H, Shah VP, Crison JR. 1995. A theoretical basis for biopharmaceutics drug classification: The correlation of *in vitro* drug product dissolution and *in vivo* bioavailability. Pharm Res 12: 413-420.

3. Yasir M, Asif M, Kumar A, Aggarval A. 2010. Biopharmaceutical Classification: An Account. Int J Pharm Tech Res 2: 1681-1690.

4. Guidance for Industry. Waiver of In Vivo Bioavailability and Bioequivalence Studies for Immediate-Release Solid Oral Dosage Forms Based on a Biopharmaceutics Classification System. USFDA. CDER. 2000.

5. Childs S, Kandi P, Lingireddy S. 2013. Formulation of a danazol cocrystal with controlled supersaturation plays an essential role in improving bioavailability. Mol Pharm 10: 3112-3127.

6. Tripathi K. 2006. Essentials of Medical Pharmacology.6th Edition.Jaypee Brothers Medical Publishers (P) Ltd.: 293.

7. Jain S, Patel N, Lin S. 2015. Solubility and dissolution enhancement strategies: current understanding and recent trends. Drug Dev Ind Pharm 41: 875-887.

8. Douroumis D, Fahr A. 2013. Drug delivery strategies for poorly water soluble drugs. Advances in Pharmaceutical Technology. Wiley Publication: UK.

9. William R, Watts A, Miller D. 2012. Formulating poorly water soluble drugs. AAPS Advances in Pharmaceutical Science Series III. Springer Publication: NY.

10. Savjani K, Gajjar A, Savjani J. 2012. Drug solubility: Importance and enhancement techniques. ISRN Pharm 2012: 1-10.

11. Mooter G. 2012. The use of amorphous solid dispersions: A formulation strategy to overcome poor solubility and dissolution rate. Drug Discov Technol Today 9: e79-e85.

12. Zhang M, Li H, Lang B, O'Donell K, Zhang H, Wang Z, Dong Y, Wu C, Williams R. 2012. Formulation and Delivery of Improved Amorphous Fenofibrate Solid Dispersion Prepared by Thin Film Freezing. Eur J Pharm Biopharm 82: 534-544.

13. Sekiguchi K, Obi N. 1961. Studies on absorption of eutectic mixtures. I. A comparison of behaviour of eutectic mixtures of sulphathiazole and that of ordinary sulphathiazole in man. Chem Pharm Bull 9: 866-872.

14. Vo C, Park C, Lee B. 2013. Current trend and future perspective of solid dispersions containing poorly water soluble drugs. Eur J Pharm Biopharm 85: 799-813.

15. Huang Y, Dai W. 2014. Fundamental aspects of solid dispersion technology for poorly soluble drugs. Acta Pharm Sin B 4: 18-25.

16. Teja S, Patil S, Shete G, Patel S, Bansal A. 2013. Drug-excipient behaviour in polymeric amorphous solid dispersions. J Excip Food Chem 4: 70-94.

17. Kumavat S, Chaudhari Y, Badhe M, Borole P. 2013. Physical stability of amorphous solid dispersion: A review. Int J Pharm Arch 2: 129-136.

18. William H, Trevaski N, Charman S, Shanker R, Pouton C. 2013. Strategies to address low drug solubility in discovery and development. Pharmacol Rev 65: 315-499.

19. Brough C, William 3rd R. 2013. Amorphous solid dispersion and nano crystal technologies for poorly water-soluble drug delivery. Int J Pharm 453: 233-252.

20. Kawakami K, Pikal M. 2005. Calorimetric investigation of the structural relaxation of amorphous materials: Evaluating validity of the methodologies. J Pharm Sci 94: 948-965.

21. Graeser K, Patterson J, Zeitler J, Rades T. 2010. The role of configurational entropy in amorphous systems. Pharmaceutics 2: 224-244.

22. Roos H. 2007. Water activity and glass transition. Water Activity in Foods. First edition. Blackwell Publishing and IFT Press: 29-46.

23. Teja S, Patil S, Shete G, Patel S, Bansal A. 2013. Drug excipients behaviour in polymeric amorphous solid dispersion. J Exip Food Chem 4: 70-94.

24. Stillinger F. 1988. Supercooled liquids, glass transition, and the kauzmann paradox. J Chem Phys 88: 7818-7825.

25. Hancock C, Parks M. 2000. What is the true solubility advantage for amorphous pharmaceuticals? Pharm Res 17: 397-404.

26. Sousa L, Reutzel-Edens S, Stephenson G, Taylor L. 2015. Assessment of the amorphous “solubility” of a group of diverse drugs using new experimental and theoretical approaches. Mol Pharm 12: 484-495.

27. Babu N, Nangia A. 2011. Solubility advantage of amorphous drugs and pharmaceutical cocrystals. Cryst Growth Des 11: 2662-2679.

28. Yu H, Hadinoto K. 2015. Mitigating the adverse effect of spray drying on the supersaturation generation capability of amorphous nanopharmaceutical powders. Powder tech 277: 97-104.

29. Sun D, Lee P. 2015. Probing the mechanism of drug release from amorphous solid dispersion in medium-soluble and medium-insoluble carriers. J Control Release 211: 85-93.

30. Sun D, Lee P. 2013. Evolution of supersaturation of amorphous pharmaceuticals: the effect of rate of supersaturation generation. Mol Pharm 10: 4330-4346.

31. Kadajji V, Betageri G. 2011. Water soluble polymers for pharmaceutical applications. Polymers 3: 1972-2009.

32. Donnelly C, Tian Y, Potter C, Jones D, Andrews G. 2015. Probing the effects of experimental conditions on the character of drug polymer phase diagrams constructed using Flory-Huggins theory. Pharm Res 32: 167-179.

33. Cui Y. 2007. A material science perspective of pharmaceutical solids. Int J Pharm 339: 3-18.

34. Kawakami K. 2015. Theory and practice of supersaturable formulations for poorly soluble drugs. Ther Deliv 6: 339-352.

35. Jahangiri A, Jalali M, Garjani A, Javadzadeh Y, Hamishekhar H, Rameshrad M, Adibkia K. 2015. Physicochemical characterization and pharmacological evaluation of ezetimibe-PVP K30 solid dispersions in hyperlipidemic rats. Colloids Surf B 134: 423-430.

36. Kannaujia P, Lau G, Hg W, Widjaja E, Hanefeld A, Fischbach M, Maio M, Tan R. 2011. Nanoparticle formation and growth during *in vitro* dissolution of ketoconazole solid dispersion. J Pharm Sci 100: 2876-2885.

37. Mahmoudi Z, Upadhye S, Ferrizzi D, Siahboomi A. 2014. In vitro characterization of a novel polymeric system for preparation of amorphous solid drug dispersions. AAPS J 16: 685-697.

38. Wu J, Ho H, Chen Y, Chen C, Sheu M. 2012. Thermal analysis and dissolution characteristics of nifedipine solid dispersions. J Food Drug Anal 20: 27-33.

39. Seo S, Han H, Chun M, Choi H. 2012. Preparation and pharmacokinetic evaluation of curcumin solid dispersion using solutol HS15 as a carrier. Int J Pharm 424: 18-25.

40. Medarevic D, Kachrimanis K, Mitric M, Djuris J, Djuric Z, Ibric S. 2015. Dissolution rate enhancement and physicochemical characterization of carbamazepine-poloxamer solid dispersions. Pharm Dev Technol. DOI: 10.3109/10837450.2014.996899.

41. Zidan A, Rahman Z, Sayeed V, Raw A, Yu L, Khan M. 2012. Crystallinity evaluation of tacrolimus solid dispersion by chemometric analysis. Int J Pharm 423: 341-350.

42. Parikh T, Gupta S, Meena A, Vitez I, Mahajan N, Serajuddin A. 2015. Application of film-casting technique to investigate drug-polymer miscibility in solid dispersion and hot-melt extrudates. J Pharm Sci 104: 2142-2152.

43. Beak I, Kim M. 2012. Improved supersaturation and oral absorption of dutasteride by amorphous solid dispersions. Chem Pharm Bull 60: 1468-1473.

44. Sun D, Lee P. 2015. Probing the mechanism of drug release from amorphous solid dispersins in medium-soluble and medium-insoluble carriers. J Control Release 211: 85-93.

45. Alshahrani S, Lu W, Park J, Morott J, Alsulays B, Majumdar S, Langley N, Kolter K, Gryczke A, Repka M. 2015. Stability enhanced hot-melt extruded amorphous solid disperisons via combinations of soluplus and HPMC-HF. AAPS PharmSciTech 16: 824-834.

46. Zhang M, Li H, Lang B, Donnell K, Zhang H, Wang Z, Dong Y, Wu C, Williams R. 2012. Fromulation and delivery of improved amorphous fenofibrate solid dispersions prepared by thin film freezing. Eur j Pharm Biopharm 82: 534-544.

47. Shamma R, Basha M. 2013. Soluplus: A novel polymeric solubilizer for optimization of carvedilol solid dispersions: Formulation design and effect of method of preparation. Powder Technol 237: 406-414.

48. Alhalaweh A, Alzghoul A, Mahlin D, Bergstrom C. 2015. Physical stability of drugs after storage above and below the glass transition temperature: Relationship to glass forming ability. Int J Pharm 495: 312-317.

49. Mahlin D, Bergstrom C. 2013. Early drug development predictions of glass-forming ability and physical stability of drugs. Eur J Pharm Sci 49: 323-332.

50. Patterson J, James M, Forster A, Lancaster R, Butler J, Rades T. 2005. The influence of thermal and mechanical preparative techniques on the amorphous state of four poorly soluble compounds. J Pharm Sci 94: 1998-2012.

51. Li j, Zhao J, Wang J, Waknis V,Pan D, Hubert M, Raghvan K, Patel J. 2015. The effect of polymeric excipients on the physical properties and performance of amorphous solid dispersions: Part I, free volume and glass transition. Pharm Res 32: 500-515.

52. Nunes T, Viciosa M, Correia N, Nunes R, Diogo H. 2014. A stable amorphous statin: solid-state NMR and dielectric studies on dynamic heterogeneity of simvastatin. Mol Pharm 11: 727-737.

53. Graeser K, Patterson J, Zeitler J, Gordon K, Rades T. 2009. Correlating thermodynamic and kinetic parameter with amorphous stability. Eur J Pharm Sci 37: 492-498.

54. Nanakwami K, Modi S, Kumar L, Bansal A. 2014. Role of thermodynamic, kinetic and structural factors in the recrystallization behaviour of amorphous erythromycin salts. Thermochim Acta 582: 77-85.

55. Marsac P, Konno H, Taylor L. 2006. A comparison of the physical stability of amorphous Felodipine and nifedipine. Pharm Res 23: 2306-2316.

56. Guo Z, Li M, Pang H, Lin L, Liu X, Wu C. 2014. The utilization of drug-polymer interactions for improving the chemical stability of hot-melt extruded solid dispersions. J Pharm Pharmacol 66: 285-296.

57. Sarode A, Sandhu H, Shah N, Malick W, Zia H. 2013. Hot melt extrusion for amorphous solid disperisons: Temperature and moisture activated drug-polymer interactions for enhanced stability. Mol Pharm 10: 3665-3675.

58. Branham M, Moyo T, Govender T. 2012. Preparation and solid dtate characterization of ball milled saquinavir mesylate for solubility enhancement. Eur J Pharm Biopharm 80: 194-202.

59. Keratichewanun S, Yoshihashi Y, Sutanthavibul, Terada K, Chatchawalsaisin J. 2015. An investigation of nifedipine miscibility in solid dispersions using Raman spectroscopy. Pharm Res 32: 2458-2473.

60. Potter C, Tian Y, Walker G, McCoy C, Hornsby P, Donnelly C, Jones D, Andrews G. 2015. Novel supercritical carbon dioxinde impregnation technique for the preparation of amorphous solid dispersions: A comparison to hot melt extrusion. Mol Pharm 12: 1377-1390.

61. Homayouni A, Sadeghi F, Nokhodchi A, Varhosaz J, Garekani H. 2015. Preparation and characterization of celecoxib dispersions in soluplus: comparison of spray drying and conventional methods. Iran J Pharm Res 14: 35-50.

62. Nielsen L, Keller S, Boisen A, Mullertz A, Rdes T. 2014. A slow cooling rate of indomethacin in microcontainers increases the physical stability of the amorphous drug withous influencing its biorelevant dissolution behaviour. Drug Deliv Transl Res 4: 268-274.

63. Paudal A, Loyson Y, Mooter G. 2013. An investigation into the effect of spray drying temperature and atomizing conditions on miscibility, physical stability and performance of naproxen-PVP K25 solid dispersions. J Pharm Sci 102: 1249-1267.

64. Keen J, Martin C, Machado A, Sandhu H, McGinity J, DiNunzio J. 2014. Investigation of process temperature and screw speed on properties of a pharmaceutical solid dispersion using corotating and counter-rotating twin-screw extruders. J Pharm Pharmacol 66: 204-217.

65. Dengale S, Hussen S, Krishna B, Musmade P, Shenoy G, Bhat K. 2015. Fabrication, solid-state characterization and bioavailability assessment of stable amorphous phases of ritonavir with quercetin. Eur J Pharm Biopharm 89: 329-338.

66. Shen T, Sun B, Xin S. 2015. Effects of metalloids on the thermal stability and glass forming ability of bulk ferromagnetic metallic glasses. J Alloys Compd 631: 60-66.

67. Petrovic A. 2015. Dynamic fragility and reduced glass transition temperature as a pair of parameters for estimating glass forming ability. J Non Cryst Solids 417-418: 1-9.

68. Kawakami K, Harada T, Yoshihashi Y, Yonemochi E, Terada K, Moriyama H. 2015. Correlation between glass-forming ability and fragility of pharmaceutical compounds. J Phys Chem B 119: 4873-4880.

69. Pina M, Pinto J, Sousa J, Craig D, Zhao M. 2015. Generation of hydrate form of paroxetine HCL from the amorphous state: An evaluation of thermodynamics and experimental predictive approaches. Int J Pharm 481: 114-124.

70. Milne M, Liebenberg W, Aucamp M. 2015. The stabilization of amorphous zopiclone in an amorphous solid dispersion. AAPS PharmSciTech. DOI: 10.1208/s12249-015-0302-4.

71. Kawakami K. 2011. Dynamics of ribavirin glass in the sub T_g temperature region. J Phys Chem B 115: 11375-11381.

72. Janssens S, Mooter G. Review: 2009. Physical chemistry of solid dispersions. J pharm Pharmacol 61: 1571-1586.

73. Surwase S, Itkonen L, Aaltonen J, Saville D, Rades T, Peltonen L , Strachan C. 2015. Polymer incorporation method affects the physical stability of amorphous indomethacin in aqueous suspension. Eur J Pharm Biopharm 96: 32-43.

74. Tian Y, Jones D, Andrews G. 2015. An investigation into the role of polymeric carriers on crystal growth within amorphous solid dispersion systems. Mol Pharm 12: 1180-1192.

75. Laitinen R, Lobmann K, Strachan C, Grohganz H, Rades T. 2013. Emerging trends in the stabilization of amorphous drugs. Int J Pharm 453: 65-79.

76. Luk E, Sandoval A, Cova A, Muller A. 2013. Anti-plasticization of cassava starch by complexing fatty acids. Carbohydr Res 98: 659-664.

77. Penzel E, Rieger J, Schneider H. 1997. The glass transition temperature of random copolymers: 1. Experimental data and the Gordon-Taylor Equation. Polymer 38: 325-327.

78. Huang Y, Dai W. 2014. Fundamental aspects of solid dispersion technology for poorly soluble drugs. Acta Pharm Sin B 4:18-25.

79. Tian B, Wang X, Zhang Y, Zhang K, Zhang Y, Tang X. 2015. Theoretical prediction of a phase diagram for solid dispersions. Pharm Res 32: 840-851.

80. Song Y, Yang X, Chen X, Nie H, Byrn S, Lubach J. 2015. Investigation of drug-excipient interaction in lapatinib amorphous solid dispersions using solid-dtate NMR spectroscopy. Mol Pharm 12: 857-866.

81. Prudic A, Lesanik A, Ji Y, Sadowski G. 2015. Thermodynamic phase behaviour of indomethacin/PLGA formulation. Eur J Pharm Biopharm 93: 88-94.

82. Mahmah O, Tabbakh R, Kelly A, Paradkar A. 2015. A comparative study of the effect of spray drying and hot-melt extrusion on the properties of amorphous solid dispersions containing Felodipine. J Pharm Pharmacol 66: 275-284.

83. Couchman P, Karasz F. 1978. A classical thermodynamic discussion of the effect of composition on glass transition temperatures. Macromol 11: 117-119.

84. Paudal A, Van Humbeeck J, Van den Mooter G. 2010. Theoretical and experimental investigation on the solid solubility and miscibility of naproxen in poly(vinylpyrrolidone). Mol Pharm 7: 1133-1148

85. Crowley K, Zografi G. 2002. Water vapour absorption into amorphous hydrophobic drug/poly(vinylpyrrolidone) dispersions. J Pharm Sci 91: 2150-2165.

86. Maniruzzaman M, Morgan D, Mendham A, Pang J, Snowden M, Douroumis D. 2013. Drug-polymer intermolecular interactions in hot-melt extruded solid dispersions. Int J Pharm 443: 199-208.

87. Paudel A, Worku A, Guns S, Mooter G. 2013. Manufacturing of solid dispersions of poorly water soluble drugs by spray drying: Formulation and process consideration. Int J Pharm 453: 253-284.

88. Khougaz K, Clas SD. 2000. Crystallization inhibition in solid dispersions of MK-0591 and Poly(vinylpyrrolidone) polymers. J Pharm Sci 89: 1325-1334.

89. Meng F, Trivino A, Prasad D, Chauhan H. 2015. Investigation and correlation of drug polymer miscibility and molecular interactions by various approaches for the preparation of amorphous solid dispersions. Eur J Pharm Sci 71: 12-24.

90. Miyazaki T, Aso Y, Yoshioka S, Kawanishi T. 2011. Differences in crystallization rate of nifedipine enantiomers in amorphous solid disperisons with HPMC and HPMCP. Int J Pharm 407: 111-118.

91. Shah N, Iyer R, Mail H, Choi D, Tian H, Diodane R. 2013. Improved human bioavailabilty of vemurafenib, a practically insoluble drug, using an amorphous polymer-stabilised solid dispersion prepared by a solvent-controlled coprecipitation process. J Pharm Sci 102: 967-981.

92. Maniruzzaman M, Morgan D, Mendham A, Pang J, Snowden M, Douroumis D. 2013. Drug-polymer intermolecular interactions in hot-melt extruded solid dispersions. Int J Pharm 443: 199-208.

93. Yang Z, Nollenberger K, Albers J, Craig D, Qi S. 2015. Molecular indicators of surface and bulk instability of hot melt extruded amorphous solid dispersions. Pharm Res 32: 1210-1228.

94. Kawakami K. 2011. Dynamics of ribavirin glass in the sub T_g temperature region. J Phys Chem B 115: 11375-11381.

95. Miura H, Kanebako M, Shirai H, Nakao H, Inagi T, Terada K. 2011. Stability of amorphous drug 2-benzyl-5-(4-chlorophenyl)-6-[4-(methylthio)phenyl]-2H-pyridazin-3-one, in silica mesopores and measurements of its molecular mobility by solid-state 13C NMR spectroscopy. Int J Pharm 410: 61-67.

96. Schamme B, Couvrat N, Malpeli P, Delbreilh L, Dupray V, Dargent E, Coquerel G. 2015. Crystallization kinetics and molecular mobility of an amorphous active pharmaceutical ingredient: A case study with biclotymol. Int J Pharm 490: 248-257.

97. Urbanova M, Sturcova A, Kredatusova J, Brus J. 2015. Structural insight into the physical stability of amorphous simvastatin dispersed pHPMA: Enhanced dynamics and local clustering as evidenced by solid-state NMR and raman spectroscopy. Int J Pharm 478: 464-475.

98. Bhardwaj S, Suryanarayanan R. 2012. Use of dielectric spectroscopy to monitor molecular mobility in glassy and supercooled trahalose. J Phys Chem 116: 11728-11736.

99. Knapik J, Wojnarowska Z, Grzybowska K, Hawelek L, Sawicki W, Wlodarski K, Markowski J, Paluch M. 2014. Physical stability of the amorphous anticholesterol agent (Ezetimibe): The role of molecular mobility. Mol Pharm 11: 4280-4290.

100. Mistry P, Mohapatra S, Gopinath T, Vogt F, Suryanarayanan R. 2015. Role of the strength of drug polymer interactions on the molecular mobility and crystallization inhibition in ketoconazole solid dispersion. Mol Pharm. DOI: 10.1021/acs.molpharmaceut.5b00333.

101. Kothari K, Ragoonanan V, Suryanarayanan R. 2015. The role of polymer concentration on the molecular mobility and physical stability of nifedipine solid dispersions. Mol Pharm 12: 1477-1484.

102. Robertis S, Bonferoni M, Elviri L, Sandri G, Caramella C, Bettini R. 2015. Advances in oral controlled drug delivery: the role of drug-polymer and interpolymer non-covalent interactions. Expert Opin Drug Deliv 12: 441-453.

103. Broman E, Khoo C, Taylor L. 2001. A comparison of alternative polymer excipients and processing methods for making solid dispersion of poorly water soluble drug. Int J Pharm 222: 139-151.

104. Knopp M, Olesen N, Holm P, Langguth P, Holm R, Rades T. 2015. Influence of polymer molecular weight on drug-polymer solubility: A comparison between experimentally determined solubility in PVP and prediction derived from solubility in monomer. J pharm Sci (In press). DOI: 10.1002/JPS.24410

105. Higashi K, Hayashi H, Yamamoto K, Moribe K. 2015. The effect of drug and EUDRAGIT® S 100 miscibility in solid dispersion on the drug and polymer dissolution rate. Int J Pharm 494: 9-16.

106. Van Krevelen, Nijenhuis K. 2009. Properties of polymers: Their correlation with chemical structures, their numerical estimations and prediction from additive group contribution method. Chapter 7. Fourth Edition. Elsevier; Amsterdam.

107. Liu J, Cao F, Zhang C, Ping Q. 2013. Use of polymer combinations in the preparation of solid dispersions of a thermally unstable drug by hot-melt extrusion. Acta Phar Sin B 3: 263-272.

108. van Krevelen, Nijenhuis K. 2009. Properties of polymers: Their correlation with chemical structures, their numerical estimations and prediction from additive group contribution method. Chapter 7. Fourth Edition. Elsevier; Amsterdam.

109. Taylor L, Li T, Marsac P. 2009. Estimation of drug-polymer miscibility and solubility in amorphous solid dispersions using experimentally determined interaction parameters. Pharm Res 26: 139-151.

110. Parikh T, Gupta S, Meena A, Vitez I, Mahajan N, Serajuddin A. 2015. Application of film-casting technique to investigate drug-polymer miscibility in solid dispersion and hot-melt extrudates. J Pharm Sci 104: 2142-2152

111. Zhao Y, Inbar P, Chokshi H, Malick W, Choi D. 2011. Prediction of the thermal phase diagram of amorphous solid dispersion by Flory-Huggins theory. J Pharm Sci 100: 3196-3207.

112. Verma S, Rudraraju V. 2014. A systematic approach to design and prepare solid dispersionsof poorly water-soluble drug. AAPS PharmSciTech 15: 641-657.

113. Liu J, Cao F, Zhang C, Ping Q. 2013. Use of polymer combinations in the preparation of solid dispersions of a thermally unstable drug by hot-melt extrusion. Acta Phar Sin B 3: 263-272.

114. Tian Y, Booth J, Meehan E, Jones D, Li S, Andrews G. 2012. Construction of drug-polymer thermodynamic phase diagrams using flory-huggins interaction theory: Identifying the relevance of temperature and drug weight fraction to phase separation within solid dispersion. Mol Pharm 10: 236-248.

115. Taylor L, Li T, Marsac P. 2009. Estimation of drug-polymer miscibility and solubility in amorphous solid dispersions using experimentally determined interaction parameters. Pharm Res 26: 139-151.

116. Amharar Y, Curtin V, Gallagher K, Healy A. 2014. Solubility of crystalline organic compounds in high and low molecular weight amorphous matrices above and below the glass transition by zero enthalpy extrapolation. Int J Pharm 472: 241-247.

117. Ahmad S, Johnston B, Mackay S, Schtzlein A, Gellert P, Sengupta D, Uchegbu I. 2010. *In silico* modelling of drug-polymer interactions for pharmaceutical formulations. J R Soc Interface 7: S423-S433

118. Ouyang D. 2012. Investigating the molecular structure of solid dispersions by the simulated annealing method. Chem Phys Lett 554: 177-184.

119. Persson L, Porter C, Charman W, Bergstrom C. 2013. Computational prediction of drug solubility in lipid based formulation excipients. Pharm Res 30: 3225-3237.

120. Gupta J, Nunes C, Vyas S, Jonnalagadda S. 2011. Prediction of solubility parameters and miscibility of pharmaceutical compounds by molecular dynamics simulations. J Phys Chem B 115: 2014-2023.

121. Maniruzzaman M, Morgan D, Mendham A, Pang J, Snowden M, Douroumis D. 2013. Drug-polymer intermolecular interactions in hot-melt extruded solid dispersions. Int J Pharm 443: 199-208.

122. Svajani k, Gajjar A, Savjani J. 2012. Drug Solubility: Importance and Enhancement Techniques. ISRN Pharm 2012: 1-10.

123. Yoo S, Krill S, Wang Z, Telang C. 2009. Miscibility/stability considerations in binary solid dispersion system composed of functional excipients towards the design of multi-component amorphous system. J Pharm Sci 98: 4711-4723.

124. Wanare R. 2013. Enhancement of dissolution rate of poorly water soluble drug by solid dispersion technique. Res J Pharm Biol Chem 4: 686-707.

125. Nabarawi M, Miligi M, Khalil I. 2012. Optimization of class II BCS drug using solid dispersion technique. Int J Pharm Pharm Sci. 4: 554-571.

126. Das S, Roy S, Kalimuthu Y, Khanam J, Nanda A. 2012. Solid dispersion: An approach to enhance the bioavailability of poorly water soluble drugs. Int J Pharmacol Pharm 1: 37-46.

127. Sekiguchi K, Obi N. 1961. Studies on absorption of eutectic mixture. I. A comparison of the behavior of eutectic mixture of sulfathiazole and that of ordinary sulfathiazole in man. Chem Pharm Bull 9: 866-872.

128. Ghebremeskel N, Vemavarpu C, Lodaya M. 2006. Use of surfactant as plasticizers in preparing solid dispersions of poorly soluble API: stability testing of selected solid dispersions. Pharm Res 23: 1928-1936.

129. Munjal M, Stodghill P, Elsohly A, Repka A. 2006. Polymeric systems for amorphous Delta 9-tetrhydrocannabinol produsedby a hot-melt method. Part I: chemical and thermal stability during processing. J Pharm Sci 95: 2473-2485.

130. Qi S, Belton P, Nollenberger K, Clayden N, Reading M, Craig D. 2010. Characterization and prediction of phase separation in hot-melt extruded solid dispersions: A thermal, microscopic and NMR relaxometry study. Pharm Res 27: 1869-1883.

131. Save T, Venkitachalam P. 1992. Studies on solid dispersion of Nifedipine. Drug Dev Ind Pharm 18: 1663-1679.

132. Patil H, Tiwari R, Repka M. 2015. Hot-melt extrusion: From theory to application in pharmaceutical formulation. AAPS Pharm Sci Tech (In press). PMID: 26159653.

133. Repka M, Battu S, Upadhye S, Thumma S, Crowler M, Zhang F, Martin C, McGinity J. 2007. Pharmaceutical application of hot-melt extrusion: Part II. Drug Dev Ind Pharm 33: 1043-1057.

134. Sharma A, Jain C. 2011. Solid dispersion: A promising technique to enhance solubility of poorly water soluble drug. Int J Drug Deliv 3: 149-179.

135. Serajuddin A. 1999. Solid dispersion of poorly water-soluble drugs: Early promises, subsequent problems and recent breakthroughs. J Pharm Sci 88: 1058-1066.

136. Vehring R. 2008. Pharmaceutical particle engineering via spray drying. Pharm Res 25: 999-1022.

137. Paudal A, Worku Z, Meeus J, Guns S, Mooter G. 2013. Manufacturing of solid dispersion of poorly water soluble drugs by spray drying: Formulation and process consideration. Int J Pharm 453: 253-284.

138. Araujo R, Teixeira C, Freitas L. 2010. The preparation of ternary solid dispersions of an herbal drug via spray drying of liquid feed. Dry Tech 28: 412-421.

139. Corrigan O. 1995. Thermal analysis of spray dried products. Thermochim Acta 248: 245-258.

140. Mahlin D, Ponnambalam S, Heidarian H, Bergstrom M. 2011. Towards in silico prediction of glass-forming ability from molecular structure alone: A screening tool in early drug development. Mol Pharm 8: 498-506.

141. Baird A, Santiago Q, Rinaldi C, Taylor S. 2012. Role of viscosity in influencing the glass forming ability of organic molecules from the undercooled melt state. Pharm Res 1: 271-284.

142. Solluhub K, Cal K. 2010. Spray drying technique. II. Current application in pharmaceutical technology. J Pharm Sci 99: 587-597.

143. Srinarong P, de Waard H, Frijlink W, Hinrichs L. 2011. Improved dissolution behaviour of lipophilic drugs by solid dispersions: the production process as starting point for formulation considerations. Expert Opin Drug Deliv 8: 1020.

144. Thakkar F, Soni T, Gohel M, Gandhi T. 2009. Supercritical fluid technology: A promising approach to enhance the drug solubility. J Pharm Sci Res 1: 1-14.

145. Sunkara G, Kompella U. 2002. Drug delivery application of supercriticalfluid technology. Drug Deliv Tech. 58: 615-619.

146. Subramaniam B, Rajewski A, Snavely K. 1997. Pharmaceutical processing with supercritical carbon dioxide. J Pharm Sci 86: 885-890.

147. Wu K, Li J, Wang W, Winstead D. 2009. Formation and characterization of solid dispersions of piroxicam and polyvinylpyrrolidone using spray drying and precipitation with compressed antisolvent. J Pharm Sci 98: 2422-2431.

148. Jun S, Kim M, Jo G, Lee S, Woo J, Park J, Hwang S. 2005. Cefuroxime axetil solid dispersions prepared using solution enhanced dispersion by supercritical fluids. J Pharm Pharmacol 57: 1529-1537.

149. Kim M, Jin S, Kim J, Park H, Song H, Neubert R, Hwang S. 2008. Preparation, characterization and *in vivo* evaluation of amorphous atorvastatin calcium nanoparticles using supercritical antisolvent (SAS) process. Eur J Pharm Biopharm 69: 454-465.

150. Corrigan O, Crean A. 2002. Comparative physicochemical properties of hydrocortisone-PVP composites prepared using supercritical carbon dioxide by the GAS anti-solvent recrystallization process, by coprecipitation and spray drying. Int J Pharm 245:75-82.

151. Lee S, Nam K, Kim M, Jun S, Park J, Woo J, Hwang S. 2005. Preparation and characterization of solid dispersion of Itraconazole by using aerosol solvent extraction system for improvement in drug solubility and bioavailability. Archiv Pharmacal Res 2: 866-874.

152. Engers D, Teng J, Jimenez J, Gent P, Hossack S, Campbell C, Thomson J, Ivanisevic I, Templeton A, Byrn S, Newman A. 2010. A solid-state approach to enable early development compounds: selection and animal bioavailability studies of an itraconazole amorphous solid dispersion. J Pharm Sci 99: 3901-3922.

153. Moes J, Koolen S, Huitema A, Schellen J, Beijnan J, Nuijen B. 2013. Development of an oral solid dispersion formulation for use in low-dose metronomics chemotherapy of paclitaxel. Eur J Pharm Biopharm 83: 87-94.

154. Zhao Y, Xin T, Ye T, Yang X Pan W. 2014. Solid dispersion in the development of a nimodipine delayed release tablet formulation. Asian J Pharm Sci 9: 35-41.

155. Al-Obaidi H, Lawrence M, Al-Saden N, Ke P. 2013. Investigation of griseofulvin and hydroxypropylmethyl cellulose acetate succinate miscibility in ball milled solid dispersions. Int J Pharm Sci 443: 95-102.

156. Chauhan A, Chauhan P. 2014. Powder XRD technique and its application in science and technology. Anal Bioanal Tech 5: 1-5.

157. Zhu Q, Toth S, Simpson G, Hsu H, Taylor L, Harris M. 2013. Crystallization and dissolution behaviour of naproxen/polyethylene glycol solid dispersions. J Phys Chem 117: 1494-1500.

158. Botker J, Karmwar P, Strachan C, Cornett C, Tian F, Zujovic Z, Rantanen J, Rades T. 2011. Assessment of crystalline disorder in cryo-milled samples of indomethacin using atomic pair-wise distribution functions. Int J Pharm 417: 112-119.

159. Nolenberger K, Gryczke A, Meier C, Dressman J, Schmidt M, Bruhne S. 2009. Pair distribution function X-Ray analysis explains dissolution characteristics of Felodipine melt extrusion products. Pharm tech 98: 1476-86.

160. Baird J, Taylor L. 2012. Evaluation of amorphous solid dispersion properties using thermal analysis techniques. Adv Drug Deliver Rev 64: 396-421.

161. Mahajan D, Raut D, Sakharkar D, Bodke P. 2011. Determination of traces of amorphpuscarvidilol content in carvidilol drug substance and drug product using modulated differential scanning Calorimetry. Der Pharm Lett 3: Pp. 1-12.

162. Ford J, Mann T. 2012. Fast-scan DSC and its role in pharmaceutical physical form characterization and selection. Adv Drug Deliver Rev 64: 422-430.

163. Jones D, Tian Y, Abu-Diak O, Andrews G. 2012. Pharmaceutical applications of dynamic mechanical thermal analysis. Adv Drug Deliver Rev 64: 440-448.

164. Zhang J, Bunker M, Chen X, Parker A, Patel N, Roberts C. 2009. Nanoscale thermal analysis of pharmaceutical solid dispersions. Int J Pharm 380: 170-173.

165. Foster A, Hempenstall J, Rades T. 2001. Characterization of glass solution of poorly water soluble drugs by melt extrusion with hydrophilic amorphous polymers. J Pharm Pharmacol 53: 303-315.

166. Ewing A, Clarke G, Kazarian S. 2014. Stability of indomethacine with relevance to the release from amorphous solid dispersions studied with ATR-FTIR spectroscopic imaging. Eur J Pharm Sci 60: 64-71.

167. Loh G, Tan Y, Peh K. 2014. Hydrophlic polymer solubilization on norfloxacin solubility in preparation of solid dispersion. Powder Technol 256: 462-469.

168. Ayenew Z, Paudel A, Mooter G. 2012. Can compression induce demixing in amorphous solid dispersion? A case study of naproxen-PVP K25. Eur J Pharm Biopharm 81: 207-213.

169. Bugay D. 2001. Characterization of the solid state: spectroscopic techniques. Adv Drug Deliv Rev 48: 43-65.

170. Furuyana N Hasegawa S, Hamaura T, Yada S, Nakagami H, Yonemochi E, Terada K. 2008. Evaluation of solid dispersions on a molecular level by the raman mapping technique. Int J Pharm 361: 12-18.

171. Sinclair W, Leane M, Clarke G, Dennis A, Tobyn M, Timmins P. 2011. Physical stability and recrystallization kinetics of amorphous ibipinabant drug product by fourier transform raman spectroscopy. J Pharm Sci 100: 4687-4699.

172. Kanaujia P, Lau G, Widjaja E, Schreyer M, Hanefeld A, Fischbach M, Saal C, Maio M, Tan R. 2011. Investigating the effect of moisture protection on solid-state stability and dissolution of fenofibrate and ketoconazole solid dispersions using PXRD, HSDSC and Raman microscopy. Drug Dev Ind Pharm 37: 1026-1035.

173. Crowley K ,Zografi G. 2002. Water vapour absorption into amorphous hydrophobic drug/poly(vinylpyrrolidone) dispersions. J Pharm Sci 91: 2150-2165.

174. Puncochova K, Heng J, Beranek J, Stepanek F. 2014. Investigation of drug-polymer interaction in solid dispersions by vapour sorption methods. Int J Pharm 469: 159-167.

175. Ticehurst M, Basford P, Dallman C, Lukas T, Marshall P, Nicholas G, Smith D. 2000. Characterization of the influence of micronization on the crystallinity and physical stability of revatropate hydrobromide. Int J Pharm 193: 247-259.

176. Enose A, Dasan P, Sivaramakrishnan H, Shah S. 2014. Formulation and characterization of solid dispersion prepared by hot melt mixing: A fast screening approach for polymer selection. J Pharm 2014: 1-13.

177. Lane R, Buckton G. 2000. The novel combination of dynamic vapour sorption gravimetric analysis and near infra-red spectroscopy as a hyphenated technique. Int J Pharm 207: 49-56.

178. Paudel A, Geppi M, Mooter G. 2014. Structural and dynamic properties of amorphous solid dispersions: The role of solid-state nuclear magnetic resonance spectroscopy and relaxometry. J Pharm Sci.103: 2635-2662.

179. Yuan X, Sperger D, Munson E. 2014. Investigating miscibility and molecular mobility of nifedipine-PVP amorphous solid dispersions using solid-ststе NMR spectroscopy. Mol Pharm 11: 329-337.

180. Litvinov V, Guns S, Adriaensens P, Scholtens B, Quaedflieg M, Carleer R, Mooter V. 2012. Solid state solubility of miconazole in poly[(ethylene glycol)-g-vinylalcohol] using hot-melt extrusion. Mol Pharm. 9: 2294-32.

181. Ito A, Watanabe T, Yada S, Hamaura T, Nakagami H, Higashi K, Moribe K, Yamamoto K. 2010. Prediction of recrystallization behaviour of troglitazone/Polyvinylpyrrolidone solid dispersion by solid-state NMR. Int J Pharm 383: 18-23.

182. Dahlberg C, Fureby A, Schuleit M, Furo I. 2010. Relationships between solid dispersion preparation process, particle size and drug release – An NMR and NMR micro imaging study. Eur J Pharm Biopharm 76: 311-319.

183. Ho R, Y Jery. 2013. A review of inverse gas chromatography and its development as a tool to characterize anisotropic surface properties of pharmaceutical solids. KONA Powder Part J 30: 164-180.

184. Buckton G, Gill H. 2007. The importance of surface energetics of powders for drug delivery and the establishment of inverse gas chromatography. Adv Drug Deliv Rev59: 1474-1479.

185. Sun Y, Zhu L, Wu T, Cai T, Gunn E, Yu L. 2012. Stability of amorphous pharmaceutical solids: crystal growth mechanisms and effect of polymer additives. The AAPS Journal 14: 380-388.

186. Hasegawa S, Ke P, Buckton G. 2009. Determination of the structural relaxation at the surface of amorphous solid dispersion using inverse gas chromatography. J Pharm Sci 98: 2133-2139.

187. Miyanishi H Nemoto T, Mizuno M, Mimura H, Kitamura S, Iwao Y, Noguchi S, Itai S. 2013. Evaluation of crystallization behaviour on the surface of nifedipine solid dispersion powder using inverse gas chromatography. Pharm Res 30: 502-511.

188. Qian F, Wang J, Hartley R, Tao J, Haddadin R, Mathias N, Hussain M. 2012. Solution behaviour of PVP-PA and HPMC-AS based amorphous solid dispersion and their bioavailability implications. Pharm Res 29: 2765-2776.

189. Yan H, Chris H. 2015. Amorphous solid dispersions: Utilization and challenges in drug discovery and development. J Pharm Sci 104: 3237-3258.

190. Raina S, Alonzo D, Zhang G, Gao Y, Taylor L. 2014. Impact of polymers on crystallization and phase transition kinetics of amorphous nifedipine during dissolution in aqueous media. Mol Pharm 11: 3635-3576.

191. Gauzman H, Tawa M, Zhang Z, Ratanabanangkoon P, Shaw P, Gardner C, Chen H, Moreau J, Almarsson O, Remenar J. 2009. Combined use of crystalline salt forms and precipitation inhibitors to improve oral absorption of celecoxib from solid oral formulations. J Pharm Sci 26: 855-864.

192. Vora C, Patadia R, Mittal K, Mashru R. 2015. Preparation and characterization of dipyridamole solid dispersions for stabilization of supersaturation: effect of precipitation inhibitors type and molecular weight. Pharm Dev Res DOI: 10.3109/10837450.2015.1069330

193. Raghuvanshi S, Pathak K. 2014. Recent advances in delivery systems and therapeutics of cinnarizine: A poorly water soluble drug with absorption window in stomach. J Drug Del 2014: 1-15.

194. http://www.accessdata.fda.gov/drugsatfda_docs/nda/99/20884_aggrenox_prntlbl.pdf

195. www.sigmaaldrich.com

CHAPTER 2. AN INVESTIGATION INTO THE CRYSTALLIZATION TENDENCY/KINETICS OF AMORPHOUS ACTIVE PHARMACEUTICAL INGREDIESNTS

2.1. Introduction

The solid state is preferred for drug formulations due to reasons of stability and ease of handling at different stages of drug product manufacture. The majority of drugs can exist in different solid-state forms such as amorphous or crystalline (hydrates, solvates and polymorphs) or both.[1] The amorphous form has the advantage of a higher apparent aqueous solubility compared to its crystalline counterpart.[2] However, inherently lower physical and chemical stability poses challenges in view of product performance and efficacy.[3] Phase transitions such as conversion of amorphous to crystalline forms are thermodynamically and kinetically driven by higher free energy and molecular mobility, respectively.[4] Given the increasing importance being attached to the stability of amorphous drug products during unit operations such as spray drying and melt extrusion (non-ambient conditions) or upon normal storage (where the conditions remain more or less constant), a robust crystallization prediction protocol may facilitate the prompt development of amorphous drug formulations with better life expectancy.[5]

Crystallization tendency describes the properties related to the crystallization behaviour of amorphous drugs. Different factors such as chemical structure, molecular weight, number of aromatic rings, symmetry of the structure, number of rotatable bonds, presence of intermolecular interactions, number of electronegative atoms and number of branches have been suggested to affect crystallization tendency.[6] In addition, physicochemical properties such as glass transition and melting temperature, melting and crystallization enthalpy/entropy, molecular mobility and viscosity of the supercooled and glassy states have been suggested to correlate with the crystallization tendency of amorphous compounds.[7] Fragility is a measure of deviation of these physical properties from Arrhenius behaviour and is considered to correlate with glass forming ability (GFA).[6] "Fragile" glass formers exhibit a large variation in properties such as molecular mobility, viscosity and/or heat capacity around the glass transition temperature, T_g, unlike "strong" glass formers which are better at remaining amorphous. Sufficient kinetic stabilization of fragile amorphous drugs may lead to the development of robust products with enhanced dissolution rates. Therefore, a systematic examination of the crystallization kinetics of an API is a critical part of formulation development of amorphous drug products.

Measurement of phase transitions from relaxation behaviour by perturbing equilibrium permits direct assessment of molecular mobility. However, powdered active pharmaceutical ingredients (APIs) are not always amenable to such measurements; for

example, measurement of shear viscosity or dielectric spectroscopy requires sample manipulation or long experiment times which may result in unwanted changes (either physical or chemical or both). Fortunately, conventional and modulated differential scanning calorimeter (DSC) overcomes both of these limitations. It can be used to study the effect of temperature on structural relaxation (characterized by the mean relaxation time, Γ) and its impact on the crystallization tendency/kinetics of amorphous drugs. The focus of this chapter is to investigate the role of molecular mobility on crystallization tendency and to study the isothermal and non-isothermal crystallization kinetics of dipyridamole and cinnarizine. The applicability of different solid-state crystallization kinetic models to identify the crystallization mechanism is also probed. Insights gained from molecular mobility/crystallization studies and a thorough understanding of the mechanism of amorphous to crystalline transformation are expected to provide formulation scientists with a road map towards more effective stabilization of glassy drug products.

2.2. Materials and Methods

2.2.1. Materials

Dipyridamole (DPM), cinnarizine (CNZ) and polyvinyl pyrrolidone (PVP) K30 were purchased from Sigma Aldrich (Ireland) and used as received.

2.2.2. Preparation of the amorphous drug form

Amorphous DPM and CNZ were prepared by heating the crystalline drug in a vacuum oven to a temperature 5°C above the melting point. The temperature was held at this point for 5 minutes and then quench cooled by dropping into liquid nitrogen. The thermal stability of the amorphous drugs was established by high-performance liquid chromatography and thermogravimetric analysis which indicate that no degradation occurred during the preparation of the amorphous form.

2.2.3. High Performance Liquid Chromatography (HPLC)

A reverse phase HPLC method was developed for thermal stability studies of DPM and CNZ. For DPM, analysis was performed on a Water's Symmetry® C18 column (150mm × 3.9 i.d., 5μm) at 25°C and a flow rate of 0.75 mL/min. The mobile phase consisted of 75:25 aqueous (0.1% v/v ortho-phosphoric acid):acetonitrile mixture. Detection was by UV at a wavelength of 283 nm and an injection volume of 40 μL was used. For CNZ, analysis was performed on XTerra® C18 column (250mm × 4.6 i.d., 5μm) at 25°C and a flow rate of 1 mL/min. The mobile phase consisted of 50:50 aqueous (0.1% v/v of trifluoroacetic

acid):acetonitrile mixture. Detection was by UV at a wavelength of 251 nm and an injection volume of 20 µL was used. The linearity was demonstrated in the range of 1-20 µg/mL for DPM and CNZ.

2.2.4. Preparation of the amorphous solid dispersions

Amorphous solid dispersions (ASDs) of DPM and CNZ using PVP K30 as a carrier matrix at 1:1 drug-polymer weight ratios were prepared in two steps. First, physical mixtures of drug and polymer were dissolved in a sufficient volume of methanol and the solvent was removed under reduced pressure at 40°C using a rotary evaporator followed by drying at room temperature under vacuum for 24 h. In the next step, the dried mixtures were melt quenched and the ASDs were stored at 25°C and 0% moisture.

2.2.5. Heat capacity measurements

The heat capacities of crystalline and amorphous DPM and CNZ were measured using modulated DSC (MDSC) (DSC Q2000; TA Instruments Corp., Elstree, Hersts, U.K.) in accordance with the previously published protocols.[8, 9] The modulation parameters chosen for this study, to ensure separation of reversing and non-reversing events, were $\pm$0.53 °C/40s at 5°C/min for both drugs. The instrument was calibrated for enthalpy, temperature and heat capacity using indium and sapphire standards as recommended by the instrument supplier.

2.2.6. Relaxation time, isothermal and non-isothermal crystallization studies

The relaxation and crystallization studies were performed using a differential scanning calorimeter equipped with an electrical cooling accessory. The temperature and heat flow calibration was carried out using a high-purity indium standard. Nitrogen was used as the purge gas at a flow rate of 50 mL/min. Five linear heating rates, 1, 2, 5, 10, and 20 °C/min from 0 to 200 °C were used. Isothermal crystallization kinetics studies were carried out by equilibrating the amorphous drugs from 313 K to specified temperatures at 350.5, 353 355.5, 358 and 360.5 °C for DPM and 325.5, 328, 330.5, 333 and 335.5 °C for CNZ to measure the heat released during crystallization over time. All measurements (in triplicate) were performed by crimping 5-10 mg of samples into hermetically sealed aluminium pans with pin-holes. Data analysis was done using Universal Analysis Software 2000 (TA Instruments Corp., Elstree, Hersts, U.K.). Sigmoidal baseline integration was used for measuring extent of crystallization (α).

2.2.7. X-ray diffraction analysis

The powdered amorphous solid dispersions were analysed using X-ray diffractometer (X'pert MPD PRO PANalytical, Almelo, Netherlands) using the following parameters: Cu radiation (wavelength 1.540598 Å) , Ni-filter, voltage 40 kV, current 40 mA, 2θ range of 5-50°C, step size 0.008° and scan rate 3.2°/min.

2.3. Results and Discussion

2.3.1. Measure of fragility and relaxation time

Fragility is an important concept to quantify the characteristics of amorphous drugs by measuring the magnitude of deviation from Arrhenius behaviour for supercooled liquids and glasses.[10] Even though fragility studies may not provide detailed information about behaviour of pharmaceutical glasses, it may be correlated with other important properties such as crystallization tendency. Different methods are described in the literature to measure fragility; however, the values sometimes do not agree with each other.[11, 12] "Thermodynamic" fragility (m_T) is a very simple concept and can be measured using the following equation:[13]

$$m_T = \frac{\Delta C_p^{conf}}{\Delta C_p} \qquad \ldots\ldots\ldots \qquad (2.1)$$

where ΔC_p^{conf} is the difference in heat capacity between the supercooled liquid and the crystal form (known as configurational heat capacity) and ΔC_p is the heat capacity change at T_g. A sudden rise in the heat capacity at T_g is an indication of increased molecular mobility which provides additional degrees of freedom and increases the recrystallization tendency. The heat capacities just above T_g of DPM for the crystalline and glassy states were found to be 0.26 and 0.67 $Jg^{-1}K^{-1}$, respectively, and for CNZ crystalline and glassy state, the values were 0.21 and 0.67 $Jg^{-1}K^{-1}$, respectively (Figure 2.1 and 2.2). The thermodynamic fragility (m_T) of DPM and CNZ were determined using Eq. 2.1 and found to be 1.09 and 1.14, respectively, which indicates the fragile nature (< 1.5) of these compounds.[6, 10]

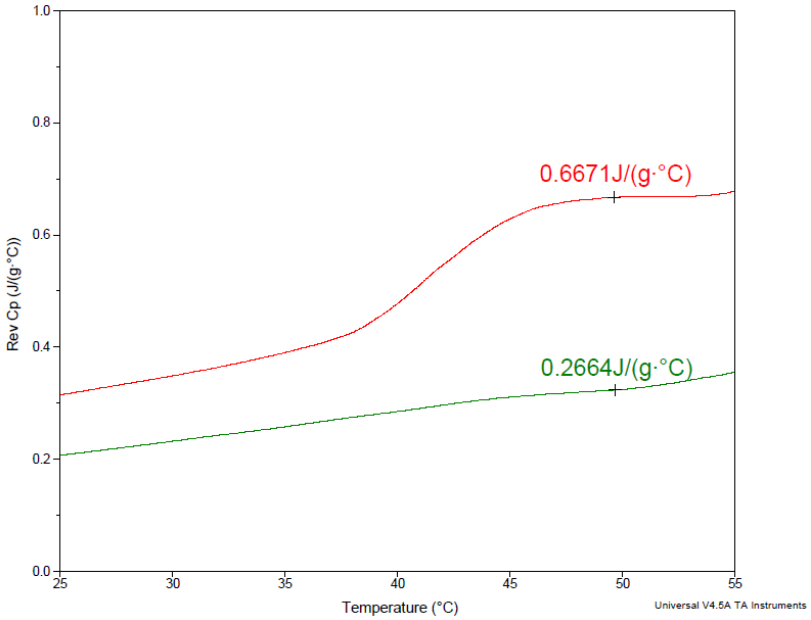

Figure 2.1. Reversing heat capacity of glassy (red) and crystalline (green) dipyridamole obtained by MDSC using ±0. 53 °C /40s as modulation parameter at a heating rate of 5 °C /min

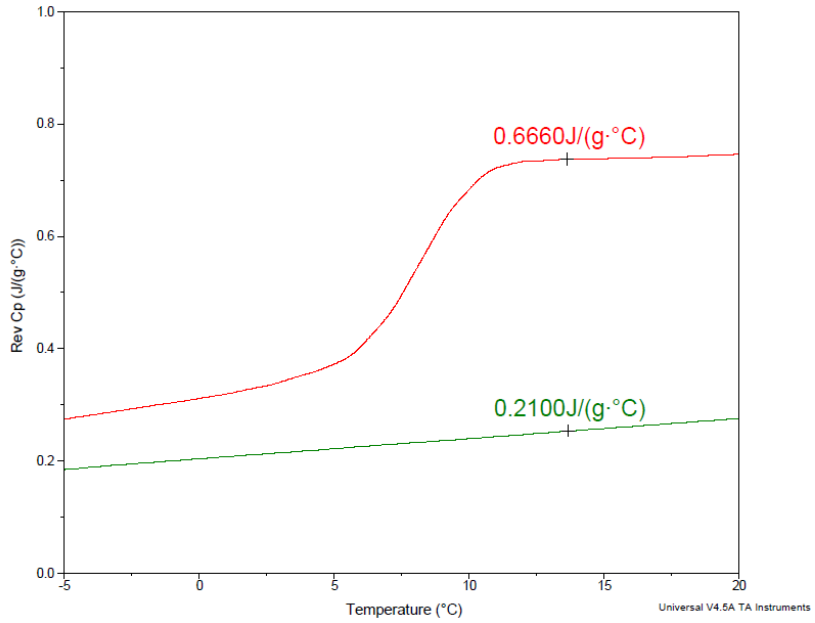

Figure 2.2. Reversing heat capacity of glassy (red) and crystalline (green) cinnarizine obtained by MDSC using ±0. 53 °C /40s as modulation parameter at a heating rate of 5 °C/min

Two different methods are employed to evaluate and compare "dynamic" fragility.[14] The first method is based on extrapolation of configurational entropy (S_c) to zero, of which the temperature dependence is described as:

$$S_c = \int_{T_K}^{T} \left(\frac{C_p^{conf}(T)}{T} \right) dT \qquad \ldots\ldots\ldots \qquad (2.2)$$

where C_p^{conf}, T_K and T are the configurational heat capacity, Kuazmann temperature and absolute temperature, respectively. Using configurational heat capacity at T_g, integration of Eq. 2.2 up to the melting temperature (T_m) gives:[15]

$$\frac{1}{T_K} = \frac{1}{T_m}\left(1 + \frac{\Delta H_m}{C_p^{conf}(T_g)T_g}\right) \qquad \ldots\ldots\ldots \qquad (2.3)$$

where ΔH_m is the melting enthalpy. Eq. 2.3 is based on the assumption that $TC_p^{conf}(T)$ is constant. The melting temperature and enthalpy for DPM were determined to be 168.08±0.03 °C and 29.06±0.29 kJ mol^{-1}, respectively, and for CNZ the values were 121.21±0.02 °C and 38.33±1.03 kJ mol^{-1}, respectively (Figure 2.3 and 2.4, respectively). Thus, T_k for DPM and CNZ was calculated as -20.15 and -55.15 °C, respectively, using Eq. 2.3.

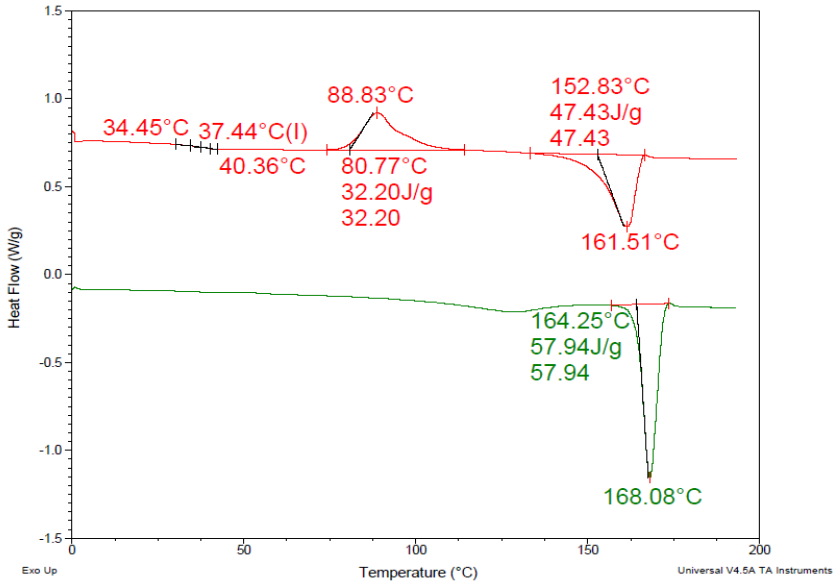

Figure 2.3. MDSC thermograms of glassy (red) and crystalline (green) dipyridamole at a heating rate of 5 °C/min

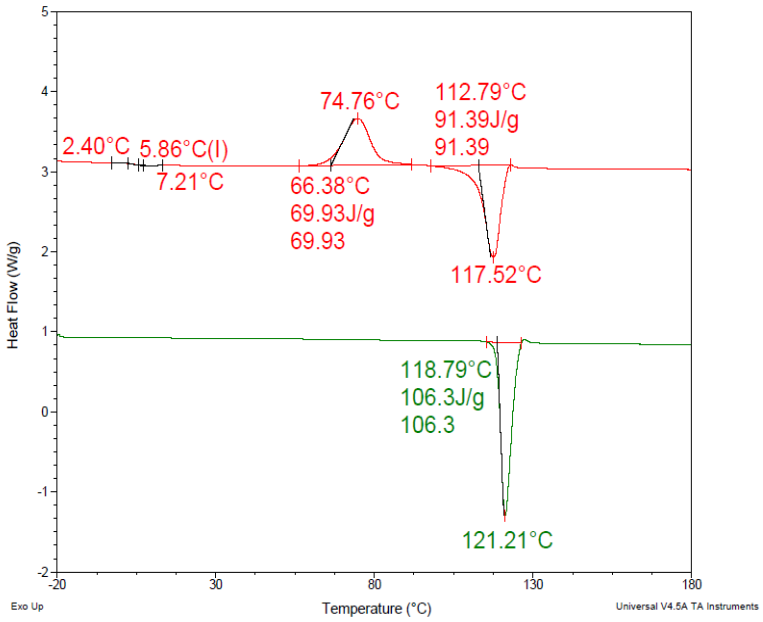

Figure 2.4. MDSC thermograms of glassy (red) and crystalline (green) cinnarizine at a heating rate of 5 °C/min

The Vogel-Tammann-Fulcher equation can be used to calculate the strength parameter, D, as shown below:[16]

$$\Gamma = \Gamma_o \exp\left(\frac{DT_o}{T-T_o}\right) \quad \ldots\ldots\ldots \quad (2.4)$$

where Γ_o is the vibrational lifetime which is approximately 10^{-14} s and T_o is a Vogel temperature which is a constant.[17] This method is based on the assumption that T_K and T_o have approximately the same value and also the value of Γ at T_g is approximately 100 s.[18] The strength parameter, D, can be calculated using Eq. 2.4 and was found to be 8.94 and 10.76 for DPM and CNZ, respectively. The strength parameter D describes the deviation from the Arrhenius behaviour with strong glass formers having D > 30 and fragile systems features D < 10.[19] Crowley and Zografi have reported that several pharmaceutical amorphous drugs have D value in the range of 7-15 suggesting moderately fragile behaviour.[14] The fragility parameter $(m_{D_{CE}})$ was calculated as 81.94 and 70.75 for DPM and CNZ, respectively, using the following equation:[16]

$$m_{D_{CE}} = \frac{D(T_o/T_g)}{\ln 10\,(1-T_o/T_g)^2} \quad \ldots\ldots\ldots \quad (2.5)$$

In general, amorphous systems having m < 40 exhibits strong glass forming ability (GFA) whereas materials having m > 75 are considered as fragile systems.[20, 21]

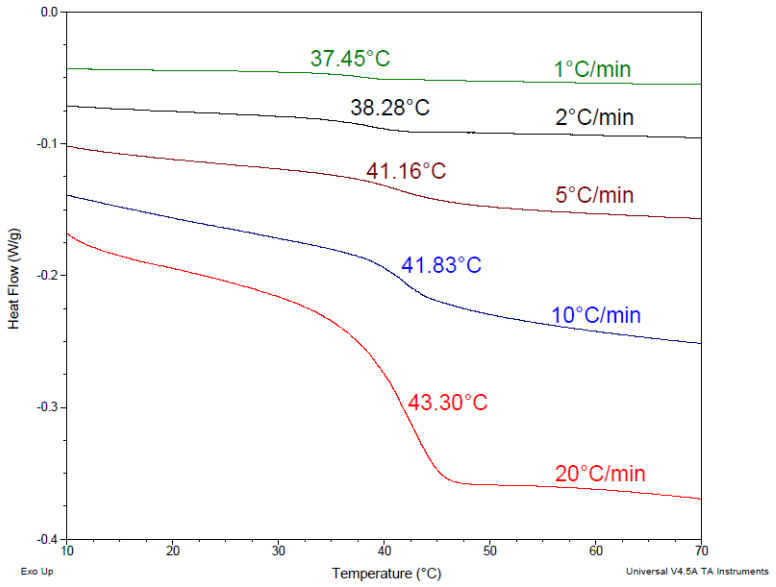

Figure 2.5. Ramp rate dependency of glass transition temperature of dipyridamole (n=3); single thermograms at each heating rate is shown for clarity

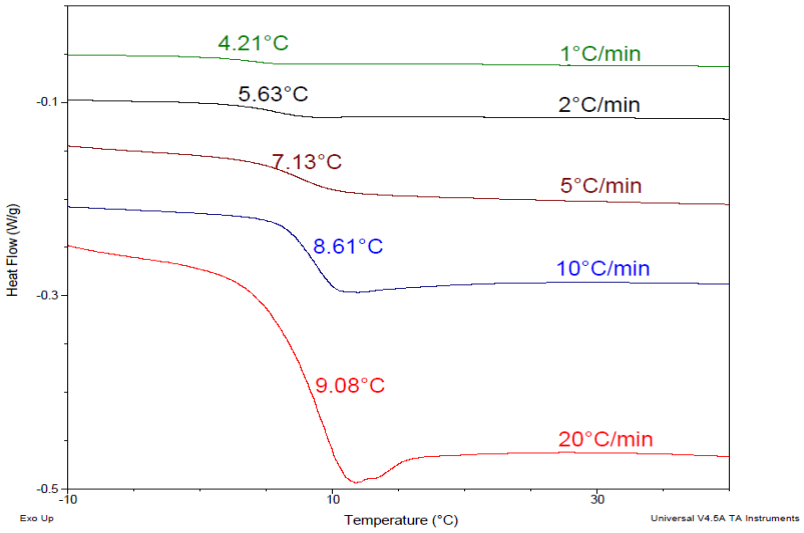

Figure 2.6. Ramp rate dependency of glass transition temperature of cinnarizine (n=3); single thermograms at each heating rate is shown for clarity

The second method is based on the dependence of T_g on the heating rate, β, in the DSC measurements as shown in Figure 2.5, 2.6, and 2.7. Using this method, D and *m* values were calculated using the following equations:[14]

$$m_{D_{Tg}} = \frac{d\,log\,\Gamma}{d(T_g/T)}\bigg|_{T=Tg} = \frac{1}{\ln 10}\frac{\Delta E_{T_g}}{RT_g} \qquad \ldots\ldots\ldots \qquad (2.6)$$

$$-\frac{\Delta E_{T_g}}{R} = \frac{d(\ln \beta)}{d(1/T_g)} \qquad \ldots\ldots\ldots \qquad (2.7)$$

$$D = 2.303(m_{min}^2)/(m - m_{min}) \quad \ldots\ldots\ldots \quad (2.8)$$

$$m_{min} = \log\left(\frac{\Gamma_{T_g}}{\Gamma_o}\right) = \log\left(\frac{100}{10^{-14}}\right) = 16 \quad \ldots\ldots\ldots \quad (2.9)$$

$$T_o = T_g\left(1 - \frac{m_{min}}{m}\right) \quad \ldots\ldots\ldots \quad (2.10)$$

D and *m* for freshly prepared DPM glass were determined to be 11.91 and 65.51, and for CNZ glass, values were 10.78 and 70.67, respectively (Table 2.1), which indicates their fragile nature. The glass transition activation energy (ΔE_{T_g}) for DPM and CNZ were found to be 394 and 381 kJ mol^{-1}, respectively, calculated using Eq. 2.7. Similar values has been reported for other fragile pharmaceutical glass formers such as indomethacin (ΔE_{T_g}= 464 kJ mol^{-1}).[14]

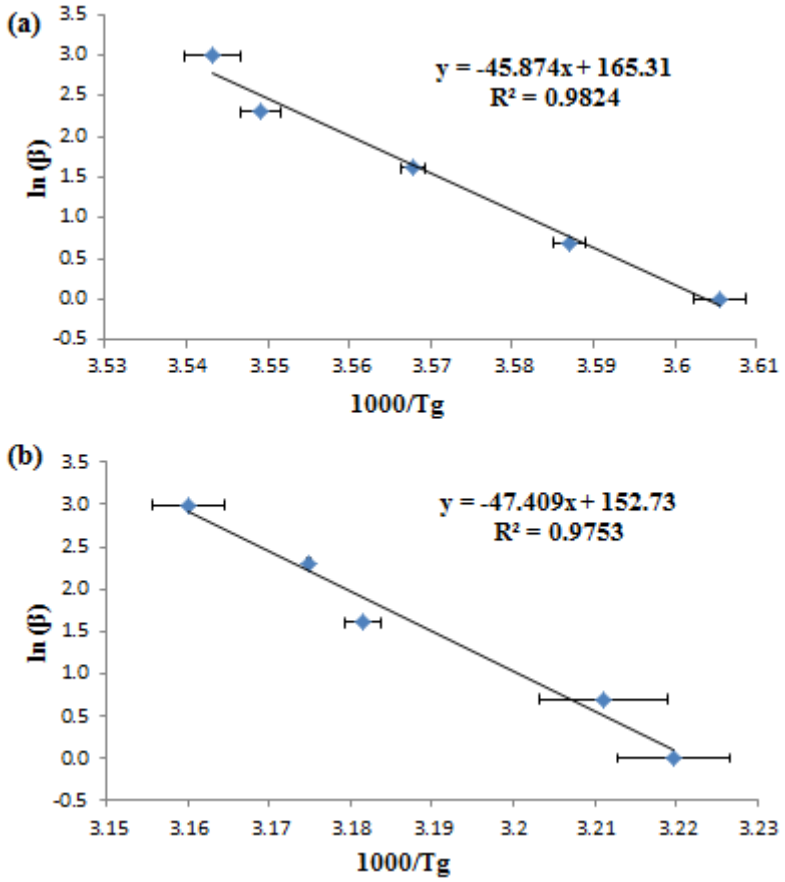

Figure 2.7. Plots of ln (β) vs. reciprocal of glass transition temperature (T_g) of amorphous dipyridamole (a) and amorphous cinnarizine (b) (n=3) to calculate the structural relaxation activation energy at the glass transition

Table 2.1. Fragility (m), strength parameter (D) and mean relaxation time (Γ) of the model drugs

		Configurational Entropy method			Heating rate method			
	m_T	$m_{D_{CE}}$	D	T_K(K)	$m_{D_{Tg}}$	D	T_o(K)	Γ(s) (25/40°C)
DPM	1.09	81.94	8.94	253.01	65.51	11.91	237.44	729/114
CNZ	1.14	70.75	10.76	218.03	70.67	10.78	217.98	13/3

Although D and m values are different for both the model drugs obtained by heating rate method as compared to those obtained by using extrapolation of configurational entropy to zero (Table 2.1), this extent of deviation has frequently been reported in literature.[10, 22] It may be attributed to the basic mathematical limitation of Eq. 2.4 which is observed when D approaches ∞, the value of *m* and m_{min} in terms of D will be more than zero in the Arrhenius limit, $T_o \rightarrow 0$, so that the product of D and T_o remains non-zero.[23] Furthermore, the configurational entropy method relies on the approximated values of Γ, Γ_o and T_o at T_g, which may not be accurate in some cases. Moreover, the discrepancy can also be partially explained by amorphous drug relaxation which decreases the T_g value if a recovery peak is found in the DSC curve. However, the effect is not very pronounced for DPM and CNZ and can be ignored. Finally, a change in cooperative rearrangement region during heating may also influence the thermodynamic and dynamic fragility.[10] The impact of these events is less significant on T_g and, therefore, it can be conclude that $m_{D_{Tg}}$ may be a better parameter to describe the fragility of the amorphous drugs. This inference is in accordance with the previously published literature on the fragility of pharmaceutical glasses.[6]

To further shed some light on the fragile behaviour of amorphous DPM and CNZ, the relaxation time of model compounds were calculated using Eq. 2.4, and the value for Angell's strength parameter, D, was obtained from the ramp rate method (second method used for the calculation of dynamic fragility). The configurational entropy method was not chosen because it was based on explicit assumption of Γ = 100 s. The heating rate dependence of the glass transition temperature, measured from DSC experiments, was fitted to Eq. 2.6 and 2.7 to plot a graph between ln (β) vs $1/T_g$. The slope of the line gives the activation energy for glass transition as shown in Figure 2.7. The value of D and T_o were calculated from Eq. 2.8 and 2.10, respectively. The resulting calculated relaxation times of amorphous DPM and CNZ are obtained using Eq. 2.4 and are summarized in Table 2.1.

The amorphous form is a non-equilibrium state which has a tendency to convert back to the more stable crystalline form. The process of approaching equilibrium is termed as structural relaxation, and the time over which relaxation occurs is known as the relaxation time.[24] It has been suggested that high molecular mobility can lead to a shorter relaxation time and higher crystallization tendency in amorphous compounds.[25] It can be seen that CNZ showed a relatively shorter relaxation time (13 s) as compared to DPM (729 s) indicating that CNZ may have higher molecular mobility and hence less physically stable. Similar results have been found for other fragile glass formers such as carbamazepine (1780 s), fenofibrate (0.4 s) and felodipine (2470 s).[26] Moreover, the results also show that mean relaxation time for both the drugs were decreased 6-7 folds as the temperature increases from 25 to 40 °C. This indicates that the amorphous DPM and CNZ are more susceptible to crystallization at higher temperature which may occur during accelerated stability studies and lead to significant change in dissolution profile.

Fragility and relaxation time studies have confirmed the fragile behaviour of the model drugs. CNZ, in particular, is found to be more fragile compared to DPM. However, fragility is a measure of change in viscosity in glass transition region and it does not tell anything about the ease with which material undergo crystallization.

2.3.2. Glass forming ability of model drugs

To further extend the discussion on crystallization tendency of glass materials, the glass forming ability (GFA) of model amorphous drugs was estimated. GFA is defined as the relative ability of materials to form an amorphous or glassy state upon super-cooling of the molten material.[27] Different numerical descriptors have been proposed for the estimation of the GFA of a material. One such parameter is the ratio of glass transition temperature (T_g) to melting temperature (T_m).[28] Assuming that viscosity remains unchanged at T_g, materials with higher T_g/T_m would be expected to be more viscous between melting and glass transition events, and consequently be more resistant to crystallization. DPM and CNZ exhibited a T_g/T_m of 0.71 and 0.72, respectively, and are expected to be fragile glass former like other fragile molecules such as acetaminophen (0.67) as compared to strong glass former such as quinapril HCl (0.91).[20, 29] Tobyn *et al.*, utilised a slightly different method to predict the fragility of amorphous drugs.[30] According to this method, materials having T_m/T_g value <1.5 signifies fragile behaviour whereas value >1.5 reflects strong GFA. DPM (1.40) and CNZ (1.39) both represent a borderline case. Hence, as per the T_g/T_m and T_m/T_g rule, DPM and CNZ show a poor GFA and are thermodynamically more inclined towards crystallization.

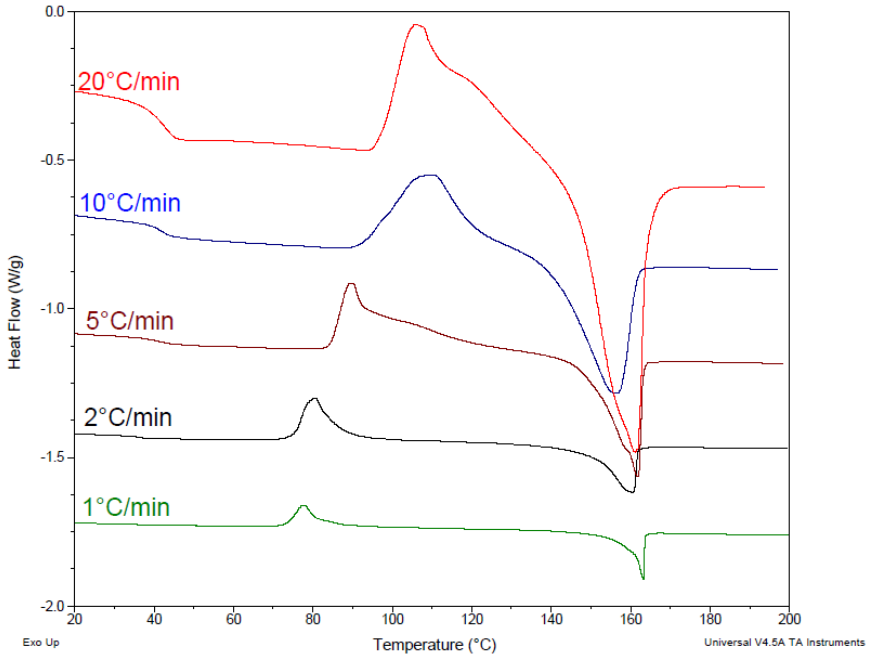

Figure 2.8. Non-isothermal DSC data for amorphous dipyridamole at five heating rates (n=3); a single thermograms at each heating rate is shown for clarity

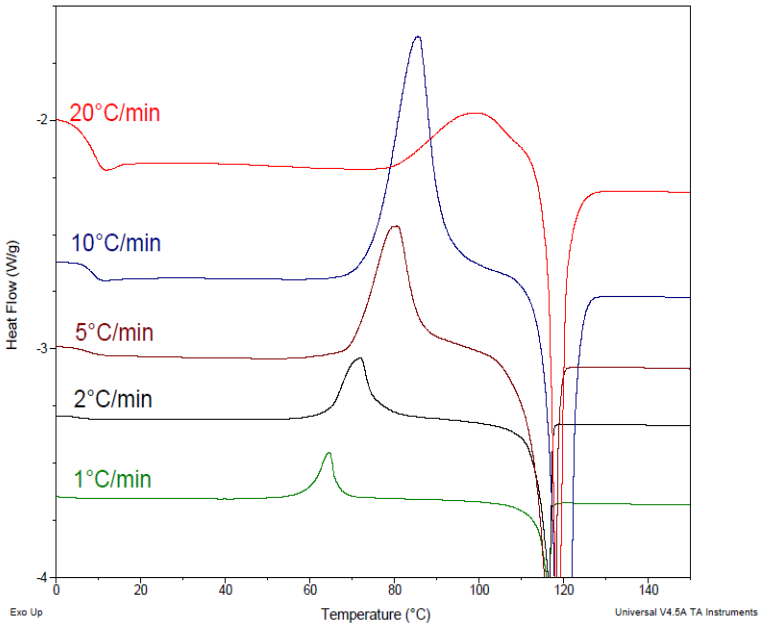

Figure 2.9. Non-isothermal DSC data for amorphous cinnarizine at five heating rates (n=3); a single thermograms at each heating rate is shown for clarity

Another frequently used method to measure GFA of amorphous drugs is based on the temperature difference between crystallization onset (T_{crys}^{Onset}) or peak (T_{crys}^{peak}) temperature and T_g. Generally, larger temperature difference between the glass transition and crystallization is an indicative of higher GFA. To describe the crystallization tendency of various

pharmaceutical glasses, a parameter called "reduced crystallization temperature", T_{red}, has been defined as shown below:[31]

$$T_{red} = \frac{T_{crys}^{onset} - T_g}{T_m - T_g} \quad \ldots\ldots\ldots \quad (2.11)$$

It is generally found that a higher T_{red} values corresponded with poor GFA or higher crystallization tendency.[32] The non-isothermal DSC data for melt-quenched amorphous DPM and CNZ at different heating rate (β) is shown in Figure 2.8 and 2.9, respectively. The values for onset/peak crystallization temperature and T_{red} are given in Table 2.2. T_{red} values were found to increase at higher heating rates which suggest that crystallization tendency for both the model drugs increases with an increase in heating rate. Moreover, at all heating rates, CNZ was found to have lower GFA as compared to DPM which is in agreement with the molecular mobility based estimation of crystallization tendency of amorphous model compounds. This shows that fragile glasses have poor GFA, which agrees with the previous observation of GFA and fragility for metallic and pharmaceutical glasses.[6, 33] Furthermore, the results for GFA are positively correlated with $m_{D_{Tg}}$where both the methods have concluded that CNZ has a higher crystallization tendency compared to DPM. This correlation can be attributed to the similar principle of measurement as both T_{red} and $m_{D_{Tg}}$are determined on the basis of a balance of thermodynamic and kinetic factors.[6] On the other hand, the thermodynamic factor is dominant for $m_{D_{CE}}$calculations where kinetic factors have no contribution. One important point to mention here is that crystallization is based on molecular structure transitions whereas glass transition is not linked with such molecular transitions. Also, the fragility and GFA predicts the crystallization tendency of the model drugs but does not tell anything about the activation energy and rate of crystallization. Therefore, a thorough examination of crystallization kinetics under isothermal and non-isothermal conditions is discussed in the next section.

Table 2.2. Non-isothermal crystallization temperature and reduced crystallization temperature (T_{red}) of amorphous dipyridamole and cinnarizine at five heating rates (Mean±SD, n=3)

β (°C/min)	T_{crys}^{Onset} (K)		T_{crys}^{peak} (K)		T_{red}	
	DPM	CNZ	DPM	CNZ	DPM	CNZ
1	347.64±0.88	331.09±1.47	353.01±0.86	335.78±1.54	0.26	0.44
2	350.39±1.51	335.30±2.34	356.06±1.87	342.37±2.52	0.28	0.48
5	359.88±2.01	342.54±0.79	364.57±1.27	351.93±1.07	0.36	0.53
10	364.88±1.44	347.74±1.13	371.17±1.30	358.02±1.81	0.40	0.59
20	369.78±0.52	356.84±1.43	377.99±1.91	370.61±0.60	0.44	0.67

β is the heating rate; T_{crys}^{Onset} is the extrapolated onset temperature for crystallization; n = 3; values represent the mean ± 1 standard deviation

2.3.3. Isothermal Crystallization Kinetics

Crystallization kinetics of amorphous drugs can be evaluated under both isothermal and non-isothermal conditions.[34] The crystallization kinetics of DPM and CNZ under isothermal conditions has been studied using Johnson-Mehl-Avrami (JMA) approach to determine the Avrami exponent 'n' which represents both the crystallization mechanism as well as the dimensionality of the crystallization process. The fraction of drug crystallized (α) can be described as a function of time (t) as shown below:[35]

$$\alpha = 1 - exp[-(Kt)^n] \quad \ldots\ldots\ldots \quad (2.12)$$

$$\ln[-\ln(1-\alpha)] = ln\,K + n\,ln\,t \quad \ldots\ldots\ldots \quad (2.13)$$

where t is the annealing time, K is the Avrami constant (or crystallization rate constant) which is dependent on the rate of nucleation and the growth rate and is assigned by Arrhenius temperature dependence as shown below:[36]

$$K = K_o exp\left(\frac{-E_a}{RT_c}\right) \quad \ldots\ldots\ldots \quad (2.14)$$

$$\ln(K) = lnK_o - \frac{E_a}{RT_c} \quad \ldots\ldots\ldots \quad (2.15)$$

where E_a is the crystallization activation energy for crystallization, K_o is the frequency factor, R is the universal gas constant and T_c is the crystallization temperature (under isothermal conditions). The isothermal crystallization exotherms of DPM and CNZ at temperatures ranging from 77.5 to 87.5 °C and 52.5 to 62.5 °C, respectively, at every 2.5 °C interval is shown in Figure 2.10 and 2.11, respectively. The fraction of amorphous drug crystallized (α)

against crystallization time during isothermal crystallization process was obtained (a typical sigmoidal shape) from the baseline integration of the crystallization peak and the value of n is obtained using Eq. 2.13 (Figures 2.12 and 2.13). The value of Avrami exponent (n) and the crystallization rate constant (K) for model drugs are given in Table 2.3. The activation energy for crystallization was determined by linear regression analysis of ln K against $1/T_c$ using Eq. 2.15 and is plotted in Figure 2.14.

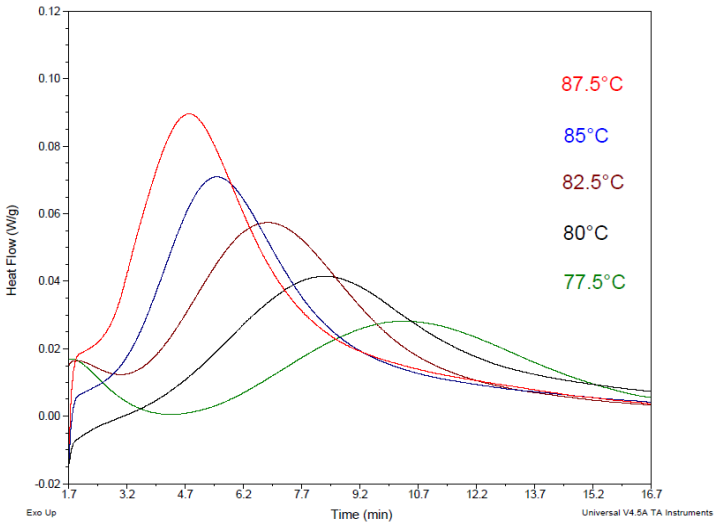

Figure 2.10. DSC isothermal curves of dipyridamole at various crystallization temperatures (n=3); single thermograms are shown at each temperature for clarity

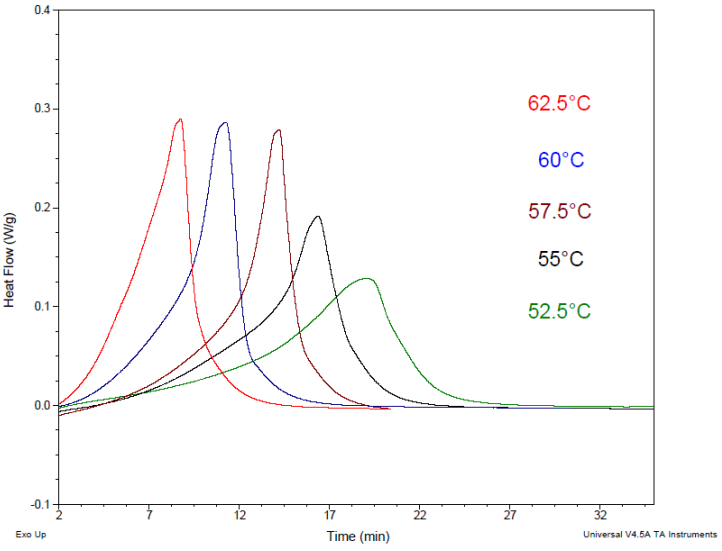

Figure 2.11. DSC isothermal curves of cinnarizine at various crystallization temperatures (n=3); single thermograms are shown at each temperature for clarity

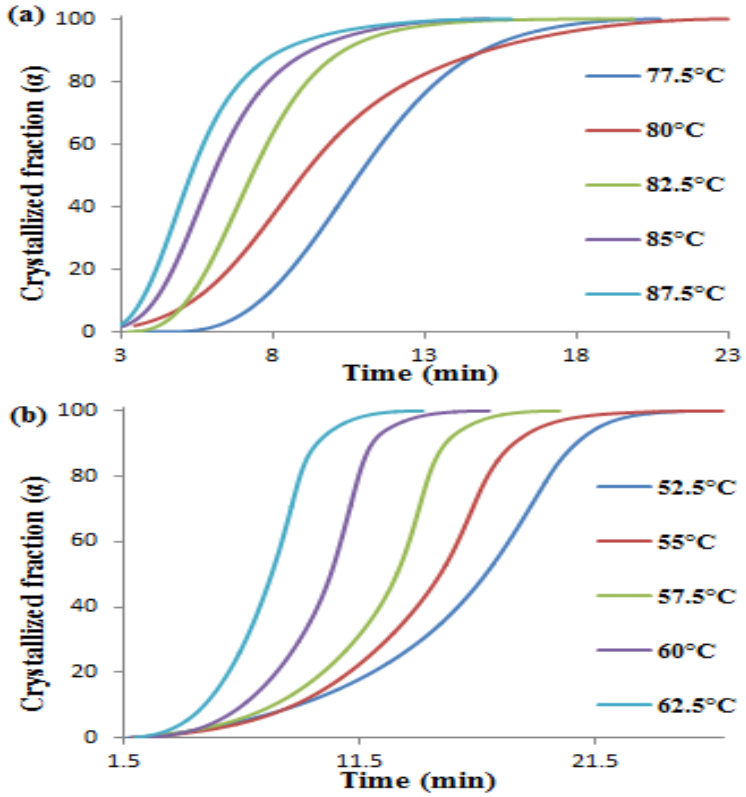

Figure 2.12. The plot of crystallized fraction (α) of amorphous dipyridamole (a) and cinnarizine (b) as a function of time at different isothermal crystallization temperature

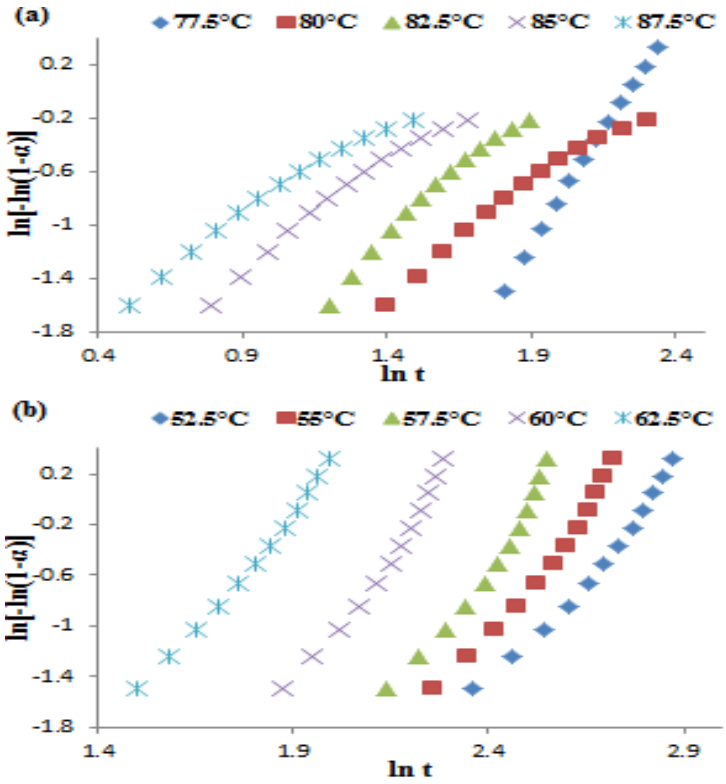

Figure 2.13. Plot of ln[-ln(1-Ft)] against ln (t) for the isothermal crystallization of dipyridamole (a) and cinnarizine (b) at the specified temperatures; Error bars are omitted for clarity

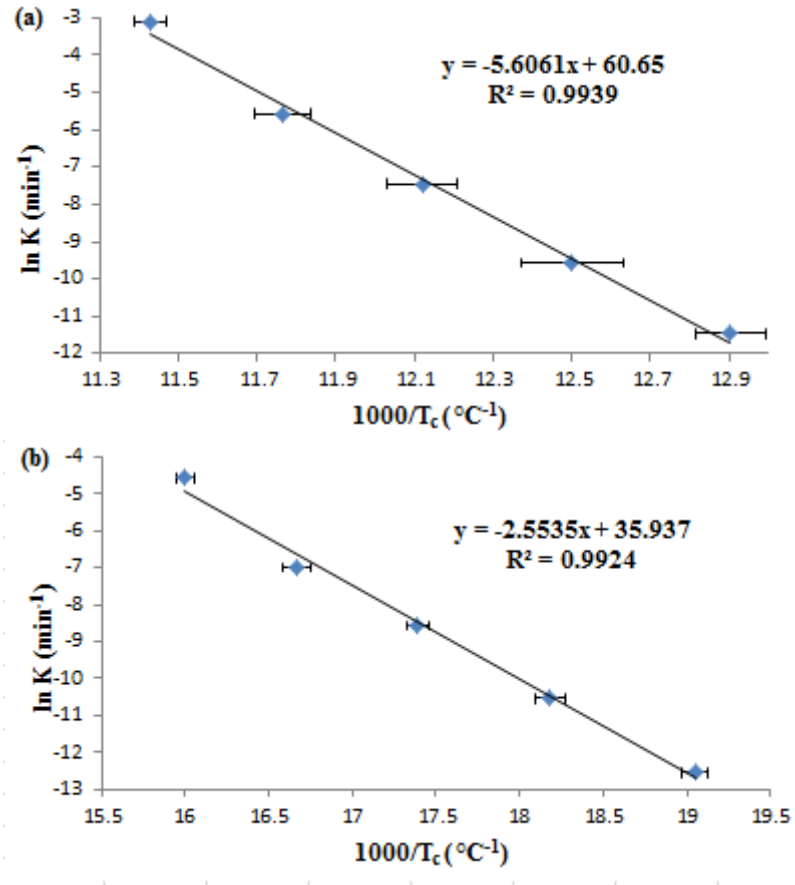

Figure 2.14. Arrhenius plot of ln K against $1/T_c$ for dipyridamole (a) and cinnarizine (b)

Table 2.3. Isothermal crystallization temperature (T_c), Avrami constant (K), Avrami exponent (n) and activation energy (E_a) of amorphous dipyridamole and cinnarizine

T_c (°C)		ln K		n		E_a (kJ mol^{-1})	
DPM	CNZ	DPM	CNZ	DPM	CNZ	DPM	CNZ
77.5	52.5	-11.46	-12.55	3.39	3.67	46.76	21.23
80	55	-9.56	-10.53	1.56	4.06		
82.5	57.5	-7.45	-8.56	2.01	4.56		
85	60	-5.57	-6.99	1.58	4.55		
87.5	62.5	-3.10	-4.57	1.42	3.78		

Table 2.4. Values of Avrami exponent, n, and expected crystallization mechanism[37]

Avrami exponent (n)	Crystallization mechanism
n = 1.5	Diffusion controlled growth of pre-existing nuclei (nucleation rate close to zero)
1.5 < n < 2.5	Growth of particle with decreasing nucleation rate
n = 2.5	Growth of particle with constant nucleation rate
n > 2.5	Growth of small particle with an increasing nucleation rate

It has been observed that the time required for crystallization during isothermal condition decreases as the temperature increases. As discussed previously, this may be due to the increased molecular mobility and shorter relaxation times at high temperatures. The K values are extremely sensitive to T_c and are dependent on the nucleation and growth rate.[36] Its value increases with an increase in T_c as shown in Table 2.3. The values of the Avrami exponent, n, and expected crystallization mechanisms are outlined in Table 2.4.[37] The n value for DPM (as shown in Table 2.3) is > 2.5 at lower temperature (77.5 °C) which corresponds to the nucleation controlled crystallization followed by growth of small particles. On the other hand, as the temperatures increases (80-85 °C), the value of n is approximately 1.5–2 which indicates a decrease in nucleation rate and diffusion controlled crystal growth becomes greater prominent. On further increasing the temperature (87.5 °C), n < 1.5 predicts the diffusion controlled crystal growth on pre-existing nuclei. In contrast, for CNZ, n value remains more than 2.5 at all temperatures indicating high nucleation rate. It has been suggested that nucleation is favored at lower temperature than crystal growth.[7, 38] Thus, CNZ crystallization (nucleation controlled) would occur relatively faster than DPM (nucleation and diffusion controlled). Indeed, the lower E_a value for CNZ (Table 2.3) suggests that it may nucleate and grow freely at the initial crystallization stage which supports its fragile nature, poor GFA and shorter relaxation time as compared to DPM. Similar results are also found for a range of polymers and are mentioned elsewhere.[39] Thus fragility and GFA can be used as an indicator of the isothermal crystallization behaviour *i.e.* compounds with large fragility and low GFA are expected to have poor stability compared to those with low fragility and high GFA.

The possibility that several process may occur during the crystallization of amorphous drug may account for the significant difference in the value of the Avrami exponent at different temperatures. The anomalous Avrami exponent values can also be attributed to assumptions made in the Avrami model.[40] The model assumes complete crystallization of the

sample which may or may not be possible and depends on the activation energy. It also assumes that no volume change occurs during crystallization with constant density and shape of the growing nuclei. Lastly, this model does not take into account any secondary crystallization. Thus, the most likely sources for Avrami exponent discrepancy can be attributed to inhomogeneous distribution of nuclei, especially at high α for DPM and CNZ crystallization under isothermal conditions.[41] Nonetheless, the correlation between fragility and GFA results to isothermal crystallization activation energy prediction suggests that this method may provide the qualitative estimation of the crystallization tendency of amorphous drugs.

2.3.4. Non-isothermal crystallization kinetics

Non-isothermal studies are preferred over isothermal studies due to the shorter experimental times and also because they are more closely related to real-life non-ambient thermal conditions during amorphous drug formulation. A robust isothermal condition is difficult to achieve because the sample must undergo heating up or cooling down to reach the desired temperature. Therefore, non-isothermal crystallization studies have been carried out to further extend the understanding of the crystallization mechanism of model compounds.

2.3.4.1. Model-Fitting kinetics

In this method, kinetics data, which is generally expressed as extent of crystallization (α), are fitted to different models at each temperature. To understand the crystallization mechanism of amorphous DPM and CNZ, a comprehensive list of different types of reaction models are provided in Table 2.5.[42, 43, 44] The model with the best correlation coefficient (r^2) value is then selected and is usually assumed to represent the actual model which describes the crystallization mechanism of the system under examination.

Table 2.5. Common solid-state reaction models and their integral forms used in this study for analysing phase transformation kinetics[43, 44]

Model Mechanism	Model notation	Integral form, g(α)
Avrami Erofeev (JMAEK), n = 2	JMAEK 2	$(-\ln(1-\alpha))^{1/2}$
Avrami Erofeev (JMAEK), n = 3	JMAEK 3	$(-\ln(1-\alpha))^{1/3}$
Avrami Erofeev (JMAEK), n = 4	JMAEK 4	$(-\ln(1-\alpha))^{1/4}$
1D diffusion	1 DD	α^2
2D diffusion	2 DD	$(1-\alpha)\ln(1-\alpha) + \alpha$
3D diffusion (Jander model)	3 DD J	$(1-(1-\alpha)^{1/3})^2$
3D diffusion (Ginstling-Brounshtein)	3 DD G	$1-2\alpha/3-(1-\alpha)^{2/3}$
First-order reaction	FOR	$-\ln(1-\alpha)$
Second-order reaction	SOR	$1/(1-\alpha)-1$
Power law, n = 1/2	PL 1/2	$\alpha^{1/2}$
Power law, n = 1/3	PL 1/3	$\alpha^{1/3}$
Power law, n = 1/4	PL 1/4	$\alpha^{1/4}$
1D phase boundary reaction (zero order)	1D PDR	α
2D phase boundary reaction	2D PDR	$1-(1-\alpha)^{1/2}$
3D phase boundary reaction	3D PDR	$1-(1-\alpha)^{1/3}$

Plotting a graph between ln[β.g(α)] vs. 1/T (where T is the crystallization temperature at each α level) gives the value of the activation energy from the slope of the plot. A higher value of E_a indicates a higher kinetic barrier for crystallization and thus amorphous drugs may have lower crystallization tendency. The non-isothermal crystallization thermograms of DPM and CNZ at five heating rates (β) are shown in Figure 2.8 and 2.9, respectively. It is recommended by International Confederation for Thermal Analysis and Calorimetry (ICTAC) to use three to five heating rates when performing crystallization kinetics by the model fitting approach and the fastest heating rate should be at least six times higher than slowest heating rate.[50] Thus, we have used 1, 2, 5, 10, and 20 °C/min heating rates. The potential impact of sample history has been minimized by using freshly quench-cooled amorphous drugs prior to DSC studies. In addition, care has been taken to avoid the possible impact of extreme strain (due to cracks) on crystallization kinetics by using intact pieces of DPM and CNZ glass.[51]

The onset (T_{crys}^{Onset}) and peak (T_{crys}^{peak}) temperatures for crystallization are summarised in Table 2.2. The crystallization temperature increases significantly with the increase in heating

rate. The overall heat flow signal (dH/dT) in DSC depends on the heat capacity of material (C_p), the heating rate (dT/dt = β) and the kinetic behaviour of the sample as shown below:[42]

$$\frac{dQ}{dt} = C_p \frac{dT}{dt} + f(T,t) \qquad \ldots\ldots\ldots \qquad (2.17)$$

The sample specific f(T,t) term depends on the heat flow (at a particular temperature) as a function of time and is shifted to higher temperatures with the increase in heating rate causing the observed crystallization temperature shift.[52] The slightly lower melting at the fastest rate suggests the lower crystal perfection due to the faster crystal growth process. The crystallization peak, for both DPM and CNZ, is clearly broader (i.e. the difference between the onset and end temperature) at higher heating rate (Figure 2.8 and 2.9, respectively). It may be assigned to the thermal lag within the sample due to low thermal conductivity of drug.

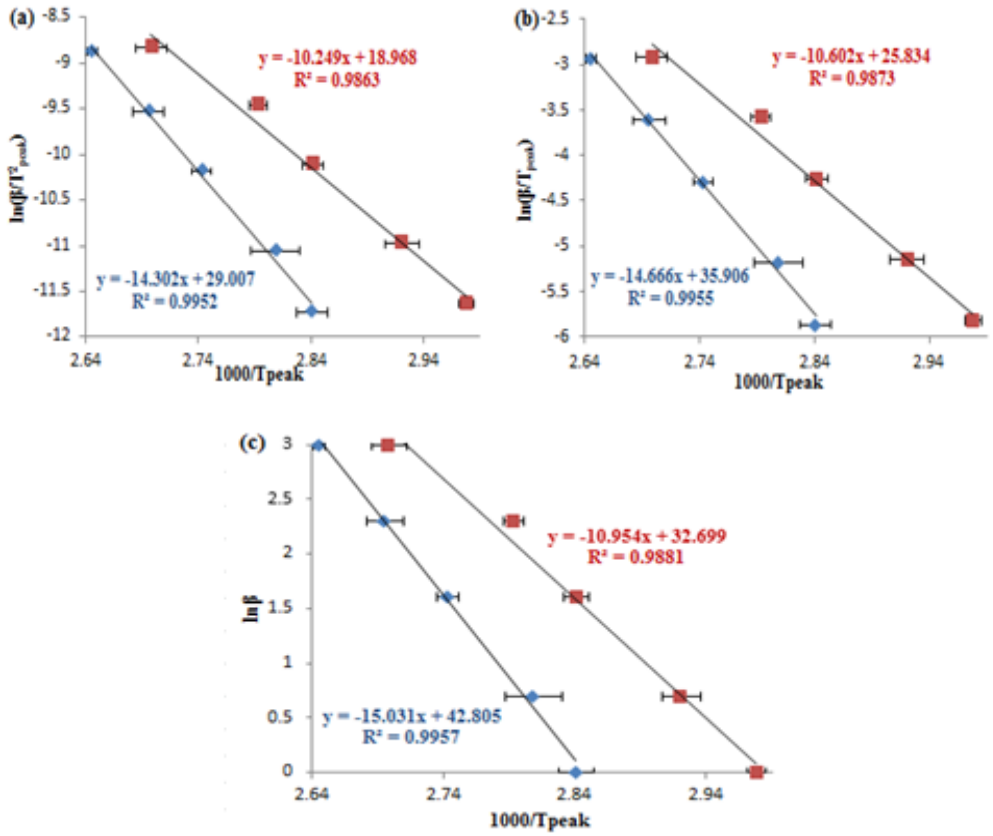

Figure 2.15. Kissinger (a) Augus-Bennett (b) and Flynn-Wall-Ozawa (c) plots for evaluating the activation energy for non-isothermal crystallization of amorphous dipyridamole (blue) and cinnarizine (red) (n=3)

As a control, the Kissinger model (Eq. 2.18), Augis-Bennett model (Eq. 2.19) and Flynn-Wall-Ozawa model (Eq. 2.20) were used for calculating activation energy, E_a, of phase transformation from amorphous to crystalline form during the non-isothermal crystallization process.[53, 54, 55]

$$ln\left(\frac{\beta}{T_{peak}^2}\right) = -\frac{E_a}{RT_{peak}} + C \quad \ldots\ldots\ldots \quad (2.18)$$

$$ln\left(\frac{\beta}{T_{peak}}\right) = -\frac{E_a}{RT_{peak}} + C \quad \ldots\ldots\ldots \quad (2.19)$$

$$ln(\beta) = -1.052\frac{E_a}{RT_{peak}} + C \quad \ldots\ldots\ldots\ldots \quad (2.20)$$

where R and C are the universal gas constant and Kissinger constant respectively. By plotting the parameter on the left hand side of the equation against the inverse of crystallization peak temperature ($\frac{1}{T_{peak}}$), the value of E_a, was obtained from the slope of the line (Figure 2.15). An average of the three methods was used (shown in Table 2.6) to eliminate the limitations of different models and to obtain a robust data for further evaluation. The main limitation of using these approaches is that it only uses the peak crystallization temperature at different heating rates, thereby giving the single activation energy value for the entire process. In contrast, the principle advantage of the model-fitting approach is that it gives activation energy value for the entire transformation range (over $0.2 < \alpha < 0.8$). Nonetheless, the three models described earlier for calculating E_a provides a good starting point towards crystallization kinetics studies under non-isothermal conditions.

Table 2.6. The non-isothermal activation energy for crystallization of amorphous dipyridamole and cinnarizine obtained by different methods

Non-Isothermal model	Activation energy of crystallization (kJ/mol)	
	DPM	**CNZ**
Kissinger	118.56	85.21
Augis-Bennett	121.59	88.15
Flynn-Wall-Ozawa	118.46	86.57
Average	119.54	86.64

The activation energies obtained by isothermal crystallization kinetics (Table 2.3) and non-isothermal crystallization kinetics (Table 2.6) are significantly different from each other. The reasons can be attributed to the underlying mechanism for the calculation of E_a values

which is the isothermal mode in the former and heating rate mode in the latter. The difference can also be aattributed to the absence of seeding nuclei (quench cooling). Schmitt *et al.* have reported similar E_a values under isothermal and non-isothermal conditions for hydrated amorphous lactose in the presence of seeding crystal.[56] However, the values differ significantly in the absence of seeding nuclei which is similar to our case where holding the drug at 5°C above melting point should have removed all the seeding nuclei. It is worth mentioning here that the physical meaning of activation energy is still matter of discussion.[57] Marotta *et al.*, have reported that even by using the same glassy system, the mechanism of crystallization may change due to sample size and thermal history.[58] Thus, E_a values for crystallization obtained from different plots and models may sometimes differ with each other.

2.3.4.2. Crystallization Activation Energy by model-fitting approach

A plot of the extent of amorphous phase crystallized, α, vs. temperature at different heating rates is shown in Figure 2.16. We have compared linear and sigmoidal baseline integration of crystallization peaks and found that the baseline choice has no effect on the rank order of the kinetic parameters measured at different heating rates. For amorphous DPM and CNZ, the shape of the crystallization plots follow sigmoidal patterns with an initial start point ($\alpha < 0.2$), followed by approximately linear zone ($0.2 < \alpha < 0.8$) and a terminal section ($\alpha > 0.8$) where the rate of crystallization approaches unity. It has been previously reported in the literature that the shape of α-T plot may be sigmoidal, decelerating or accelerating for any phase transformation for a variety of organic and inorganic glasses. [42, 59] The linear portion of each α-T plot has been selected for model-fitting kinetics.[48]

The non-isothermal crystallization kinetics at each extent of crystallization (α) have been described by several types of models such as diffusion models, nucleation models, power laws, geometric contraction models and reaction order models.[42] Although the majority of pharmaceutical compounds follow nucleation and diffusion based models for a range of solid-state phase transformations, there are certain exceptions as well.[60, 61, 62, 63] It is important to emphasize here that no single model can describe all the aspects of a crystallization phenomenon.[7] In the light of this information, 15 different kinetic models have been selected to assess the role of model selection on non-isothermal crystallization activation energy of amorphous DPM and CNZ at different heating rates (Table 2.5). Analyzing different crystallization models is required to investigate the effect of thermodynamic, molecular and kinetic factors on the crystallization event.

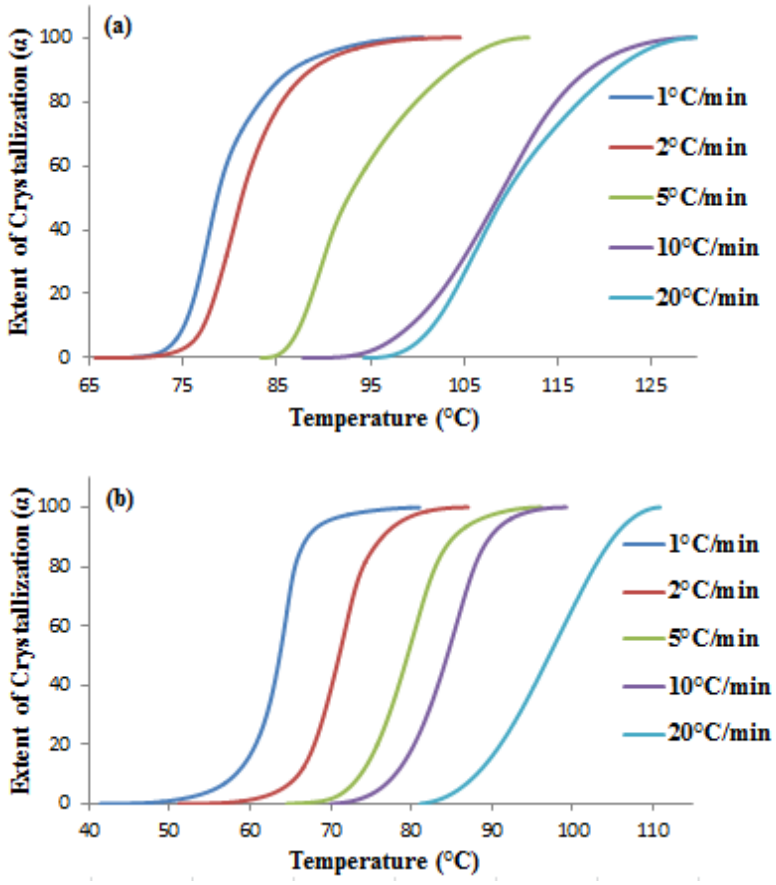

Figure 2.16. A sigmoidal plot of extent of crystallization (α) vs. crystallization temperature (T) at different heating rates for amorphous dipyridamole (a) and cinnarizine (b) (n=3)

Crystallization kinetics data collected from DSC experiments was fitted to different models to determine the most appropriate solid-state kinetic model of DPM (Table 2.7) and CNZ (Table 2.8). Interestingly, the results show that activation energy, E_a, values can vary significantly depending on the selected model and heating rate. It was found that for DPM none of the selected models can accurately describe the kinetics (r^2 ranges from 0.87 to 0.99) and similar results have been previously reported.[64] On the other hand, for CNZ it is extremely difficult to define the best model by comparing the r^2 value as several models gave high and comparable values. Similar trends have been previously observed for non-isothermal crystallization kinetics of amorphous nifedipine.[42]

Table 2.7. Activation energy for non-isothermal crystallization of amorphous dipyridamole based on model-fitting approach at five heating rates (β); mean value of three readings

Model notation	E_a (kJ/mol)									
	β = 1°C/min		β = 2°C/min		β = 5°C/min		β = 10°C/min		β = 20°C/min	
	Mean	r^2	Mean	r^2	Mean	r^2	Mean	r^2	Mean	r^2
JMAEK 2	133.07	0.9305	138.22	0.9646	86.14	0.9488	94.55	0.9955	82.95	0.9693
JMAEK 3	88.72	0.9305	92.19	0.9646	57.43	0.9488	63.02	0.9955	55.30	0.9693
JMAEK 4	66.54	0.9305	69.11	0.9646	43.07	0.9488	47.27	0.9955	41.48	0.9693
1 DD	352.70	0.8733	371.90	0.9204	228.32	0.8943	261.97	0.9743	224.16	0.9628
2 DD	402.66	0.8929	422.57	0.9361	260.74	0.9136	294.91	0.9829	254.40	0.9421
3 DD J	465.29	0.9138	485.60	0.9522	301.27	0.9335	335.29	0.9906	291.87	0.9576
3 DD G	423.32	0.9006	443.38	0.9421	274.11	0.921	308.26	0.9859	266.77	0.9479
FOR	266.15	0.9305	276.43	0.9646	172.29	0.9488	189.09	0.9955	80.59	0.9693
SOR	388.35	0.9656	398.42	0.9882	250.26	0.9788	265.99	0.9997	238.12	0.9907
PL 1/2	92.66	0.9216	92.98	0.9204	57.08	0.8943	65.49	0.9743	56.04	0.9268
PL 1/3	58.78	0.8733	61.98	0.9204	38.05	0.8943	43.66	0.9743	37.36	0.9268
PL 1/4	44.09	0.8733	46.49	0.9204	28.54	0.8943	32.75	0.9743	28.02	0.9268
1D PDR	176.35	0.8733	185.95	0.9204	114.16	0.8943	130.99	0.9743	112.08	0.9268
2D PDR	217.26	0.9046	227.31	0.9452	140.68	0.9247	157.72	0.9874	136.72	0.9509
3D PDR	232.65	0.9138	242.80	0.9522	150.63	0.9335	167.64	0.9906	145.94	0.9576

It has also been found that the E_a values obtained at higher heating rates are lower than those obtained at lower heating rate. The dependence of E_a on the heating rate has been further illustrated using different nucleation and diffusion models (as they have been shown as suitable for a range of solid-state phase transformation) in Figure 2.17.[65] One principle factor responsible for the drop in E_a is the effect of temperature on the crystallization process.[66] The crystallization peak shifts towards higher temperature at faster heating rates. Qualitatively, molecular mobility increases at higher temperature which favors crystallization. Another possibility might be the effect of heating rates on the relative predominance of nucleation and crystal growth which shifts the onset crystallization temperature compared to glass transition temperature.[67] At higher heating rate, the crystallization is dominated by crystal growth whereas at slower heating rates there is the possibility of some nucleation because of the relatively slow crystal growth.[54] As a result, nucleation dominates the crystallization phenomenon at lower heating rates. This dependence of crystallization on two different events, nucleation and crystal growth, may cause a thermal lag to the E_a values measured at higher heating rate.[68]

Table 2.8. Activation energy for non-isothermal crystallization of amorphous cinnarizine based on model-fitting approach at five heating rates (β); mean value of three readings

Model notation	E_a (kJ/mol)									
	β = 1°C/min		β = 2°C/min		β = 5°C/min		β = 10°C/min		β = 20°C/min	
	Mean	r^2	Mean	r^2	Mean	r^2	Mean	r^2	Mean	r^2
JMAEK 2	194.79	0.9961	163.02	0.9967	141.55	0.9979	139.57	0.9996	94.24	0.9973
JMAEK 3	129.85	0.9961	108.68	0.9967	94.37	0.9979	93.04	0.9996	62.83	0.9973
JMAEK 4	97.39	0.9961	81.51	0.9967	70.78	0.9979	69.78	0.9996	47.12	0.9973
1 DD	558.76	0.9985	454.48	0.9783	396.35	0.9814	393.04	0.9882	264.80	0.9803
2 DD	422.57	0.9982	510.65	0.9858	444.76	0.9883	440.24	0.9934	296.85	0.9874
3 DD J	698.48	0.9985	579.29	0.9925	503.74	0.9943	497.57	0.9977	335.77	0.9936
3 DD G	647.39	0.9992	533.34	0.9885	464.26	0.9907	459.20	0.9953	309.72	0.9899
FOR	398.57	0.9961	326.05	0.9967	283.12	0.9979	279.13	0.9996	188.49	0.9973
SOR	532.37	0.9823	456.29	0.9994	294.66	0.9990	387.22	0.9966	261.82	0.9989
PL 1/2	139.69	0.9985	113.62	0.9783	99.08	0.9814	98.26	0.9882	66.20	0.9803
PL 1/3	93.13	0.9985	75.74	0.9783	66.06	0.9814	65.51	0.9882	44.13	0.9803
PL 1/4	69.84	0.9985	56.81	0.9783	49.54	0.9814	49.13	0.9882	33.10	0.9803
1D PDR	279.38	0.9985	227.24	0.9783	198.17	0.9814	196.52	0.9882	132.40	0.9803
2D PDR	330.45	0.9991	272.77	0.9897	237.36	0.9919	234.68	0.9961	158.31	0.9911
3D PDR	349.24	0.9985	289.64	0.9925	251.86	0.9943	248.78	0.9977	167.88	0.9936

2.3.4.3. Model-free approach to identify the predominant crystallization model

The model-fitting approach has certain limitations and identification of the most suitable model for amorphous DPM and CNZ is difficult. Thus, to further understand the crystallization mechanism, model-free approach was employed. This method was originally proposed for solid-state desolvation kinetics and employs both model-fitting and model-free methods for identifying the most suitable kinetic model.[69] First, the activation energy, E_a, using the model free approach has been calculated and then these values were compared with those obtained by using the model-dependent method. Depending on the closeness of values of E_a obtained from model-dependent and model-free approach, the best model may be identified.

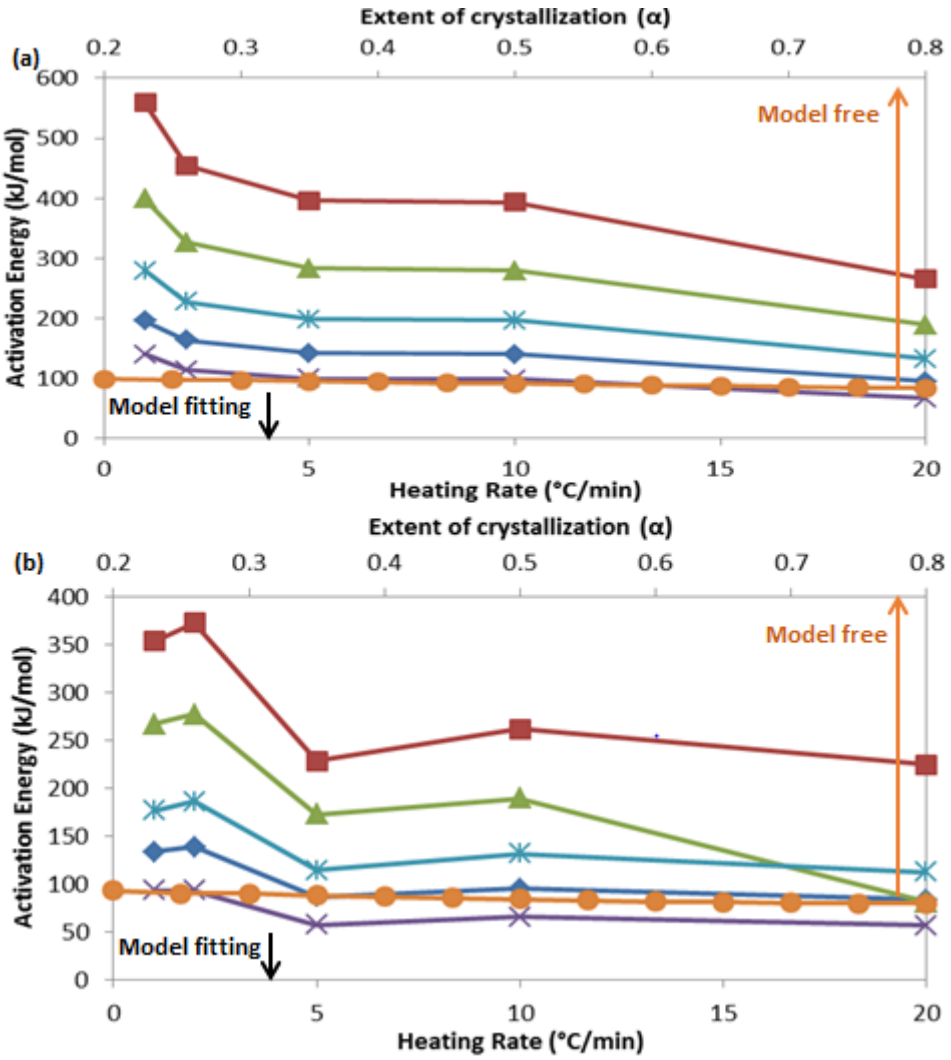

Figure 2.17. Effect of heating rate on activation energy of crystallization of amorphous dipyridamole (a) and cinnarizine (b) obtained by fitting nucleation and diffusion models of different orders; 1D diffusion (square), First order reaction (triangle), 1D phase boundary (star), JMAEK (diamond) and Power law (cross) (from top to bottom); Model-free kinetics (circle) for amorphous dipyridamole (a) and cinnarizine (b) calculated by Kissinger-Akahira-Sunose isoconversional kinetics to identify the most suitable kinetic model; (n=3)

In the model-free method, the crystallization kinetics are evaluated without assuming any particular model. The dependence of the crystallization kinetics on the extent of phase transformation may be evaluated from isoconversional kinetics technique which gives the value of E_a at different extents of crystallization, (α).[48] The Kissinger-Akahira-Sunose method (Eq. 2.21) is usually employed to perform model-free isoconversional analysis of non-isothermal crystallization kinetics data over the range of α = 0.2 to 0.8 at increment of α = 0.05 by plotting ln $(\beta_i/T^2_{\alpha\, i})$ vs 1/T thereby giving activation energy at each α increment.[70]

$$ln\left(\frac{\beta_i}{T_{\alpha i}^2}\right) = k - \frac{(E_a)_\alpha}{RT_\alpha} \quad \ldots\ldots\ldots \quad (2.21)$$

The model-free analysis for amorphous DPM and CNZ crystallization is illustrated in Figure 2.17. As per ICTAC recommendation, the kinetic parameter was analysed over a wide range of α with an increment of 0.05 for any amorphous to crystalline transformation.[50] We have selected the Kissinger-Akahira-Sunose kinetic method over other models (Flynn-Wall-Ozawa method, Tang method and Staink method) because it is considered better and gives more accurate E_a value.[50]

The E_a calculated by model-free kinetics for amorphous DPM and CNZ varies from 79 to 93 kJ/mol and 83 to 98 kJ/mol, respectively, as α increases from 0.2 to 0.8 (Figure 2.17). On the basis of the E_a values obtained from the model-free method, some of the models significantly overestimate E_a (such as all diffusion models and phase boundary models) whereas others underestimate it (such as power law models; n = 1/3 and 1/4) for both DPM (Table 2.7) and CNZ (Table 2.8). Furthermore, on increasing the heating rate, the model that yields the comparable E_a values changes from one model to another at different heating rates.

However, for both drugs, the activation energy values obtained from model-free analysis are generally comparable with that obtained from the nucleation- and growth-based models (such as JMAEK and power law; n = ½) as shown in Figure 2.17. Furthermore, for DPM (with increasing heating rate), the model that gives the similar E_a changes from, with no clear distinction, the third order JMAEK to the power law (n = ½) and finally to three dimensional JMAEK model. On the other hand, for CNZ, matching E_a values models changes from power law (n = 1/3) to JMAEK (n = 4), JMAEK (n = 3), power law (n = ½), and finally to JMAEK (n = 2). This suggests that crystallization of amorphous DPM and CNZ starts as a two-dimensional process and transition into three-dimensional crystal growth as heating rate is increased which is in agreement with the isothermal crystallization kinetics data. Therefore, it can be concluded that no single kinetic model is sufficient to describe the non-isothermal crystallization kinetics of amorphous DPM and CNZ. Furthermore, it is also observed that kinetic models are dependent on the heating rate for non-isothermal crystallization. These observations are similar to those of other amorphous pharmaceutical compounds such as nifedipine and felodipine.[42 70]

The E_a values for DPM and CNZ obtained from isothermal studies (Table 2.3) are lower compared to those calculated from the model-free approach. Zhou *et al.*, have reported a mathematical explanation for this discrepancy.[64] They showed that the calculation of the activation energy (for both isothermal and non-isothermal data) is the sum of the true activation energy and a correction term. The correction term is zero for isothermal kinetic data, but is not zero in the case of non-isothermal studies. This explains the lower activation energy calculated from isothermal studies as compared to E_a values from non-isothermal studies. The E_a values obtained by the model-fitting approach for CNZ are higher compared to those of DPM which demonstrates the limitation of the model-fitting approach to study crystallization kinetics of the model drugs. On the other hand, the model-free approach gives nearly similar E_a values for both the drugs. The discrepancies in the activation energy obtained from the model-fitting and model-free approach may be explained by examining the limitations of the different models. These models were originally derived for the crystallization kinetics in isothermal mode,[71] but later have been modified for non-isothermal crystallization.[72, 73] An important assumption of nucleation models is that the crystallization kinetics is only dependent on the temperature of the system without considering the effect of time or crystal size on the kinetics.[7 72] This assumption holds true for crystallization of equilibrium phase such as supercooled liquids where crystallization starts above T_g. However, the same assumption is invalidated when crystallization starts in the glass phase (below T_g) because the properties of the glass state are influenced by thermal history and age. Another assumption is the low anisotropy of the growing crystals.[74] On the contrary, most organic crystals exhibit anisotropy which influences the crystallization kinetics. Finally, both model-based and model-free kinetic approaches are based on an implicit assumption that the rate constant of crystallization, *k*, follows an Arrhenius dependence.[47] Although Arrhenius dependence holds true for most solid-state phase transformation, there are certain exceptions as well.[75] Non-Arrhenius dependence may lead to systematic error in E_a. Thus, the two most likely sources of E_a discrepancies can be attributed to crystal anisotropy and the possibility of non-Arrhenius behaviour of the crystallization rate constant.

2.3.5. Amorphous Drug Stability

Recently, fragility and GFA have been considered worthwhile parameters to predict the stability of amorphous drugs.[6, 22] Both model drugs were found to be fragile glasses (Table 2.1), CNZ, in particular, was found to be more fragile than DPM. This result was further supported by relaxation time measurements (Table 2.1) and T_{red} values (Table 2.2). Based on the above assessment, it can be predicted that a certain fraction of our model drugs may undergo crystallization which may have a significant effect on the amorphous drug product performance.[76]

Stability was first predicted based on the difference between the storage temperature and glass transition temperature of amorphous drugs.[77] It has been suggested that storing the amorphous drug below T_g (usually 50°C) could prevent crystallization maintaining the physical stability of drug during its shelf-life.[78] Storage condition can also be defined in terms of hypothetical thermodynamic temperatures such as Kauzmann temperature (T_K) or Vogel temperature (T_o) at which the molecular mobility is assumed to be close to zero.[57] The T_g, T_K and T_o for DPM/CNZ were found to be 38/6°C, -20/-55°C and -36/-55°C, respectively. Storing the amorphous drug at T_g – 50°C (*i.e.* -12 and -44°C for DPM and CNZ, respectively) or at T_K/T_o would be practically very inconvenient. Therefore, different approaches have to be developed to improve the stability of amorphous drug such as the use of polymeric solid dispersions which significantly improves the shelf life expectancy of amorphous drug formulations.

In order to shed further light on the role of crystallization tendency on the stability of amorphous drug products, amorphous solid dispersions of DPM and CNZ using PVP K30 as the carrier matrix (1:1 ratio) were prepared. The DSC thermograms of the freshly prepared and aged (2 months in desiccator at 25°C) amorphous solid dispersion products are shown in Figure 2.18. Both the freshly prepared and aged DPM-PVP solid dispersions show no sign of a melting endotherm (crystallization) and form a homogenous (single T_g) phase. Despite the fragile nature of the DPM, PVP K30 is effective in stabilizing the drug. This can be attributed to several factors such as antiplasticization, drug polymer interaction, and reduction in molecular mobility which are discussed in Chapter 3.[79] In contrast, the freshly prepared CNZ-PVP solid dispersion shows a melting endotherm ($\Delta H_m = 0.14$ kJ mol^{-1}) indicating some crystallization (0.36%) of amorphous CNZ in the solid dispersion. The DSC results were further confirmed using X-ray powder diffraction of aged solid dispersions and are shown in Figure 2.19. This is expected as the molecular mobility of amorphous CNZ is considerably

higher (shorter relaxation time) compared to DPM. The melting endotherm ($\Delta H_m = 13.25$ kJ mol^{-1}) increases further in the aged CNZ-PVP solid dispersion (34.6% crystallization). Furthermore, as shown in Table 2.1, the relaxation time for both drugs decreases at higher temperatures (113.5 and 2.5 s at 40°C for DPM and CNZ, respectively) and thus, the tendency to crystallize further increases leading to a higher probability of batch failure during accelerated stability studies.

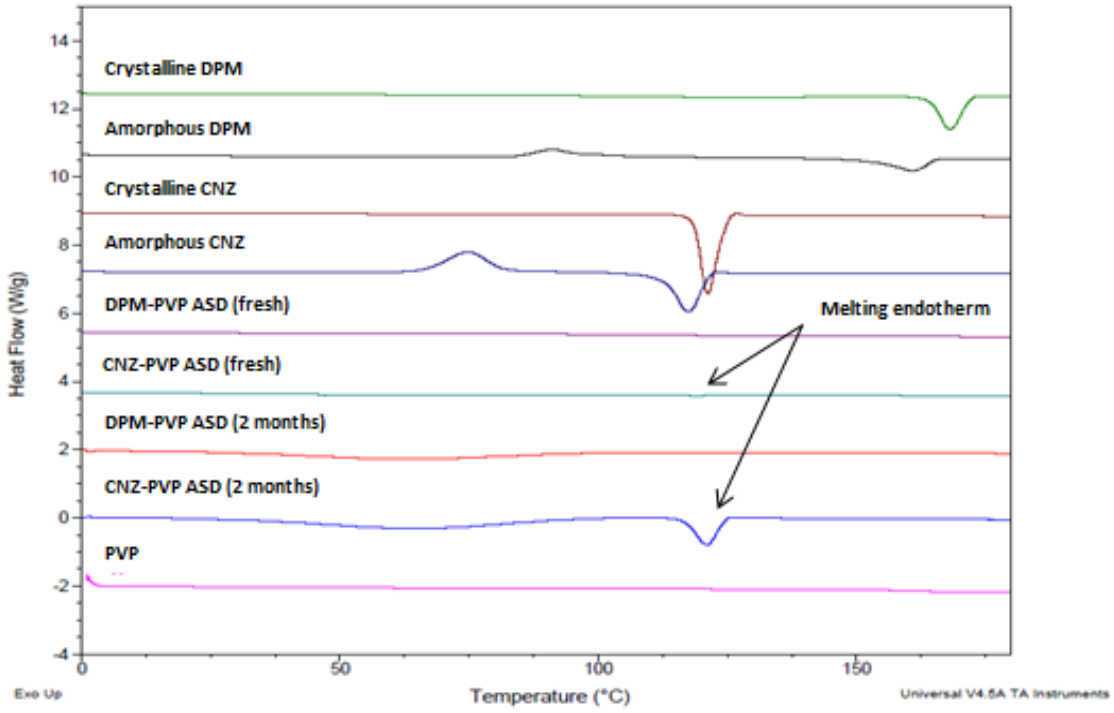

Figure 2.18. MDSC thermograms of model drugs, polymer and their solid dispersions using ± 0.53 °C /40s as modulation parameter at a heating rate of 5 °C /min; (n = 2)

These observations are further supported by the crystallization kinetic studies (isothermal and non-isothermal) which predict that both model amorphous drugs are susceptible to crystallization due to low E_a values. Moreover, the E_a values for DPM and CNZ obtained from the model fitting approach are nearly identical which implies that not only the activation energy but also the mechanism of crystallization may have a significant effect on the crystallization tendency of amorphous drugs under identical conditions. Crystallization kinetic studies have shown that during DPM crystallization both nucleation and diffusion/crystal growth are dominant factors whereas CNZ crystallization is governed by nucleation. Since nucleation is favoured at a lower temperature than crystal growth,[7] crystallization of amorphous CNZ in solid dispersions may be attributed to its nucleation

based mechanism which requires lower temperatures and thus lower activation energy to crystallize compared to DPM where diffusion also plays an important role.

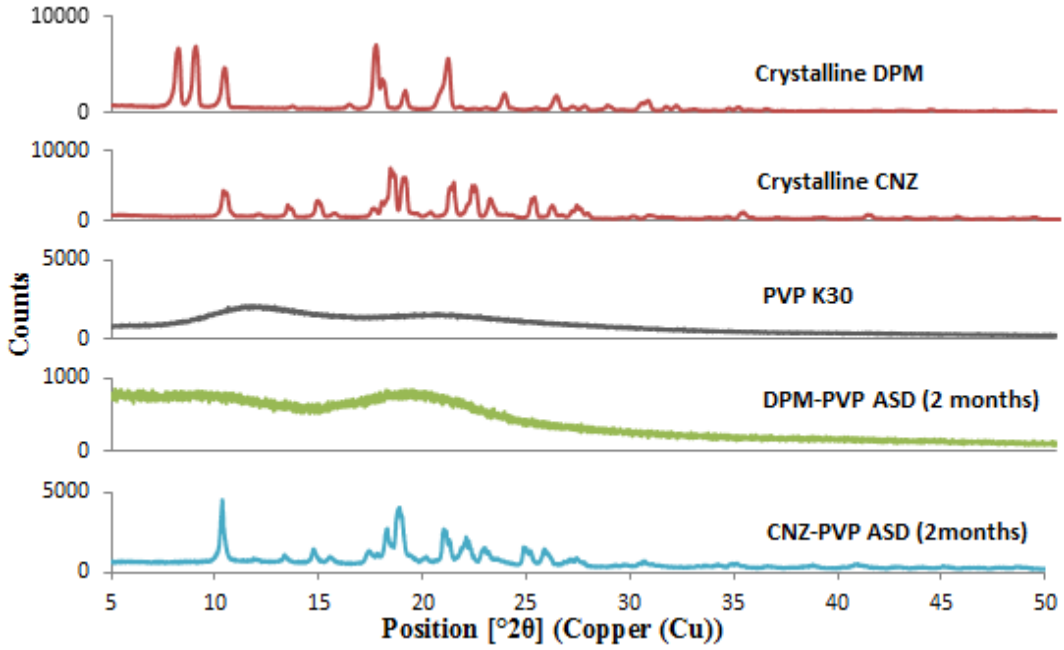

Figure 2.19. XRD scans of model drugs, polymer and their solid dispersions

At this point, it is clear that the crystallization of an amorphous drug is a complicated process and several factors may impact crystallization of an amorphous form. A detailed discussion on the factors effecting crystallization can be found elsewhere.[7] It must be pointed out that the above mentioned theories (fragility, GFA and crystallization kinetics) are only an approximation and they may not provide more than qualitative predictions for the real system. Moreover, the exact mechanism of crystallization at each level of transformation or accurate determination of molecular mobility (relaxation time) may not be accessible experimentally, thereby significantly restricting quantitative predictions. However, qualitative insights gained from this study are expected to facilitate more reliable classification of glasses based on the activation energy of crystallization and more effective stabilization of amorphous drugs and their products.

2.4. Conclusion

In this chapter, the crystallization tendency of amorphous APIs have been estimated using fragility and GFA approaches. Fragility can be determined by different methods; however, the values obtained may vary significantly. Significant correlation was found between m_T, $m_{D_{T_g}}$ and GFA whereas $m_{D_{CE}}$ did not correlate with any of them. Nonetheless,

this correlation suggests that fragile glasses have poor GFA and have higher crystallization tendency. Furthermore, the mean relaxation time of model drugs was also calculated and the result suggests that CNZ tends to recrystallize faster than DPM due to high molecular mobility. This result was corroborated by higher T_{red} and faster crystallization of CNZ during isothermal and non-isothermal experiments as compared to DPM. Other direct evidence for this observation was obtained from the activation energy measurement of glass transition and crystallization for DPM and CNZ. The results are in complete agreement with each other suggesting both APIs are unstable and CNZ, in particular, would have a smaller energy barrier to crystallization compared to DPM. Thus, fragility and GFA have been established as an important parameters for predicting the glass transition and crystallization behaviour of amorphous drugs. In addition, the crystallization kinetics of model drugs under isothermal and non-isothermal conditions has also been examined. It has been found that the crystallization mechanism for DPM follows one-dimensional growth with surface crystallization and for CNZ it is an interface-controlled three-dimensional isotropic growth and early nucleation site saturation. Moreover, it has also been shown that the conventional approach of comparing statistical data by the model fitting method is insufficient for identifying the most appropriate model for the crystallization process. The model free approach shows that nucleation- and growth- models are precise to the crystallization kinetics obtained for DPM and CNZ. Also, for both drugs, the crystallization mechanism changes from a two-dimensional process to three-dimensional process as crystallization proceeds. Finally, the validity of stability predictions on DPM and CNZ amorphous solid dispersion products has been checked and the results are in good agreement with predicted crystallization tendency and kinetics. Thus, fragility, GFA and crystallization kinetics are shown to be useful parameters in predicting the life expectancy of amorphous drugs from a practical standpoint.

2.5. References

1. Vippangupta S, Brittain H, Grant D. 2001. Crystalline Solids, Adv Drug Del Rev 48 : 3-26.

2. Diak A, Jones D, Andrews G. 2011. An investigation into the dissolution properties of celecoxib melt extrudates: Understanding the role of polymer type and concentration in stabilizing supersaturated drug concentrations. Mol Pharm 8: 1362-1371.

3. Babu N, Nangia A. 2011. Solubility advantage of amorphous drugs and pharmaceutical cocrystal, Cryst Growth Des 11: 2662-2779.

4. Hilden L, Morris K. 2004. Physics of amorphous solids. J Pharm Sci 93: 3-12.

5. Kawakami K. 2009. Modification of physicochemical characteristics of active pharmaceutical ingredients and application of supersaturable dosage forms as formulations for early clinical phases. J Pharm Sci 98: 2875-2885.

6. Kawakami K, Harada T, Yoshihashi Y, Yonemochi E, Terada K, Moriyama H. 2015. Correlation between glass forming ability and fragility of pharmaceutical compounds. J Phys Chem 119: 4873-4880.

7. Bhugra C, Pikal M. 2008. Role of thermodynamic, molecular and kinetic factors in crystallization from the amorphous state. J Pharm Sci 97: 1329-1349.

8. Guinot S, Leveiller F. 1997. The use of MDSC to assess the amorphous phase content of a micronized drug substance. Int J Pharm 192: 63-75.

9. Harada T, Kawakami K, Yoshihashi Y, Yonemochi E, Terada K, Moriyama H. 2013. Practical approach for measuring heat capacity of pharmaceutical crystals/glasses by modulated-temperature differential scanning calorimetry. Chem Pharm Bull 61: 315-319.

10. Kawakami K. 2011. Dynamics of ribavirin glass in the sub Tg temperature region. J Phys Chem B 115: 11375-11381.

11. Huang D, Mckenna G. 2001. New insights into the fragility dilemma in liquids. J Chem Phys 114: 5621-5630.

12. Hancock B, Dalton C, Pikal M, Shamblin S. 1998. A pragmatic test of a simple calorimetric method for determining the fragility of some amorphous pharmaceutical materials. Pharm Res 15: 762-767.

13. Angell C. 1991. Relaxation in liquids, polymers and plastic crystals – strong/fragile patterns and problems. J Non-Cryst Solids 131-133: 13-31.

14. Crowley K, Zografi G. 2001. The use of thermal methods for predicting glass-former fragility. Thermochim Acta 380: 79-93.

15. Richert C, Angell C. 1998. Dynamics of glass-forming liquids. V. On the link between molecular dynamics and configurational entropy. J Chem Phys 108: 9016-9026.
16. Zhang D, Zhang G, Law D, Grant D, Schmitt E. 2008. Thermodynamics, molecular mobility and crystallization kinetics of amorphous griseofulvin. Mol Pharm 5: 927-936.
17. Shamblin S, Zografi G. 1999. The effect of absorbed water on the properties of amorphous mixtures containing sucrose. Pharm Res 16: 1119-1124.
18. Moynihan C, Easteal A, Debolt M, Tucker J. 1976. Dependence of fictive temperature of glass on cooling rate. J Am Ceram Soc 59: 12-16.

19. Baird J, Eerdenbrugh B, Taylor L. J. 2010. A classification system to assess the crystallization tendency of organic molecules from undercooled melts. J Pharm Sci 90: 3787-3806.
20. Gupta P, Chawla G, Bansal K. 2004. Physical stability and solubility advantage from amorphous celecoxib: the role of thermodynamic quantities and molecular mobility. Mol Pharm 1: 406-413.
21. Greaser K, Patterson J, Zeitler J, Gordon K, Tades T. 2009. Correlating thermodynamic and kinetic parameters with amorphous stability. Eur J Pharm Sci 37: 492-498.
22. Grzybowska K, Paluch M, Grzybowski A, Wojnarowska Z, Hawelek J, Kolodziejczyk K. 2010. Molecular dynamics and physical stability of amorphous anti-inflammatory drug: Celecoxib. J Phys Chem B 114: 12792-12801.
23. Hodge L. 1996. Strong and fragile liquids – a brief critique. J Non-Cryst Solids 202: 164-172.
24. Shamblin S, Hancock B, Dupuis Y, Pikal M. 2000. Interpretation of relaxation time constants for amorphous pharmaceutical systems. J Pharm Sci 89: 417-427.
25. Hancock B, Shamblin S, Zografi G. 1995. Molecular mobility of amorphous pharmaceutical solids below their glass transition temperatures. Pharm Res 12: 799-806.
26. Yang Z. 2013. PhD Dissertation, University of East Anglia, Norwich, United Kingdom.
27. Alhalaweh A, Alzghoul A, Kailey W, Mahlin D, Christel A. 2014. Computational predictions of glass forming ability and crystallization tendency of drug molecules. Mol Pharm 11: 3123-3132.
28. Law D, Krill S. L, Schmitt E. A, Fort J. J, Qui Y, Wang W, Porter W. R. 2001. Physicochemical considerations in the preparation of amorphous ritonavir-poly(ethylene glycol) 8000 solid dispersions. J Pharm Sci 90: 1015-1025.

29. Guo Y, Bym R, Zografi G. 2000. Physical characteristics and chemical degradation of amorphous quinapril hydrochloride. J Pharm Sci 89: 128-143.
30. Tobyn M, Brown J, Dennis A. B, Fakes M, Gao Q, Gamble J, Khimyak Y. Z, McGeorge G, Patel C, Sinclair W, Timmins P, Yin S. 2009. Amorphous drug-PVP dispersions: Application of theoretical, thermal and spectroscopic analytical techniques to the study of a molecule with intermolecular bonds in both the crystalline and pure amorphous state. J Pharm Sci 98: 3456-3468.
31. Zhou D, Zhang G, Law D, Grant E, Schmitt E. 2002. Physical stability of amorphous pharmaceuticals: Importance of configurational thermodynamic quantities and molecular mobility. J Pharm Sci 91: 1863-1872.
32. Masuda K, Tabata S, Sakata Y, Hayese T, Yonemochi E, Terada K. 2005. Comparison of molecular mobility in the glassy state between amorphous indomethacin and salicin based on spin-lattice relaxation times. Pharm Res 22: 797-805.
33. Senkov N. 2007. Correlation between fragility and glass forming ability of metallic alloys. Phys Rev B 76: 104202.
34. Yu L. 2001. Amorphous pharmaceutical solids: Preparation, characterization and stabilization. Adv Drug Del Rev 48: 27-42.
35. Avrami M. 1939. Kinetics of phase change. I Genaral theory. J Chem Phys 7: 1103
36. Avrami M. 1940. Kinetics pf phase change. II. Transformation time relations for random distribution of nuclei. J Chem Phys 8: 212.
37. Wu J, Pan Y, Huang J, Pi J. 2013. Non-isothermal crystallization kinetics and glass-forming ability of Cu-Zr-Ti-In bulk metallic glasses. Thermochim Acta 552: 15-22.
38. Andronis V, Zografi G. 2000. Crystal nucleation and growth of indomethacin polymorphs from the amorphous state. J Non-Cryst Solids 271: 236-248.
39. Feldman D. Polymer chemistry-The basic concept. J Polym Sci 22: 673.
40. Verhoyen O, Dupret F, Legras R. Isothermal and non-isothermal crystallization kinetics of polyethylene terephthalate: Mathematical modelling and experimental measurement. Polym Eng Sci 38: 1594-1610.
41. Sinha I, Mandal R. 2011. Avrami exponent under transient and heterogenous nucleation transformation conditions. J Non-Cryst Solids 357: 919-925.
42. Zhou D, Schmitt E. A, Zhang G. G, Law D, Vyazovkin S. 2003. Crystallization kinetics of amorphous nifedipine studied by model-fitting and model-free approaches. J Pharm Sci 92: 1779-1792.

43. Garmer W. Chemistry of the solid state, Academic Press, New York.
44. Byrn S, Pfeiffer R, Stowell J. 1999. Solid-state chemistry of drugs. second ed., West Lafayette: SSCI, Inc.
45. Brown M. 2001. Introduction to thermal analysis: Techniques and applications. Second ed., Kluver, Amsterdam, Netherland.
46. Galwey A, Brown M. Introduction to thermal analysis: Chemical properties and reactivities of ionic phases, Elsevier, Amsterdam, Netherland.
47. Galwey A, Brown M. 2002. Application of the Arrhenius equation to solid state kinetics: Can this be justified? Thermochim Acta 386: 91-98.

48. Khawam A, Flanagan D. 2006. Basics and applications of solid state kinetics: A pharmaceutical perspective. J Pharm Sci 95: 472-498.
49. Vyazovkin S, Wight C. Model-free and model-fitting approaches to kinetic analysis of isothermal and non-isothermal data. Thermochim Acta 340-341: 53-68.
50. Vyazovkin S, Bumham A. K, Criado J. M, Maqueda L. A, Popescu C, Sbirrazzouli N. ICTAC Kinetic committee recommendations for performing kinetic computations on thermal analysis data. Thermochim Acta 520: 1-9.
51. Bhugra C, Shmeis R, Pikal M. 2008. Role of mechanical stress in crystallization and relaxation behaviour of amorphous indomethacin. J Pharm Sci 97: 4446-4458.
52. Russo U, Lemini D, Lacaita A. 2007. Analytical modelling of chalcogenic crystallization for PCM data-retention extrapolation. IEEE Trans Electronic Devices 54: 2769-2777.

53. Karmwar P, Boetkar J, Graeser K, Strachan C, Rades T. 2011. Investigations on the effect of different cooling rates on the stability of amorphous indomethacin. Eur J Pharm Sci 44: 341-350.
54. Soliman A, Kashif I, Sakr E, Ratep A. 2010. Elucidation of the crystallization kinetics for sodium-alumino-silicate glasses containing different amounts of manganese oxide, Phase. Transit 83: 1096-1113.
55. Fandaruff C, Sibaja A, Pereira R, Hoffmeister C, Rocha H, Silva M. 2013. Thermal behaviour and decomposition kinetics of efavirenz under isothermal and non-isothermal conditions J Therm Anal Calorim 115: 1-6.
56. Schmitt E, Law D, Zhang G. 1999. Nucleation and crystallization kinetics of hydrated amorphous lactose above the glass transition temperature. J Pharm Sci 88: 291-296.

57. Schamme B, Couvrat N, Malpeli P, Delbreilh L, Duprey V, Dargent E, Coquerel G. 2015. Crystallization kinetics and molecular mobility of an amorphous active pharmaceutical ingredient: A case study with biclotimol. Int J Pharm 490: 248-257.
58. Marotta A, Buri A, Branda F. 1980. Surface and bulk crystallization in non-isothermal devitrification of glasses. Thermochim Acta 40: 397-403.
59. Kong L, Gao Y, Song T, Wang G, Zhai Q. 2011. Non-isothermal crystallization kinetics of FeZrB amorphous alloy. Thermochim Acta 522: 166-172.

60. Maciejewski M. 2000. Computational aspect of kinetic analysis. Part B: The ICTAC kinetics project – The decomposition kinetics of calcium carbonate revisited, or some tips on survival in the kinetic minefield. Thermochim Acta 355: 145-154.
61. Vyazovkin S. 2000. Computational aspects of kinetic analysis: Part C: The ICTAC kinetics project – the light at the end of the tunnel? Thermochim Acta 355: 155-163.
62. Bumham A. Computational aspects of kinetic analysis: Part D: The ICTAC kinetics project – multi-thermal-history model-fitting methods and their relation to isoconversional methods. Thermochim Acta 355: 165-170.
63. Roduit B. 2000. Computational aspects of kinetic analysis: Part E: The ICTAC kinetics project – numerical techniques and kinetics of solid state processes. Thermochim Acta 355: 171-180.
64. Zhou D, Grant D. Model dependence of the activation energy derived from non-isothermal kinetic data. J Phys Chem A 108: 4239-4246.
65: Roduit B. 2000. Computational aspects of kinetic analysis: Part E: The ICTAC kinetics project – numerical techniques and kinetics of solid state processes. Thermochim Acta 355: 171-180.
66. Bosq N, Guigo N, Zhuraylev E, Sbirrazzuoli N. 2013. Non-isothermal crystallization of polytetrafluoroethylene in a wide range of cooling rates. J Phys Chem B 117: 3407-3415.
67. Kelton F. 1997. Analysis of crystallization kinetics. Mater Sci Eng A 226-228: 142-150.
68. Lam R, Rogers M. 2011. Activation energy of crystallization for trihydroxystearin, stearic acid and 12-hydroxystearic acids under non-isothermal cooling conditions. Crys Growth Des 11: 3593. 3599.
69. Khawam A, Flanagan D. 2005. Complementary use of model-free and modelistics methods in the analysis of solid state kinetics. J Phys Chem B 109: 10073-10080.

70. Chattoraj S, Bhugra C, Li Z, Sun C. 2014. Effect of heating rate and kinetic model selection on activation energy of non-isothermal crystallization of amorphous Felodipine. J Pharm Sci 103: 3950-3957.
71. Avrami M. 1941. Granulation, phase change and microstructure of kinetics of phase change. III. J Chem Phys 9: 177-184.
72. Handerson D. 1979. Thermal analysis of non-isothermal crystallization kinetics in glass forming liquids. J Non-Cryst Solids 30: 301-315.
Wang H, Gao Y, Ye Y, Min G, Chen Y, Teng X. 2003. Crystallization kinetics of an amorphous Zr-Cu-Ni alloy: Calculation of the activation energy. J Alloy Compd 353: 200-206.
74. Malek J. 2000. Kinetic analysis of crystallization process in amorphous materials. Thermochim Acta 255: 239-253.
75. Vyazovkin S. 2008. The handbook of thermal analysis and calorimetry, Elsevier, Amsterdam. Netherland.

76. Grohganz H, Priemel P. A, Lobmann K, Nielsen L. H, Laitinen R, Mullertz A, Mooter van der G. 2014. Refining stability and dissolution rate of amorphous drug formulations. Expert Opin Drug Deliv 11: 977-989.
77. Zhou D, Grant D, Zhang G, Law D, Schmitt E. 2007. A calorimetric investigation of thermodynamic and molecular mobility contributions to the physical stability of two pharmaceutical glasses. J Pharm Sci 96: 71-83.
78. Capen R, Christopher D, Forenzo P, Ireland C, Liu O, Lyapustina S, Neill J, Patterson N. 2012. , On the shelf life of pharmaceutical Products. AAPS Pharm Sci Tech 13: 911-918.
79. Teja S, Patil S, Patel S, Bansal A. 2013. Drug-excipient behaviour in polymeric amorphous solid dispersions. J Exip Food Chem 4: 70-94.

CHAPTER 3. THEORETICAL AND EXPERIMENTAL INVESTIGATION OF DRUG-POLYMER INTERACTION AND MISCIBILITY

3.1. Introduction

As discussed previously (Chapter 1 and 2), active pharmaceutical ingredients (APIs) may exist either in a crystalline form or in the amorphous state.[1] The former consists of an orderly arrangement of molecules whereas the latter lacks molecular periodicity. The random molecular arrangement gives the amorphous APIs a higher free energy compared to their crystalline counterparts which contributes to their higher apparent aqueous solubility.[2] However, the higher free energy also makes the amorphous systems inherently unstable which may lead to crystallization during storage and/or upon exposure to humidity. Such limitations often necessitate the incorporation of polymeric excipients as a stabilizer for the amorphous APIs producing solid dispersions.[2]

The solubility and miscibility of a drug within a polymeric carrier system has a significant effect on the stability of the amorphous solid dispersion (ASD) formulation.[3] Several factors are involved in stabilizing an amorphous drug within a polymeric carrier such as a reduction in chemical potential and molecular mobility, an increase in the activation energy for crystallization, an increase in T_g, strong drug-polymer interactions or a combination of these factors.[4 5] To achieve the maximum crystallization inhibition, regardless of the specific mechanism, intimate mixing of the drug in the polymeric matrix at the molecular level is highly desirable; poor mixing may lead to drug crystallization as observed with sucrose-PVP or indomethacin-PVP physical mixtures.[6 7] A better understanding of the phase behaviour of ASD systems helps to avoid supersaturation-driven phase separation or crystallization of the API at drug loadings beyond the solubility/miscibility limit of a specific polymer.[1 3 8 9] Therefore, it is of interest to assess drug-polymer miscibility in order to rationally select the optimal formulation for the desired storage conditions.

In view of these challenges, the focus of the present chapter aims to investigate the strength of drug-polymer interactions and solid state solubility/miscibility of the two poorly water soluble APIs, dipyridamole (DPM) and cinnarizine (CNZ), in two different polymeric carriers, polyvinyl pyrrolidone (PVP) and polyacrylic acid (PAA), using a multi-methodological approach. Flory-Huggins (F-H) binary interaction theory has been used to estimate drug-polymer interactions and miscibility (phase diagram) towards the successful development of ASD-based formulations of DPM and CNZ. Ternary F-H interaction parameters (drug-polymer-water) have also been calculated using dynamic vapor sorption (DVS) analysis to understand the effect of moisture on amorphous DPM and CNZ within PVP and PAA solid dispersions. The main objective of this study is to investigate the

usefulness of F-H theory as a preformulation tool for evaluating different polymers in order to gain an insight into the drug-polymer interaction and miscibility. This information is further correlated with the role of polymers in maintaining *in-vitro* drug supersaturation (Chapter 4). Subsequently, this information can be used as a road map to guide the selection of an appropriate drug loading for the chosen polymer and also help to optimize the processing conditions to maintain long term stability of the ASD products.[10]

3.2. Materials and methods

3.2.1. Materials

Dipyridamole (DPM), cinnarizine (CNZ), polyvinyl pyrrolidone (PVP) K30 and polyacrylic acid (PAA) were purchased from Sigma Aldrich, Ireland. The chemical structure of model drugs and polymers are shown in Figure 1.13. All reagents were of analytical grade and used without further purification.

3.2.2. Preparation of physical mixtures

Physical mixtures were prepared by manually mixing (using mortar and pestle) model crystalline drugs and polymers at 100%, 95%, 90%, 85% and 80% (w/w) drug concentrations. Sample preparation was carried out in triplicate at each concentration. During preparation of the physical mixture, the amorphous to crystalline drug ratio may have changed. It must be noted that, grinding may increase the amorphous content of the drug which may reduce its chemical potential.[11] Thus, care was taken to attain optimum mixing with minimum amorphization of drugs. Similarly, interaction between drug and polymer may also reduce the chemical potential and decrease the melting point of the drug in the mixture.

3.2.3. Preparation of solid dispersion

Amorphous solid dispersions (at 10, 20, 35, 50 and 60% w/w drug loading) were prepared in two steps. First, the drug and polymer were dissolved in a common solvent (methanol). The solvent was removed using rotary evaporation under reduced pressure. The mixture was then dried in a vacuum oven for 24 hr at 40°C. The dried mixture was then heated to the melting temperature of the drug, held isothermally for 5 min, and then cooled at 40°C/min to -60°C in a DSC pan. This additional step was performed to ensure complete mixing of drug and polymer at molecular level. It is important to mention here that different preparative techniques may generate solid dispersions with different physico-chemical properties for the same drug- polymer combination.[12 13]

3.2.4. Differential scanning calorimetry

Thermal analysis was performed using a TA Instruments Q2000 differential scanning calorimeter equipped with an electrical cooling accessory. Nitrogen was used as the purge gas at a flow rate of 50 mL/min. Temperature and heat flow calibration was carried out using a high-purity indium standard. Melting point depression analysis was conducted at a heating rate of 2°C/min from 0 to 200°C. The rate of 2°C/min is expected to provide sufficiently slow heating rate to induce molecular mixing of drug and polymer to meet the pseudo-equilibrium condition for Eq. 3.7. Validation experiments were carried out by modulated differential scanning calorimetry using an underlying heating rate of 5°C/min from 0 to 200°C, modulation amplitude of $\pm$0.53°C and a period of 40 s for both model compounds.[14] The onset of the melting peak was used for subsequent calculations.[15 16 17] A detailed explanation regarding the impact of heating rate on the melting point depression and the choice of onset of melting for calculations is available in literature.[18] All measurements (in triplicate) were performed by placing 5-10 mg of samples into aluminium pans with pin-holes. Data analysis was performed using Universal Analysis software (TA Instruments).

3.2.5. Dynamic vapour sorption

Dynamic vapour sorption (DVS) (DVS-1000 Advantage, Surface Measurement Systems, UK) analysis was used to study the moisture sorption behaviour of the ASDs. The samples (10-15 mg) were first dried to a constant mass (0% RH) for 3 hrs and then exposed to 10, 20, 30, 40, 50, 60, 70, 80 and 90% RH for 2 hrs at each stage to achieve equilibrium. All the measurements were done in duplicate.

3.2.6. Fourier-Transform Infrared Spectroscopy

Fourier-transform Infrared Spectroscopy (FTIR) was performed on a Varian 660-IR FT-IR Spectrometer (32 scans at 4 cm^{-1} resolution). Test samples were mixed with KBr and then compressed into disk and analysed immediately.

3.2.7. X-ray diffraction analysis

The powdered amorphous solid dispersions were analysed using X-ray diffractometer (X'pert MPD PRO PANalytical, Almelo, Netherlands) using the following parameters: Cu radiation (wavelength 1.540598 Å) , Ni-filter, voltage 40 kV, current 40 mA, 2θ range of 5-50°C, step size 0.008° and scan rate 3.2°/min.

3.3. Results and Discussion

3.3.1. Prediction of drug-polymer miscibility using solubility parameter approach

The solubility parameter is often used to quantitatively measure the cohesive properties of a drug-polymer system and is defined as the square root of cohesive energy density (CED) (cohesive energy per unit volume).[19] A number of excellent texts are available for more detailed information on solubility parameters and other cohesion parameters.[20] [21] The solubility parameters were calculated using two different methods, the Fedor and the van Krevelen methods. An average of both the methods has been taken for subsequent calculations.

Table 3.1. Physical properties of DPM, CNZ, PVP K30 and PAA

	Molecular weight (g/mol)	**Density (g/cm^3)**	**Molar volume[e] V_m (cm^3/mol)**	**ΔH_f (kJ/mol)**	**T_m (K)**
DPM	504.63	1.40[a]	360.23	29.06	441.26
CNZ	368.51	1.13[b]	326.12	38.33	394.40
PVP K30	40000	1.23[c]	32,520.33	-	
PAA	450,000	1.27[d]	3,54,330.71	-	

[a]Data reported.[26] [b]Value obtained from literature.[27] [c]Value obtained from literature.[28] [d]Value Taken from literature.[29] [e]Values obtained by dividing molecular weight by true density. [f]Values obtained from DSC (n=3)

The Fedor equation for calculating solubility parameter is as follows:[22]

$$\delta = \sqrt{CED} = \sqrt{\Delta E_{coh}/V} \quad \ldots\ldots\ldots \quad (3.1)$$

where δ is the solubility parameter, ΔE_{coh} is the cohesive energy and V is the lattice volume. According to van Krevelen, the total cohesive energy (E_{coh}) is the sum total of three types of interactions:[23]

$$E_{coh} = E_d + E_p + E_h \quad \ldots\ldots\ldots \quad (3.2)$$

where E_d, E_p and E_h are the contributions from the dispersive forces, polar forces and hydrogen bonding, respectively. The corresponding equation for solubility parameter (δ) is:

$$\delta^2 = \delta_d^2 + \delta_p^2 + \delta_h^2 \quad \ldots\ldots\ldots \quad (3.3)$$

$$\delta_d = \frac{\sum F_{di}}{V_m},\ \delta_p = \frac{\sqrt{\sum F_{pi}^2}}{V_m} \text{ and } \delta_h = \sqrt{\frac{\sum E_{hi}}{V_m}} \quad \ldots\ldots\ldots \quad (3.4)$$

where F_{di} is the molar attraction constant due to the dispersive components; F_{pi} is the molar attraction constant due to the polar components, E_{hi} is the hydrogen bonding energy, and V_m is the molar volume. The group contribution values for the drugs and polymers was obtained from literature.[24] The drug-polymer interaction parameter, χ, was calculated using the method developed by Hildebrand and Scott as shown in Eq. 3.5:[25]

$$\chi = \frac{V_m}{RT}\left(\delta_{drug} - \delta_{polymer}\right)^2 \quad \ldots\ldots\ldots \quad (3.5)$$

where V_m is the molar volume of the solvent, R is the universal gas constant and T is the absolute temperature.

Table 3.2. Solubility parameter and interaction parameter values of model drugs and polymers at 25°C

Drug/Polymer	δ Hoftyzer and van Krevelen method ($MPa^{1/2}$)	δ Fedor method ($MPa^{1/2}$)	Average	$\delta_{drug} - \delta_{polymer}$ Difference		χ (at 25°C)	
				DPM	CNZ	DPM	CNZ
DPM	28.57	29.57	29.07				
CNZ	21.00	21.10	21.05				
PVP K30	26.28	23.75	25.02	4.06	3.97	2.39	2.07
PAA	27.00	28.73	27.87	1.21	6.82	0.21	6.11

The values of the physical properties used to calculate the interaction parameter (Eq. 3.5) were taken from Table 3.1. The values of the solubility parameter (δ) and the interaction parameter (χ) for different drug-polymer systems used in this work are shown in Table 3.2. The solubility parameter difference between the drugs and polymers were determined to evaluate miscibility.[30] Generally, mixtures with lower difference are predicted to have higher miscibilities. Greenhalgh *et al.* showed that compounds with solubility parameter differences of < 7 $MPa^{1/2}$ are more likely to be miscible compared to compounds with solubility parameters differing by more than 10 $MPa^{1/2}$, which are generally immiscible.[31] For all the drug-polymer systems used in this study, the solubility parameter difference was found to be less than 7 $MPa^{1/2}$, suggesting their miscibility (Table 3.2). DPM, in particular, is expected to have higher miscibility with PAA as compared to PVP which may have higher miscibility with CNZ. Although widely applied, this approach has several limitations. For instance, the theoretical principle behind this method applies to simple organic structures where van der Waals interactions are dominant. However, for drug-polymer systems involving long range orders (e.g. ionic interaction) or highly directional bonds (e.g. H-bonding), this approach can

be erroneous.[32] In addition, the solubility parameter approach does not take into account lattice energy for miscibility predictions. Alternate methods, such as glass transition approach or molecular dynamic simulation for the estimation of interaction parameters have been reported in the literature but also have their own limitations.[33 34]

3.3.2. Drug-polymer binary interaction parameter and phase diagram

F-H theory is a modification of the original solution theory and has been widely applied to investigate the free energy of mixing (ΔG_{mix}) of polymer-polymer and/or polymer-solvent systems. The F-H lattice theory provides a rational explanation of the thermodynamics of the drug-polymer solution by considering an amorphous drug as analogous to a solvent molecule.[10] Hence, ΔG_{mix} for a drug-polymer dispersion is described by:

$$\frac{\Delta G_{mix}}{RT} = \Phi_{drug} \ln \Phi_{drug} + \frac{\Phi_{poly}}{m} \ln \Phi_{poly} + \chi \Phi_{drug} \Phi_{poly} \qquad \ldots\ldots\ldots \qquad (3.6)$$

where Φ is the volume fraction, T is the temperature of the system and *m* is the ratio of the volume of the polymer chain to a drug molar volume.[10] The mixing of the drug in the polymer will be thermodynamically favourable only if the free energy change associated with the mixing is negative ($\Delta G_{mix} < 0$). The theory also accounts for the contributions due to enthalpy and non-ideal entropy of mixing of small solvent molecules with a large polymer compound. On the right hand side of Eq, 3.6, the first two terms describes the entropy of mixing of a drug and polymer while the last term denotes the contribution from the enthalpy of mixing. The entropy always favours mixing, so it is the enthalpy which determines whether the mixing will be spontaneous or not. Thus, the drug-polymer binary interaction parameter,χ, is critical for understanding and predicting the behaviour of the system.

In this work, the F-H interaction parameter (χ) was calculated using the melting point depression method.[35] For miscible systems, the partial Gibbs free energy or the chemical potential of the drug in the mixture on melting will be smaller than the chemical potential of pure crystalline drug in the absence of polymer. This causes a depression in the onset of melting point of the drug in the mixture. However, if the drug and polymer are immiscible, the chemical potential of the drug remains unchanged and there will be no depression in the melting point. This method is not applicable for systems having very high melting point as these experiments may cause decomposition of either component.

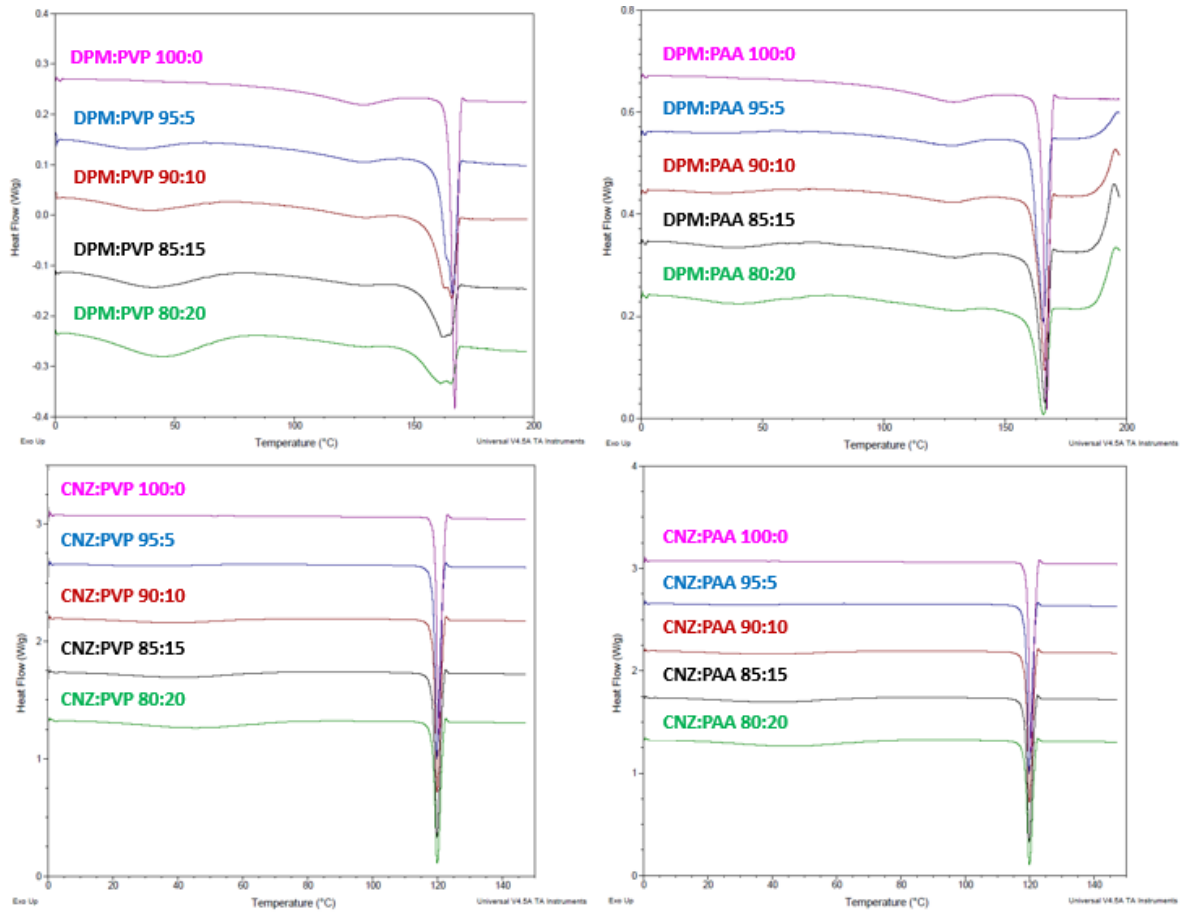

Figure 3.1. MDSC thermograms of depression in melting point onset of drug-polymer physical mixture at a heating rate of 2° C/min (n=3)

Figure 3.1 shows MDSC thermograms showing depression in melting point for drug-polymer physical mixtures containing different weight fractions of drug. Clearly, there is significant evidence of depression in the melting point onset of DPM and CNZ with an increasing fraction of PVP or PAA, indicating a substantial degree of mixing at the melting temperature of the respective drug-polymer systems. To further investigate drug-polymer solubility and miscibility, the value χ for different drug polymer combinations from the melting point depression data was calculated using the following equation:[36]

$$\left(\frac{1}{T_m}-\frac{1}{T_m^o}\right)=\frac{-R}{\Delta H_f}\left[ln\Phi_{drug}+\left(1-\frac{1}{m}\right)\Phi_{poly}+\chi\Phi_{poly}^2\right] \quad \ldots\ldots\ldots \quad (3.7)$$

where T_m is the melting temperature of drug in the drug-polymer mixture, T_m^o is the melting temperature of the pure drug, and ΔH_f is the heat of fusion of the pure drug. On plotting $\left(\frac{1}{T_m}-\frac{1}{T_m^o}\right)*\frac{\Delta H_f}{-R}-ln\Phi_{drug}-\left(1-\frac{1}{m}\right)\Phi_{poly}$ vs. Φ_{poly}^2, a linear plot was obtained for all the drug-polymer systems and the value of χ was estimated from the slope of the graph as shown in Figure 3.2.

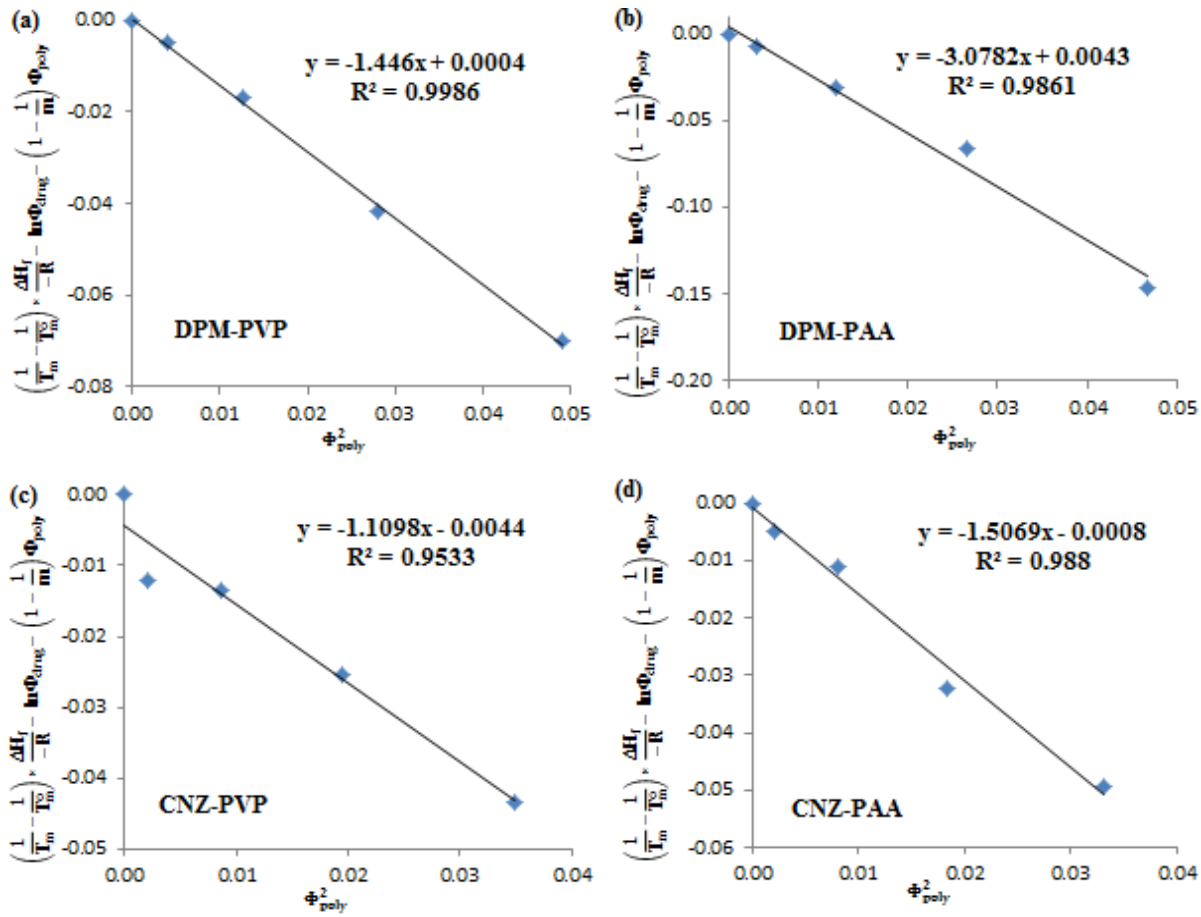

Figure 3.2. F-H interaction plot of the physical mixtures of drugs and polymers used to determine the F-H interaction parameter near melting point of DPM and CNZ (n=3).

Table 3.3. Calculated values of F-H interaction parameter by melting-point depression method

Drug-polymer combination	χ (at melting temperature of drug)
DPM-PVP K30	-1.45
DPM-PAA	-3.08
CNZ-PVP K30	-1.11
CNZ-PAA	-1.51

F-H, Flory-Huggins

A negative value of χ indicates heteronuclear interaction between drug and polymer which would facilitate mixing. A positive value is indicative of strong homonuclear interaction between drug or polymer molecules which is expected to offset the entropic gain due to mixing.[32] In this study, the χ value for each system was found to be negative (Table 3.3), indicating that PVP and PAA were miscible with both drugs at the melting temperature of the drug. It also suggests an exothermic heat of mixing which reduces the free energy of the system and makes it more stable. On the basis of these results, the degree of interaction and miscibility of the model drugs with PAA were found to be greater than with PVP K30.

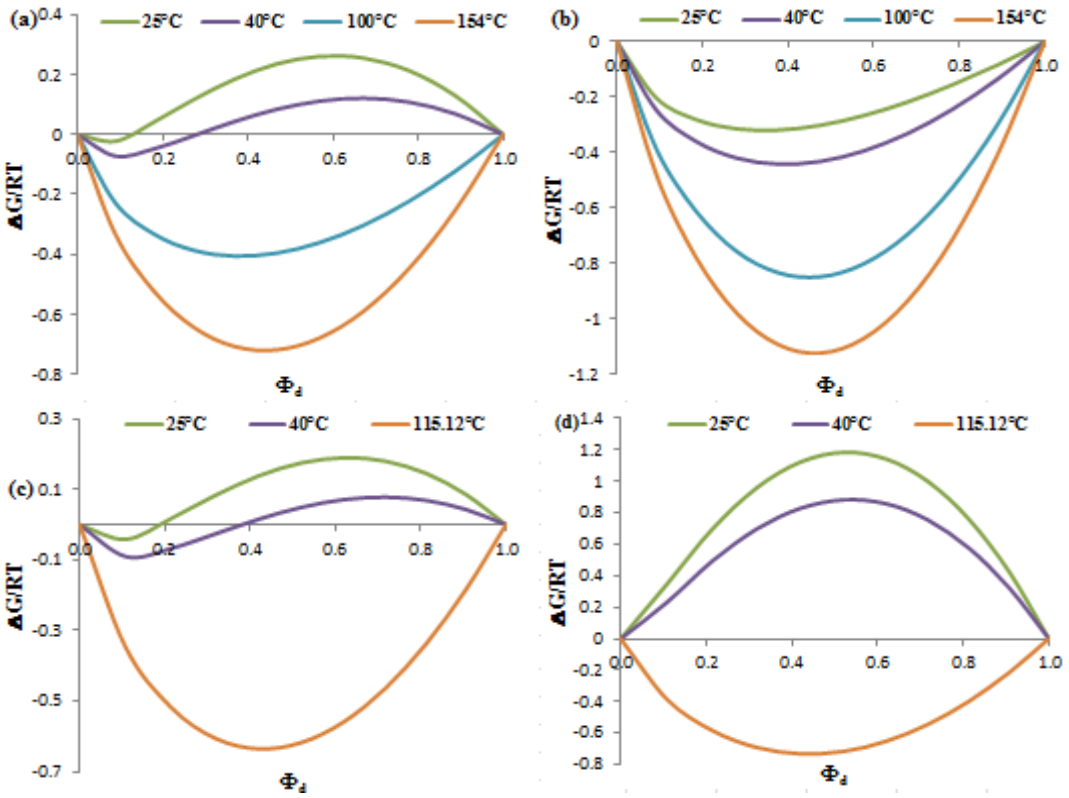

Figure 3.3. Plot of $\frac{\Delta G_m}{RT}$ vs drug weight fraction (Φ_d) for DPM-PVP K30 (a), DPM-PAA (b), CNZ-PVP K30 (c), and CNZ-PAA (d) systems at different temperatures.

Using Eq. 3.6 and the χ values (obtained from the melting point depression data), the change in Gibb's free energy upon mixing at DPM and CNZ melting temperature as a function of drug weight fraction was examined as shown in Figure 3.3 (orange line). The Gibb's energy of mixing can be either positive (promoting phase separation) or negative (promoting stability) depending on the value of χ and the drug composition. As expected, due to negative value of χ, the Gibb's free energy is negative showing the mixing is thermodynamically favorable at the melting temperature of the model drugs. These results suggest that at higher temperatures (hot-melt extrusion) it would be possible to obtain miscible DPM-PVP, DPM-PAA, CNZ-PVP and CNZ-PAA systems. However, this information does not enable us to predict the miscibility and phase stability at lower temperatures (such as room temperature). Therefore, constructing an appropriate phase diagram would give a more rational thermodynamic standpoint to determine miscibility and predict whether crystallization would occur at lower temperatures.

Table 3.4. Values of constants A and B for different drug-polymer systems

	DPM-PVP K30	DPM PAA	CNZ-PVP K30	CNZ-PAA
A	-10.31	-10.68	-8.53	-19.11
B	3786.6	3247.3	3161.2	7520.1

The value of the interaction parameter, χ, shows a non-trivial dependence on the temperature and volume fraction of the polymer.[37] The correlation between χ and these variables cannot be simply estimated. Often, to simplify the study, the temperature dependence of the χ has been written as the sum of the two components:[10]

$$\chi(T) \cong A + B/T \qquad \ldots\ldots\ldots \qquad (3.8)$$

The constants A (entropic contribution) and B (enthalpic contribution) were determined from the two known values of χ; χ_1 obtained at room temperature (25°C) using the solubility parameter approach and χ_2 obtained at the melting temperature of the drug using the melting point depression method (summarized in Table 3.4).[15] Eq. 3.8 can be combined with Eq. 3.6 to obtain Gibb's free energy at different temperatures as shown in Figure 3.3. From the curve it is evident that for the DPM-PVP K30 system at 25°C, the free energy is only negative for drug volume fractions (Φ_d) < 0.126, whereas for DPM-PAA it is negative at all drug loadings with a free energy minimum at Φ_d ~ 0.35. The free energy of mixing for CNZ-PVP at 25°C is negative at Φ_d < 0.19 while for the CNZ-PAA system it is found to be positive at all drug fractions. Thus, it can be predicted that at room temperature, only certain drug-polymer compositions will be able to generate thermodynamically stable ASDs.

To obtain a better understanding of miscibility at different drug volume fractions we constructed solid-liquid equilibrium (SLE) curve (using Eq. 3.6 and 3.8) as shown in Figure 3.4. Furthermore, the spinodal curve was constructed using the second derivative of free energy of mixing with respect to the volume fraction of drug using the following equation:

$$\frac{1}{\Phi_{drug}} + \frac{1}{m\Phi_{poly}} - 2\chi = 0 \qquad \ldots\ldots\ldots \qquad (3.9)$$

And finally, the glass transition curve was obtained using the Gordon-Taylor equation:[38]

$$T_g = \frac{W_1 T_{g1} + K_G W_2 T_{g2}}{W_1 + K_G W_2} \qquad \ldots\ldots\ldots \qquad (3.10)$$

where T_g, T_{g1} and T_{g2} are glass transition temperatures of the drug polymer mixture, the amorphous drug and the polymer respectively, and K_G is a constant which can be calculated using the equation as shown:

$$K_G = \frac{\rho_1 T_{g1}}{\rho_2 T_{g2}} \qquad \ldots\ldots\ldots \qquad (3.11)$$

where ρ_1 and ρ_2 are the densities of amorphous drug and polymer respectively. This generates phase diagram of four drug-polymer systems (DPM-PVP, DPM-PAA. CNZ-PVP and CNZ-PAA) having a solid-liquid equilibrium (SLE) or solubility curve, spinodal or miscibility curve and glass transition curve, as shown in Figure 3.4, determined using solubility parameter and melting point depression data.[39]

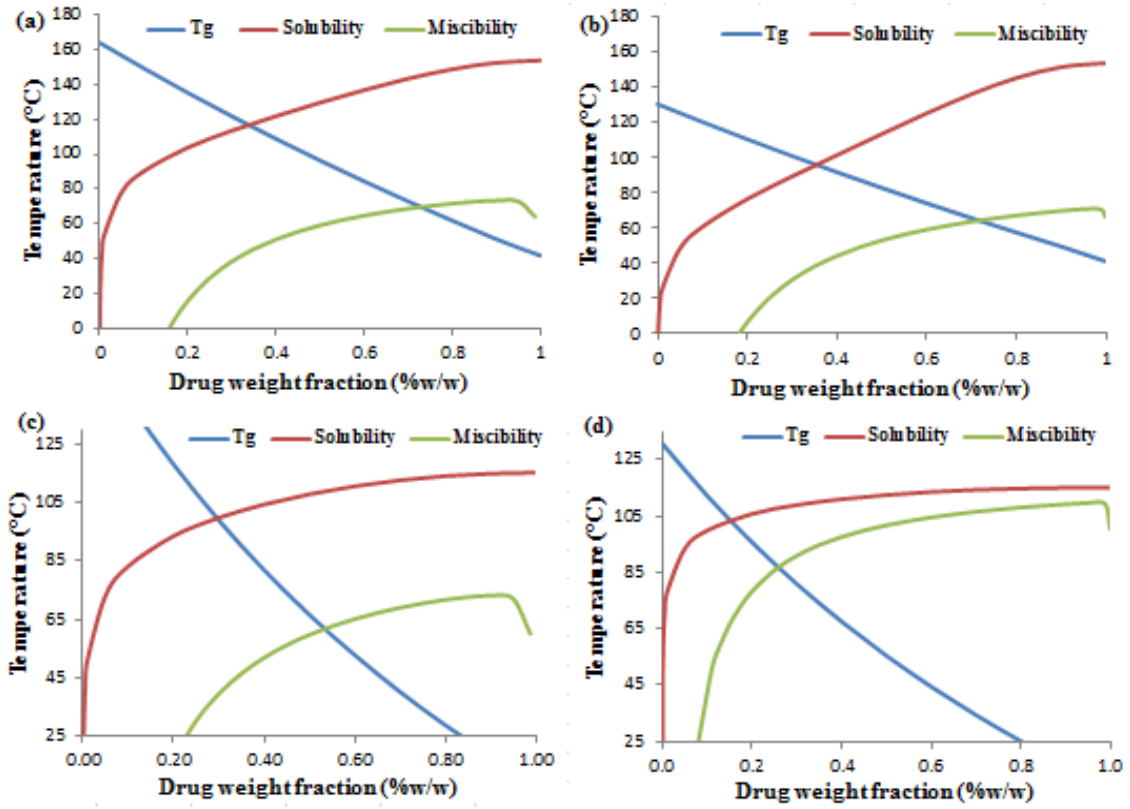

Figure 3.4. Binary phase diagram for DPM-PVP K30 (a), DPM-PAA (b), CNZ-PVP K30 (c) and CNZ-PAA (d); Solid-liquid equilibrium curve (red), miscibility curve (green) and glass transition curve (blue)

The temperature-composition phase diagram provides a fair estimation of thermal stability and allows formulation scientists to predict whether a mixture is locally stable or will undergo spontaneous phase separation as a result of fluctuations in temperature or composition. For instance, a drug-polymer hot-melt extrudate containing 70% drug loading can form an oversaturated solid dispersion as the system cools to normal room temperature. It is worth mentioning that phase separation of a metastable system is a kinetically controlled process which depends on the processing parameters, system perturbation, crystal nuclei formation and growth.[40] As shown in Figure 3.4, above the SLE curve (red color), the drug-polymer mixtures are expected to remain thermodynamically stable. Below this boundary and above Spinodal curve (green color), a metastable zone exists representing a metastable state.[10] In this region, specific drug-polymer compositions have the potential to separate into

coexisting amorphous phase leading to the formation of drug-rich or polymer rich amorphous domains without transforming directly into crystalline state which may occur later. Accordingly, single-phase and two-phase thermodynamic regions can be identified for the given drug-polymer binary mixture. Therefore, to evaluate the constructed phase diagram, ASDs of different drug-polymer combinations (DPM, CNZ, PVP K30 and PAA) and at different drug loading (10, 20, 35, 50 and 65% w/w) were prepared and analysed using MDSC as shown in Figure 3.5.

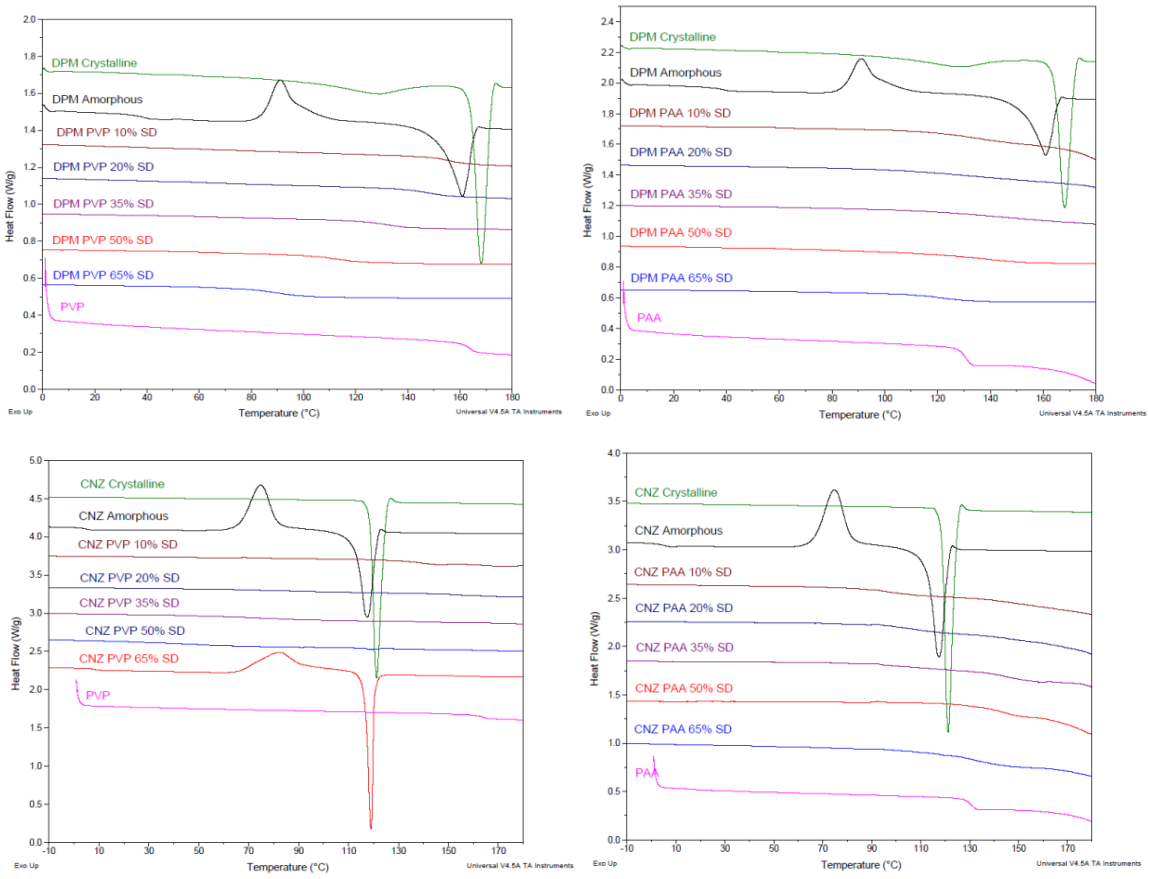

Figure 3.5. MDSC thermograms of freshly prepared amorphous solid dispersions of DPM and CNZ using ± 0.53 °C /40s as modulation parameter at a heating rate of 5 K/min (clockwise from top) (n=2).

From the phase diagram (Figure 3.4) it can be predicted that below the solubility curve the system will enter metastable region followed by unstable zone below the miscibility curve. In the unstable zone, spontaneous crystallization should occur without any significant energy barrier. However, it has been observed experimentally that three of the systems, DPM-PVP, DPM-PAA and CNZ-PAA, exhibited a single T_g (Figure 3.5) indicating the formation of single-phase homogenous system despite having compositions/temperatures in the unstable zone. No crystallization peaks were observed at any drug loading for these

systems which shows complete amorphization and miscibility of the drugs within the solid dispersion. CNZ-PVP crystallized at higher drug loadings (50 and 65% w/w) but formed a homogenous amorphous solid dispersion at lower drug loadings (10, 20 and 35% w/w). A glass transition and a small endothermic melting peak ($\Delta H_f = 0.37$ J/g) was observed to the 50% w/w CNZ/PVP system indicating a mainly amorphous system with a low level of crystalline drug. At higher CNZ weight fraction (65% w/w in PVP), a glass transition was observed along with a large melting peak ($\Delta H_f = 35.96$ J/g). This transition was lower than the T_g of PVP indicating the presence of amorphous drug. The solid dispersions were re-analysed after 2 months storage in a desiccator at 25°C. It was found that DPM-PVP, DPM-PAA and CNZ-PAA systems had remained stable as shown in Figures 3.6 and 3.7 (lower drug loadings are not shown). The CNZ-PVP solid dispersion also remained stable at lower drug loading (10, 20 and 35%) while at higher drug loadings the melting enthalpy had increased ($\Delta H_f = 21.94\ J/g$ and $40.74\ J/g$ for 50 and 65% drug loading, respectively).

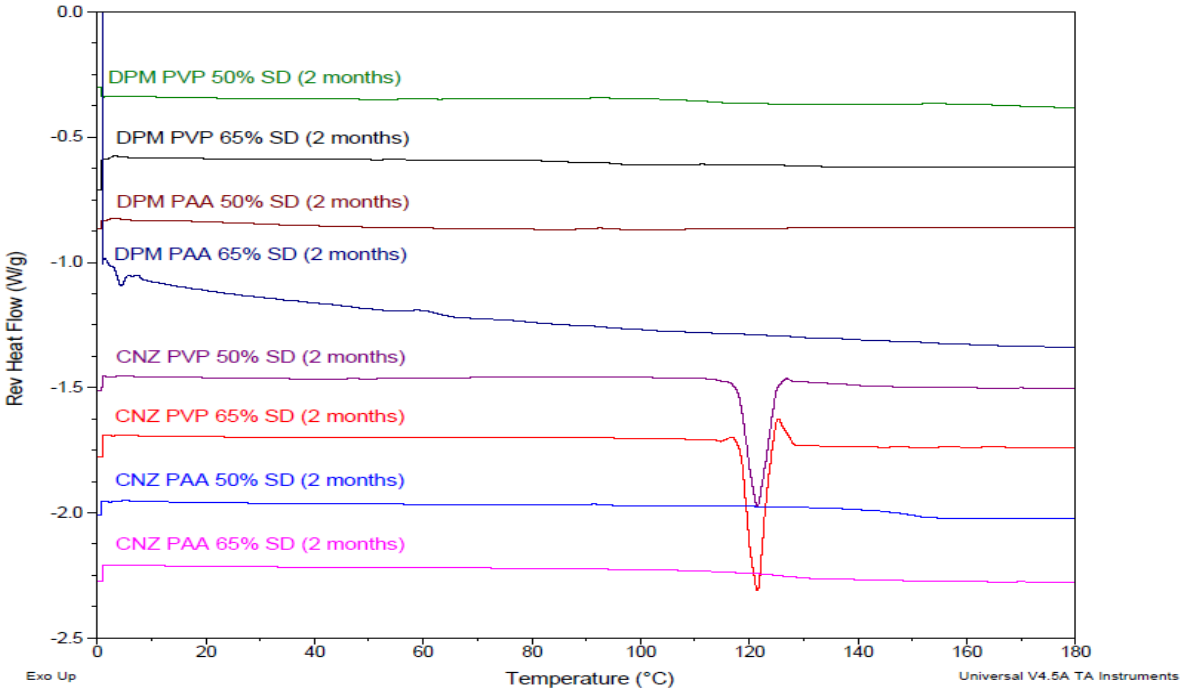

Figure 3.6. MDSC thermograms of aged solid dispersion (2 months) (n=2) using ± 0.5 K/40s as modulation parameter at a heating rate of 5 °C /min; aged represent SD stored in desiccator at 25°C for 2 months.

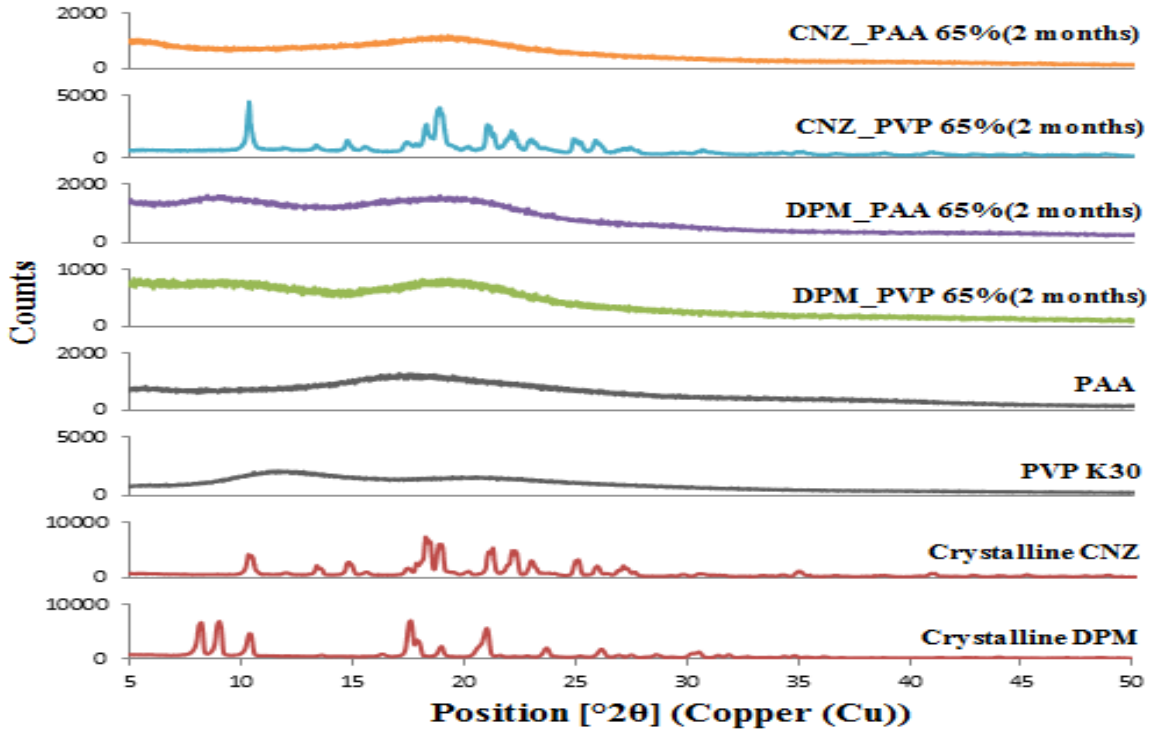

Figure 3.7. XRD spectra of model drugs, polymers and their respective aged solid dispersion at 65% w/w drug loading; aged represent SD stored in desiccator at 25°C for 2 months.

The observed stability of the ASD's within the metastable zone may be due to kinetic effects.[40 41] Within the metastable region, the drug is supersaturated inside the polymeric matrix; however, with apparent drug-polymer miscibility and storage below T_g of the ASD, with proper formulation engineering, drug supersaturation may be maintained without crystallization/phase separation increasing the shelf life of the product. Indeed, it has been found that DPM-PVP, DPM-PAA and CNZ-PAA systems are stable at drug concentration beyond the solubility curve which might be attributed to the slow kinetics of recrystallization. At room temperature, the DPM systems are all below the glass transition temperature of the drug system ($T_{g,DPM}$ = 37.44 °C) providing a kinetic barrier to recrystallization. The molecular mobility is low below T_g which may impede crystallization if the system is stored below T_g. CNZ systems, where the glass transition temperature is lower than room temperature ($T_{g,CNZ}$ = 5.86 °C), are more susceptible to recrystallization due to an insufficient kinetic barrier. We observed CNZ crystallization within PVP matrix at 50 and 65% w/w drug loadings whereas no crystallization was observed in CNZ-PAA systems. This suggests two important stabilizing factors *i.e.* the antiplasticization effect and drug-polymer interaction. Undoubtedly, a polymer that is capable of offering better antiplasticization and complementary bonds will provide greater resistance to devitrification.

3.3.3. Antiplasticization effect

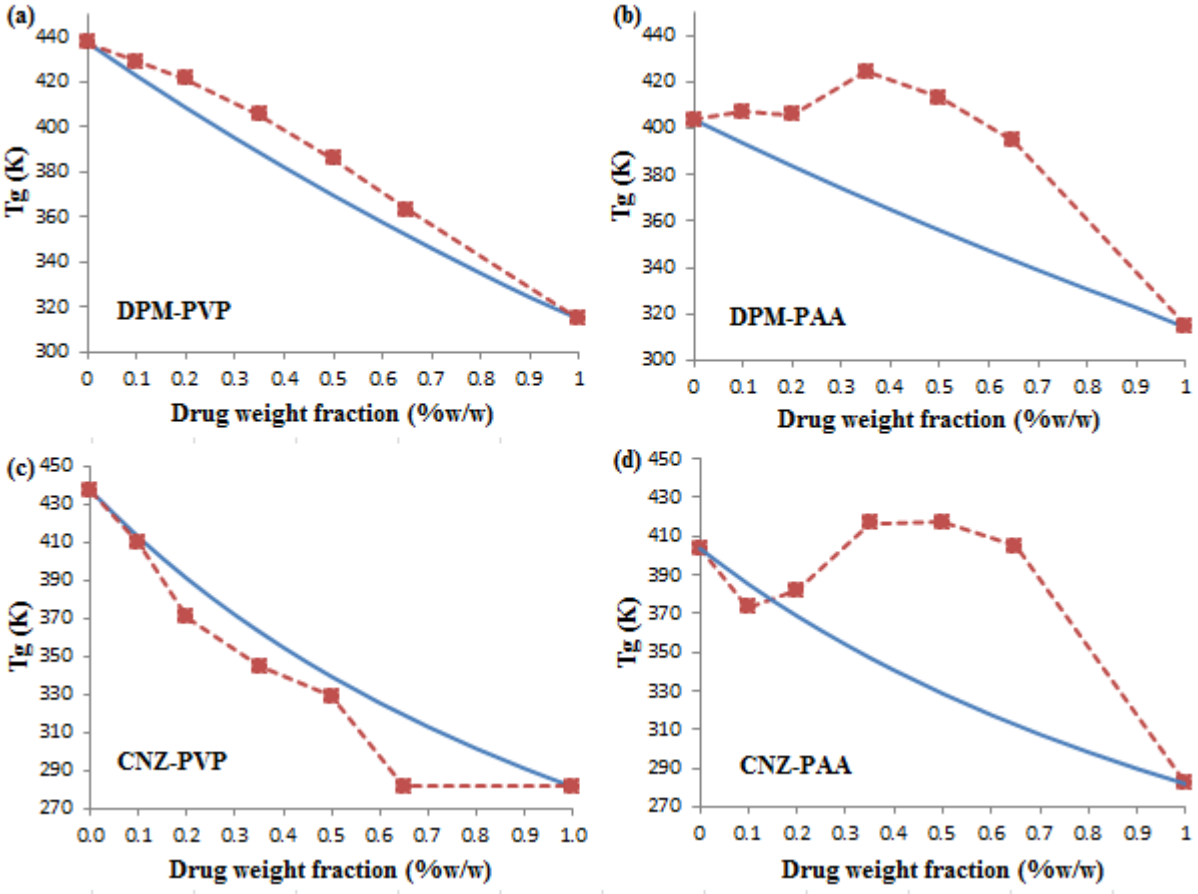

Figure 3.8. Predicted (blue line) and experimentally (red dots) obtained glass transition values of freshly prepared amorphous solid dispersions of DPM and CNZ (n=2).

To further examine the stability of amorphous solid dispersions, by comparing the predicted T_g values to those obtained experimentally, the stabilization due to drug-polymer interaction is shown in Figure 3.8. Negative deviation (observed T_g values below predicted values) suggest strong homonuclear interactions which will have a destabilizing effect. Positive deviation suggests strong heteronuclear interaction leading to enhanced stabilization of the drug within the polymer.[42] Deviations from the predicted T_g were minor at lower drug loading (10%) in all the four drug-polymer systems. However, at higher drug loadings, significant deviations were observed. A positive deviation from the ideal mixing behaviour was observed for DPM-PVP, DPM-PAA and CNZ-PAA solid dispersions suggesting that these systems are capable of forming strong bonds which increase the T_g. This explains the stability of these solid dispersions at higher drug loadings within the metastable and unstable regions at 25°C (Figure 3.4 and 3.5) due to antiplasticization effect of polymer on drug. On the other hand, only the CNZ-PVP system experienced a negative deviation from the predicted T_g, indicating that the heteronuclear interactions (CNZ- PVP) in the dispersions were less than the sum of the homonuclear interactions (CNZ-CNZ and PVP-PVP) of the

pure components at these compositions. This may explain the crystallization of CNZ in PVP solid dispersions at higher drug loadings. Similar results have been reported previously for CNZ-Soluplus® system where 35% w/w drug loading appears to be a critical value above which CNZ may crystallize.[43] The large positive deviation observed in PAA systems compared to PVP suggests that PAA is more effective at forming stable solid dispersions with both drugs.

3.3.4. FTIR analysis of drug polymer interaction

FT-IR analysis of pure DPM, CNZ, PVP K30, PAA and the ASDs was performed to look for possible interactions between drugs and polymers (Figure 3.9). The FT-IR spectra of DPM revealed characteristic peaks at 1533 and 1359 cm^{-1} peaks corresponding to C = N ring and C – N bonds; 2923 and 2851 cm^{-1}, due to asymmetrical and symmetrical stretch of CH_2 group; and 3377 and 3303 cm^{-1} corresponding to OH stretching vibration. The important bands of PVP K30 are 2956 cm^{-1} (C-H stretch) and 1665 cm^{-1} (C = O). A very broad band visible at 3400 cm^{-1} was attributed to the presence of water which was detected as broad endotherm in DSC thermograms. The OH stretching vibration almost disappeared in DPM-PVP system which can be attributed to the presence of the intermolecular H-bonds between the carbonyl groups (-N-CO-R) of PVP (H-bond acceptor) and the hydroxyl groups (-OH) of DPM (H-bond donor) causing the OH stretching vibration to weaken. This led to the presence of a weak and broad peak that was covered by broad band stretches from PVP. PAA shows important bands at 3441 cm^{-1} (stretching vibration of hydroxyl group) and 1714 cm^{-1} (stretching vibration of C = O group). The weaker bands at 1453 and 1413 cm^{-1} are associated with scissor and bending vibration of $–CH_2–$ and CH–CO groups, respectively. Bands associated with in-plane OH bending and C–O stretching of neighboring carboxyl groups are present at 1246 and 1172 cm^{-1}, respectively. Interactions were observed between DPM and PAA within solid dispersion characterized by changes in the C = N and C–N bands at 1533 and 1359 cm^{-1} respectively. Thus it could be anticipated that OH group of PAA might be interacting with C–N group present in DPM through hydrogen bonding. In addition, the stretching vibration of C = O of PAA at 1714 cm^{-1} was shifted to lower wavenumber indicating the presence of another H-bonding with OH group of DPM (broad band in ASD). This explains the higher interaction parameter of DPM-PAA system compared to DPM-PVP system (Table 3.3) and also the large positive deviation in T_g (Figure 3.8).

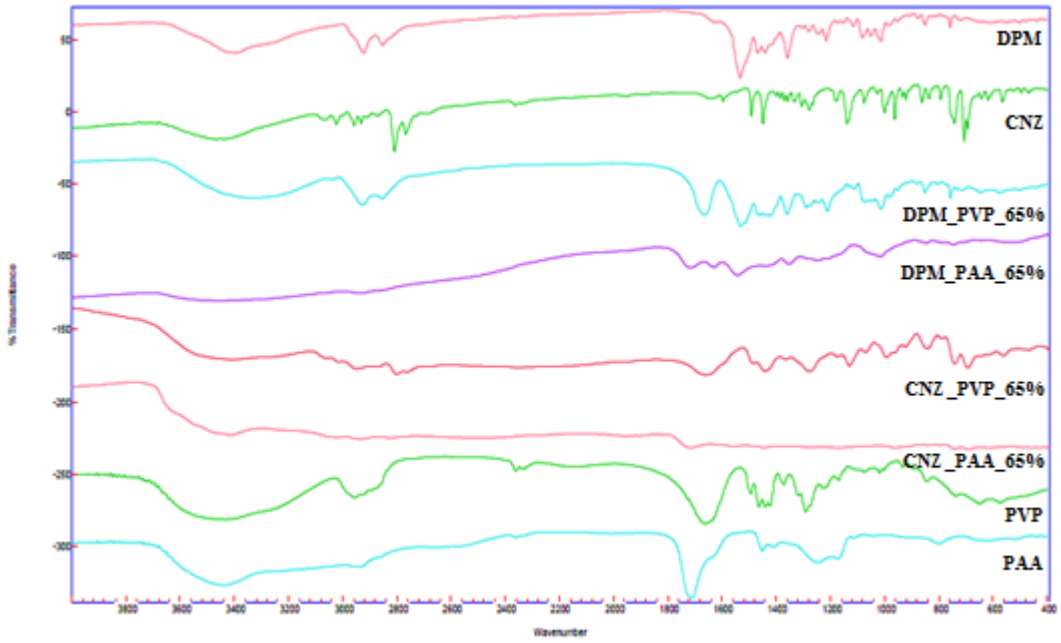

Figure 3.9. FTIR spectra of model drugs, polymers and their respective solid dispersions at 65% w/w drug loading

The pure cinnarizine spectra showed aromatic and alkene CH stretching peaks at 3066 and 3021 cm^{-1}, respectively, an aliphatic CH stretching peak at 2956 cm^{-1}, a C–N stretching peak at 1141 cm^{-1} and =C–H alkene and aromatic (out of plane) peaks at 1001 and 963 cm^{-1}, respectively.[44] The CNZ-PVP solid dispersion showed no change in spectra compared to the pure drug except that some peaks became broader and merged, suggesting the presence of amorphous drug and no H-bond interaction between CNZ and PVP. It can be inferred that the drug-drug interactions are stronger than drug-polymer interactions which explains the negative deviation in T_g (Figure 3.8). However, as shown in Figure 3.5 and 3.6, no crystallization peak was observed at 10, 20 and 35% drug loading suggesting that CNZ was uniformly dispersed within PVP to produce mixing at a molecular level. This disagreement suggests that CNZ formed a solid solution with the PVP at high temperatures and was kinetically frozen during the cooling process, rather than being a thermodynamic equilibrium. If this is the case then increasing the drug loading would lead to self-association of CNZ molecules and, as a result, crystallization. As can be seen from Figure 3.5 and 3.6, the CNZ-PVP systems with 50 and 65% drug loading both displayed a characteristic crystalline drug melting peak. On the other hand, CNZ-PAA spectra clearly demonstrated the presence of H-bonding between C–N group of CNZ and carboxyl group of PAA leading to the formation of stable system with strong positive deviation in T_g and no observed crystallization.

3.3.5. Drug-Polymer-Water ternary interaction parameter

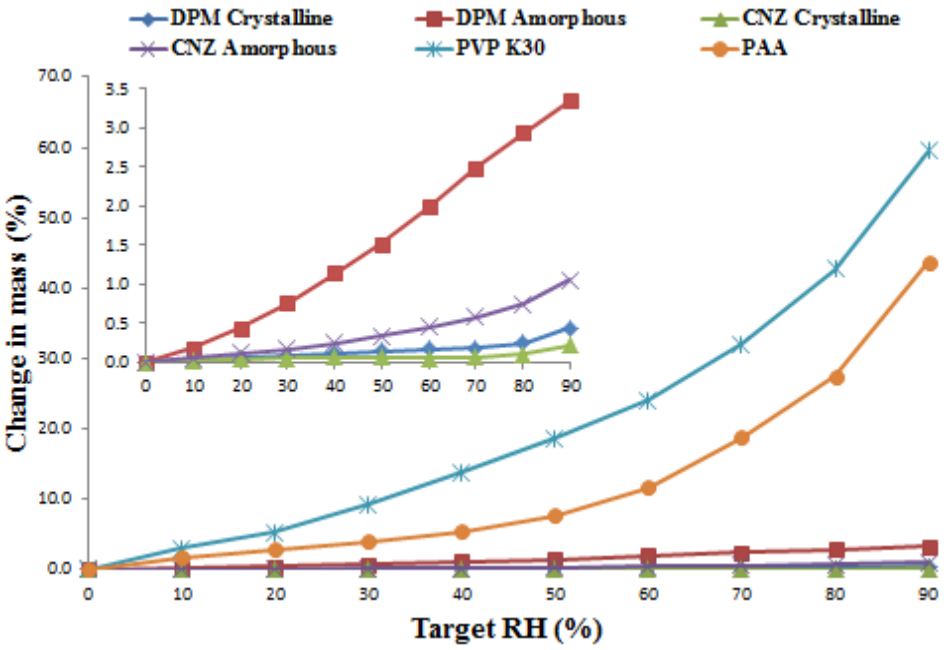

Figure 3.10. Water sorption isotherm of pure drugs and polymers; DPM/CNZ curves are expanded in inset

Moisture sorption analysis has been widely used to study the affinity of pharmaceutical compounds towards moisture. A typical moisture sorption isotherm at a constant temperature and pressure shows the change in mass of the sample due to water sorption (absorption/adsorption) which reflects the interaction between the sample and water.[45] As shown in Figure 3.10, PVP was found to be more hygroscopic than PAA (59% and 44% increase in mass at 90% RH, respectively). The hydrophobic nature of the pure crystalline drugs was demonstrated by their low moisture sorption (Figure 3.10 Inset). Amorphous DPM and CNZ sorbed 3.34 and 1.05% water by mass at 90% RH, respectively, suggesting that DPM is slightly more hydrophilic than CNZ. The solid dispersions, on the other hand, showed a significant increase in moisture sorption compared to the pure drugs as shown in Figure 3.11 at 50% w/w drug loading. The PVP solid dispersion had a higher moisture sorption than the PAA, probably due to more hydrophilic nature of the polymer.

The moisture sorption isotherm of a binary physical mixtures can be predicted by assuming isotherm additivity of each component present in the mixture as shown below:[42]

$$W_{mix} = \frac{(W_{API}m_{API} + W_{poly}m_{poly})}{(m_{API} + m_{poly})} \qquad \ldots\ldots\ldots \qquad (3.12)$$

where *m* is the component mass in the mixture and *W* is the mass of the absorbed water per unit dry mass of the solid. This equation is based on the assumption that there is no interaction between the components and implies ideal behaviour. However, if the drug and the polymer interact with each other, a deviation from the ideal behaviour would be observed and the extent of deviation may be regarded as a measure of the strength of the drug-polymer interaction.[46] Furthermore, improving the wetting properties of an amorphous drug within a solid dispersion may lead to enhanced diffusion of water molecules into the dispersion and consequently, an improved dissolution rate.[47]

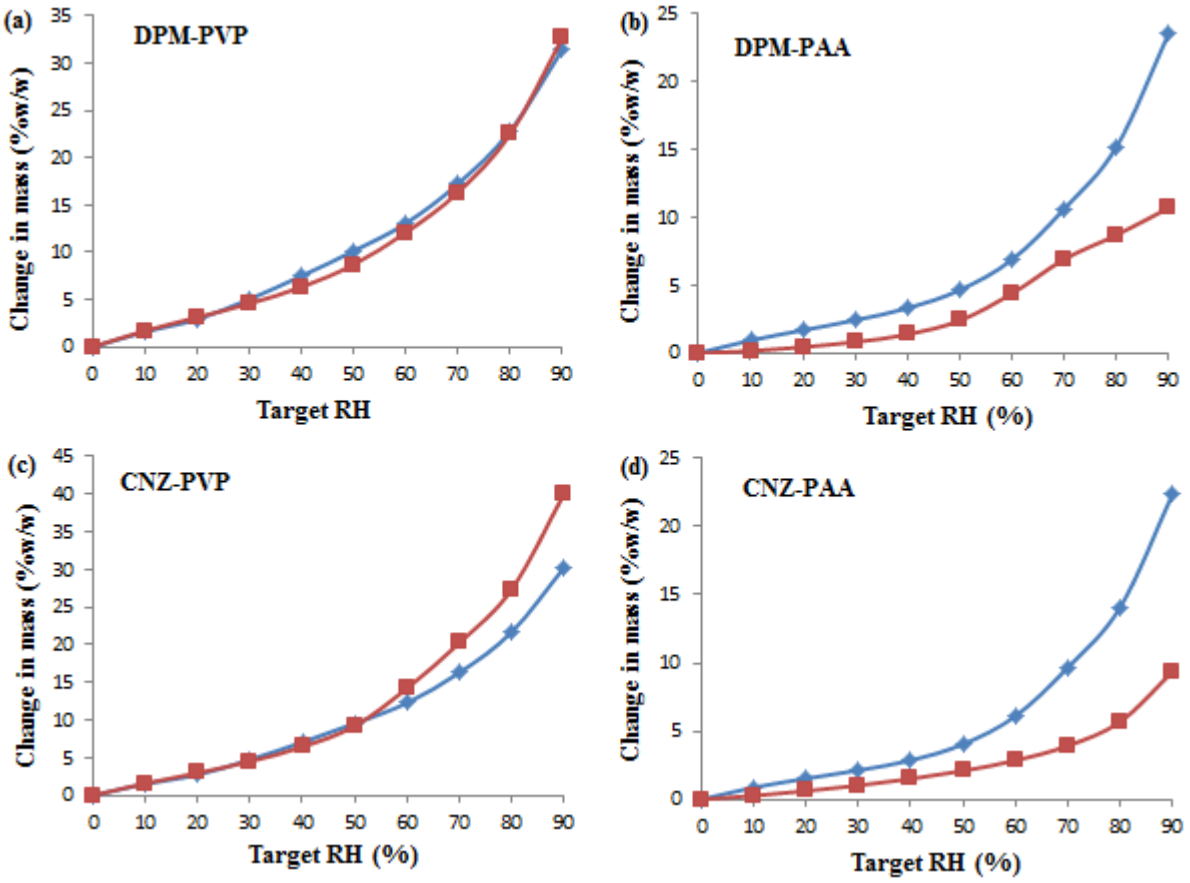

Figure 3.11. Predicted (blue line) and experimental (red line) water sorption isotherm of DPM and CNZ solid dispersion within PVP and PAA at 50% w/w drug loading

On comparing the predicted isotherms (Eq. 3.12) with the experimental sorption isotherms (at 50% w/w drug loading), a decrease in the equilibrium moisture sorption was generally observed (Figure 3.11). This can be attributed to the arrangement of drug-polymer structure (steric effect) and their mutual interactions, which may reduce the number and availability of polar functional groups that interact with moisture. The moisture sorption profile of each drug-polymer system at 10% w/w drug loading (data not shown) was positively deviated from the predicted values suggesting the possibility that the structural

properties of the drug-polymer combination required for moisture sorption is altered leading to a composition dependent moisture sorption.[48] However, it is not clear how molecular-level inhomogeneity would affect the behaviour of solid dispersions with temperature fluctuation or in the presence of moisture. Similar results were observed previously in case of valsartan solid dispersion with PVP.[46]

The deviation from the predicted moisture sorption isotherms shows that the nature of the water-drug, water-polymer and drug-polymer interactions affects the amount of moisture sorbed by the solid dispersion. Therefore, at this stage, it is useful to employ the ternary F-H model which includes these interactions and that allows one to calculate the composition dependent interaction parameter.[42] Firstly, to assess the interaction parameter between the water and each of the individual components we employed the F-H model for binary systems as shown below:

$$\ln\left(\frac{p}{p_o}\right) = ln\Phi_1 + \left(1 - \frac{1}{\chi_{12}}\right)\Phi_2 + \chi_{12}\Phi_2^2 \qquad \text{……..} \qquad (3.13)$$

where $\frac{p}{p_o}$ represents partial vapour pressure 1 and 2 represent the water and drug or polymer, respectively, and Φ represents the volume fraction. In this study, water-DPM, water-CNZ, water-PVP and water-PAA interaction parameters of 2.40, 3.93, 0.30 and 0.81, respectively, were obtained. A large χ value represents a weak interaction between the components, thereby explaining the decreasing order of moisture sorption PVP>PAA>DPM>CNZ as shown in Figure 3.10.[42 49] The lipophilic nature of dipyridamole (Log P = 3.71)[50] and cinnarizine (Log P = 5.71)[51] could have prevented their interaction with water. In the next step, we employed ternary F-H equation to include mutual interaction parameters between water-drug, water-polymer and drug-polymer as follows:[42 52]

$$\ln\left(\frac{p}{p_o}\right) = ln\Phi_1 + (\Phi_2 + \Phi_3) - \left(\frac{\Phi_2}{X_{12}}\right) - \left(\frac{\Phi_3}{X_{13}}\right) + \left[(\chi_{12}\Phi_2 + \chi_{13}\Phi_3)(\Phi_2 + \Phi_3)\right] - \left(\frac{\chi_{23}\Phi_2\Phi_3}{\chi_{12}}\right)$$

……. (3.14)

where 1,2 and 3 represents the water, drug and polymer, respectively. X_{12} and X_{13} are the number of molecules of drug and the number of segments (monomer units) of polymers per unit water molecule respectively.

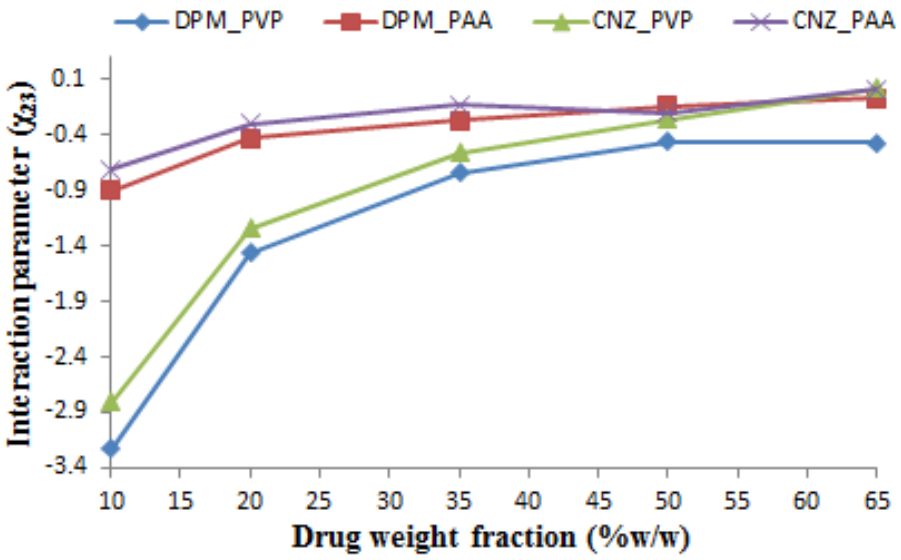

Figure 3.12. Drug-polymer interaction parameter (χ_{23}) from moisture sorption analysis

The values of χ_{23} obtained by the moisture sorption based calculation (at 90% target RH) are shown in Figure 3.12. The drug-polymer interaction parameter obtained by this method showed significant dependence on composition. The positive values of χ_{23} at 65% w/w CNZ loading in PVP and PAA implied weaker or unfavorable interaction.[53] However, lower DPM and CNZ contents give negative values suggesting good miscibility. This may be due to strong adsorption and better steric hindrance of the drugs by PVP and PAA which may result in better inhibition effect on drug precipitation. Though the values from the ternary moisture sorption analysis are not precisely comparable with the values obtained from the binary melting point depression analysis, an idea about the extent of composition dependent interaction can be obtained in the presence of water. This equation has been previously employed successfully to model moisture sorption and to calculate the F-H interaction parameter of sucrose-PVP and trehalose-PVP solid dispersions.[54] It has also been reported in the literature that the results obtained from ternary moisture sorption analysis are good predictors of dissolution performance.[53]

The moisture sorption based methodology provided the composition dependent χ values and to some extent predicts the fate of drug-polymer miscibility in the presence of moisture. With increased supersaturation, the solubility of drug in polymer decreases due to the sorbed moisture, known as the $\Delta\chi\ (=\ \chi_{12} - \chi_{13})$ effect. The large difference between interaction of water with hydrophobic DPM ($\chi_{12} = 2.40$) and CNZ ($\chi_{12} = 3.93$) and hydrophilic PVP ($\chi_{13} = 0.3$) and PAA ($\chi_{13} = 0.81$) can induce the composition dependent miscibility. Similar results of moisture induced phase separation of pharmaceutical

amorphous solid dispersions are reported previously.[52 55] This can be more pronounced at higher drug loading as the systems are already supersaturated. Thus, the interaction parameters calculated by this method are perhaps more qualitative.

Having compared the relative ability of PVP and PAA in stabilizing DPM and CNZ ASDs in the solid-state, the importance of drug-polymer interaction in generating and prolonging drug supersaturation in solution after dissolution is also of great importance. At this stage it could be hypothesized that PAA will stabilize the DPM and CNZ supersaturation more efficiently compared to PVP. This stabilizing polymeric effect in aqueous solution may be attributed to strong drug-polymer interaction that might prevent the association of drug molecules into a crystalline lattice. Obviously, at this stage, one could conclude that further investigation is required to understand the molecular level processes involved in the stabilization of amorphous drugs using polymers and to decode the dissolution behaviour and physical stability of ASD systems. These studies will form the basis of Chapter 4 and 5, respectively.

3.4. Conclusion

The work is important to develop a thorough theoretical methodology for the rational selection of polymers and the optimization of processing conditions for preparing amorphous solid dispersions. This study has presented a small scale thermal and moisture sorption based method that can be used in combination with binary and ternary F-H interaction theory to predict the suitability of polymers for the preparation of amorphous solid dispersions. The binary interaction parameter was successfully determined from the solubility parameter approach and melting point depression analysis for DPM-PVP, DPM-PAA, CNZ-PVP and CNZ-PAA systems. The solubility and miscibility of DPM was higher than CNZ in both of the polymers. The constructed phase diagrams were assessed at five different drug loadings using MDSC and XRD. The results clearly identified metastable and unstable drug weight fractions for each system. Furthermore, an indication of increased moisture sorption ability for the solid dispersions and a composition dependence of the drug-polymer interaction in the presence of moisture has been shown using dynamic vapor sorption. From a formulation point of view, an important question is whether F-H interaction theory (binary and ternary) can be used as a tool for the rational selection of polymers and to predict the stability of ASDs in both the dry and wet states. In the specific cases investigated here, a correlation was found between solid dispersion performance and F-H interaction parameter predictions, once kinetic effects were considered in addition to thermodynamic effects.

3.5. References

1. Lu J, Shah S, Jo S, Mjaumdar S, ryczke A, Kolter K, Langley N, Repka M. A. 2015. Investigation of phase diagrams and physical stability of drug-polymer solid dispersions. Pharm Dev Technol 20: 105-117.

2. Kaushal A, Gupta P, Bansal A. 2004. Amorphous drug delivery systems: molecular aspects, design and performance. Crit Rev Ther Drug Carrier Syst 21: 133-193.

3. Qian F, Huang J, Hussain M. 2010. Drug-polymer solubility and miscibility: Stability considerations and practical challenges in amorphous solid dispersion development. J Pharm Sci 99: 2941-2947.

4. Kaushal A, Gupta P, Bansal A. 2004. Amorphous drug delivery systems: molecular aspects, design and performance. Crit Rev Ther Drug Carrier Syst 21: 133-193.

5. Baghel S, Cathcart H, O'Reilly NJ. 2016. Polymeric amorphous solid dispersions: A review of amorphization, crystallization, stabilization, solid-state characterization and aqueous solubilization of biopharmaceutical classification system class II drugs. J Pharm Sci 105: 2527-2544.

6. Shamblin S. L, Zografi G. 1999. The effect of absorbed water on the properties of amorphous mixtures containing sucrose. Pharm Res 16: 1119-1124.

7. Matsumoto T, Zografi G. 1999. . Physical properties of solid molecular dispersions of indomethacine with poly(vinylpyrrolidone) and poly(vinylpyrrolidone-co-vinylacetate) in relation to indomethacin crystallization. Pharm Res 16: 1722-1728.

8. Janssen S, Mooter van der G. 2009. Review: Physical chemistry of solid dispersions. J Pharm Pharmacol 61: 1571-1586.

9. Rumondor A, Ivanisevic I, Bates S, Alonzo D, Taylor L. 2009. Evaluation of drug polymer miscibility in amorphous solid dispersion systems. Pharm Res 26: 2523-2534.

10. Tian Y, Booth J, Meehan E, Jones D, Li S, Andrews G. 2013. Construction of drug-polymer phase diagrams using Flory-Huggins interaction theory: Identifying the relevance of temperature and drug weight fraction to phase separation within solid dispersions. Mol Pharm 10: 236-248.

11. Verma S, Rudraraju V. 2014. A systematic approach to design and prepare solid dispersions of poorly water-soluble drug. AAPS Pharm Sci Tech 15: 641-657.

12. Joe J, Lee W. M, Park Y. J, Joe K. H, Oh D. H, Seo Y. G, Woo J. S, Yong C. S, Choi H. G. 2010. Effect of the solid-dispersion method on the solubility and crystalline property of tacrolimus. Int J Pharm 395: 161-166.

13. Guns S, Dereymaker A, Kayaert P, Mathot V, Martens J, Mooter van der G. 2011. Comparison between hot-melt extrusion and spray-drying for manufacturing solid dispersions of the graft copolymer of ethylene glycol and vinylalcohol. Pharm Res 28: 673-682.

14. Patterson J, James M, Forster A, Lancaster R, Butler J, Rades T. 2007. Preparation of glass solutions of three poorly water soluble drugs by spray drying, ,melt extrusion and ball milling. Int J Pharm 336: 22-34.

15. Zhao Y, Inbar P, Chokshi H, Malick A, Choi D. 2011. Prediction of the thermal phase diagram of amorphous solid dispersions by Flory-Huggins theory. J Pharm Sci 100: 3196-3207.

16. Pina M, Zhao M, Pinto J, Sousa J, Craig D. 2014. The influence of drug physical state on the dissolution enhancement of solid dispersions prepared via hot melt extrusion: A case study using olanzapine. J Pharm Sci 103: 1214-1223.

17. Osama A, Diak A, Jones D, Andrews G. 2012. Understanding the performance of melt extruded poly(ethylene oxide)-bicalutamide solid dispersions: Characterization of microstructural properties using thermal, spectroscopic and drug release methods. J Pharm Sci 101: 200-213.

18. Taylor L, Li T, Marsac P. 2009. Estimation of drug-polymer miscibility and solubility in amorphous solid dispersions using experimentally determined interaction parameters. Pharm Res 26: 139-151.

19. Coleman M, Serman C, Bhagwagar D, Painter P. 1990. A practical guide to polymer miscibility. Polymer 31: 1187-1203.

20. Hansen C. 1991. Hansen solubility parameter: A user's handbook. 2nd edition. Florida: CRC Press.

21. Burton A. Handbook of Solubility Parameter and Other Cohesion Parameters. 2nd edition. Florida: CRC Press.

22. Chokshi R, Sandhu H, Iyer R, Shah N, Malick W, Zia H. 2005. Characterization of physico-mechanical properties of indomethacin and polymers to assess their suitability for hot-melt extrusion process as a means to manufacture solid dispersion/solution. J Pharm Sci 94: 2463-2474.

23. Liu J, Cao F, Zhang C, Ping Q. 2013. Use of polymer combinations in the preparation of solid dispersions of a thermally unstable drug by hot-melt extrusion. Acta Pharm Sin B 3: 263-272.

24. Krevelen, V.; Nijenhuis, K. 2009. Properties of polymers: Their correlation with chemical structures, their numerical estimations and prediction from additive group contribution method. Chapter 7. Fourth Edition. Elsevier; Amsterdam.

25. Bansal K, Baghel U, Thakral S. 2015. Construction and validation of binary phase diagram for amorphous solid dispersion using Flory-Huggins Theory. AAPS Pharm Sci Tech. Ahead of print. DOI: 10.1208/s12249-015-0343-8

26. http://www.chemspider.com/Chemical-Structure.2997.html

27. Eerdenbrugh B, Vermant J, Martens J. A, Froyen L, Humbeek J, Augustijns P, Mooter G. 2009. A screening study of surface stabilization during the production of drug nanocrystals. J Pharm Sci 98: 2091-2103.

28. Khougaz K, Clas S. D. 2000. Crystallization inhibition in solid idspersions of MK-0591 and poly(vinylpyrrolidone) polymers. J Pharm Sci 89: 1325-1334.

29. Yu H, Huang A, Xiao C. 2006. Characteristics of konjac glucomannan and poly(acrylic acid) blend films for controlled drug release. J Appl Phys 100: 1561-1570.

30. Foster A, Hempenstall J, Tucker I, Rades T. 2001. Selection of excipients for melt extrusion with two poorly water soluble drugs by solubility parameter calculation and thermal analysis. Int J Pharm 226: 147-161.

31. Greenhalgh D, Williams A, Timmins P, York P. 1999. Solubility parameters as predictors of miscibility in solid dispersions. J Pharm Sci 88: 1182-1190.

32. Meng F, Trivino A, Prasad D, Chauhan H. 2015. Investigation and correlation of drug polymer miscibility and interactions by various approaches for the preparation of amorphous solid dispersions. Eur J Pharm Sci 71: 12-24.

33. Lu X, Weiss A. 1992. Relationship between glass transition temperature and the interaction parameter of miscible binary polymer blends. Macromol 25: 3242-3246.

34. Yuan L, Xu Y, Cai T, Jian S. 2003. Molecular simulation studies on the interaction between different polymers in aqueous solutions. Colloid Polym Sci 281: 66-72.

35. Djuris J, Nikolakakis I, Ibric S, Djuric Z, Kachrimanis K. 2013. Preparation of carbamazepine-soluplus solid dispersions by hot-melt extrusion, and prediction of drug-polymer miscibility by thermodynamic model fitting. Eur J Pharm Biopharm 84: 228-237.

36. Nishi T, Wang T. 1975. Melting point depression and kinetic effects of cooling on crystallization in poly(vinyledene fluoride)-poly(methyl methacrylate) mixtures. Macromol 8: 909-915.

37. Koningsveld R, Stockmayer W, Nies E. 2001. Polymer Phase Diagram: A text book. Oxford: Oxford University Press.

38. Huang Y, Dai W. 2014. Fundamental aspects of solid dispersion technology for poorly soluble drugs. Acta Pharm Sin B 4: 18-25.

39. Cheng S. 2008. Phase transitions in polymers: The role of metastable states. Amsterdam: Elsevier.

40. Bhugra C, Pikal M. 2007. Role of thermodynamic, molecular and kinetic factors in crystallization from the amorphous state. J Pharm Sci 97: 1329-1349.

41. Bhardwaj S, Arora K, Kwong E, Templeton A, Clas S, Suryanarayanan R. 2014. Mechanism of amorphous itraconazole stabilization in polymer solid dispersions: role of molecular mobility. Mol Pharm 11: 4228-37.

42. Crowley K, Zografi G. 2002. Water vapour absorption into amorphous hydrophobic drug/poly(vinylpyrrolidone) dispersions. J Pharm Sci 91: 2150-2165.

43. Tian B, Wang X, Zhang Y, Zhang K, Zhang Y, Tang X. 2015. Theoretical prediction of a phase diagram of solid dispersions. Pharm Res 32: 840-851.

44. Haress N. G. 2015. Cinnarizine Comprehensive Profile. In Profile of Drug Substance, Excipients, and Related Methodology, 1st ed.; Brittain, H. G.; Elsevier Pubilcation: Oxford, 7-8.

45. Jones D. S, Margetson D. N, McAllister M. S, Yu T, Shu Li, McCoy C. P, Andrews G. p. 2014. Thermodynamically stable amorphous drug dispersion in amorphous hydrophilic polymers engineered by hot-melt extrusion. Chem Eng Res Des 92: 3046-3054.

46. Puncochova K, Heng J, Beranek J, Stepanek F. 2014. . Investigation of drug-polymer interaction in solid dispersions by vapour sorption methods. Int J Pharm 469: 159-167.

47. Frizon F, Eloy J, Donaduzzi C, Mitsui M, Marchetti J. 2013. Dissolution rate enhancement of loratadine in polyvinylpyrrolidone K30 solid dispersion by solvent method. Powder Technol 253: 532-539.

48. Taylor L, Langkilde F, Zografi G. 2001. Fourier transform Raman spectroscopic study of the interaction of water vapour with amorphous polymers. J Pharm Sci 90: 888-901.

49. Rumondor A, Konno H, Marsac P, Taylor L. 2010. Analysis of the moisture sorption behaviour of amorphous drug-polymer blends. J Appl Polym Sci 117: 1055-1063.

50. http://www.accessdata.fda.gov/drugsatfda_docs/nda/99/20884_aggrenox_prntlbl.pdf

51. Raghuvanshi S, Pathak K. 2014. Recent advances in delivery systems and therapeutics of cinnarizine: A poorly water soluble drug with absorption window in stomach. J Drug Deliv 2014: 1-15.

52. Paudal A, Van Humbeek J, Mooter van der G. 2010. Theoretical and experimental investigation on the solid solubility and miscibility of naproxen in poly(vinylpyrrolidone). Mol Pharm 7: 1133-1148.

53. Chen Y, Liu C, Chen Z, Su C, Hageman M, Hussain M, Haskell R, Stefanski K, Qian F. 2014. Drug-polymer-water interaction and its implication for the dissolution performance of amorphous solid dispersions. Mol Pharm 12: 576-589.

54. Zhang Z, Zografi G. 2001. Water vapour absorption into amorphous sucrose-poly(vinylpyrrolidone) and trehalose-poly(vinylpyrrolidone) mixtures. J Pharm Sci 90: 1375-1385.

55. Tian B, Zhang L, Pan Z, Zhang Y, Tang X. 2014. A comparison of the effect of temperature and moisture on the solid dispersions: Aging and crystallization. Int J Pharm 475: 385-392.

CHAPTER 4. UNDERSTANDING THE GENERATION AND MAINTENANCE OF SUPERSATURATION DURING THE DISSOLUTION OF AMORPHOUS SOLID DISPERSIONS USING MODULATED DSC AND ^{1}H NMR

4.1. Introduction

Poor dissolution rate of drugs hampers drug formulation development process and several strategies are reported to improve the solubility of poorly soluble drugs.[1 - 4] Amorphization is an effective approach to improve the solubility and bioavailability of poorly water-soluble biopharmaceutical classification system (BCS) class II drugs.[5 - 21] In the solid-state, several mechanisms are involved in stabilizing an amorphous drug inside a polymer matrix such as drug-polymer interaction, antiplasticization, reduction in molecular mobility, reduction in chemical potential or higher activation energy for crystallization.[5 21 22 23] Once the amorphous drugs (or their solid dispersions) are dissolved in water, a supersaturated solution, in which the drug is apparently dissolved more than its solubility, can be formed.[7] While it is imperative to stabilize the amorphous drug against crystallization in the solid state to improve the shelf-life of the product, the prolongation of supersaturation achieved during dissolution is also of critical importance.[24 25]

The apparent solubility of the amorphous form is often theoretically predicted to be much higher than practically observed.[26] Generally, this discrepancy is mainly attributed to the rapid formation of a lower solubility crystalline form from the supersaturated solution.[27] In dissolution studies of amorphous solid dispersions (ASDs), it has been observed that the drug solution concentrations are still much higher than the crystalline drug solution concentration, indicating the supersaturated solutions are being generated.[28] Furthermore, the concentration-time profiles attained with ASDs may be higher than those achieved with the pure amorphous drug.[29] This suggests that certain polymers are able to maintain and prolong the supersaturation concentrations of amorphous drug. The experimentally achieved higher solution concentrations following dissolution of ASDs have been attributed to drug crystallization inhibition by the polymer from the supersaturated solution and increased equilibrium solubility of the crystalline drug due to solution complexation with the polymer.[7 30 31] Despite the aforementioned studies, prediction of the *in vitro* dissolution mechanism remains challenging due to the many interdependent processes that occur simultaneously upon wetting of the ASD in dissolution media such as the crystallization of drug or change in drug-polymer interaction within the undissolved yet hydrated ASD.[32 - 35]

In Chapter 2, we have shown the relative physical instability of the amorphous forms compared to their crystalline counterparts.[15] In Chapter 3, the impact of drug-polymer interaction and miscibility (binary and ternary Flory-Huggins theory) on the solid-state stability of ASDs have been shown.[21] Having compared the relative abilities of amorphous

DPM and CNZ to crystallize and the role of the polymer as a crystallization inhibitor in the solid state, this chapter aims to understand the molecular level dissolution behaviour of each ASD system and the effect of polymer type and concentration on the dissolution of poorly water-soluble model compounds, dipyridamole (DPM) and cinnarizine (CNZ). To date, there have been limited articles describing the drug-polymer interaction in a supersaturated solution although a large number of studies have been performed to examine the interaction in a solid dispersion. Furthermore, what has been published regarding molecular level understanding of drug-polymer interaction in a supersaturated solution is largely restricted to a few polymeric systems such as hydroxypropyl methyl cellulose acetate succinate, Eudragit 4155F or polyvinyl pyrrolidone vinyl acetate.[7 36 37 38] In light of this, an attempt has been made to broaden the overall understanding of the dissolution mechanism and the role of drug-polymer interaction in prolonging supersaturation.

Based on our solid-state drug-polymer interaction studies, using binary and ternary Flory-Huggins interaction parameter (chapter 3), it has been hypothesized that strong drug-polymer interactions and an anti-plasticization effect may also improve dissolution performance of ASDs and suggested that further investigation is required at a molecular level to decode the dissolution mechanism of ASD systems. Therefore, this chapter takes the previous work towards a better understanding of the dissolution behaviour of ASDs and the effect of drug-polymer interactions on the dissolution profile of ASDs. In this study, the dissolution profiles of DPM and CNZ from various ASDs are investigated. Furthermore, the dissolution profiles (drug concentration vs. time) are compared to supersaturated drug solution profiles (concentration vs. time) which are created by adding a concentrated solution of the drug to a dissolution medium in which an amount of the polymer has been previously dissolved. Thus, the *supersaturation parameter* and the *dissolution performance parameter* were used to assess the ability of different polymers to maintain drug supersaturation and to quantify the dissolution performance of different ASDs.[38] Additionally, solution state proton nuclear magnetic resonance (^{1}H NMR) spectroscopic studies were conducted to investigate the interaction between drug and polymer and to better understand the dissolution mechanism of the drug from the ASD.

4.2. Materials and Methods

4.2.1. Materials

Dipyridamole (DPM), cinnarizine (CNZ), polyvinyl pyrrolidone (PVP) K30 and polyacrylic acid (PAA) were purchased from Sigma Aldrich, Ireland. All reagents were of analytical grade and used without further purification. The chemical structure and key physicochemical properties of the model drugs and polymers used in this study are summarized in Figure 1.13 and Table 4.1, respectively.

Table 4.1. Physicochemical properties of model drugs and polymers

	Molecular weight (g/mol)	ΔH_f **(kJ/mol)[a]**	T_m **(°C)[a]**	T_g **(°C)[a]**	**Log P [b]**	**pK$_a$**
DPM	504.63	29.06	168.11	37.44	3.71	6.4[39]
CNZ	368.51	38.33	121.25	5.86	5.71	8.4[40]
PVP	40000	-		164.13		
PAA	450,000	-		130.61		

[a]Values obtained from DSC (n=3), [b]Values obtained from literature[21]

4.2.2. Preparation of amorphous solid dispersion

The spray dried solid dispersions were prepared using a Pro-C-epT 4M8-TriX spray drier (Zelzate, Belgium) with a bifluid nozzle. The spray drying solutions were prepared by dissolving the drug and polymer in methanol at 20, 50 and 80% w/w drug concentration within the ASD. The key processing parameters are feed concentration (10% w/v in methanol solution), spray rate (6 mL/min), nozzle size (0.2 mm), atomization air flow rate (5 L/min), inlet temperature (80 $\pm$ 5°C), outlet drying temperature (50 $\pm$ 5°C) and drying air rate (100 $\pm$ 10 L/min). The spray dried solid dispersions were collected using a small cyclone separator and stored in a vacuum desiccator at room temperature for further analysis. Similar methodology has been used to produce amorphous drug.

4.2.3. Thermogravimetric analysis (TGA)

The residual solvent content of the prepared solid dispersions was assessed using a TGA Q50 (TA Instruments Corp., Elstree, Herts, U.K.). Samples were heated at 10°C/min from 25 to 200°C. During all TGA experiments nitrogen was used as the purging gas at 50 mL/min. All analyses were performed in duplicate.

4.2.4. Modulated Differential scanning calorimeter (MDSC)

Thermal analysis was performed using a MDSC Q2000 (TA Instruments Corp., Elstree, Herts, U.K.) equipped with an electrical cooling accessory. Enthalpy, temperature

and heat capacity calibrations were carried out using high-purity indium and sapphire standards as recommended by the instrument supplier. Samples between 3 and 10 mg were accurately weighed and placed into crimped aluminium pan with a pin hole. Nitrogen, at a flow rate of 50 mL/min, was used as the purge gas. The modulation parameters chosen to ensure separation of reversing and non-reversing events was ± 0.53 °C/40s at a ramp rate of 5 °C/min. Data analysis was performed using Universal Analysis software (TA Instruments Corp., Elstree, Herts, U.K.). All analyses were performed in duplicate.

4.2.5. X-Ray diffractometry (XRD)

The powdered amorphous solid dispersions were analysed using an X-ray diffractometer (X'pert MPD PRO PANalytical, Almelo, Netherlands) using the following parameters: Cu radiation (wavelength 1.540598 Å) , Ni-filter, voltage 40 kV, current 40 mA, 2θ range of 5-50°C, step size 0.008° and scan rate 3.2°/min

4.2.6. Effect of polymer on the solubility of crystalline drug

The equilibrium solubility of crystalline DPM and CNZ, in the presence and absence of polymer, was measured at 37.0 ±0.2 °C using phosphate buffer solutions (pH 6.8) (PBS 6.8). 25 mg of crystalline DPM or CNZ was dispersed in 500 mL of PBS 6.8, in which 500 or 1000 mg of polymer (PVP or PAA) had been previously dissolved, leading to a final PVP or PAA concentration of 1.0 and 2.0 mg/mL, respectively. The solution was stirred at 100 rpm using a United State Pharmacopeia (USP) II paddle apparatus (Varian VK 7010 L1168, Santa Clara, United State). Samples were collected after 24 h and centrifuged (Hettich Centrifuge, Tuttlingen, Germany) for 5 min at 15000 rpm. The concentrations of DPM and CNZ were determined using a UV-Vis spectrophotometer (UV-2401PC, Shimadzu Corp., Duisburg, Germany) and a standard calibration curve that was linear over the concentration range (0.5-20 μg/mL). The wavelengths selected were 292 nm for DPM and 251 nm for CNZ. No interference from PVP or PAA on the DPM and CNZ assay was observed at these respective wavelengths. The solubility of DPM and CNZ in PBS 6.8 in the absence of polymer was also evaluated. All measurements were carried out in duplicate.

4.2.7. Effect of polymer on maintaining and prolonging drug supersaturation

A concentrated solution of DPM and CNZ in methanol was prepared by dissolving 25 mg of crystalline DPM and CNZ in 10 mL methanol. This solution was subsequently added to 500 mL of PBS 6.8 at 37.0 ± 0.2 °C. This generated an initial drug concentration of 50 μg/mL in PBS 6.8, into which 100, 25 or 6.25 mg of polymer (PVP or PAA) had been

previously dissolved, leading to final polymer concentration of approximately 200, 50 and 12.5 µg/mL, respectively. The solution was stirred at 100 rpm using a USP II paddle. 2 mL samples were withdrawn from each vessel at predefined intervals (5, 10, 15, 30, 60, 120, 180, 240, 300 and 360 min) and centrifuged for 5 min at 15000 rpm. At each time point the same volume of fresh medium was replaced. The concentrations of DPM and CNZ were determined using a UV-Vis spectrophotometer. The same experiments were performed in PBS 6.8 in the absence of any polymer. All measurements were carried out in duplicate. The ability of different polymers to maintain and prolong DPM and CNZ supersaturation in PBS 6.8 can be quantified by using the *supersaturation parameter* (SP) as described by Chen *et. al.*[38] The concentration-time curve of a drug supersaturated in aqueous medium in the presence ($C_iC_f^{poly}$) and absence ($C_iC_f^{no\ poly}$) of polymers is shown in Figure 4.1. The ideal situation where no drug crystallization from supersaturated solution occurred is represented by curve $C_iC_i^{'}$. The s*upersaturation parameter* (SP) is defined as:

$$Supersaturation\ parameter = \frac{Area_{C_iC_f^{no\ poly}C_f^{poly}}}{Area_{C_iC_f^{no\ poly}C_i'}} \qquad \ldots\ldots\ldots \qquad (4.1)$$

where $area_{C_iC_f^{no\ poly}C_f^{poly}}$ is the integral area between curve $C_iC_f^{no\ poly}$ and $C_iC_i^{'}$ and can be theoretically regarded as "the amount of drug crystallized over time" in the absence of polymer. When polymer was employed to maintain drug supersaturation, curve $C_iC_f^{no\ poly}$ was elevated to curve $C_iC_f^{poly}$, thus $area_{C_iC_f^{no\ poly}C_f^{poly}}$, the integral area between curves $C_iC_f^{no\ poly}$ and $C_iC_f^{poly}$, could provide theoretical estimation of the amount of drug whose crystallization was inhibited by a certain type and amount of polymer. Thus, the SP is a dimensionless quantity and its value ranges from 0 to 1, where 0 represents no supersaturation maintenance power at all while 1 signifies complete inhibition of drug crystallization from aqueous solution. Practically SP is dependent on drug/polymer structure and concentration.

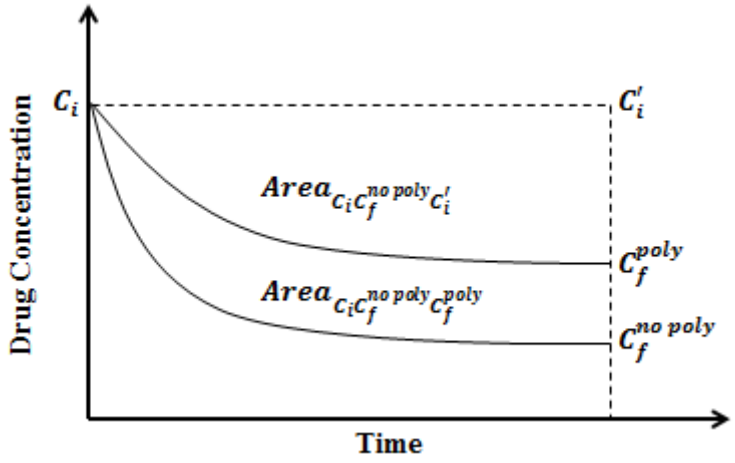

Figure 4.1. Theoretical illustration of the concentration-time curve of supersaturated drug solution in aqueous medium in the presence ($C_iC_f^{poly}$) and absence of polymers ($C_iC_f^{no\ poly}$)

4.2.8. In-vitro dissolution study of solid dispersion

The dissolution rate of DPM and CNZ from various powdered ASDs was measured using the USP II paddle method. Samples containing 25 mg of DPM and CNZ were added to 500 mL of PBS 6.8 at 37.0 ± 0.2 °C. The solution was stirred at 100 rpm using a USP II paddle apparatus. 2 mL samples were withdrawn from each vessel at predefined intervals (5, 10, 15, 30, 60, 120, 180, 240, 300 and 360 min) and centrifuged for 5 min at 15000 rpm. At each time-point the same volume of fresh medium was replaced. The concentration of DPM and CNZ was determined using a UV-Vis spectrophotometer. All measurements were carried out in duplicate.

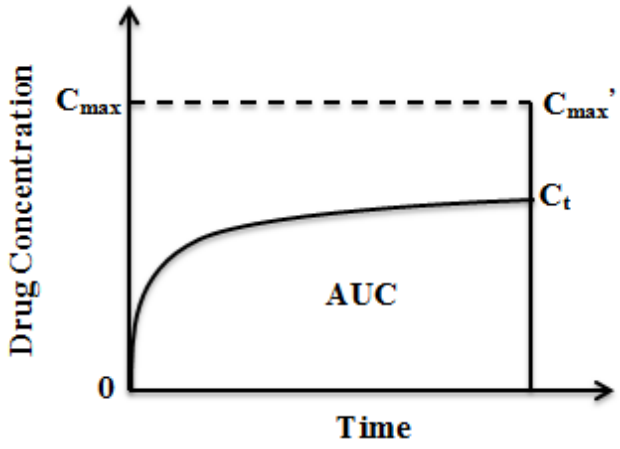

Figure 4.2. Theoretical illustration of dissolution profile of ASD where AUC_{actual} is the integral area under the curve $0C_t$ and $AUC_{theoretical}$ is the integral area under the curve $C_{max}C_{max}$'

Figure 4.2 shows a theoretical dissolution profile of an ASD where C_{max}' represents the maximum drug concentration achieved by complete dissolution of the drug in the dissolution medium. The area under the curve (AUC) is an indicator of dissolution performance *i.e.* higher AUC represents better dissolution performance. The theoretical maximum AUC is defined by the AUC of line $C_{max}C_{max}'$ which signifies that the drug concentration reached the C_{max} immediately after dosing and this concentration was maintained consistently throughout the dissolution time. The dissolution performance of various ASDs in PBS 6.8 have been compared quantitatively by using the *dissolution performance parameter* (DPP) as described by Chen *et al:*[38]

$$Dissolution\ performance\ parameter = \frac{AUC_{actual}}{AUC_{theoretical}} \quad \ldots\ldots\ldots \quad (4.2)$$

where AUC_{actual} and $AUC_{theoretical}$ are the integrated areas under curves $0C_t$ and $C_{max}C_{max}'$, respectively. DPP is a dimensionless parameter whose value range between 0 and 1, where 0 indicates no dissolution and 1 represents an ideal complete dissolution without crystallization.

4.2.9. Solution state Nuclear Magnetic Resonance (NMR)

In order to understand the molecular mechanism of the drug-polymer interaction, ^1H NMR spectra were recorded on a Jeol ECX-400 spectrometer operating at 400 MHz. The measurements were performed at 40°C in dimethylsulfoxide (DMSO-d6) using tetramethylsilane (TMS) as an internal standard. Initial trials were performed using D_2O. However, the poor solubility of the model drugs in D_2O leads to weak signals and the chemical shifts were not clear. Therefore, DMSO has been selected due to its high dielectric constant and hydrophilic nature. Both drugs and polymers were completely soluble in DMSO. It is important to mention here that DMSO is used only for qualitative purpose to obtain a general representation of drug-polymer interaction in solution. The NMR spectrum was recorded for the pure drugs, polymers and their ASDs (at 20%, 50% and 80% w/w drug weight fraction).

4.3. Results and Discussions

4.3.1. Solid State Characterization of Spray Dried dispersions

In a standard TGA ramp test all the spray dried ASD systems showed a residual solvent content of ≤ 5% w/w. As shown in Figure 4.3 and 4.4, pure DPM and CNZ showed a distinctive crystalline drug pattern. No DPM crystal peaks were detected in the XRD spectra of spray dried dispersions with PVP and PAA at 20 and 50% w/w drug loading. The XRD

spectra at high DPM loading (80% w/w) within PVP and PAA displayed characteristic crystalline DPM peaks, indicating the presence of drug crystals within the ASD. XRD spectra of CNZ dispersions (at 20% w/w drug loading) with PVP and PAA displayed a halo pattern. Interestingly, at 50% w/w CNZ loading, only PAA was able to produce complete amorphous dispersion whereas the XRD spectra of the PVP dispersions displayed the crystalline CNZ peaks. At 80% w/w CNZ loading the XRD profile of PVP and PAA dispersions showed the presence of CNZ crystals. These XRD results are in good agreement with the MDSC findings (data not shown).

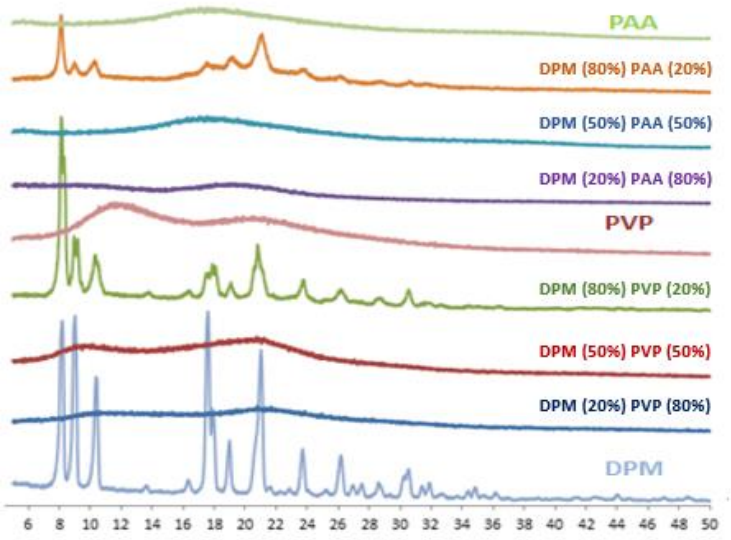

Figure 4.3. XRD spectra of DPM solid dispersions; % values represent drug or polymer weight fraction within ASD

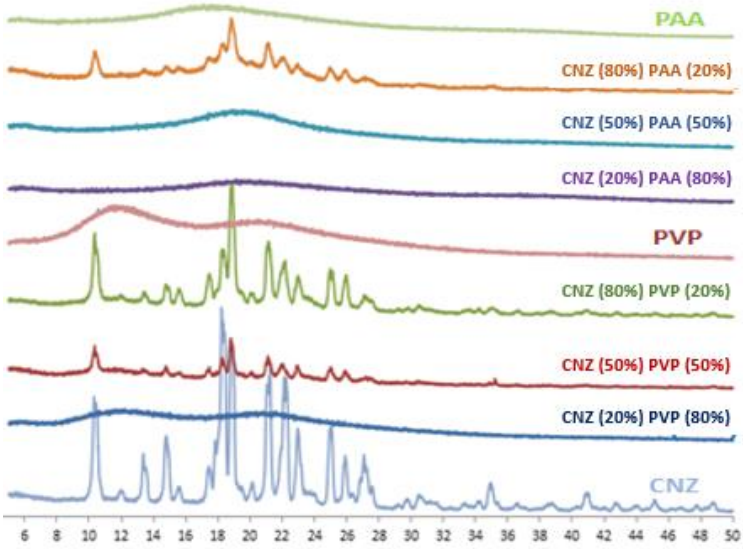

Figure 4.4. XRD spectra of CNZ solid dispersions; % values represent drug or polymer weight fraction within ASD

4.3.2. Equilibrium solubility of crystalline drug in the polymeric solution

The equilibrium solubility of the crystalline drug in the presence of concentrated polymeric solutions can help explain the mechanism of dissolution of a spray dried solid dispersions.[41] To determine the solubilizing power of PVP and PAA, the equilibrium solubility of crystalline DPM and CNZ in 500 mL PBS 6.8 at 1 mg/mL and 2 mg/mL of each of the respective polymers was determined and compared to the equilibrium solubility of DPM and CNZ in PBS 6.8 in the absence of polymer. It should be noted that this polymer concentration far exceeds the solution concentration described in drug supersaturation and in-vitro dissolution studies (Section 4.2.7 and 4.2.8, respectively). The high polymer to drug ratios was chosen to represent the conditions wherein it would be most likely to increase the crystalline drug solubility.

As shown in Table 4.2, the equilibrium solubility of DPM increases (~1.22-fold) in the presence of PVP at 1 and 2 mg/mL. In contrast, PAA has a high solubilizing effect on DPM. The crystalline DPM solubility increased 1.5 and 2.9-fold at 1 and 2 mg/mL of PAA, respectively. The equilibrium solubility of CNZ did not change significantly when 1 mg/mL of PVP or PAA was present in the PBS 6.8, however there was a significant increase in the solubility of crystalline CNZ (~1.84-fold) when 2 mg/mL of PVP and PAA was present. These results indicate that highly concentrated polymer solutions have a solubilizing effect on CNZ which is otherwise practically insoluble in PBS 6.8. Furthermore, PAA has a relatively higher solubilizing efficiency for DPM compared to PVP whereas both polymers have nearly equal solubilizing effect on CNZ (Table 4.2). Previous studies have shown that the solubility of poorly soluble drugs was improved significantly in aqueous solution in which polymeric carriers had been dissolved due to the formation of weakly soluble complexes.[7 42]

Table 4.2. Equilibrium solubility of crystalline DPM and CNZ in PBS 6.8 with or without dissolved polymer at 37 ± 0.2 °C

Polymer concentration (mg/mL)	Equilibrium solubility in PBS 6.8 (µg/mL) (n = 2)	
	DPM	**CNZ**
Without polymer	6.88 ± 0.19	2.35 ± 0.17
PVP		
1.0	8.18 ± 0.17	2.61 ± 0.06
2.0	8.59 ± 0.03	4.35 ± 0.03
PAA		
1.0	10.04 ± 0.21	2.67 ± 0.15
2.0	19.76 ± 0.11	4.49 ± 0.02

4.3.3. Polymer effect in maintaining and prolonging drug supersaturation in PBS 6.8

The inhibitory effects of PVP and PAA on the crystallization of DPM and CNZ from supersaturated solution were evaluated by adding a concentrated solution of DPM and CNZ in methanol (25 mg in 10 mL) to PBS 6.8 (in which the polymers had been pre-dissolved) and examining the drug solution concentration as a function of time. Figure 4.5 and 4.6 shows the results for DPM and CNZ respectively, obtained at polymer solution concentrations of 200, 50 and 12.5 µg/mL. These concentrations correspond to the polymer solution concentration that would be produced by the complete dissolution of solid dispersions containing 80, 50 and 20% w/w polymer respectively. For reference, results obtained for PBS 6.8 in the absence of polymer are also shown. As shown in Figure 4.5 and 4.6, in the absence of polymer, both drugs crystallized immediately (within 5 mins) and the concentrations of DPM and CNZ rapidly diminish until they reach values close to the equilibrium solubility of crystalline drug. This rapid decrease in concentration suggested that the crystallization tendency of pure DPM and CNZ from supersaturated solution in PBS 6.8 is very high. These results were consistent with those reported previously by Konno *et al.,* wherein rapid recrystallization of felodipine was observed in the absence of polymeric excipients.[6] By comparison, the polymer solutions were found to have a stabilizing effect on the supersaturation level of the dissolved drugs.

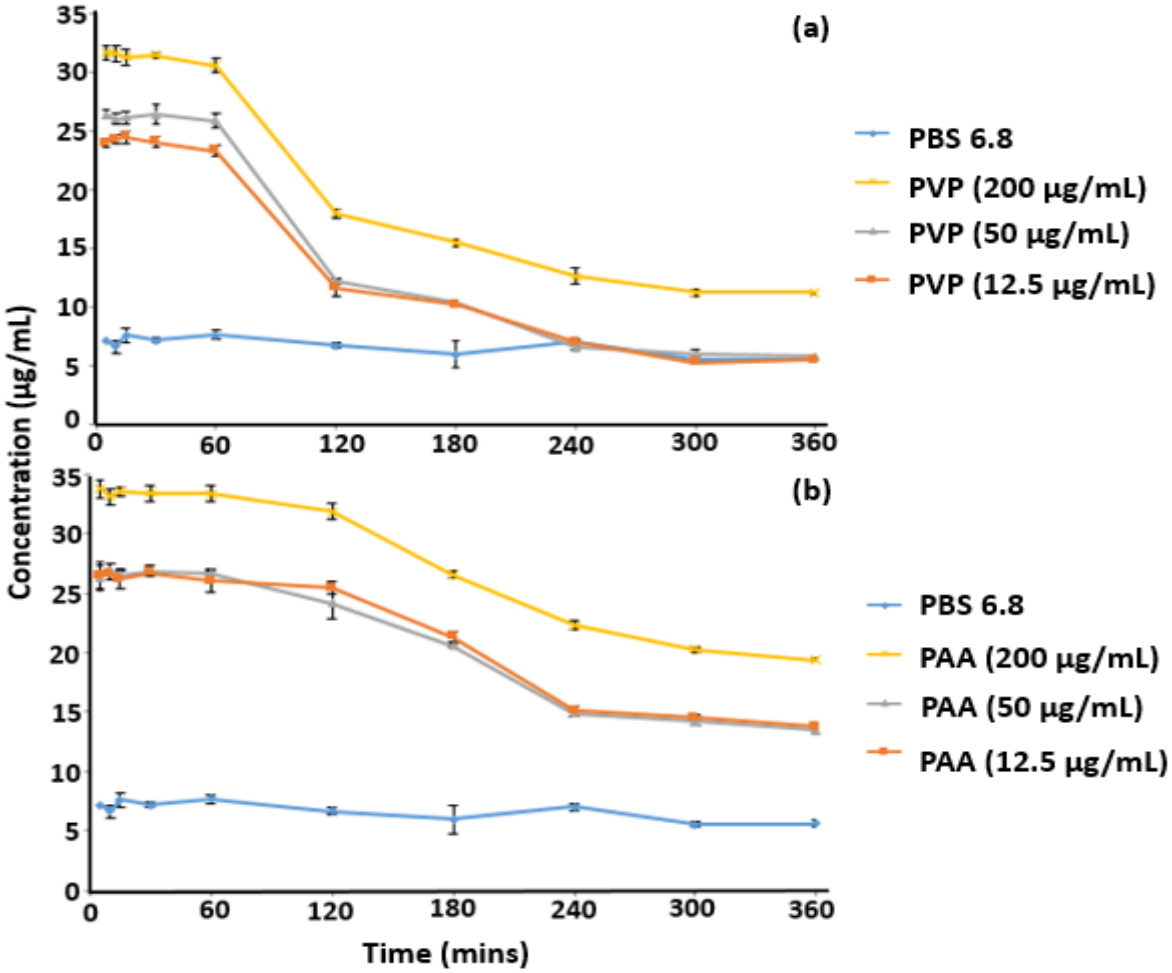

Figure 4.5. Supersaturation profile of DPM in PBS 6.8 with dissolved PVP (a) and PAA (b) at 37°C. The initial DPM concentration in each solution was 50 µg/mL; Each point represents mean ± SD; n = 2

The initial drug concentration, measured 5 min after addition of a concentrated solution of DPM and CNZ, were significantly higher in PBS 6.8 containing 200 µg/mL of PVP than other lower concentrations of PVP (50 and 12.5 µg/mL) as shown in Figure 4.5 (a) and 4.6 (a). Conversely, there was only a small difference between the DPM and CNZ concentration achieved in PBS 6.8 containing PVP concentrations 50 and 12.5 µg/mL. These results show that PVP has significant inhibitory effect at all concentration on DPM and CNZ recrystallization from their supersaturated solutions in PBS 6.8. After 360 min, only the 200 µg/mL of PVP concentration in PBS 6.8 was able to maintain significantly higher DPM solution concentration whereas the drug concentration, for lower PVP concentration, approximated to the equilibrium solubility of crystalline DPM (Table 4.2). On the other hand, after 360 min, the differences in CNZ concentrations were still apparent (at all PVP concentration) which is much higher than equilibrium solubility of crystalline CNZ (Table 4.2) and were also a function of PVP concentration.

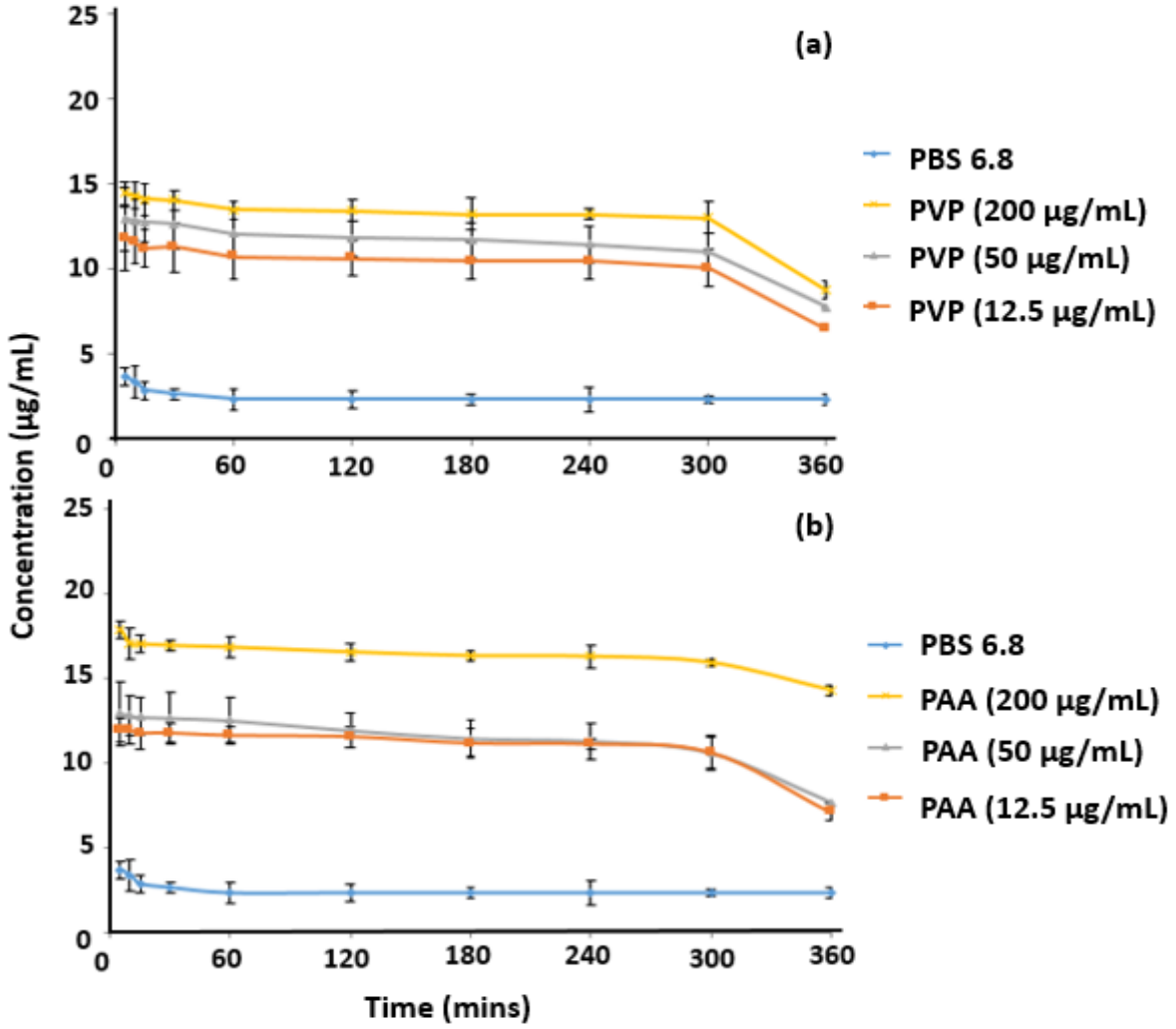

Figure 4.6. Supersaturation profile of CNZ in PBS 6.8 with dissolved PVP (a) and PAA (b) at 37°C. The initial CNZ concentration in each solution was 50 µg/mL; Each point represents mean ± SD; n = 2

Dispersions of PAA performed better in maintaining higher supersaturation level of DPM and CNZ solution in PBS 6.8 (Figure 4.5 (b) and 4.6 (b)). The concentration of DPM and CNZ remaining in solution, 5 min after addition of a supersaturated concentration of the drug, was significantly higher for solutions containing PAA than buffer containing no polymer. Interestingly, the initial concentration, achieved 5 min after addition of a concentrated DPM and CNZ solution, was significantly higher in PBS 6.8 containing 200 µg/mL of PAA than other lower concentrations of PAA. Moreover, no significant difference was observed between the DPM and CNZ concentration achieved after 5 min in PBS 6.8 containing 50 and 12.5 µg/mL of PAA. However, PAA at the lower concentration was also effective in maintaining DPM and CNZ concentrations above their equilibrium solubility in crystalline form (Table 4.2). It is clear that the highest concentration of PAA (200 µg/mL) maintained significantly higher levels of DPM and CNZ in solution compared to PVP at same

concentration in PBS 6.8. By comparison, the difference was not very significant at lower PAA concentration when compared to PVP, at a similar concentration, in maintaining DPM and CNZ supersaturation. The differences in drug concentration in solution (compared to crystalline drug solubility) were still apparent after 360 min and were also a function of PAA concentration. Similarly, the inhibition of celecoxib and felodipine recrystallization from a supersaturated drug concentration was dependent upon polymer concentration in phosphate buffer.[6 7] The comparison of inhibitory effect of PVP and PAA (Figure 4.5 and 4.6) suggests that PAA, at 200 µg/mL, was more efficient in stabilizing DPM and CNZ once a supersaturated concentration was achieved. The lower concentration of PVP and PAA performed equally well in prolonging DPM and CNZ crystallization from supersaturated solution in PBS 6.8.

Amorphous drug solubility: It has been reported that amorphous drug offers a higher apparent solubility as compared to their crystalline counterpart due to their higher thermodynamic properties (enthalpy, entropy, free energy and volume).[5 6 7] The relative increase in solubility can be estimated using the following equation:[43]

$$\Delta G_T^{a,c} = -RTln\ (\sigma_T^a/\sigma_T^c) \qquad \ldots\ldots\ldots \qquad (4.3)$$

where (σ_T^a/σ_T^c) is the solubility ratio of the amorphous and crystalline forms, $\Delta G_T^{a,c}$, the difference in the free energy, R is the universal gas constant and T is the absolute temperature. It is important to mention here that Eq. 4.3 is used only for apparent amorphous drug solubility and does not predict exact amorphous drug solubility. Nevertheless, when combined with the in-vitro dissolution results, they help build a better understanding of the amorphous drug solubility profile from their solid dispersions.

An estimate of the free energy difference between the two forms can be obtained from the Hoffman equation if the heat of fusion (ΔH_f) and the melting temperature (T_m) of the crystalline form is known as shown below:[44]

$$\Delta G_T^{a,c} = \Delta H_f \frac{(T_m - T)T}{T_m^2} \qquad \ldots\ldots\ldots \qquad (4.4)$$

It is clear from Eq. 4.4 that the higher the heat of fusion and the melting temperature of a drug, the greater the solubility increase that would be expected from the amorphous form of the drug. However, the experimentally determined apparent solubility of the amorphous APIs remains lower than the theoretically predicted values in most cases.[45] The amorphous form

dissolves to produce the supersaturated solution but this is followed by a decrease in concentration due to recrystallization. The nucleation rate (J), according to classical nucleation theory, is dependent on many factors as shown below:[46]

$$J = A \exp\left[-\frac{16\pi\gamma^3 v^2}{3k^3T^3(\ln S)}\right] \quad \ldots\ldots\ldots \quad (4.5)$$

where v is the molar volume, γ is the interfacial tension, k is the Boltzman constant, T is the absolute temperature and S is the supersaturation defined as the ratio of the solution concentration to the equilibrium solubility. Thus, it is clear from Eq. 4.5 that the nucleation rate is strongly dependent on the degree of supersaturation that is present. This shows that a high theoretical solubility ratio for an amorphous-crystalline system would have a greater tendency to nucleate and crystallize from solution making it difficult to achieve the theoretically predicted concentration experimentally. Using Eq. 4.4 and thermodynamic information calculated in our previous study for DPM and CNZ, amorphous DPM and CNZ should yield maximum solution concentration of approximately 10 and 12 times that of the crystalline form, respectively.[5] Thus at 37 °C, concentrations of 68.8 μg/mL (DPM) and 28.2 μg/mL (CNZ) could theoretically be achieved based on the equilibrium solubility measured for crystalline DPM and CNZ (Table 4.2). On the contrary, as shown in Figures 4.5 and 4.6, when the DPM and CNZ are introduced into polymer solution at a concentration of 50 μg/mL, the drug concentration decreases rapidly indicating rapid crystallization of DPM and CNZ. This suggests that the dissolution of amorphous DPM and CNZ is followed by rapid crystallization.

4.3.4. In-vitro dissolution of spray dried solid dispersion

Figure 4.7 and 4.8 shows the dissolution profiles of DPM and CNZ ASDs containing different weight fractions of PVP and PAA. Dissolution from DPM and CNZ ASDs resulted in higher solution concentrations than the equilibrium solubility of crystalline DPM and CNZ (Table 4.2), indicating that supersaturated solutions were generated and maintained for up to 360 min at all drug/polymer ratio. Furthermore, the supersaturation level increases with increasing polymer load within the ASDs. However, the maximum drug concentration in solution is still below the maximum theoretical amorphous drug solubility values calculated earlier (68.8 μg/mL for DPM and 28.2 μg/mL for CNZ). As discussed previously, this could be due to rapid crystallization of some of the drug in the solution. Nonetheless, the drug solubility increases significantly at all polymer concentrations which could arise from dissolution of the ASD and stabilization of drug supersaturation by the polymer, and/or by an

increase in the DPM and CNZ equilibrium crystalline solubility due to complexation with polymer in the solution.[6]

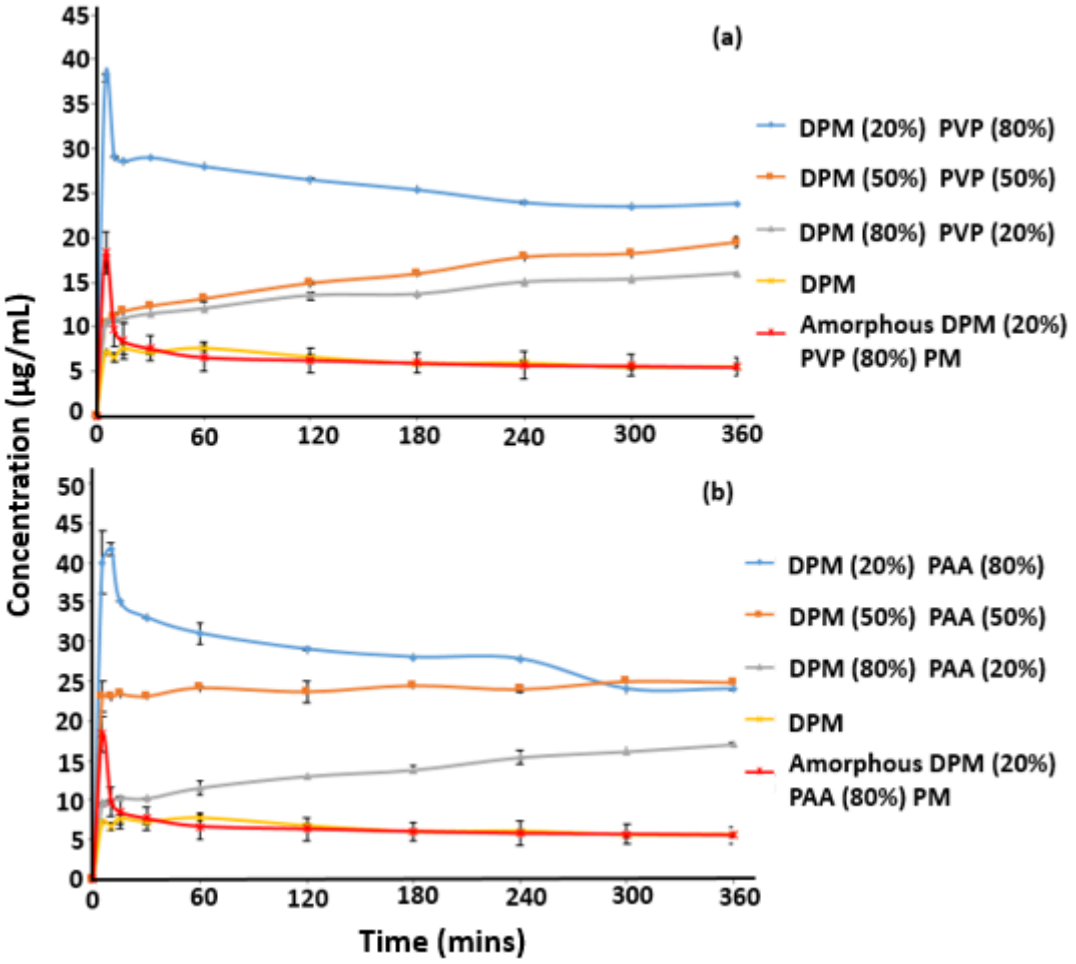

Figure 4.7. Dissolution profile of DPM solid dispersion with PVP (a) and PAA (b) in PBS 6.8 at 37°C; % values represent polymer weight fraction within ASD, samples equivalent to 25 mg of drug was added to PBS 6.8; PM means Physical Mixture; Each point represents mean ± SD; n = 2

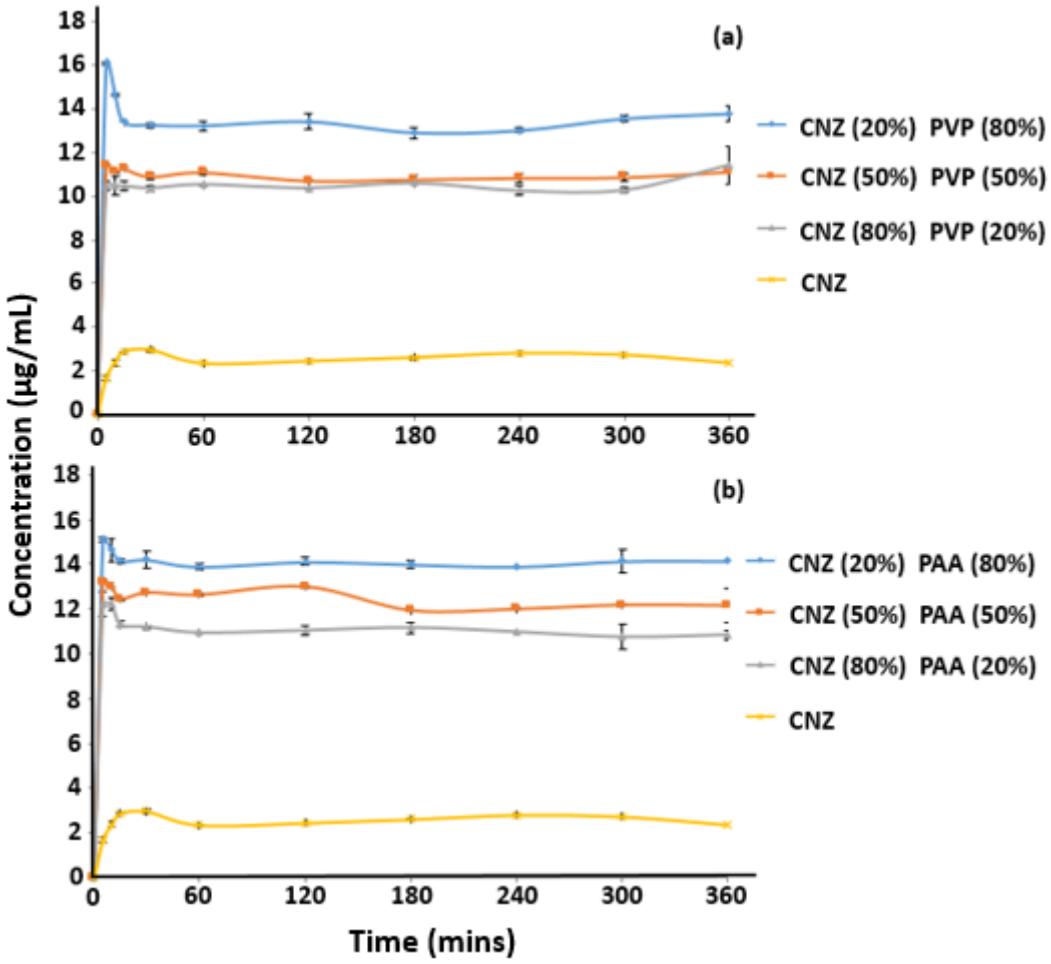

Figure 4.8. Dissolution profile of CNZ solid dispersion with PVP (a) and PAA (b) in PBS 6.8 at 37°C; % values represent polymer weight fraction within ASD, samples equivalent to 25 mg of drug was added to PBS 6.8; Each point represents mean ± SD; n = 2

In Figure 4.9, the data from the dissolution studies has been replotted to enable a comparison between solid dispersions containing different polymers at the same weight fraction. While the PAA has a higher MW than the PVP (450 kDa vs. 40 kDa respectively), they are present in low concentrations in the dissolution media (max. 200 µg/l) and therefore the effect of solution viscosity is expected to be negligible. The supersaturation parameter (SP) and dissolution performance parameter (DPP) values are reported in Table 4.3. At a very high polymer loading (80% w/w) within the dispersion there was minimal differences between the DPM supersaturation level achieved with PVP and PAA during dissolution. Also, there was no difference with CNZ concentrations at 80% w/w polymer loading and both polymers maintained nearly equal CNZ solution concentration at all time. At 50% w/w polymer loading, PAA maintained a much higher level of DPM concentration in solution

when compared to PVP and the difference was also apparent with CNZ, where PAA performed marginally better than PVP in maintaining CNZ supersaturation. On further reducing the amount of polymer to 20% w/w in the solid dispersion, both the polymers performed equally well in maintaining DPM and CNZ supersaturation.

Table 4.3. Table representing glass transition temperature, phase behaviour, solubility and supersaturation/dissolution performance parameter of DPM and CNZ with PVP and PAA; % represents drug weight fraction within ASD

Drug loading	T_g (GT equation) (°C)[21]	T_g experimental (°C)	No. of Phases	Concentration, 6 hr (µg/mL)		SP	DPP
PVP				**PM**	**SD**		
DPM 20%	135.36	147.98	1	7.16	23.85	0.58	0.55
DPM 50%	96.48	113.4	1	6.23	19.50	0.55	0.21
DPM 80%	61.96	102.7/152.47	3	6.95	15.98	0.52	0.20
PAA							
DPM 20%	110.61	149.88	1	7.98	24.44	0.60	0.62
DPM 50%	82.88	148.39	1	7.43	24.87	0.57	0.40
DPM 80%	57.54	117.73	2	7.12	17.03	0.57	0.18
PVP							
CNZ 20%	118	106.54	1	2.39	13.77	0.36	0.25
CNZ 50%	66.53	57.11	2	2.36	11.13	0.35	0.20
CNZ 80%	28.77	79.43	2	2.07	11.42	0.33	0.18
PAA							
CNZ 20%	95.63	110.37	1	2.79	14.14	0.37	0.26
CNZ 50%	55.43	128.11	1	2.38	12.15	0.34	0.23
CNZ 80%	25.11	102.51	2	2.01	10.84	0.33	0.21

GT represents Gordon-Taylor equation and PM represents physical mixture of crystalline drug and polymer; No. of phase represents the presence of uniformly mixed drug-polymer system with one T_g (1), drug-polymer system with one amorphous and one crystalline domain (2) and presence of two amorphous domains as well as crystalline domain (3); SP and DPP are supersaturation and dissolution performance parameter, respectively; n = 2

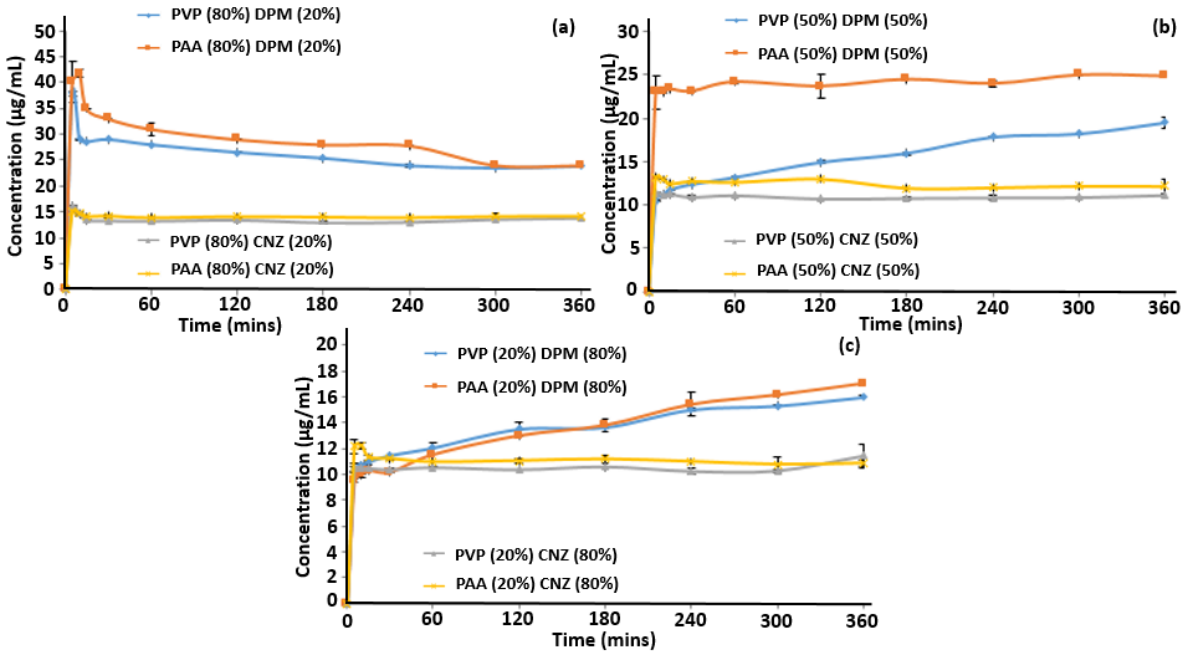

Figure 4.9. Dissolution profile of DPM and CNZ at 80% (a), 50% (b) and 20% (c) w/w of polymer loading in PBS 6.8; Each point represents mean ± SD; n = 2

Mehta *et al.* have reported that water sorption led to the plasticization of amorphous drug due to a decrease in both the relaxation (increase in molecular mobility) and crystallization times.[47] The rapid crystallization of amorphous DPM during the dissolution of physical mixtures of amorphous DPM with PVP and PAA (Figure 4.7) may be attributed to the powerful plasticization effect of water molecules once amorphous DPM contacts the aqueous PBS, particularly given the low glass transition (T_g) values of the amorphous drugs (Table 4.1). Furthermore, amorphous CNZ also crystallizes very rapidly and attains crystalline drug solubility (within 5 mins) when its physical mixture with PVP or PAA were dispersed in PBS 6.8 (data not shown). On the other hand, spray drying with high T_g polymers (PVP and PAA, Table 4.1) causes intimate mixing of drug and polymer and the generated ASDs have a single T_g (single phase) between the T_g of the two individual components (Table 4.3). The exception to this was the DPM-PAA system at 80% w/w drug loading where amorphous drug-rich (T_g = 102.7 ºC) and polymer rich domains (T_g = 152.47 ºC) was observed in addition to the crystalline drug domain (3 phase system). Nevertheless, the resultant T_g's observed were significantly higher than the pure drug T_g (Table 4.1 and 4.3) and also demonstrated a positive deviation from the Gordon-Taylor (GT) predicted T_g (except for the CNZ-PVP systems at low drug loadings), indicating strong heteronuclear interaction between the drug and polymers.[21] The increased T_g of the ASDs may result in greater physical stability during dissolution. Thus, the greater supersaturation levels generated for

DPM and CNZ with increasing PVP and PAA concentration may be attributed to the higher T_g values for PVP and PAA based systems at elevated polymer concentrations by increasing amorphous drug stabilization during dissolution. This antiplasticization effect by PVP and PAA on amorphous DPM and CNZ may enable amorphous DPM and CNZ to remain in amorphous form for longer periods of time especially given that it is in direct contact with PVP and PAA during dissolution. Thus the intimate drug-polymer mixing achieved in solid ASDs formed using spray drying results in supersaturated levels of DPM and CNZ in solution.

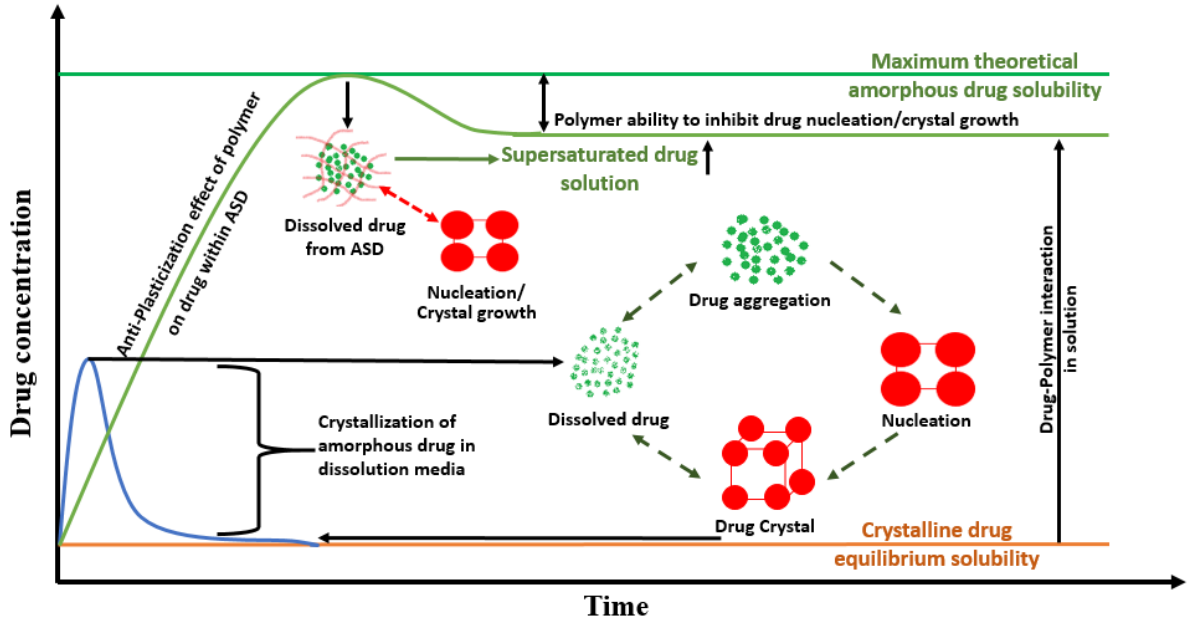

Figure 4.10. Generalized mechanism of drug supersaturation generation and maintenance from the dissolution of amorphous drug-polymer physical mixture and ASD

As reported in Table 4.2, only high concentrations of polymer significantly increase the solubility of the crystalline drugs. The solution concentration of polymer produced by the dissolution of the ASD is low (200 µg/mL at highest polymer loading), compared to 1000-2000 µg/mL of polymer concentration during crystalline drug solubility study (Table 4.2), suggesting that the drug dissolution profile is mainly due to amorphous drug solubility rather than polymer enhanced crystalline drug solubility. This is supported from the results reported in Table 4.3 where the concentration generated from DPM and CNZ ASDs were significantly higher than the concentration obtained from their physical mixture (crystalline drug and polymer) at equivalent drug and polymer loading. Thus, it can be inferred that the main mechanism for drug solubility improvement can be attributed to the polymer's ability to generate and maintain drug supersaturation from ASD. This is supported by the dissolution

results (Figure 4.8 and 4.9) where elevated drug concentrations persist following the generation of supersaturation. As shown in Figure 4.10 the dissolution profile can be rationalized as follows: Generation of a highly-supersaturated solution, due to immediate release of amorphous drug from polymer matrix, causes rapid nucleation of DPM and CNZ particles and precipitation from solution. The extent of this precipitation depends on the polymer's antiplasticization effect on drug which further depends on the weight fraction of polymer within ASD. As shown in Eq. 4.5, a high concentration of drug causes a high nucleation rate leading to the creation of more crystals and a more extensive initial drop in the drug solution concentration. PVP and PAA do not appear to have prevented the initial nucleation of DPM and CNZ under these conditions. However, upon reaching the plateau region the drug concentration in PBS 6.8 remains higher than the equilibrium solubility values, strongly indicating that the polymers are able to inhibit further nucleation and crystal growth. A similar observation has been made previously.[6]

4.3.5. Solution ^{1}H NMR

^{1}H NMR studies were performed to investigate the drug-polymer interaction in solution to try to correlate this information with the results obtained from the dissolution of ASDs. The electron density around the hydrogen atom of DPM and CNZ varied as a result of interaction between the drug and polymer. This was reflected in the NMR spectra as chemical shift variations and peak broadening, since the electron density around the interacting atom and the mobility changed.[50]

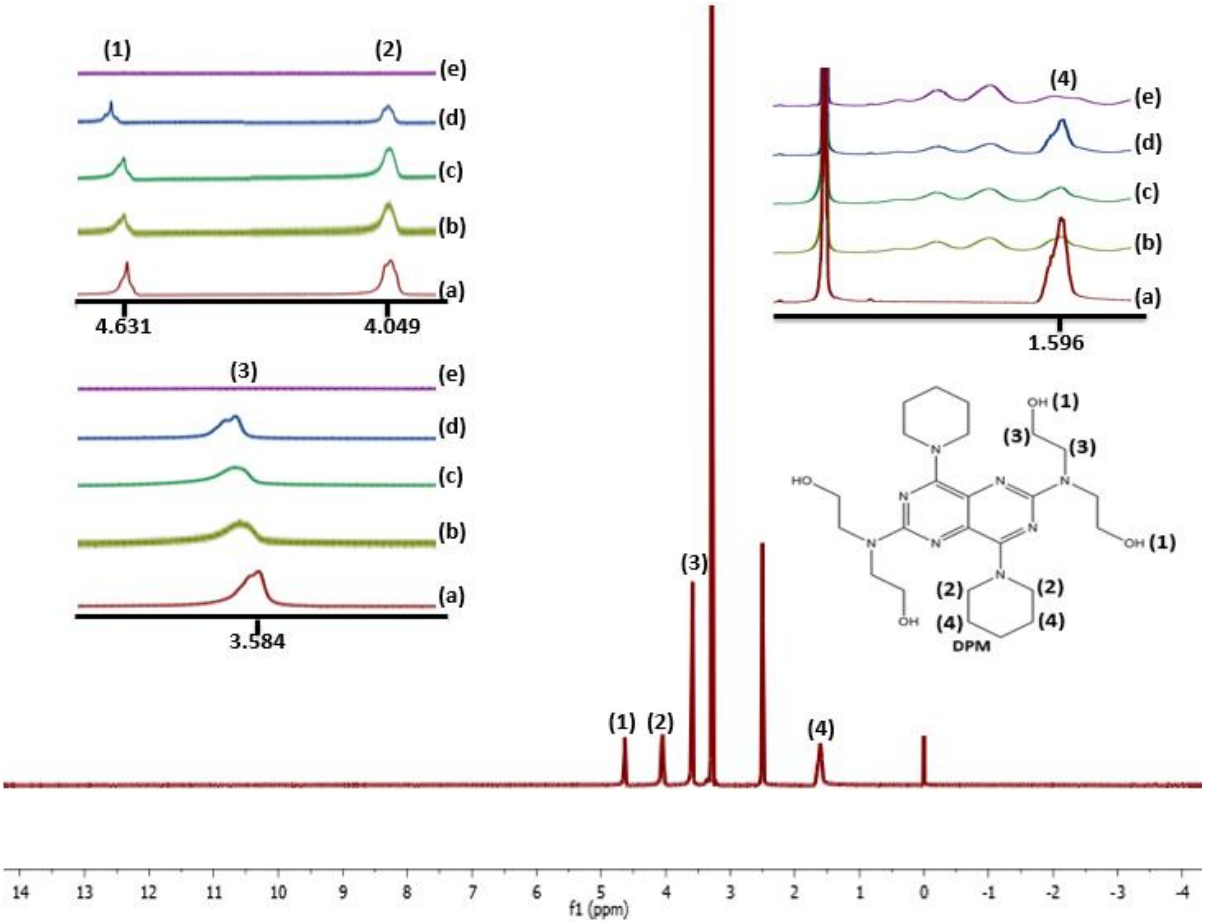

Figure 4.11. Solution ^{1}H NMR spectra of DPM in DMSO-d6. Figures in inset represent the chemical shift of DPM-PVP ASDs at 100% (a), 80% (b), 50% (c), 20% (d) and 0% (e) drug loadings. The numbers at the top of each inset figure represent the peak number in the DPM spectra. Assignments of DPM resonance is based on spectral database[48] Numbers are assigned arbitrarily

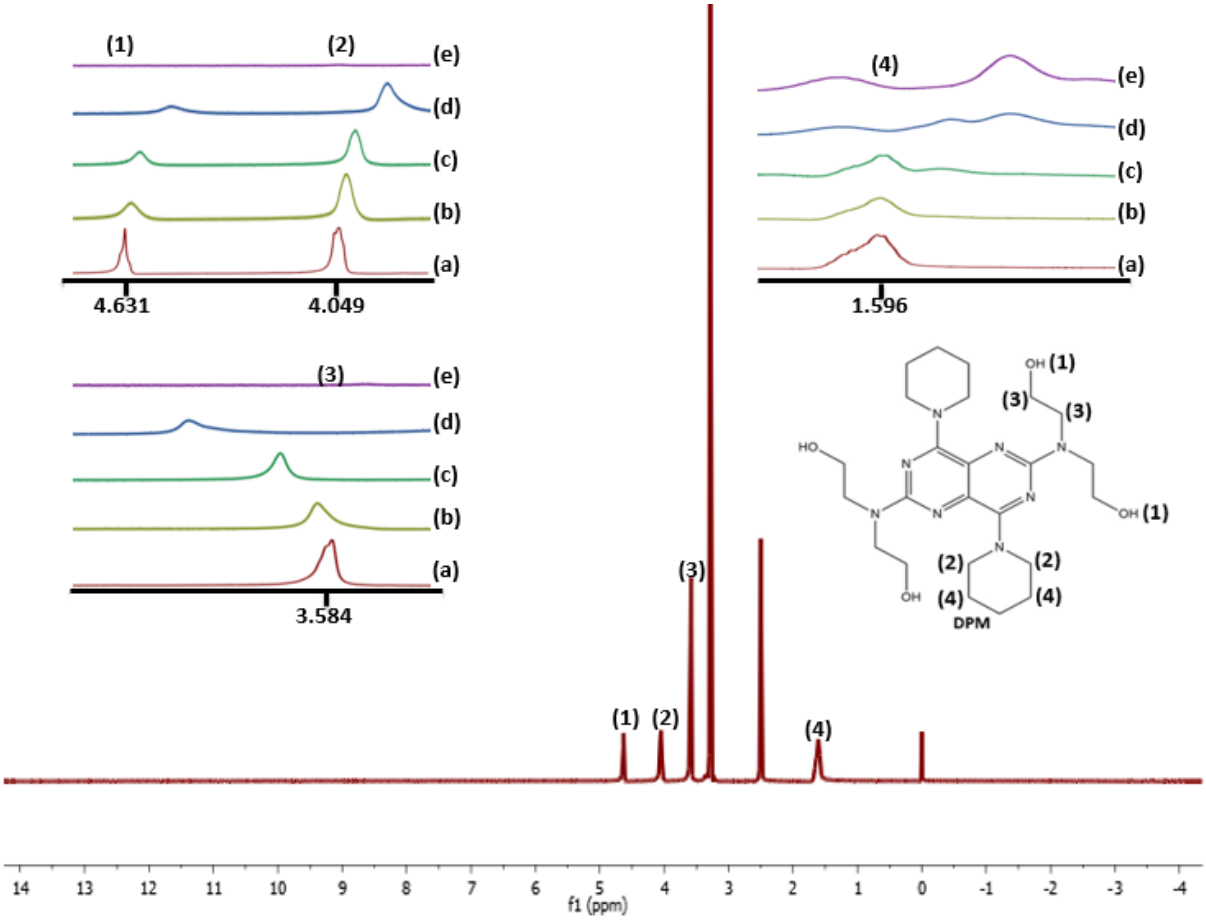

Figure 4.12. Solution ^{1}H NMR spectra of DPM in DMSO-d6. Figures in inset represent the chemical shift of DPM-PAA ASDs at 100% (a), 80% (b), 50% (c), 20% (d) and 0% (e) drug loadings. The numbers at the top of each inset figure represent the peak number in the DPM spectra. Assignments of DPM resonance is based on spectral database[48] Numbers are assigned arbitrarily

As shown in Figure 4.11, the chemical shift (δ) of hydroxyl protons (1) of DPM have been shifted to higher values (deshielding) in solution resulted from dissolution of PVP solid dispersions compared to corresponding protons in pure DPM. Conversely, the peak (1) shifted to lower values (shielding) in PAA solid dispersion solution (Figure 4.12). The deshielding and shielding effect on the hydroxyl protons suggest a change in electron density as a result of interaction with PVP and PAA and also indicates that PVP and PAA interact in a different manner with DPM. The change in electron density in DPM OH group confirmed the formation of H-bonding between the OH group of DPM with the -C=O of PVP and -COOH group of PAA. Furthermore, no shift was observed for proton in piperidine ring (2) in PVP based dispersions. However, upfield shifts (to lower values) was recorded for these protons (2) in PAA based dispersions due to shielding effects. The protons in ethanolamine group (3) of DPM were shifted to higher values (downfield) in both PVP and PAA based dispersions (deshielding). No shift for peak (4) was observed in DPM-PVP systems

compared to DPM-PAA systems where upfield shift was recorded at 20% w/w DPM loading. The change in electron density of proton attached to different groups (2, 3 and 4) in DPM may be attributed to the conjugative interaction resulting in the formation of dipole-induced complex formation between the drug and the polymer. For CNZ systems, addition of PVP and PAA had a significant impact on the chemical shift of several peaks due to the interaction between the drug and the polymer. The interactions were most pronounced for protons 1, 2, 6 and 7 in PVP based dispersions (Figure 4.13) and for protons 1, 2, 3, 4, 5, 6, and 7 in PAA solid dispersions (Figure 4.14). This suggest that CNZ interacts in a different way with PVP as compared to PAA which goes some way towards explaining the different polymeric effect, particularly in terms of inhibition of CNZ recrystallization and dissolution of CNZ ASDs. The shifts were downfield (higher values) for all the protons in both the systems. The nature of the CNZ proton interactions with PVP or PAA are currently not fully understood, but might be due to H-bonds, ionic-bonds or van der Waals forces.[51]

The chemical shifts of protons of different functional groups of DPM and CNZ correlate well with the solubilizing effect of PVP and PAA. Furthermore, the relative shifts in DPM and CNZ peaks are higher for PAA system compared to PVP based system which indicates the formation of stronger interaction between the drug and PAA. This observation is in keeping with the results observed during supersaturation and dissolution studies where PAA maintained relatively higher level of DPM and CNZ supersaturation in PBS 6.8 than PVP. Furthermore, the relative shifts in the peaks were found to be dependent on the drug-polymer concentration in solution which further explains the difference in drug supersaturation level achieved at different polymer concentrations during ASD dissolution (Figure 4.7 and 4.8). Similar shifts and complex formation mechanism have been reported in the literature.[7 29 52]

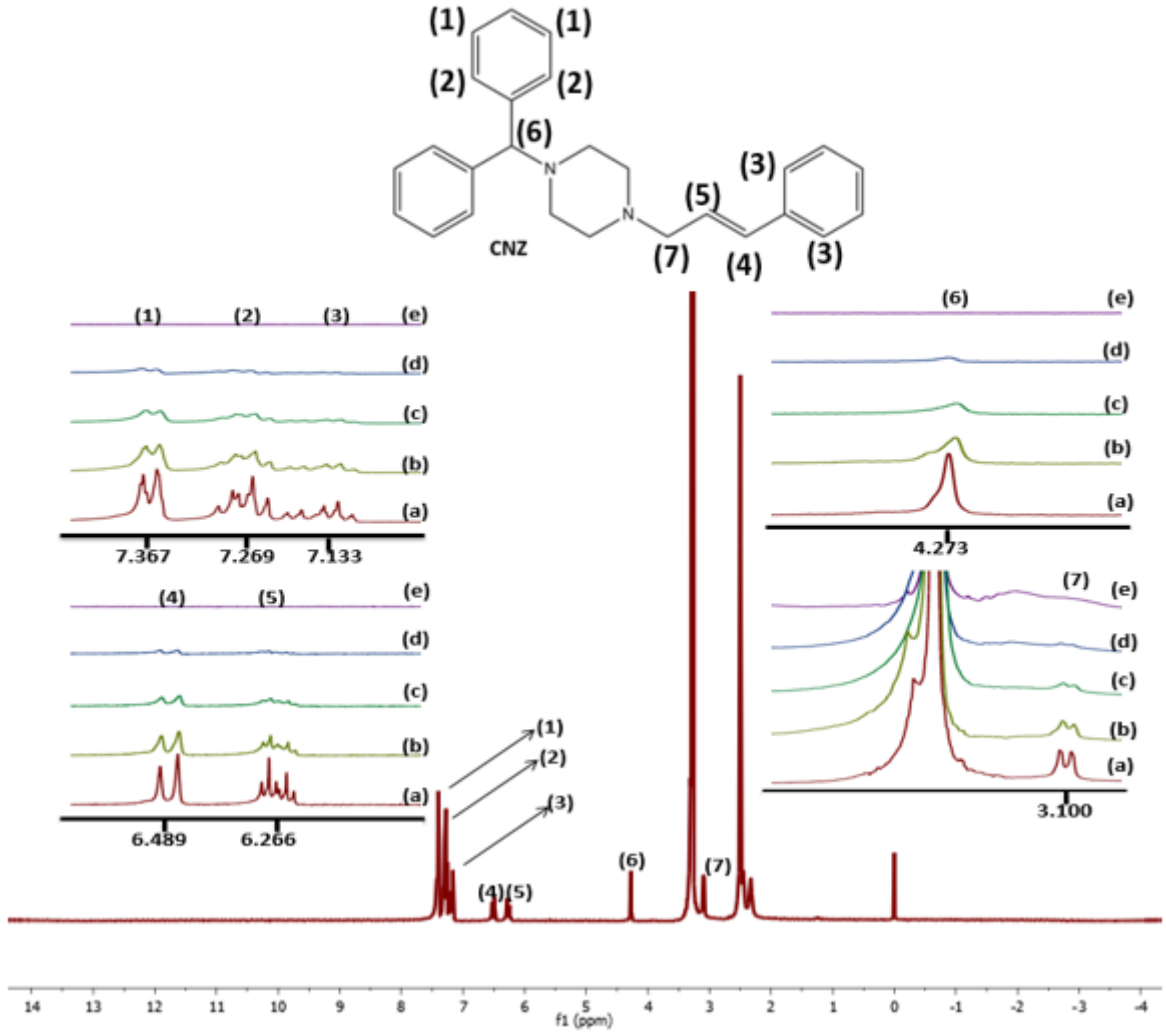

Figure 4.13. Solution ^{1}H NMR spectra of CNZ in DMSO-d6. Figures in inset represent the chemical shift of CNZ-PVP ASDs at 100% (a), 80% (b), 50% (c), 20% (d) and 0% (e) drug loadings. The numbers at the top of each inset figure represent the peak number in the CNZ spectra. Assignments of CNZ resonance is based on Sassene *et al.*[49] Numbers are assigned arbitrarily

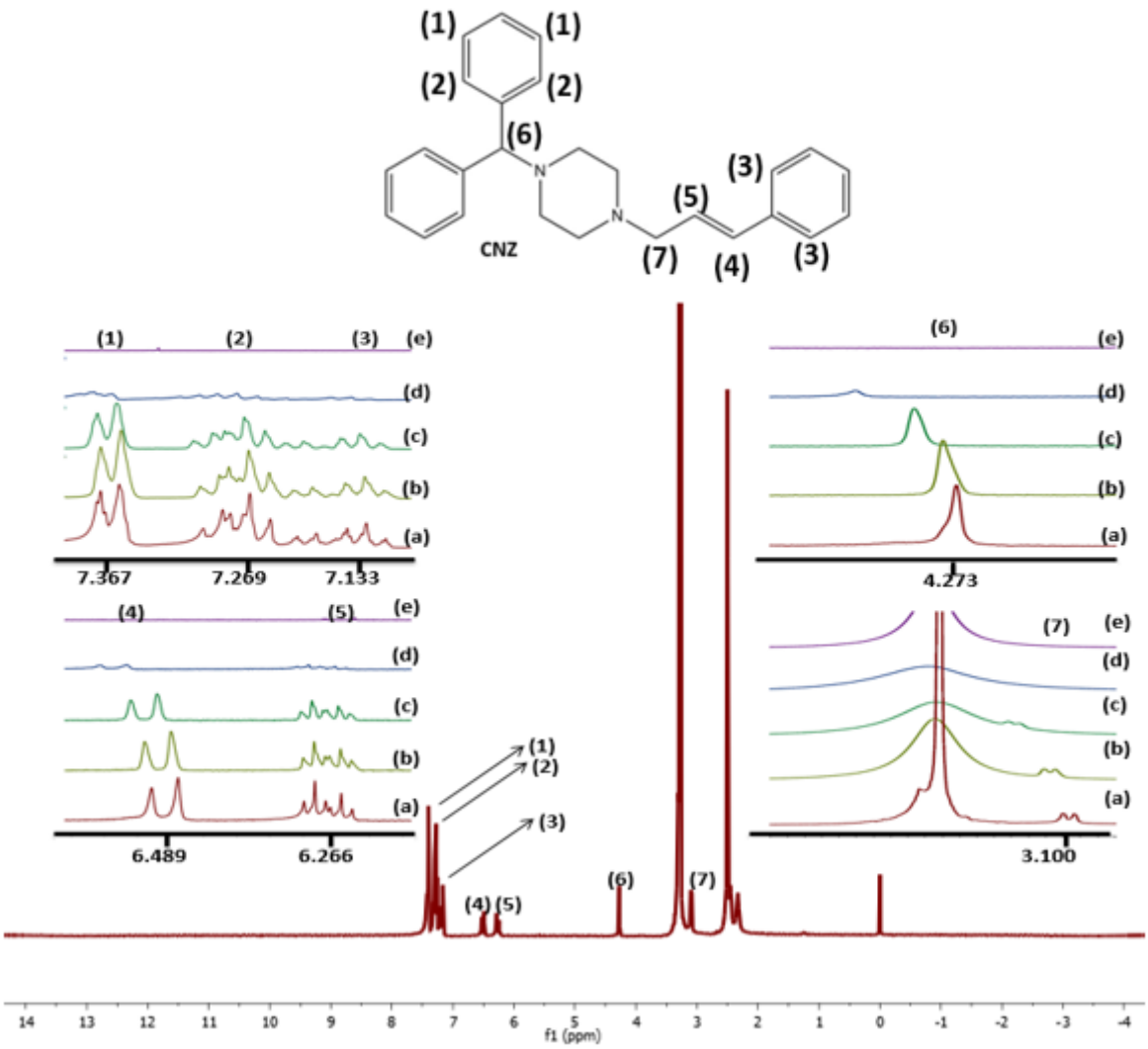

Figure 4.14. Solution ^{1}H NMR spectra of CNZ in DMSO-d6. Figures in inset represent the chemical shift of CNZ-PAA ASDs at 100% (a), 80% (b), 50% (c), 20% (d) and 0% (e) drug loadings. The numbers at the top of each inset figure represent the peak number in the CNZ spectra. Assignments of CNZ resonance is based on Sassene *et al.*[49] Numbers are assigned arbitrarily

4.4. Conclusions

The dissolution behaviour of the ASDs of DPM and CNZ prepared with PVP and PAA have been investigated and compared. We have shown that different types and concentrations of polymers have different effects on the supersaturated drug concentrations generated from the ASD. ASDs formulated with PAA were found to result in solutions with the highest extent of supersaturation. At equivalent supersaturations, both polymers were observed to reduce crystal growth rates relative to the growth rate of the drug alone in PBS 6.8. In addition, this study also highlighted the importance of intimate drug-polymer mixing achieved by spray drying in increasing the supersaturated drug concentration. The relatively high stabilizing effect of PAA compared to PVP may be attributed to specific interactions

between the drug and polymer in the solid-state as well as in solution. These results suggest that it is important to select appropriate polymers for a solid dispersion by considering the solid state stability and the stability of the supersaturated solution generated following dissolution of the amorphous solids.

4.5. References

1. Nkansah P, Antipas A, Lu Y, Varma M, Rotter C, Rago B, El-Kattan A, Taylor G, Rubio M, Litchfield J. 2013. Development and evaluation of novel solid nanodispersion system for oral delivery of poorly water-soluble drugs. J Control Release 169: 150-161.

2. Aytac Z, Sen HS, Durgun E, Uyar T. 2015. Sulfisoxazole/cyclodextrin inclusion complex incorporated in electrospun hydroxypropyl cellulose nanofibers as drug delivery systems. Colloids Surf B 128: 331-338.

3. Harmon P, Galipeau K, Xu W, Brown C, Wuelfing WP. 2016. Mechanism of dissolution-induced nanoparticle formation from a copovidone based amorphous solid dispersion. Mol Pharm 13:1467-1481.

4. Moribe K, Makishima T, Higashi K, Liu N, Limwikrant W, Ding W, Masuda M, Shimizu T, Yamamoto K. 2014. Encapsulation of poorly water-soluble drugs into organic nanotubes for improving drug dissolution. Int J Pharm 469:190-196.

5. Baghel S, Cathcart H, O'Reilly NJ. 2016. Polymeric amorphous solid dispersions: A review of amorphization, crystallization, stabilization, solid-state characterization and aqueous solubilization of biopharmaceutical classification system class II drugs. J Pharm Sci 105: 2527-2544.

6. Konno H, Handa T, Alonzo DE, Taylor LS. 2008. Effect of polymer type on the dissolution profile of amorphous solid dispersions containing felodipine. Eur J Pharm Biopharm 70:493-499.

7. Abu-Diak OA, Jones DS, Andrews GP. 2011. An investigation into the dissolution properties of celecoxib melt extrudates: Understanding the role of polymer type and concentration in stabilizing supersaturated drug concentration. Mol Pharm 8:1362-1371.

8. Zhu D, Zografi G, Gao P, Gong Y, Zhang GGZ. 2016. Modelling physical stability of amorphous solids based on temperature and moisture stresses. J Pharm Sic 105: 2932-2939.

9. He Y, Ho C. 2015. Amorphous solid dispersions: Utilization and challenges in drug discovery and development. J Pharm Sci 104: 3237-3258.

10. Huang Y, Dai WG. 2014. Fundamental aspects of solid dispersion technology for poorly soluble drugs. Acta Pharm Sin B 4: 18-25.

11. Van den Moooter G. 2012. The use of amorphous solid dispersions: A formulation strategy to overcome poor solubility and dissolution rate. Drug Discov Today Technol 9: e79-e85.

12. Sawiki E, Beijnen JH, Schellens JHM, Nuijen B. 2016. Pharmaceutical development of an oral tablet formulation containing a spray dried amorphous solid dispersions. Int J Pharm 511: 765-773.
13. Hancock BC, Zografi G. 1997. Characteristics and significance of the amorphous state in pharmaceutical systems. J Pharm Sci 86: 1-12.
14. Greaser KA, Patterson JE, Zeitler JA, Gordon KC, Rades T. 2009. Correlating thermodynamics and kinetic parameters with amorphous drug stability. Eur J Pharm Sci 37:492-498.
15. Baghel S, Cathcart H, Redington W, O'Reilly NJ. 2016. An investigation into the crystallization tendency/kinetics of amorphous active pharmaceutical ingredients: A case study with dipyridamole and cinnarizine. Eur J Pharm Biopharm 104:59-71.
16. Meng F, Trivino A, Prasad D, Chauhan H. 2015. Investigation and correlation of drug polymer miscibility and molecular interaction by various approaches for the preparation of amorphous solid dispersions. Eur J Pharm Sci 71:12-24.
17. Song Y, Yang X, Chen X, Nie H, Byrne S, Lubach JW. 2015. Investigation of drug-excipient interactions in lapatinib amorphous solid dispersions using solid-state NMR spectroscopy. Mol Pharm 12: 857-866.
18. Konno H, Taylor LS. 2006. Influence of different polymers on the crystallization tendency of molecularly dispersed amorphous felodipine. J Pharm Sci 95: 2692-2705.
19. Konno H, Taylor LS. 2008. Ability of different polymers to inhibit the crystallization of amorphous felodipine in the presence of moisture. Pharm Res 25: 969-978.
20. Tiann Y, Caron V, Jones DS, Healy AM, Andrews GP. 2014. Using Flory-Huggins phase diagram as a pre-formulation tool for the production of amorphous solid dispersions: a comparison between hot melt extrusion and spray drying. J Pharm Pharmacol 66:256-274.
21. Baghel S, Cathcart H, O'Reilly NJ. 2016. Theoretical and experimental investigation of drug-polymer interaction and miscibility and its impact on drug supersaturation in aqueous medium. Eur J Pharm Biopharm 107: 16-31.
22. Teja AB, Patil SP, Shete G, Patel S, Bansal AK. 2013. Drug-excipient behaviour in polymeric amorphous solid dispersions. J Excipients Food Chem 4: 70-94.
23. Maniruzzaman M, Morgan DJ, Mendham AP, Pang J, Snowden MJ, Doroumis D. 2013. Drug-polymer intermolecular interactions in hot-melt extruded solid dispersions. Int J Pharm 443: 199-208.
24. Fu Q, Li B, Zhang D, Fang M, Shao J, Guo M, Guo Z, Li M, Sun J, Zhai Y. 2015. Comparative studies of the *in vitro* dissolution and *in vivo* pharmacokinetics for different

formulation strategies (solid dispersion, micronization, and nanocrystals) for poorly water-soluble drugs: A case study for lacidipine. Coll Surf B Biointerfaces 132: 171-176.
25. Tian B, Wang X, Zhang Y, Zhang K, Zhang Y Yang X. 2015. Theoretical prediction of a phase diagram for solid dispersions. Pharm Res 32: 840-852.
26. Sousa LA, Reutzel-Edens SM, Stephenson GA, Taylor LS. 2016. Supersaturation potential of salt, co-crystal and amorphous forms of a model weak base. Cryst Growth Des 16: 737-748.
27. Jackson MJ, Kestur US, Hussain MA, Taylor LS. 2016. Dissolution of danazol amorphous solid dispersions: Supersaturation and phase behaviour as a function of drug loading and polymer type. Mol Pharm 13: 223-231.
28. Duong TV, Van den Mooter G. 2016. The role of the carrier in the formulation of pharmaceutical solid dispersions. Part II: amorphous carriers. Expert Opin Drug Deliv 13: 1681-1694.
29. Ohyagi N, Ueda K, Higashi K, Yamamoto K, Kawakami K, Moribe K. 2017. Synergistic role of hypromellose and methacrylic copolymer in the dissolution improvement of amorphous solid dispersions. J Pharm Sci 106: 1042-1050.
30. Xie T, Taylor LS. 2016. Dissolution performance of high drug loading celecoxib amorphous solid dispersions formulated with polymer combinations. Pharm Res 33; 739-750.
31. Sun DD, Lee PI. 2015. Probing the mechanism of drug release from amorphous solid dispersions in medium-soluble and medium-insoluble carriers. J Control Rel 211: 85-93.
32. Qian F, Wang J, Hartley R, Tao J, Haddadin R, Mathias N, Hussain M. 2012. Solution behaviour of PVP-VA and HPMC-AS based amorphous solid dispersions and their bioavailability implications. Pharm Res 29: 2765-2776.
33. Simonelli AP, Mehta SC, Higuchi WI. Dissolution rates of high energy polyvinylpyrrolidone (PVP) sulfathiazole coprecipitates. J Pharm Sci 99: 4023-4031.
34. Rumondor ACF, Marsac PJ, Stanford LA, Taylor LS. 2010. Effect of polymer hygroscopicity on the phase behaviour of amorphous solid dispersins in the presence of moisture. Mol Pharm 7: 477-490.
35. Jackson MJ, Toth SJ, Kestur US, Huang J, Qian F, Hussain MA, Simpson GJ, Taylor LS. 2014. Impact of polymers on the precipitation behaviour of highly supersaturated aqueous danazol solutions. Mol Pharm 11: 3027-3038.
36. Keisuke U, Kenjirou H, Kaiji Y, Kunikazu M. 2013. Inhibitory effect of Hydroxypropyl methylcellulose acetate succinate on drug recrystallizationfrom a supersaturated solution assessed using nuclear magnetic resonance measurements. Mol Pharm 10: 3801-3811.

37. Keisuke U, Kenjirou H, Kaiji Y, Kunikazu M. 2015. Equilibrium state at supersaturated drug concentration achieved by Hydroxypropyl methylsuccinate: Molecular characterization using 1H NMR technique. Mol Pharm 12: 1096-1104.

38. Chen Y, Liu C, Chen Z, Su C, Hageman M, Hhussain MA, Haskell R, Stefanski K, Qian F. 2015. Drug-polymer-water interaction and its implication for the dissolution performance of amorphous solid dispersions. Mol Pharm 12: 576-589.

39. Vora C, Patadia R, Mittal K, Mashru R. 2015. Preparation and characterization of dipyridamole solid dispersions for stabilization of supersaturation: effect of precipitation inhibitors type and molecular weight. Pharm Dev Technol 3: 1-9.

40 http://www.drugbank.ca/drugs/DB00568

41. Craig DQM. 2002. The mechanism of drug release from solid dispersions in water-soluble polymers. Int J Pharm 213: 131-144.

42. Ahuja N, Katare OP, Singh B. 2007. Studies on dissolution enhancement and mathematical modelling of drug release of a poorly water-soluble drug using water-soluble carriers. Eur J Pharm Biopharm 65: 26-38.

43. Hancock C, Parks M. 2000. What is the true solubility advantage for amorphous pharmaceuticals? Pharm Res 17: 397-404.

44. Marsac PJ, Konno H, Taylor LS. 2006. A comparison of the physical stability of amorphous felodipine and nifedipine systems. Pharm Res 10: 2306-2316.

45. Sousa L, Reutzel-Edens S, Stephenson G, Taylor L. 2015. Assessment of the amorphous "solubility" of a group of diverse drugs using new experimental and theoretical approaches. Mol Pharm 12: 484-495.

46. Turnbull D, Fischer JC. 1949. Rate of nucleation in condensed system. J Chem Phys 17: 1722-1728.

47. Mehta M, Kothari K, Ragoonanan V, Suryanarayanan R. 2016. Effect of water on the molecular mobility and physical stability of amorphous pharmaceuticals. Mol Pharm 13: 1339-1346.

48. http://sdbs.db.aist.go.jp/sdbs/cgi-bin/cre_index.cgi

49. Sassene PJ, Mosgaard MD, Loebmann K, Mu H, Larsen FH, Rades T, Mullertz A. 2015. Elucidating the molecular interactions occurring during drug precipitation of weak bases from lipid based formulations – a case study with cinnarizine and a long chain self nano-emulsifying drug delivery system. Mol Pharm 12: 4067 4076.

50. Van der Mooter G, Abu-Diak OA, Jones DS. 2010. Physiochemical characterization of hot-melt extruded bicalutamide-polyvinylpyrrolidone solid dispersions. J Pharm Sci 99: 1322-1335.
51. Misic Z, Jung DS, Sydow G, Kuentz M. 2012. Understanding the interaction of oleic acid with basic drugs in solid lipids on different biopharmaceutical levels. J Excip Food Chem 5: 113-134.
52. Hosono T, Tsuchiya S, Matsumaru H. 1980. Model of interaction of ajmaline with polyvinylpyrrolidone. J Pharm Sci 69: 824-826

CHAPTER 5. AN INVESTIGATION INTO THE EFFECT OF TEMPERATURE AND MOISTURE ON THE PHYSICAL STABILITY AND DISSOLUTION PROFILE OF SPRAY DRIED AMORPHOUS SOLID DISPERSIONS: PHASE SEPARATION AND CRYSTALLIZATION

5.1. Introduction

Thermodynamically solid dispersions are referred to as "solid solutions" (single-phase systems with molecularly dispersed APIs) and will be formed when the API concentration is less than the solubility of the API in polymer.[1 2] These dispersions will be thermodynamically stable with minimum tendency of phase separation or crystallization during the shelf life of the product. [3 4] However, the solubility of crystalline API in an amorphous polymer is always too low to meet practical needs.[5] Consequently, most ASDs are metastable or unstable and may lead to amorphous-amorphous phase separation and recrystallization of the amorphous API from ASDs during storage.[6]

Crystalline APIs adsorbs water by a surface adsorption mechanism.[7] Amorphous APIs are more hygroscopic due to their higher free energy and disordered structure compared to their crystalline counterpart and, therefore, water can penetrate into the bulk (in addition to surface adsorption) of the amorphous material.[8] Water (glass transition temperature, T_g = -137 °C) can effectively reduce the T_g of the ASD and thereby increase the molecular mobility which can be detrimental to the stability of ASDs.[9 10] Water can also interfere with the drug-polymer interaction and thus alter the drug-polymer miscibility by competitively forming hydrogen bonds (H-bond) with a hydrophilic polymer.[11] This may lead to phase separation and crystallization.[12 13]

Due to their higher free energy and metastable conditions, ASDs are sensitive to environmental conditions. It has been previously reported that elevated temperature and relative humidity can promote phase separation and crystallization of ASDs by increasing the overall molecular mobility, reducing the T_g or interfering the drug-polymer interaction in ASDs leading to a decreased drug-polymer miscibility.[14 15] The effect of stressed conditions on ASDs have been widely studied in the past, however, little has been published in literature about which has greater influence on ASDs, temperature or humidity?[16 17 18] Investigation of this question is required because it will help formulation scientists to select appropriate storage conditions for ASDs.

Another important question that has not been investigated to any great extent is the relationship between solid-state of the drug within ASDs and its effect on the dissolution profile. Crystallization of an amorphous API in ASDs leads to reduced dissolution and bioavailability. However, some ASDs may retain their amorphous nature under certain conditions without crystallization and may exist as phase separated system. Therefore, it is

interesting to see the effect of those phase separated systems on the physical stability and dissolution behaviour during storage and how will they change over time.

The main objective of this Chapter is to investigate the effect of temperature and moisture on ASDs and measure the changes of ASDs over time during the stability testing. Dipyridamole (DPM), cinnarizine (CNZ) ASDs were prepared by spray drying and exposed to three different temperatures (25, 40 and 60 °C) at 0 and 75% RH at each temperatures for 4 weeks. The crystallinity and dissolution profiles were then determined to understand the effect of different stress conditions on ASDs. The samples were also stored in desiccator at room temperature for one year to evaluate changes in solid state and dissolution due to the physical aging process.

5.2. Materials and Methods

5.2.1. Materials

Dipyridamole (DPM), cinnarizine (CNZ), polyvinyl pyrrolidone (PVP) K30 and polyacrylic acid (PAA) were purchased from Sigma Aldrich, Ireland. All reagents were of analytical grade and used without further purification. The chemical structure and key physicochemical properties of the model drugs and polymers used in this study are summarized in Figure1.13.

5.2.2. Preparation of amorphous solid dispersions

The spray dried solid dispersions were prepared using a Pro-CepT 4M8-TriX spray drier (Zelzate, Belgium) with a bifluid nozzle. The spray drying solutions were prepared by dissolving the component mixtures in methanol. The drug-polymer proportion in the binary mixture was 20:80 w/w. For the ternary solid dispersion systems, the proportion of drug-polymer-surfactant was 20:75:5 and drug-polymer-polymer was 20:40:40. The proportion of drug-polymer-polymer-surfactant in quaternary systems was 20:37.5:37.5:5 w/w. The key processing parameters were feed concentration (10% w/v in methanol solution), spray rate (6 mL/min), nozzle size (0.2 mm), atomization air flow rate (5 L/min), inlet temperature (80 $\pm$ 5°C), outlet drying temperature (50 $\pm$ 5°C) and drying air rate (100 $\pm$ 10 L/min). The spray dried solid dispersions were collected using a small cyclone separator and stored in a vacuum desiccator at room temperature for further analysis. Typical product yields were approximately 70%.

5.2.3. Thermogravimetric analysis (TGA)

The residual solvent content of the spray dried solid dispersions was assessed using a TGA Q50 (TA Instruments Corp., Elstree, Herts, U.K.). Samples were heated at 10°C/min from 25 to 200 °C. During all TGA experiments nitrogen was used as the purging gas at 50 mL/min. All analyses were performed in duplicate.

5.2.4. X-Ray diffractometry (XRD)

The powdered amorphous solid dispersions were analysed using an X-ray diffractometer (X'pert MPD PRO PANalytical, Almelo, Netherlands) at the Uiversity of Limerick using the following parameters: Cu radiation (wavelength 1.540598 Å) , Ni-filter, voltage 40 kV, current 40 mA, 2θ range of 5-50°C, step size 0.008° and scan rate 3.2°/min

5.2.5. Modulated differential scanning calorimetry (MDSC)

Thermal analysis was performed using a MDSC Q2000 (TA Instruments Corp., Elstree, Herts, U.K.) equipped with an electrical cooling accessory. Enthalpy, temperature and heat capacity calibrations were carried out using high-purity indium and sapphire standards as recommended by the instrument supplier. Samples between 3 and 10 mg were accurately weighed and placed into crimped aluminium pan with a pin hole. Nitrogen, at a flow rate of 50 mL/min, was used as the purge gas. The modulation parameters chosen to ensure separation of reversing and non-reversing events was $\pm$ 0.53 °C/40s at a ramp rate of 5 °C/min. Data analysis was performed using Universal Analysis software (TA Instruments Corp., Elstree, Herts, U.K.). All analyses were performed in duplicate.

The relative crystallinity (α) of ASDs was approximately calculated from the MDSC data using the following equation:[19]

$$\alpha = \frac{\Delta H_s}{\Delta H_c} * 100\% \qquad \ldots\ldots\ldots \qquad (5.1)$$

where ΔH_s and ΔH_c are the enthalpy of fusion of ASDs and drug-polymer physical mixture containing the crystalline drug in the same weight ratio, respectively. Physical mixtures (PM) were prepared by manually mixing the drug and polymer using mortar and pestle.

5.2.6. Dynamic Vapour Sorption (DVS)

Moisture sorption analysis of ASDs was done using dynamic vapour sorption (DVS)-1000 Advantage, Surface Measurement Systems, U.K. Amorphous drug samples (5-10 mg)

were analysed using double ramp method from 0-90-0% RH (2 cycles) in 10% increment ($\frac{dm}{dt} \leq 0.001$ at each step) at 25 °C. All the measurements were done in duplicate.

5.2.7. Stability testing under stress conditions

ASDs were stored at 60 °C/75% RH, 60 °C/ 0% RH, 40 °C/ 75% RH, 40 °C/ 0% RH, 25 °C/ 75% RH and 25 °C/ 0% RH for 4 weeks. Humidity conditions at each temperature was maintained using saturated sodium chloride salt solutions. 0% RH was maintained using silica gel. Temperature and humidity conditions were monitored throughout the experimental timeframes using MicroLogPRO II data loggers, FOURTEC, U.K. To investigate the physical aging of ASDs, samples were also stored in desiccator at room temperature for one year. Periodically samples were removed from the stability chambers and subjected to MDSC and in-vitro dissolution testing to investigate the changes of the dispersions.

5.2.8. In-vitro dissolution testing

The dissolution rate of DPM and CNZ from various powdered ASDs was measured using the USP II paddle method. Samples containing 25 mg of DPM and CNZ were added to 500 mL of PBS 6.8 at 37.0 $\pm$ 0.2 °C. The solution was stirred at 100 rpm using a USP II paddle apparatus. 2 mL samples were withdrawn from each vessel at predefined intervals (5, 10, 15, 30, 60, 120, 180, 240, 300 and 360 min) and centrifuged for 5 min at 15000 rpm. At each time-point the same volume of fresh medium was replaced. The concentration of DPM and CNZ was determined using a UV-Vis spectrophotometer. All measurements were carried out in duplicate.

5.3. Results and Discussion

5.3.1. Crystallization tendency of amorphous DPM and CNZ

As shown in Figure 5.1, amorphous DPM has a very high tendency to crystallize in the presence of moisture. DVS measurements showed that the moisture sorption of amorphous DPM initially displayed a steady uptake of moisture which is typical of an amorphous material. This was followed by moisture induced crystallization of amorphous DPM which leads to the expulsion of water. In the second cycle, most of the amorphous DPM was already crystallized as indicated by the small step changes (mass %) suggesting the presence of a crystalline material. Crystallization of amorphous DPM was confirmed by DSC analysis post DVS analysis (data not shown). CNZ, on the other hand, crystallizes very rapidly before the start of DVS cycle (confirmed using DSC by analyzing the sample after 60 mins in DVS, data not shown) due to its highly fragile nature.[4] Furthermore, as shown in

Figure 5.1 (c) and (d), freshly prepared amorphous DPM and CNZ, respectively, displayed a broad exothermic peak due to crystallization of the drug under DSC heating cycle followed by crystalline drug melting peak. In Chapter 2, it has been shown that both DPM and CNZ have high tendency to crystallize when stored at non-ambient temperature conditions.[4] Thus, both our model drugs in amorphous form are very sensitive to temperature and moisture and it would be interesting to see their crystallization behaviour in ASDs when exposed to stress conditions.

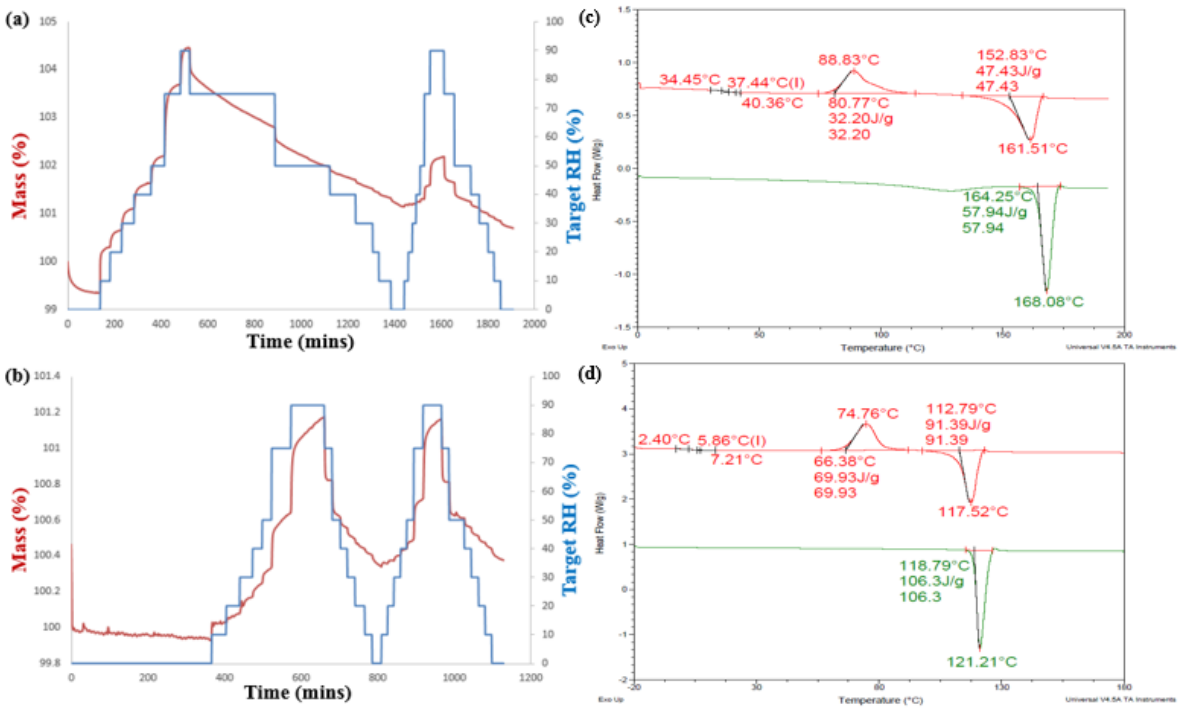

Figure 5.1. DVS analysis of Amorphous DPM (a) and CNZ (b) using double ramp method from 0-90-0% RH (2 cycles) in 10% increment ($\frac{dm}{dt} \leq 0.001$ at each step) at 25 °C; (c) and (d) represents DSC thermograms of amorphous and crystalline DPM and CNZ, respectively, n = 2

5.3.2. Physical aging of ASDs

The DSC thermograms of freshly prepared DPM and CNZ ASDs are shown in Figure 5.2 (a) and (c), respectively. It can be seen that all freshly spray dried DPM ASDs at 20 and 50% w/w presented only a single T_g, suggesting a completely amorphous state of the drug and uniform drug-polymer miscibility within the dispersions. Equally, CNZ-PVP 20%, CNZ-PAA 20% and CNZ-PAA 50% also displayed a single T_g, suggesting complete miscibility and homogeneity. For CNZ-PVP 50%, a small endothermic peak attributed to the melting of crystalline drug was observed, which seemed to indicate a small amount of crystalline CNZ in the initially formed ASD. The DSC thermograms of all the systems 80% w/w drug loading

(DPM-PVP, DPM-PAA, CNZ-PVP and CNZ-PAA) displayed the crystalline drug melting peak. These MDSC results are in good agreement with the XRD findings (Figure 5.2 (b) and (d)).

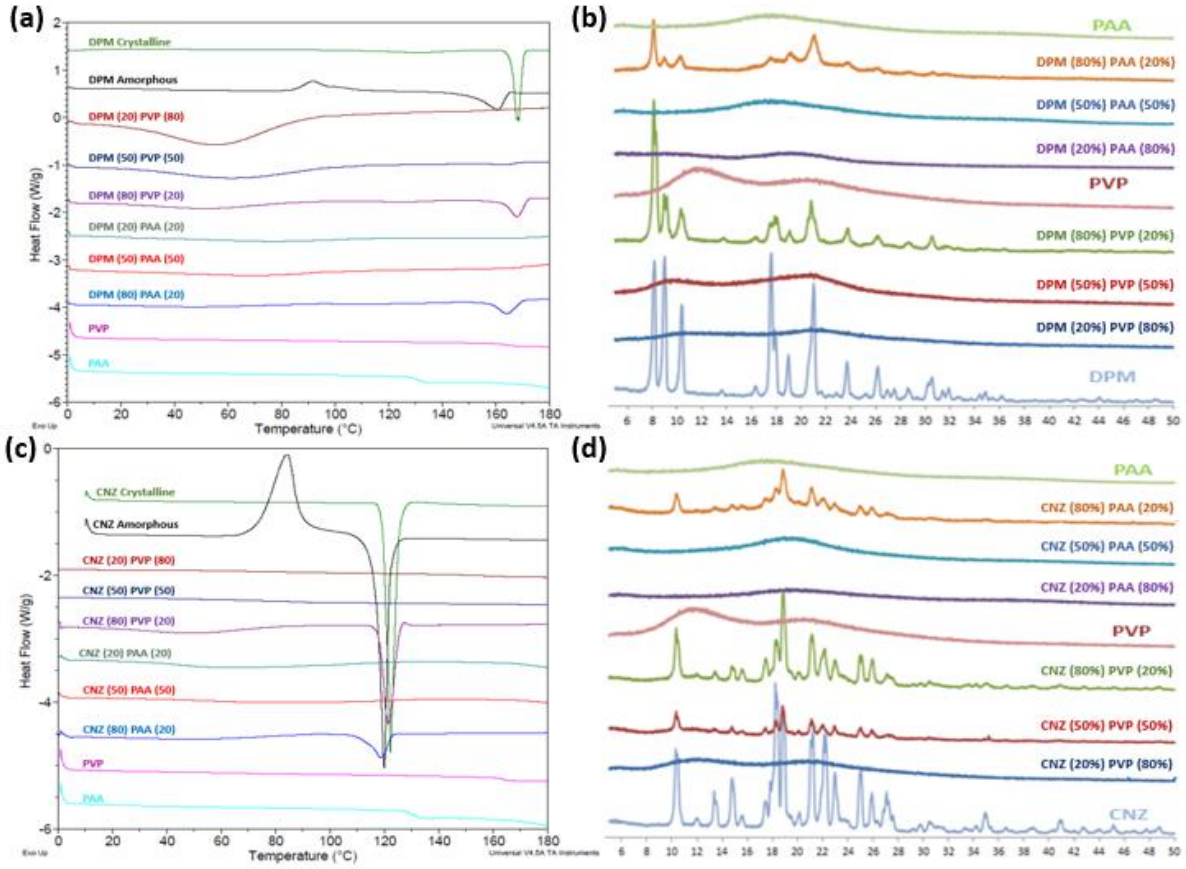

Figure 5.2. DSC thermogram and XRD spectra of DPM (a) and CNZ (b) solid dispersions; % values represent drug or polymer weight fraction within ASD

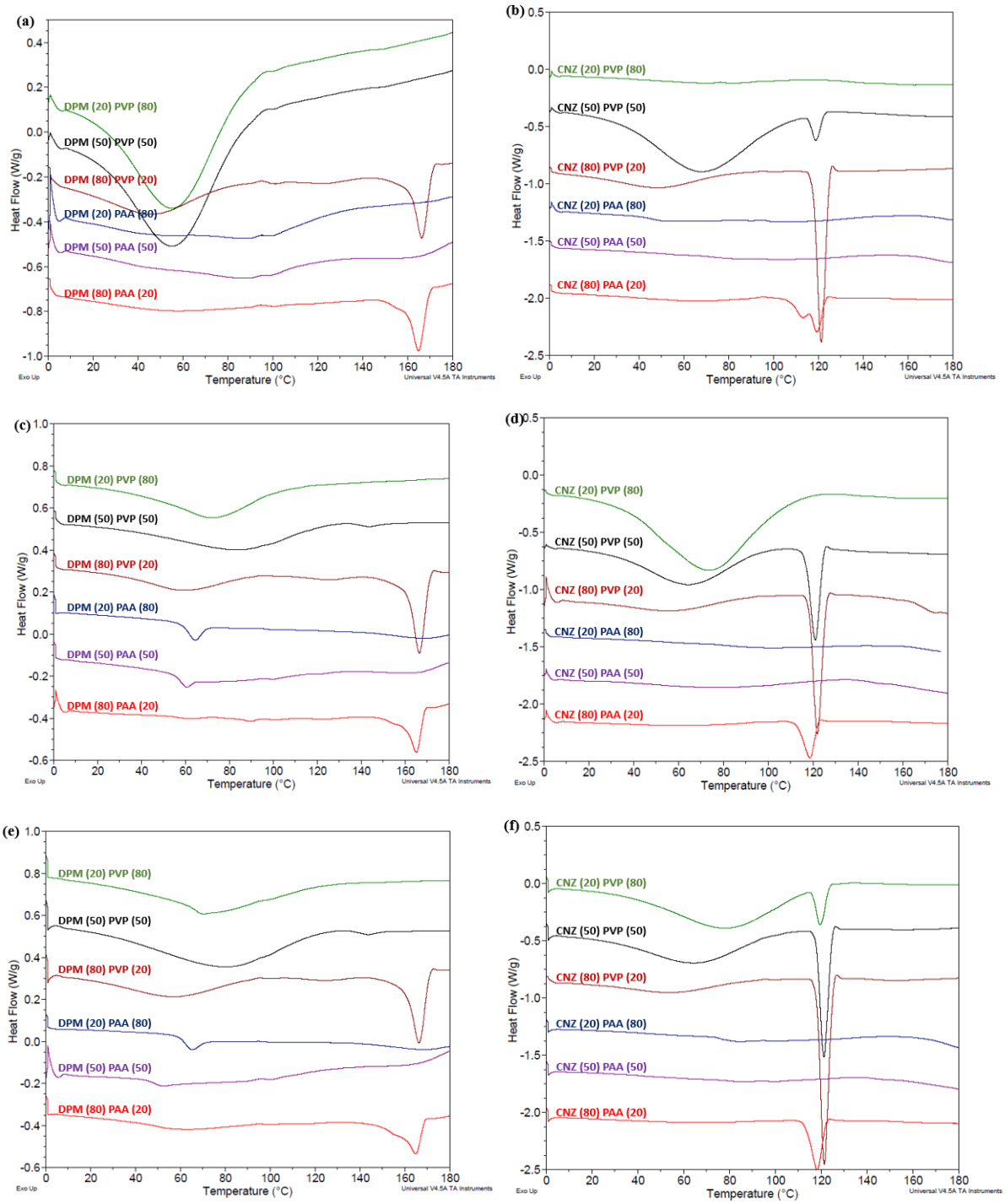

Figure 5.3. DSC thermograms of aged ASDs of DPM and CNZ stored at room temperature in desiccator for 1 month (a and b), 6 months (c and d) and 1 year (e and f); n = 2

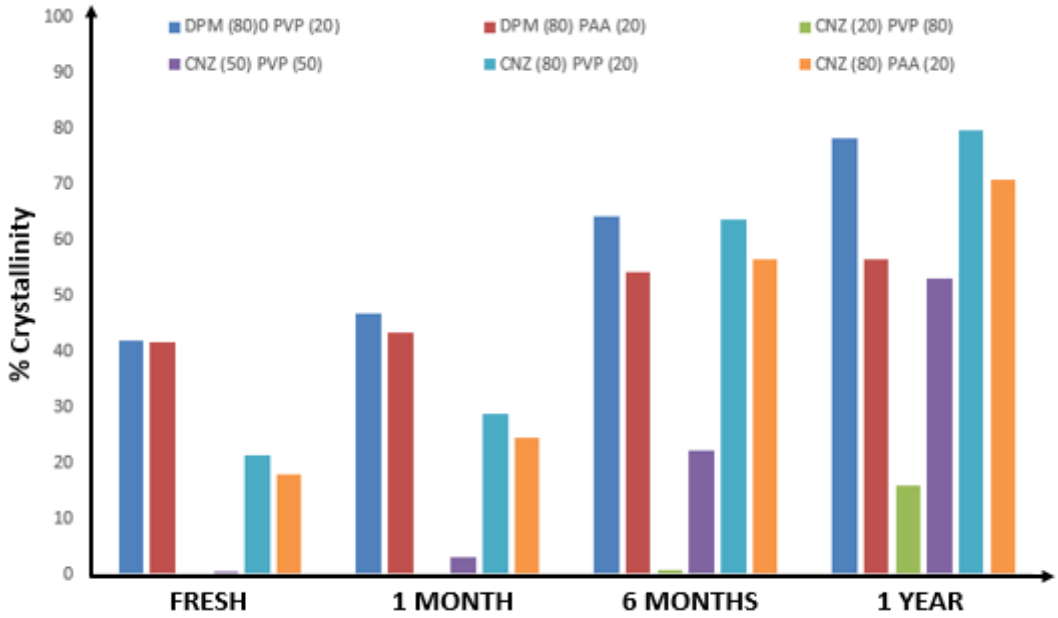

Figure 5.4. % Crystallization of amorphous DPM and CNZ within PVP and PAA based ASDs; Each point represents mean; n = 2; samples which remained complete amorphous are not shown in the figure

Samples were further analysed after 1 month (Figure 5.3 (a) and (b)), 6 months (Figure 5.3 (c) and (d)) and 1 year (Figure 5.3 (e) and (f)) of storage at room temperature within a desiccator. The results after 1 month were similar to the freshly prepared samples for both the drugs at 20 and 50% w/w drug loadings within PVP and PAA based ASDs. The melting enthalpy of crystalline drug within DPM-PVP 80%, DPM-PAA 80%, CNZ-PVP 50%, CNZ-PVP 80% and CNZ-PAA 80% increased after 1 month suggesting further crystallization of amorphous drug within polymeric carrier.

The T_g values of DPM and CNZ ASDs-20% (PVP and PAA) decreased significantly after 6 months of storage within desiccator at room temperature compared to freshly prepared sample suggesting physical aging. After 6 months, the DSC thermograms of the PVP based DPM ASD-50% displayed a small endothermic peak at drug melting point whereas CNZ ASD-50% showed a crystallization exotherm in addition to melting peak. These results suggest that both the model drugs have tendency to crystallize within PVP matrix at 50% drug loading or above after 6 months due to physical aging as shown in Figure 5.3 (c) and (d) and Figure 5.4. PAA based DPM and CNZ ASDS-50% showed reduced T_g and no melting peak was observed. The melting enthalpy of DPM and CNZ ASDs-80% (PVP and PAA) further increased after 6 month compared to fresh or 1 month aged samples suggesting further crystallization of amorphous drug within polymeric carrier.

After 1 year of storage, only the DPM-PVP 20%, DPM-PAA 20 and 50%, and CNZ-PAA 20 and 50% samples remained completely amorphous (Figure 5.3 (e) and (f). The melting enthalpies of crystalline drug within DPM-PVP 50 and 80%, DPM-PAA 80%, CNZ-PVP 50 and 80% and CNZ-PAA 80% had increased further after 1 year (Figure 5.4). CNZ-PVP 20%, which was amorphous for 6 months, also displayed a melting endotherm suggesting crystallization of amorphous CNZ within the dispersion (Figure 5.3 (f)).

5.3.3. Crystallization under stress conditions

Having confirmed the physical aging of the dispersions, the next step was to evaluate if immiscibility or phase separation could be induced by exposure to high temperature and relative humidities. To investigate into the effect of temperature and moisture on the crystallization of DPM and CNZ ASDs, samples were stored at different conditions (60 °C/75% RH, 60 °C/ 0% RH, 40 °C/ 75% RH, 40 °C/ 0% RH, 25 °C/ 75% RH and 25 °C/ 0% RH) for 4 weeks. Samples were removed at different time intervals (1, 2, 3 and 4 weeks) and examined by DSC to investigate the solid state of the drug in the ASDs (Figure 5.5 and 5.6). The glass transition temperature (T_g) of all the dispersions are reported in Table 5.1. If amorphous-amorphous phase separation occurs, two different T_g's are expected in DSC thermograms since drug molecules will predominantly interact with other drug molecules in the amorphous drug-rich regions. The same is true for polymer-polymer interactions also. If phase separation occurs due to crystallization, the melting enthalpy is expected to increase. As reported in Table 5.1, amorphous-amorphous phase separation was observed for DPM ASDs (4 weeks) at 20 and 50% w/w drug loadings for both PVP and PAA. Furthermore, phase separation led to crystallization of amorphous DPM within the DPM-PVP 50% ASD. Similar results were observed CNZ-PVP 20% ASD where amorphous-amorphous phase separation led to crystallization of CNZ. No signs of phase separation or crystallization was observed for CNZ-PAA 20 and 50% dispersions. However, the T_g of these systems decreased significantly after 4 weeks of storage under stress conditions. As shown in Figure 5.5, the DPM-PVP 20% and DPM-PAA 20 and 50% thermograms showed no indication of crystallization whereas the thermograms for DPM-PVP 50 and 80% and DPM-PAA 80% displayed endothermic peaks corresponding to the melting of crystalline drug. On the other hand, only the CNZ-PAA 20 and 50% ASDs remained amorphous. All other CNZ systems displayed drug crystallization within the ASDs after 4 weeks of storage under stress conditions. This demonstrated that stress conditions have caused crystallization of amorphous

DPM and CNZ from the system. Furthermore, PAA has better crystallization inhibition efficiency of amorphous DPM and CNZ compared to PVP.

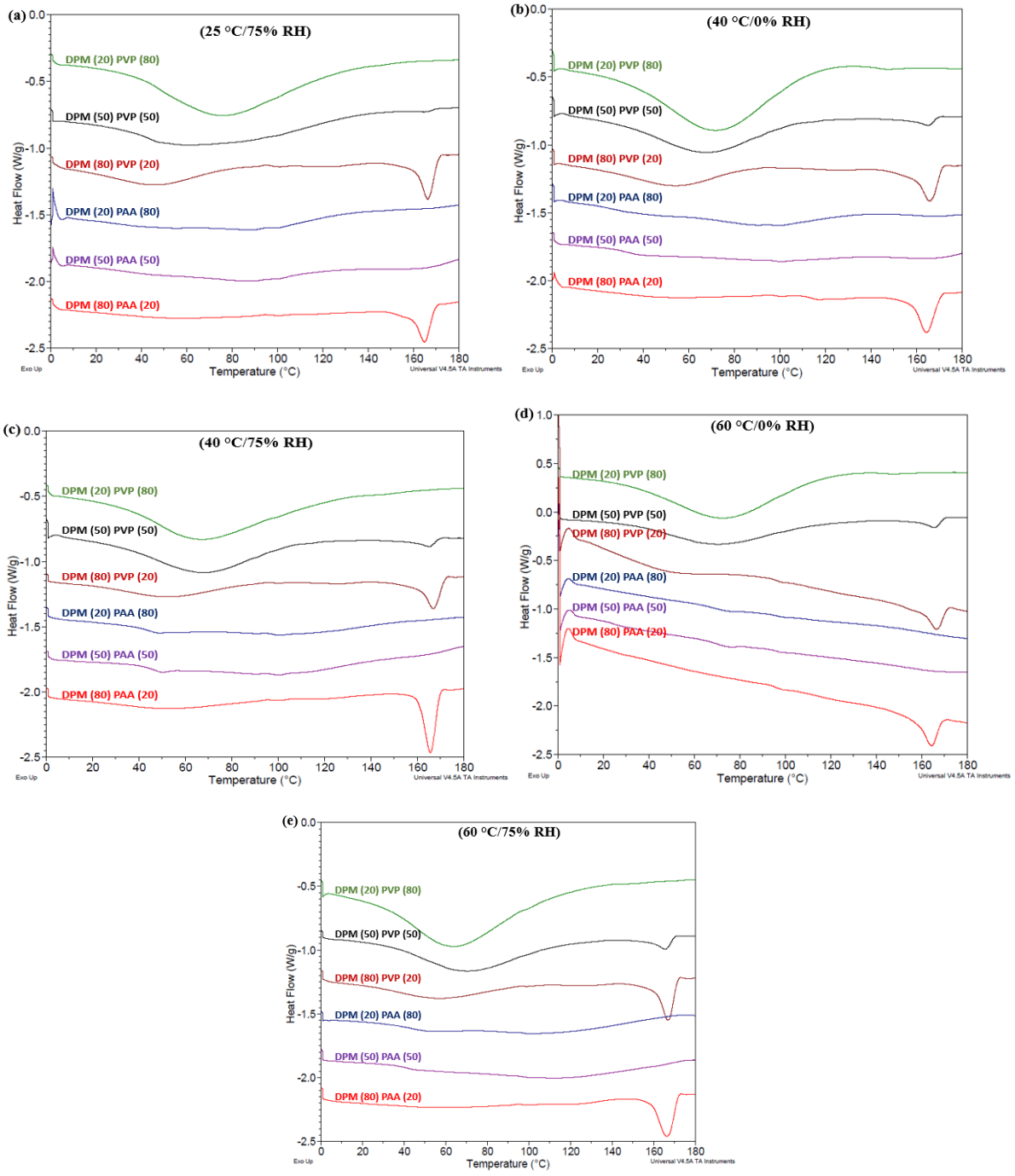

Figure 5.5. DSC thermograms of freshly prepared DPM ASDs stored at different conditions of temperature and moisture for 4 weeks; n = 2

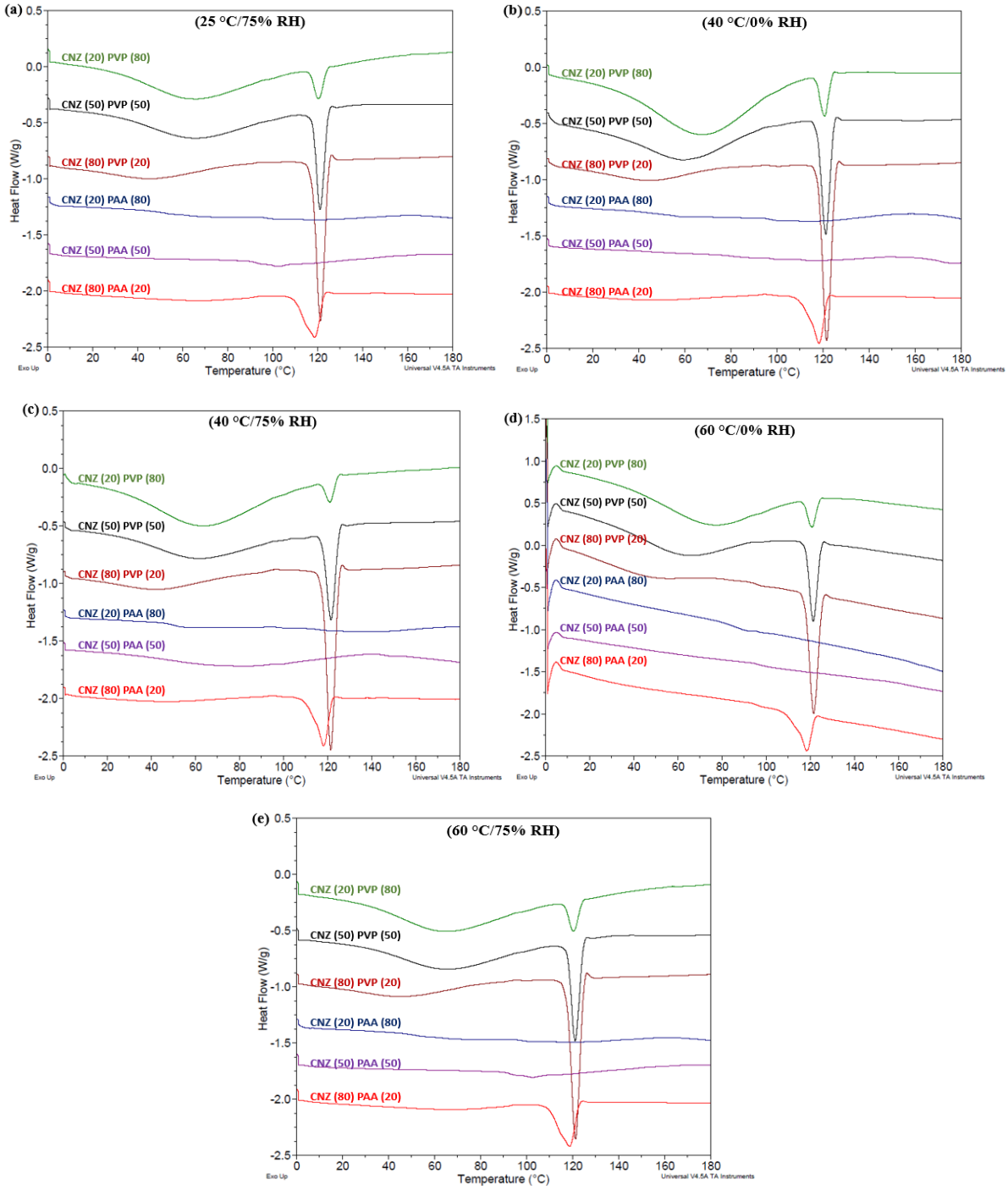

Figure 5.6. DSC thermograms of freshly prepared CNZ ASDs stored at different conditions of temperature and moisture for 4 weeks; n = 2

Table 5.1. Glass transition temperature (T_g, °C) of DPM and CNZ ASDs

	ASD FORMULATIONS (Each point represents mean; n = 2)						
	1 week						
	Fresh	25°C/0% RH	25°C/75%R RH	40°C/0% RH	40°C/75% RH	60°C/0% RH	60°C/75% RH
PVP Based							
DPM-20	147.9	147.8	147.5	147.8	148.0	147.7	147.2
DPM-50	113.4	113.2	113.4	114.0	113.5	113.7	113.8
DPM-80	102.7/152.4	113.0	112.9	112.4	113.5	102.2/151.7	106.1/149.8
PAA Based							
DPM-20	149.9	149.8	147.2	149.3	54.3/153.2	46.0/166.7	52.5/154.3
DPM-50	113.4	143.3	143.5	148.0	55.0/144.5	55.6/155.6	47.8/150.9
DPM-80	117.7	112.0	116.5	113.0	113.2	112.2	119.5
	2 week						
PVP Based							
DPM-20		146.5	147.5	147.1	147.1	147.9	147.9
DPM-50		113.7	113.6	113.4	113.1	114.1	113.4
DPM-80		113.6	113.3	105.2	113.3	113.4	85.0
PAA Based							
DPM-20		149.8	55.2/153.8	149.3	48.5/153.9	76.8/152.2	52.2/152.9
DPM-50		148.3	57.9/144.4	147.2	46.8/139.0	56.4/148.0	47.0/135.7
DPM-80		111.4	110.4	112.0	113.4	113.0	114.1
	3 week						
PVP Based							
DPM-20		147.8	147.6	147.7	146.9	148.0	147.8
DPM-50		114.2	114.9	115.3	114.0	114.1	114.1
DPM-80		113.0	113.6	115.1	113.6	114.0	115.6
PAA Based							
DPM-20		149.0	51.7/148.7	38.7/148.2	52.1/132.7	74.6/150.3	51.7/135.8
DPM-50		148.0	56.0/141.7	147.4	41.7/135.4	78.5/146.9	50.4/126.2
DPM-80		112.0	114.9	113.0	113.6	116.9	113.4
	4 week						
PVP Based							
DPM-20		147.9	54.1/146.5	147.1	55.3/138.7	146.9	51.3/136.5
DPM-50		113.4	50.2/112.2	112.7	50.2/114.7	114.3	38.5/114.7
DPM-80		102.7/152.4	50.0/120.4	113.2	114.0	109.7	114.0

PAA Based							
DPM-20		149.8	51.3/124.1	38.7/148.9	49.7/151.9	73.1/143.5	51.7/135.4
DPM-50		148.3	48.5/140.2	140.7	41.7/130.1	78.8/142.3	50.9/114.3
DPM-80		117.7	114.0	113.7	114.0	113.8	114.7
				1 Week			
PVP Based							
CNZ-20	105.5	106.4	83.7	104.5	78.0	62.5/155.8	75.6
CNZ-50	57.1	56.9	56.3	54.8	52.3	52.2	50.9
CNZ-80	79.4	78.9	77.9	78.9	74.2	76.4	75.4
PAA Based							
CNZ-20	110.4	109.9	96.2	94.4	90.5	92.7	87.2
CNZ-50	128.1	121.0	107.5	110.0	105.5	110.5	105.4
CNZ-80	102.5	102.9	89.7	102.4	83.4	101.2	71.7
				2 Week			
PVP Based							
CNZ-20		105.9	68.3	54.8/155.4	58.4	51.0/149.2	49.2
CNZ-50		56.6	56.1	54.8	51.9	51.2	50.1
CNZ-80		78.5	77.9	78.5	70.2	74.8	66.2
PAA Based							
CNZ-20		108.8	90.3	88.1	75.2	86.9	72.9
CNZ-50		115.3	107.7	88.6	84.7	87.1	80.2
CNZ-80		103.8	88.1	102.5	82.9	101.0	68.3
				3 Week			
PVP Based							
CNZ-20		106.0	58.7	55.6/155.7	58.4	51.0/149.2	49.2
CNZ-50		55.1	55.4	54.03	51.9	51.2	50.1
CNZ-80		78.7	77.6	75.1	70.2	74.8	66.2
PAA Based							
CNZ-20		108.7	84.2	87.2	75.2	86.9	72.9
CNZ-50		113.1	102.9	87.5	84.7	87.1	80.2
CNZ-80		102.3	88.2	101.4	82.9	101.0	68.3
				4 Week			
PVP Based							
CNZ-20		106.2	54.3	54.6/155.6	50.7	50.4/148.8	47.5
CNZ-50		55.4	55.2	54.5	50.5	50.1	49.8
CNZ-80		78.2	76.4	75.2	70.0	74.3	62.1
PAA Based							
CNZ-20		104.4	86.4	83.2	73.5	75.1	61.7
CNZ-50		111.7	100.2	85.3	84.3	84.1	72.6
CNZ-80		101.7	88.6	101.3	81.1	100.4	61.8

To better understand the impact of stress conditions on amorphous drug crystallization within ASDs, we have chosen DPM-PVP 50 and 80%, DPM-PAA 80%, CNZ-PVP 20, 50 and 80%, and CNZ-PAA 80% to assess crystallinity under various storage conditions using Eq. (5.1). The results are shown in Figure 5.7. All other systems (DPM-PVP 20%, DPM-PAA 20 and 50% and CNZ-PAA 20 and 50%) remained completely amorphous after 4 weeks of storage under stress conditions. It is clear that crystallinity increased in the order of 25 °C/0% RH, 25 °C/75% RH, 40 °C/0% RH, 60 °C/0% RH, 40 °C/75% RH and 60 °C/75% RH for DPM and 25 °C/0% RH, 40 °C/0% RH, 25 °C/75% RH, 60 °C/0% RH, 40 °C/75% RH and 60 °C/75% RH for CNZ. The results indicate that ASDs are most sensitive to 60 °C/75% RH for both DPM and CNZ, while 25 °C/0% RH and 40 °C/0% RH had the least effect on the amorphous DPM and CNZ crystallization, respectively.

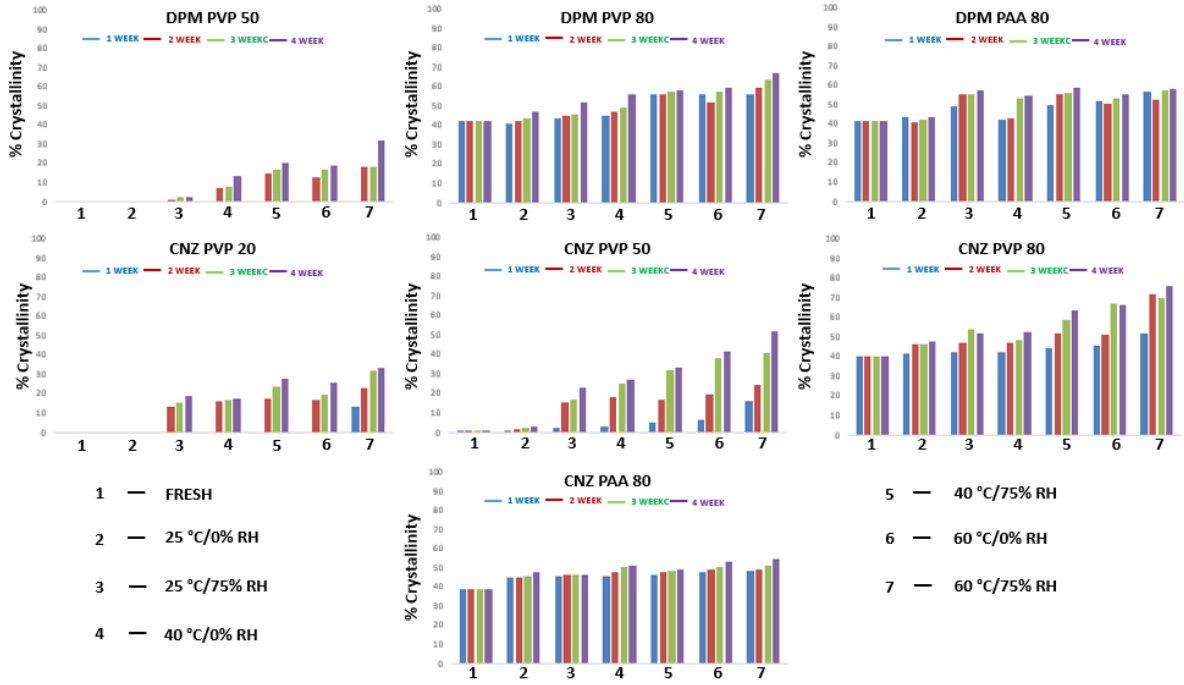

Figure 5.7. Relative crystallinity of DPM and CNZ ASD after 4 weeks of storage under stress conditions; Each point represents mean; n = 2

5.3.4. In-vitro dissolution behaviour of ASDs

Effect of physical aging on the dissolution profile of ASDs: It has been shown that high temperature and humidity can cause recrystallization of amorphous DPM and CNZ, reducing the rate and extent of dissolution of ASDs. To investigate the changes in the solid state (physical aging) of DPM and CNZ ASDs stored within a desiccator at room temperature, DSC was performed at different time points (Figure 5.3). After 1 year of storage, DPM-PVP 20%, DPM-PAA 20%, DPM-PAA 50%, CNZ-PAA 20% and CNZ-PAA 50% were still amorphous without drug crystallization. However, some changes did occur as

detected by MDSC. The increase in enthalpy of relaxation at glass transition (DPM-PAA 20 and 50%) and the decreased T_g in the MDSC thermogram indicated that physical ageing had occurred.[20] [21] To investigate the effect of physical aging on the dissolution behaviour of ASDs, dissolution tests were performed and the results are shown in Figure 5.8 and 5.9. The results indicated a reduction in the rate and extent of dissolution over time which suggested a negative effect of physical aging on the dissolution of ASDs.

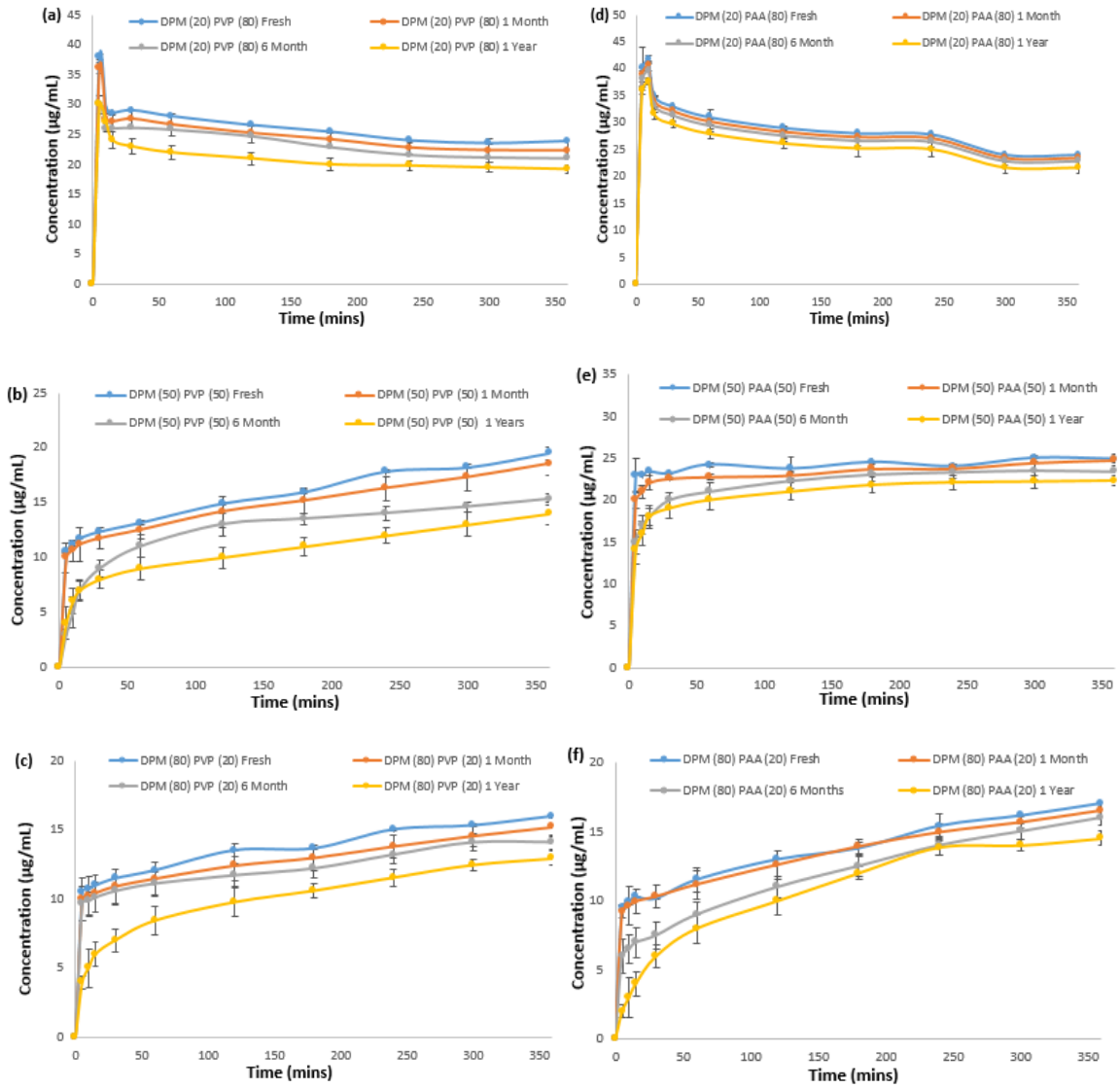

Figure 5.8. Dissolution profile of DPM ASDs stored within desiccator at room temperature; Value in brackets represent weight fraction of the component; Each point represents mean ± SD; n = 2

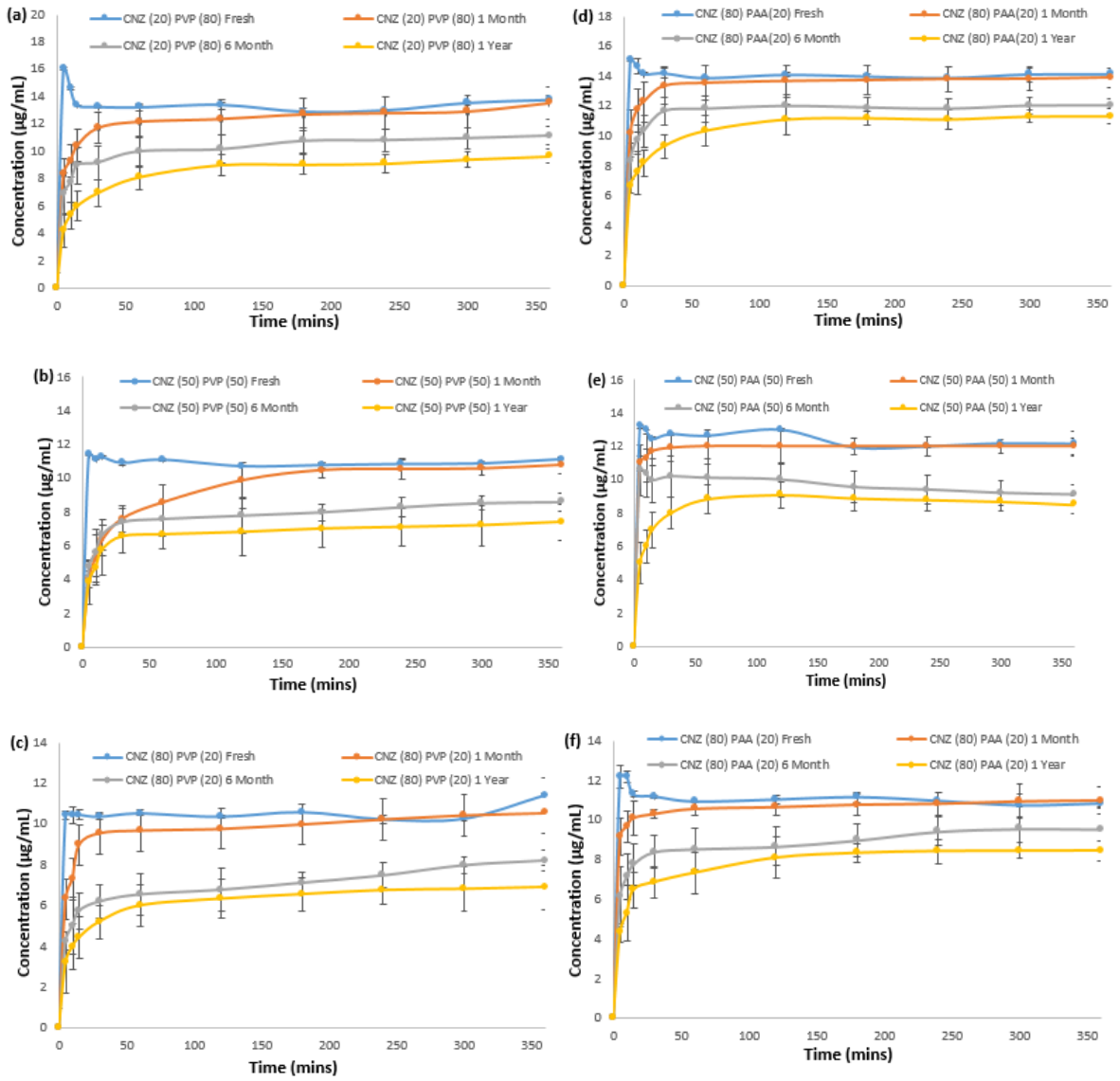

Figure 5.9. Dissolution profile of CNZ ASDs stored within desiccator at room temperature; Value in brackets represent weight fraction of the component; Each point represents mean ± SD; n = 2

Effect of stress conditions on the dissolution profile of ASDs: As stress conditions caused phase separation and/or crystallization of DPM and CNZ ASDs, dissolution tests were subsequently performed to investigate effect of stress conditions on the dissolution profile of ASDs. The dissolution profile of DPM and CNZ ASDs within PVP and PAA subjected to various stress conditions for 4 weeks are shown in Figure 5.10 and 5.11. As expected, stress conditions caused a reduction both in the rate and extent of dissolution due to the drug recrystallization. Compared with the solid-state crystallization under stress conditions (Figure 5.5, 5.6 and 5.7), similar trends were observed in the effect of stress conditions on the dissolution behaviour of ASDs: 60 °C/75% RH has the greatest effect and 25 °C/0% RH has the least effect. The results also showed that the changes in dissolution behaviour under

various stress conditions correlated with the drug loading. A higher drug loading would lead to a lower rate and extent of dissolution after storage (Figure 5.10 and 5.11). To further asses the effect of stress condition on the dissolution profile of phase separated yet amorphous systems, we studied the dissolution profiles of completely amorphous systems which had been subjected to various stress conditions for 4 weeks. As shown in Figure 5.10 and 5.11, stress conditions caused a reduction in the dissolution rate in the phase separated amorphous system. Thus, it may be suggested that even if the system is still amorphous, phase separation it is more susceptible to crystallization. Trends were similar in this case also where 60 °C/75% RH has the greatest effect and 25 °C/0% RH has the least effect.

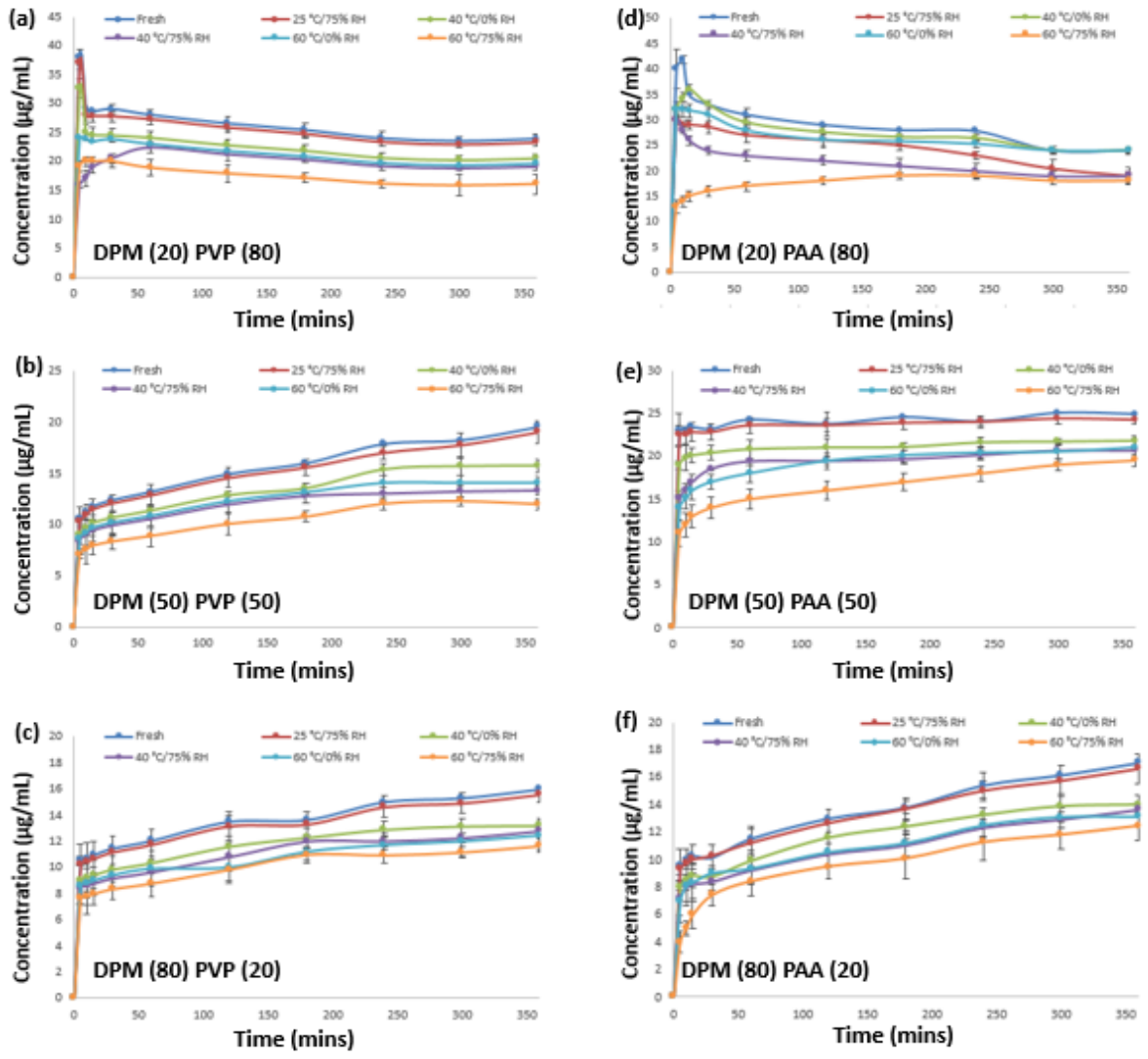

Figure 5.10. Dissolution profile of DPM ASDs stored at stressed conditions for 4 weeks; Value in brackets represent weight fraction of the component; Each point represents mean ± SD; n = 2

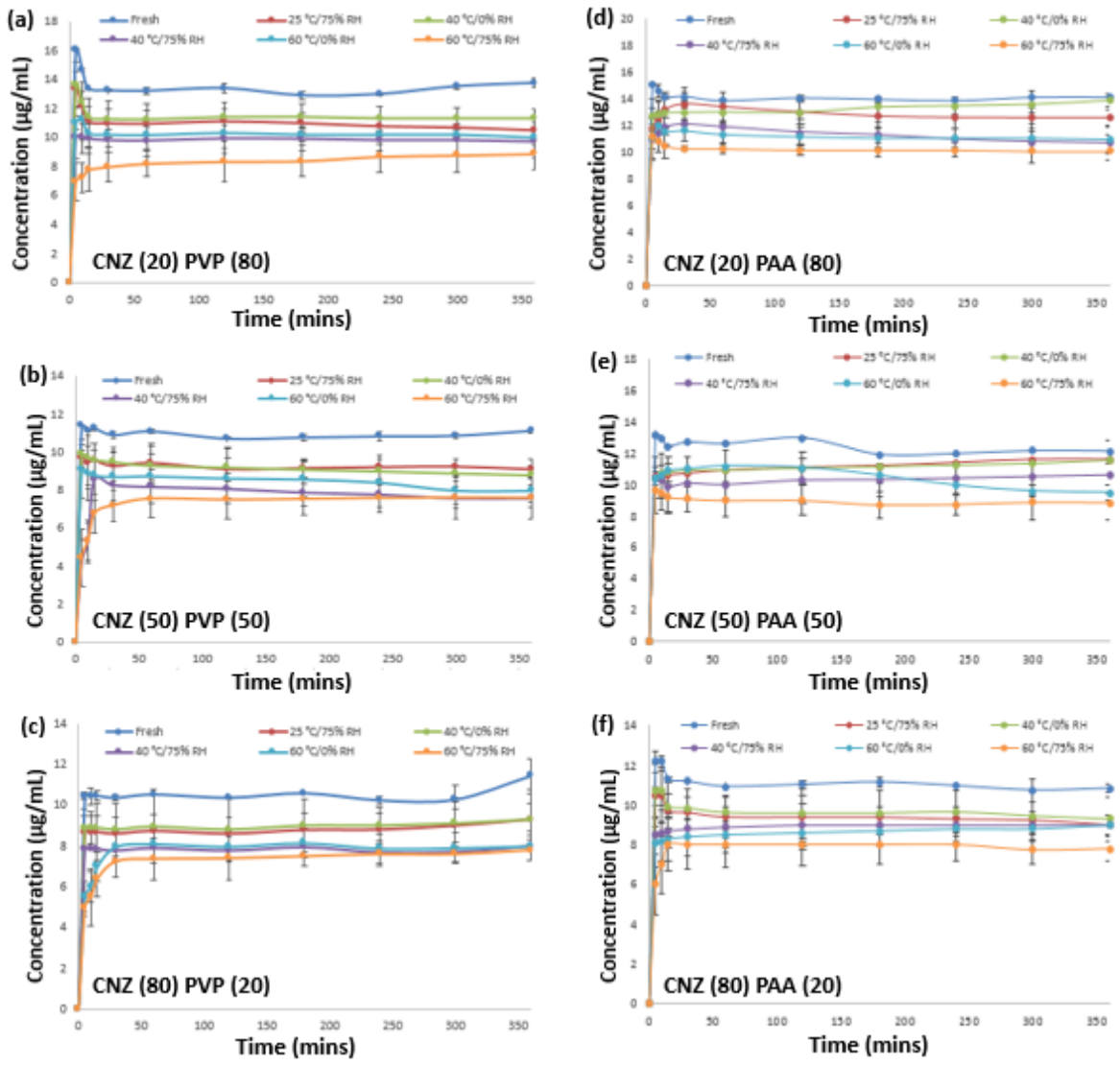

Figure 5.11. Dissolution profile of CNZ ASDs stored at stressed conditions for 4 weeks; Value in brackets represent weight fraction of the component; Each point represents mean ± SD; n = 2

5.4. General Discussions

Crystallization is the process by which a crystalline lattice (anisotropic nature and long-range three-dimensional order) is formed.[22] Generally, this process occurs either from an undercooled melt or from a supersaturated solution. If occurring from an under-cooled melt, crystallization can also be described as the process by which a supercooled liquid or a glass undergoes a phase transition (first-order) to form the more thermodynamically stable crystalline lattice. Crystallization is generally described using two sequential sub-processes: nucleation and crystal growth.[23] The process of development of nuclei or seed which act as the center of crystallization is known as nucleation, and depends on the thermodynamic and

kinetic factors mentioned above, as well as other factors including interfacial surface energy. Post nucleation, crystal growth is also affected by thermodynamic and kinetic factors.[23] To have a clear understanding of the effect of moisture on the crystallization behaviour of a drug from an ASD, it is important to consider the different factors mentioned above.

Different thermodynamic, kinetic as well as other molecular factors affect this process.[24 25] Crystallization of an amorphous drug is affected by the thermodynamic driving force (ΔG_c) for crystallization, also known as "degree of undercooling".[26] ΔG_c for pure amorphous drugs can be approximated using the Hoffman equation or calculated as the difference in the enthalpy and the entropy of the amorphous and crystalline forms of the drug.[27 28] However, in the presence of a second component such as polymer which is mixed at the molecular level with the amorphous drug, ΔG_c for the crystallizable component of the system is not easily quantifiable. In Chapter 3, the additional free energy change upon mixing (ΔG_{mix}) of DPM-PVP, DPM-PAA, CNZ-PVP and CNZ-PAA systems have been calculated by performing melting point depression experiments and found that PAA have better stabilizing effect against crystallization compared to PVP.[5] It is apparent from Figure 5.3, 5.4, 5.5, 5.6 and 5.7 that DPM and CNZ crystallization rates from PVP dispersions are extremely sensitive to temperature and RH compared to PAA based dispersions. Also, in the presence of a third component, such as moisture, which is sorbed by the system (comprised of drug and polymer) at molecular level will further affect ΔG_{mix}. However, an exact estimation is extremely difficult, since different contributing factors effecting ΔG_{mix} will include the relative amount of drug, polymer and water, as well as drug-drug, drug-polymer, drug-water and polymer-water interactions, which are liable to change in the presence of other components.[5]

Kinetically, intimately mixing large molecules such as polymers with an amorphous drug may reduce the overall molecular mobility within the dispersion, for example, as shown by an increase in the T_g of the ASDs (Table 5.1). Previously (Chapter 2 and 3), it has been found that reducing the molecular mobility may increase the stability of amorphous systems by reducing the crystallization rate of amorphous DPM and CNZ.[4,5] Aside from this, drug-polymer interaction and the degree of drug-polymer mixing have also been shown to impact crystallization from the amorphous phase. ASDs composed of a poorly water-soluble drug and a polymer are mixed and processed with the intention of maintaining the drug as an amorphous solid over the shelf-life of the product, thereby ensuring higher and reproducible dissolution rates. It is generally expected that, for the polymer to act as an effective

crystallization inhibitor, the drug and polymer should be intimately mixed to produce a homogenous system; this is usually inferred by the presence of a single T_g in DSC thermogram. DPM-PVP (20 and 50%), DPM-PAA (20 and 50%), CNZ-PVP 20% and CNZ-PAA (20 and 50%) drug loadings, investigated in this study, form miscible amorphous systems displaying a single T_g event, as well as evidence of drug-polymer intermolecular interactions (Figure 5.2 and Table 5.1). On the other hand, DPM-PVP 80%, DPM-PAA 80%, CNZ-PVP 50 and 80%, and CNZ-PAA 80% displayed two-phase amorphous-crystalline systems.

To further probe into the effect of storage at high temperatures and RH, it is necessary to consider an interesting phenomenon reported for the PVP and PAA based DPM and CNZ dispersions, namely that exposure of the samples to high temperature and RH resulted in the formation of drug-rich and polymer-rich phases (Table 5.1). In the event of stress-induced amorphous-amorphous phase separation, it would be expected that the physical stabilization of the amorphous drug due to the formation of an ASD within the polymer matrix would be significantly reduced, if not altogether eliminated in the most extreme cases (where phase separation has been observed leading to crystallization) of high drug loadings and high temperature/RH exposure (Table 5.1). Therefore, the overall rate of crystallization rate would be expected to be dependent on the nature of amorphous drug, drug-polymer miscibility, drug-polymer interaction and the stress conditions to which they are exposed. This is exactly in agreement with the previous studies on DPM and CNZ systems (Table 5.1).[4 5] In Chapter 2, we found that DPM and CNZ, both, are highly fragile amorphous drugs having high tendency to recrystallization. CNZ, in particular, is more unstable in amorphous form compared to DPM. Furthermore, it has also been shown that drug-polymer interaction is present in DPM-PVP system whereas amorphous CNZ was kinetically stabilized within PVP matrix and no CNZ-PVP interaction was observed (Chapter 3). This is exactly in agreement with the stability results observed in this study, supporting the supposition that the crystallization of an amorphous drug is an interplay of different mechanisms.

It is also of interest to compare crystallization of DPM and CNZ from PAA-containing ASDs to those from PVP-containing ASDs. Generally, the extent of DPM and CNZ crystallization from PAA dispersions tended to be lower than for PVP based ASDs at equivalent drug loadings (Figure 5.4 and 5.7). PAA based dispersions of DPM and CNZ at 20 and 50% drug loadings remained completely amorphous during physical aging (1 year within desiccator at room temperature) and stress testing (4 weeks at different temperature and

moisture conditions) as shown in Figure 5.3, 5.4, 5.5, 5.6 and 5.7. DPM and CNZ ASDs within PAA at 20 and 50% w/w displayed no signs of crystallization during 4 weeks of stress testing or during physical aging tests at 25 °C/0% RH. However, a significant reduction in T_g was observed (Table 5.1). Furthermore, as reported in Table 5.1, the crystallization rate of DPM and CNZ from PAA-containing dispersions was clearly much less sensitive to changes in storage in stress conditions as compared to PVP-containing dispersions. In Chapter 3 Flory-Huggins theory has been employed to predict drug-polymer interaction in the presence and absence of moisture and found that PAA has better stabilizing efficiency for amorphous DPM and CNZ compared to PVP.[5] Predictions made from previous studies (Chapter 3) on DPM and CNZ PAA or PVP based dispersions prepared by different method (solvent evaporation followed by quench cooling) are in complete agreement with these results.

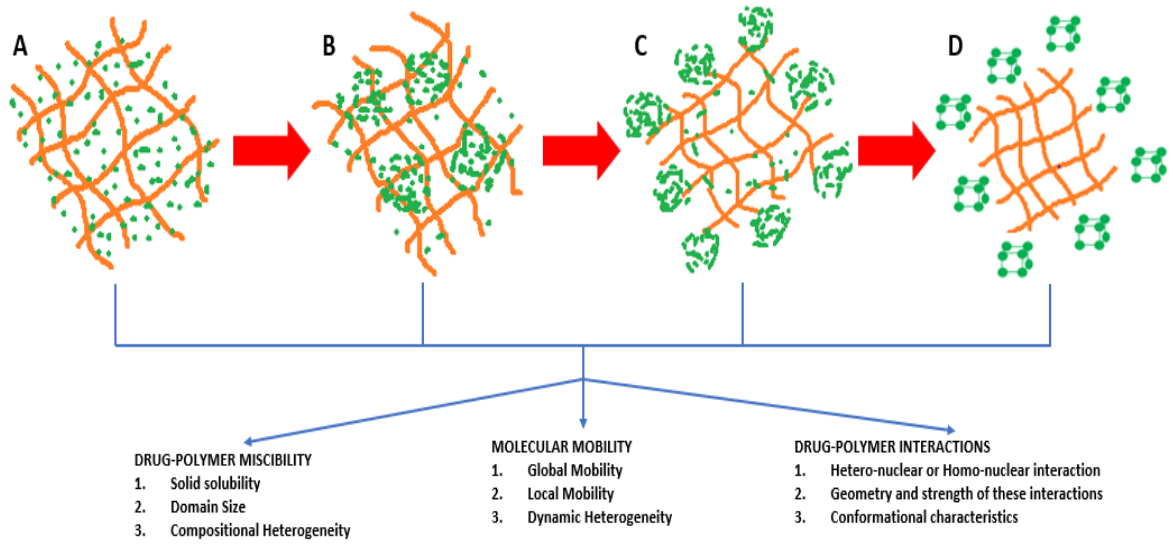

Figure 5.12. Schematic illustration of the aging and crystallization process of spray dried DPM and CNZ ASDs

DPM and CNZ ASDs in this work exhibited different physical stabilities under different conditions. For instance, physical aging and crystallization was observed for those stored within desiccator at room temperature or under stress conditions. Based on the results observed in this study, an aging and crystallization mechanism was proposed as shown in Figure 5.12. During spray drying, drugs might dissolve in polymers to form a solution and, as a result, the drug molecules might be dispersed uniformly throughout the polymer immediately after preparation (Figure 5.12 (A)). However, due to the higher free energy of amorphous form compared with its crystalline counterpart, ASDs will lose their excess free energy inevitably through physical aging first. It has been shown that aging can lead to increased phase separation, and/or crystallization. During phase separation, drug molecules

dispersed within the polymer matrix gather together to form amorphous clusters, resulting in amorphous drug-rich phase (with a lower concentration of polymer) and a polymer-rich phase (with a lower concentration of amorphous drug). The aging phenomenon is diffusion controlled leading to the formation of amorphous drug clusters within polymers (Figure 5.12 (A to B)). In the early stage of the phase separation process, drug molecules diffuse rapidly due to their high concentration and decreased T_g of the system under stress conditions. As a result, CNZ crystallizes faster than DPM as reported in Table 5.1. Afterwards, the diffusion of molecules became slower and slower due to the decreased concentration of molecularly dispersed drug molecules (Figure 5.12 (B to C)). The rate of phase separation followed by crystallization (Figure 5.12 (C to D)) depends on many factors including drug-polymer miscibility during preparation process, molecular mobility of drug molecules within dispersions and drug-polymer interactions.[3 4 5] In addition, alignment and orientation of drug molecules are required to form a crystal lattice and initiate crystallization. During the aging process, ASDs can retain their amorphous state or crystallize depending on the storage conditions (Figure 5.3 and 5.4). In this study, it has been shown that crystallization can cause a reduction in dissolution. Interestingly, it has also been shown that it is not reasonable to assume that the dissolution of ASDs will not decrease in the absence of crystallization. As shown in this study, aging or stress conditions may lead to phase separation which may have negative affect on dissolution, although the systems were still amorphous.

5.5. Conclusion

For DPM and CNZ ASDs, high temperature and humidity can cause, both, crystallization and reduced dissolution. It was found that ASDs were most affected by 60 °C/75% RH and, in contrast, 75% RH at 25 °C had the least effect on the system. Results also showed that temperature and humidity seemed to have comparable effect on the crystallization and/or phase separation of DPM and CNZ ASDs. Furthermore, PAA is more effective crystallization inhibitor of amorphous DPM and CNZ compared to PVP. It should also be noted that the physical aging can also lead to decreased dissolution in the absence of crystallization, and the T_g of ASDs may be a good indicator of changes in dissolution.

5.6. References

1. Feng J, Xu L, Gao R, Luo Y, Tang X. 2012. Evaluation of polymer carriers with regards to the bioavailability enhancement of bifendate solid dispersions prepared by hot melt extrusion. Drug Dev Ind Pharm. 38: 735-743.

2. Leuner C, Dressman J. 2000. Improving drug solubility for oral delivery using solid dispersions. Eur J Pharm Biopharm. 399: 47-60.

3. Baghel S, Cathcart H, O'Reilly N.J. 2016. Polymeric amorphous solid dispersions: A review of amorphization, crystallization, stabilization, solid-state characterization and aqueous solubilisation of biopharmaceutical classification system class II drugs. J Pharm Sci. 105: 2527-2544.

4. Baghel S, Cathcart H, O'Reilly N.J. 2016. An investigation into the crystallization tendency/kinetics of amorphous active pharmaceutical ingredients: A case study with dipyridamole and cinnarizine. Eur J Pharm Biopharm. 104: 59-71.

5. Baghel S, Cathcart H, O'Reilly N.J. 2016. Theoretical and experimental investigation of drug-polymer interaction and miscibility and its impact on drug supersaturation in aqueous medium. Eur J Pharm Biopharm. 107: 16-31.

6. Zhang J, Bruker M, Parker A, Madden-Smith C.E, Patel N, Roberts C.J. 2011. The stability of solid dispersions of felodipine in polyvinylpyrrolidone characterized by nanothermal analysis. Int J Pharm. 414: 210-217.

7. Zographi G. 1988. States of water associated with solids. Drug Dev Ind Pharm. 14: 1905-1926.

8. Andronis V, Yoshioka M, Zografi G. 1997. Effects of sorbed water on the crystallization of indomethacin from the amorphous pharmaceutical solids. J Pharm Sci. 86: 346-351.

9. Katkov I.I, Levine F. 2004. Prediction of the glass transition temperature of water solutions: comparison of different models. Cryobiology. 49: 62-82.

10. Hancock B.C, Zografi G. 1994. The relationship between the glass transition temperature and the water content of amorphous pharmaceuticals solids. Pharm Res. 11: 471-477.

11. Marsac P.J, Rumondor A.C, Nivens D.E, Kestur U.S, Stanciu KL, Taylor L.S. 2010. Effects of temperature and moisture on the iscibility of amorphous dispersions of felodipine and poly (vinyl pyrrolidone). J Pharm Sci. 99: 169-185.

12. Rumondor A.C.F, Taylor L.S. 2010. Effect of polymer hygroscopicity on the phase behaviour of amorphous solid dispersions in the presence of moisture. Mol Pharm. 7: 477-490.

13. Purohit H.S, Taylor L.S. 2015. Taylor, Phase separation kinetics in amorphous solid dispersions upon exposure to water. Mol Pharm. 12: 1623-1635.
14. Xie T, Taylor L.S. 2017. Effect of temperature and moisture on the physical stability of binary and ternary amorphous solid dispersions of celecoxib. J Pharm Sci. 106: 100-110.
15. Tian B, Zhang L, Pan Z, Gou J, Zhang Y, Tang X. 2014. A comparison of the effect of temperature and moisture on the solid dispersions: Aging and crystallization. Int J Pharm. 475: 385-392.
16. Adronis V, Yoshioka M, Zografi G. 1997. Effects of sorbed water on the crystallization of indomethacin from amorphous state. J Pharm Sci. 86: 346-351.
17. Gupta P, Kakumanu V.K, Bansal A.K. Stability and solubility of celecoxib PVP amorphous dispersions. Pharm Res. 21: 1762-1769.
18. Rumondor A.C, Stanford L.A, Taylor L.S. 2009. Effect of polymer type and storage relative humidity on the kinetics of felodipine crystallization from amorphous solid dispersions. Pharm Res. 26: 2599-2606.
19. Kanaujia P, Lau G, Ng W.K, Widjaja E, Schreyer M, Hanefeld A, Fischlbach M, Saal C, Maio M, Tan R.B. 2011. Investigating the effect of moisture protection on solid-state stability and dissolution of fenofibrate and ketoconazole solid dispersions using PXRD, HSDSC, and Raman microscopy. Drug Dev Ind Pharm. 37: 1026-1035.
20. Kakumanu V.K, Bansal A.K. 2002. Enthalpy relaxation studies of celecoxib amorphous mixtures. Pharm Res. 19: 1873-1878.
21. Maiti P, Dikshit A.K, Nandi A.K. 2001. Glass-transition temperature of poly (vinylidene fluoride)-poly(methyl acrylate) blends: influence of aging and chain structure. J Appl Polym Sci. 79: 1541-1548.
22. Mullin J.W. 1997. Crstallization, Oxford: Butterwirth Heinemann.
23. Andronis V, Zografi G, Crystal nucleation and growth of indomethacin polymorphs from the amorphous state. J Non Cryst Solids. 271: 236-248.
24. Bhugra C, Pikal M.J. 2008. Role of thermodynamic, molecular and kinetic factors in crystallization from the amorphous state. J Pharm Sci. 97: 1329-1349.
25. Yu L. 2001. Amorphous pharmaceutical solids: preparation, characterization and stabilization. Adv Drug Deliv Rev. 48: 27-42.
26. Rumondor A.C.F, Stanford L.A, Taylor L.S. 2009. Effect of polymer type and storage relative humidity on the kinetics of felodipine crystallization from amorphous solid dispersions. Pharm Res. 26: 2599-2606.

27. Marsac P.J, Konno H, Taylor L.S. 2006. A comparison of the physical stability of amorphous felodipine and nifedipine systems. Pharm Res. 23: 2306-2316.
28. Zhou D.L, Zhang G.G.Z, Law D, Grant D.J.W, Schmitt E.A. 2002. Physical stability of amorphous pharmaceuticals: Importance of configurational thermodynamic quantities and molecular mobility. J Pharm Sci. 91: 1863-1872.

CHAPTER 6. AN INVESTIGATION INTO THE SOLID-STATE PROPERTIES AND DISSOLUTION PROFILE OF SPRAY DRIED TERNARY AMORPHOUS SOLID DISPERSIONS; A RATIONAL STEP TOWARDS THE DESIGN AND DEVELOPMENT OF MULTI-COMPONENT AMORPHOUS SYSTEM

6.1. Introduction

As discussed in the previous chapters, the majority of new chemical entities in the development pipeline are poorly water soluble and various strategies are employed to enhance their solubility and dissolution rate.[1 - 7] Amorphization of crystalline drugs is a promising strategy to overcome the solubility challenge, however, they have inherent tendency to convert to crystalline form.[8 - 14] In an attempt to delay crystallization and improve physical stability and dissolution, different polymers (which interfere with either nucleation or crystal growth or both) have been used to prepare binary ASDs.[15 - 18] Different mechanisms have been proposed to explain the improvement in drug dissolution and stability from binary ASDs including the formation of fine particles, drug-polymer interaction in solution, formation of a physical barrier to crystallization (adsorption of the polymer molecules onto the crystal surfaces), viscosity enhancement, reduction in Gibb's free energy and an anti-plasticization effect of polymer on the drug.[9, 19]

Conceptually, multi-component ASDs are considered to be an option to further improve the solubility of poorly water-soluble drugs. A multi-component system, incorporating other pharmaceutical excipients in addition to the drug and amorphous polymer matrix, modifies the drug particles' microenvironment at the dissolution front leading to the enhancement of API solubility.[20] The physical stability of the amorphous dispersions can be improved by the selection of appropriate matrix components for multi-component system.[21] Therefore, multi-component ternary ASDs composed of API, amorphous polymer matrix and functional excipients are considered to be a propitious step towards the improvement of physical stability and enhancement of dissolution of poorly water-soluble drugs. However, in formulating such systems several issues, such as the formation of homogenous dispersions and the physical stability, should be considered. It has been observed that in some cases the solution concentration of free drug during the dissolution of ternary ASDs (drug, polymer and an additive) declined due to the recrystallization of an amorphized additive.[22] It has also been reported that multi-component systems of drug and polymer may undergo phase separation due to the addition of an additive to the binary ASD system.[23] There is a paucity of literature on the application of multi-component spray dried solid dispersions and further research is required to understand and optimize ternary ASDs. Thus it would seem that the choice and quantity of functional additive may be critical to formulating stable, multi-component ASDs. Therefore, a rational starting point towards the design of a multi-component ternary ASDs,

where the API is one of the amorphous state components, would be a ternary mixture of amorphous polymer and functional excipients forming drug-polymer-excipient system.

Generally the third component is either a polymer or surfactant to form ternary ASDs. To date, very few studies have examined the effect of a third component on the stability and dissolution of ASDs.[23 - 26] The addition of a third component commonly aims to further improve the physical stability and increase the dissolution by inhibiting drug recrystallization during shelf life and in solution state, respectively. Moreover, it would be interesting to see the effect of combining two different polymers which have different types of interactions with the drug on the physical stability and dissolution behaviour of ternary ASDs. Although there are many publications on amorphous drug crystallization inhibition in the presence of a single polymer (binary ASDs), there is a need to understand drug crystallization (both in the solid-state and during dissolution) in the presence of two polymers (ternary ASDs). Due to an increase in the overall number of poorly soluble APIs, ternary ASDs having two different polymers may be utilised to further enhance their physical stability and apparent solubility.

Another class of pharmaceutical excipient used to improve the aqueous solubility and dissolution performance of poorly water-soluble drugs are surfactants.[27, 28] As a consequence, it may be expected that incorporating surfactants into ASDs to form drug-polymer-surfactant ternary ASDs may further enhance the dissolution rate of the poorly water-soluble drug by promoting wettability of the particles. In this work, the main reason for choosing surfactants as third component in addition to binary drug-polymer combinations was based on the fact that polymer may dissolve the amorphous drug in the solid state, leading to a stable system without crystallization or phase separation, while the surfactant may promote wettability in solution which can lead to an increase in solubility and dissolution rate of the drug. Previously, surfactants have been used as plasticizers for polymers during hot melt extrusion processes to enhance drug-polymer miscibility.[29, 30] However, currently there is very limited literature available on the preparation and characterization of spray dried drug-polymer-surfactant dispersions and therefore, it is of interest to study the effect of surfactants on ASD properties when incorporated within spray dried ASDs.[31, 32] Furthermore, the role of surfactants on drug release from ASDs has also been reviewed, with some studies finding a positive impact on the release kinetics of hydrophobic APIs and others reporting a negative effect of surfactants on the dissolution of amorphous drugs from solid dispersions.[33, 34] It is therefore reasonable to suggest that surfactants, like polymers, may have an impact on the physical stability and dissolution behaviour of ASDs and it is of interest to explore this

possibility. Consequently, the physical stability and dissolution behaviour of spray dried ASDs with and without surfactants as a ternary agent will also be investigated in this study.

Polyvinyl pyrrolidone K30 (PVP), hydroxypropyl methylcellulose K100 (HPMC) and a combination of both have been chosen as a carrier matrix for ASDs. The surfactants selected for this study are poloxamer 188 (P188) and sodium dodecyl sulphate (SDS). P188, which is a non-ionic, triblock copolymer, comprised of a hydrophobic block of polypropylene glycol and two hydrophilic blocks of polyethylene glycol, is categorized as a surfactant in this work as the use of this excipient in the pharmaceutical area is related to its surfactant properties. The other surfactant investigated in this study is SDS, which is an anionic surfactant. The selection of these excipients was based on the anticipation that differences in their physicochemical characteristics may allow one to distinguish the critical factors affecting the drug-polymer interactions and miscibility more clearly. Another criteria for choosing these excipients (polymer-surfactant combination) was based on the fact that one must dissolve the amorphous drug in the solid state, leading to a stable system without crystallization or phase separation, while the other one must increase the solubility and dissolution rate of the drug. As a control, drug-polymer-polymer-surfactant (quaternary ASDs) combinations has also been studied to probe the effect of surfactant on drug-polymer-polymer system. Dipyridamole (DPM) and cinnarizine (CNZ) were selected as model drugs because of their poorly water-soluble properties. In Chapter 2, it has been reported that the DPM and CNZ are very unstable in their amorphous forms and have high crystallization tendency.[11] In Chapter 3-5, the role of drug-polymer interaction and anti-plasticization in improving solid-state stability and increasing supersaturation of DPM and CNZ binary ASDs has also been studied.[19] This is a continuation of previous work which showed significant differences in the dissolution profile of binary ASDs when drug-polymer interactions were changed (using two different polymers),[19] to understand the role of polymer-surfactant and polymer-polymer combinations on the physical stability and dissolution profile of ASDs by preparing and characterizing spray dried binary (drug-polymer), ternary (drug-polymer-surfactant or drug-polymer-polymer) and quaternary (drug-polymer-polymer-surfactant) solid dispersions. The ASDs were characterized by differential scanning calorimetry (DSC), modulated DSC, Fourier-transform infrared (FTIR), dynamic vapour sorption (DVS), in-vitro dissolution and ^{1}H nuclear magnetic resonance (NMR). This study will add to the overall understanding of the use of excipients in ASDs and will help in future multi-component amorphous product development.

6.2. Materials and Methods

6.2.1. Materials

Dipyridamole (DPM), cinnarizine (CNZ), polyvinyl pyrrolidone K30 (PVP) and poloxamer 188 were supplied by Sigma Aldrich, Ireland. Hydroxypropyl methylcellulose K100 (HPMC) was obtained from Colorcon, England, and sodium dodecyl sulphate (SDS) was obtained from Fisher Scientific, U.K. All reagents were of analytical grade and used without further purification. The chemical structure and key physicochemical properties of the model drugs and polymers used in this study are shown in Figure 6.1 and Table 6.1, respectively.

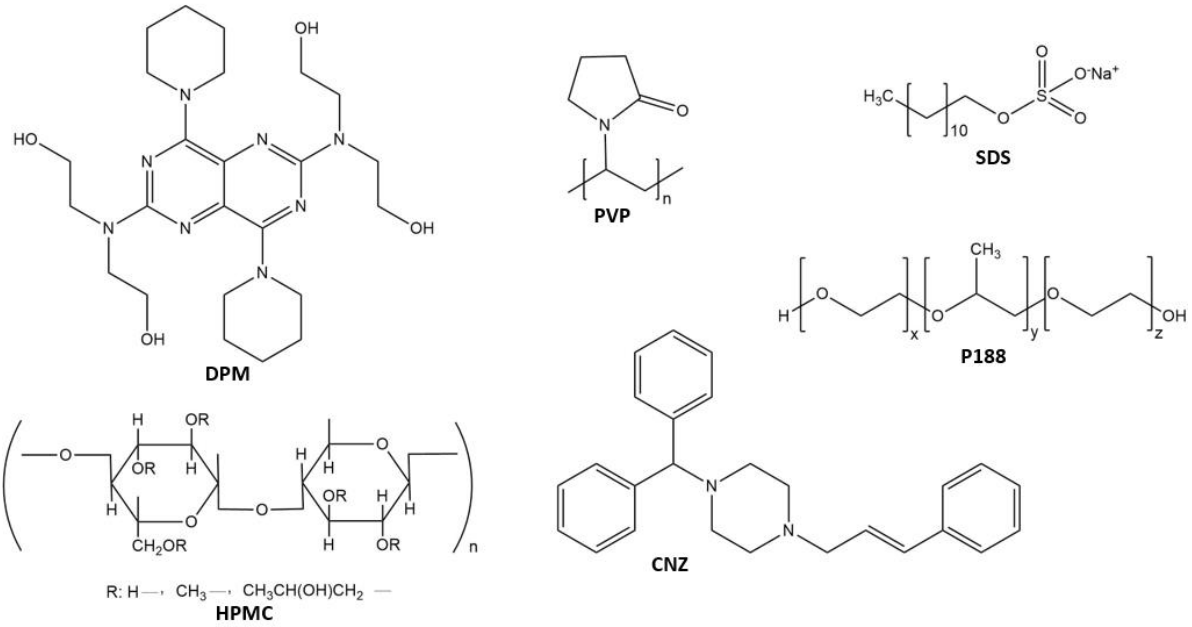

Figure 6.1. Chemical structure of DPM, CNZ, PVP K30, SDS, P188 and HPMC K100 (clockwise from top)

Table 6.1. Physicochemical properties of model drugs and polymers

	Molecular weight (g/mol)	ΔH_f (kJ/mol)[a]	T_m (°C)[a]	T_g (°C)[a]	Log P [b]	pK$_a$
DPM	504.63	29.06	168.11	37.44	3.71	6.4[35]
CNZ	368.51	38.33	121.25	5.86	5.71	8.4[36]
PVP	40000	-	-	164.13	-	-
HPMC	450,000	-	-	153.83	-	-
SDS	288.37	-	-	-	-	-
P188	102.13	-	48.67	-	-	-

[a]Values obtained from DSC (n=3), [b]Values obtained from literature[19]

6.2.2. Preparation of amorphous solid dispersions

The spray dried solid dispersions were prepared using a Pro-CepT 4M8-TriX spray drier (Zelzate, Belgium) with a bifluid nozzle. The spray drying solutions were prepared by dissolving the component mixtures in dichloromethane-ethanol mixture (50:50 v/v). The drug-polymer proportion in the binary mixture was 20:80 w/w. For the ternary solid dispersion systems, the proportion of drug-polymer-surfactant was 20:75:5 and drug-polymer-polymer was 20:40:40. The amount of surfactant in ternary ASDs was kept low as they are not well tolerated in the body at high concentration.[9] The proportion of drug-polymer-polymer-surfactant in quaternary systems was 20:37.5:37.5:5 w/w. The key processing parameters were feed concentration (dichloromethane-ethanol mixture (50:50 v/v), spray rate (6 mL/min), nozzle size (0.2 mm), atomization air flow rate (5 L/min), inlet temperature (80 $\pm$ 5°C), outlet drying temperature (50 $\pm$ 5°C) and drying air rate (100 $\pm$ 10 L/min). The spray dried solid dispersions were collected using a small cyclone separator and stored in a vacuum desiccator at room temperature for further analysis.

6.2.3. Preparation of physical mixtures

Physical mixtures for in-vitro dissolution testing and melting point depression (MPD) analysis were prepared by manually mixing the components by mortar and pestle. The weight fraction of drug, polymer and surfactant for in-vitro dissolution testing was similar to weight fraction used for preparing spray dried solid dispersion. The ratio of drug and polymer chosen for binary systems to perform MPD analysis was 95:5, 90:10, 85:15 and 80:20 w/w. For ternary systems the ratios of drug-polymer-polymer were 95:2.5:2.5, 90:5:5, 85:7.5:7.5 and 80:10:10 w/w for MPD analysis.

6.2.4. Thermogravimetric analysis (TGA)

The residual solvent content of the spray dried solid dispersions was assessed using a TGA Q50 (TA Instruments Corp., Elstree, Herts, U.K.). Samples were heated at 10°C/min from 25 to 200 °C. During all TGA experiments nitrogen was used as the purging gas at 50 mL/min. All analyses were performed in duplicate.

6.2.5. Differential scanning calorimetry (DSC)

Thermal behaviour of the ASDs was analysed using a TA instrument Q2000 DSC. Temperature and heat flow calibration was carried out using a high-purity indium standard. Nitrogen was used as the purge gas at a flow rate of 50 mL/min. 3-5 mg of samples were accurately weighed into aluminium pans with pin holes. The samples were heated from 0 to 200 ºC at a heating rate of 10 ºC/min. MPD analysis was carried out at a heating rate of 2

ºC/min from 0 to 200 ºC. The glass transition temperature (T_g) of the freshly prepared and aged samples was analysed using modulated DSC (mDSC). 3-5 mg of the samples were accurately weighed into aluminium pans with pin holes. The experiment was performed under nitrogen gas flow (50 mL/min) using an underlying heating rate of 5 ºC/min from 0 to 200 ºC and a modulation amplitude of ± 0.53 ºC over a period of 40 s for all the samples. All measurements were performed in triplicate and data analysis was performed using Universal Analysis Software (TA instruments).

6.2.6. Fourier-Transform Infrared Spectroscopy

Fourier-transform Infrared Spectroscopy (FTIR) was performed using a Varian 660-IR FT-IR Spectrometer (32 scans at 4 cm^{-1} resolution). Test samples were mixed with KBr and then compressed into a disk and analysed immediately.

6.2.7. In-vitro dissolution study of solid dispersion

The equilibrium solubility of crystalline drugs and dissolution rate of amorphous DPM and CNZ from various powdered physical mixtures and ASDs, respectively, were measured using the USP II paddle method. Samples containing 25 mg of DPM and CNZ were added to 500 mL of PBS 6.8 at 37.0 $\pm$ 0.2 °C. The solution was stirred at 100 rpm using a USP II paddle apparatus. 2 mL samples were withdrawn from each vessel at predefined intervals (5, 10, 15, 30, 60, 120, 180, 240, 300, 360 and 1440 min) and centrifuged for 5 min at 15000 rpm. At each time-point the same volume of fresh medium was replaced. The concentration of DPM and CNZ was determined using a UV-Vis spectrophotometer (Varian VK 7010 L1168, Santa Clara, United State). All measurements were carried out in duplicate.

6.2.8. Solution state Nuclear Magnetic Resonance (NMR)

In order to understand the molecular mechanism of drug-polymer interaction, ^1H NMR spectra were recorded on a Jeol ECX-400 spectrometer operating at 400 MHz. The measurements were performed at 40°C in dimethylsulfoxide (DMSO-d6) using tetramethylsilane (TMS) as an internal standard. It is important to mention here that initial trials were performed using D_2O. However the poor solubility of the model drugs in D_2O leads to weak signals and the chemical shifts were not clear. Therefore, DMSO-d6 has been selected due to its high dielectric constant and hydrophilic nature. All the model drugs and polymers were completely soluble in DMSO-d6. Furthermore, to clearly elucidate the molecular interactions between polymer and surfactant were characterize by two-dimensional Nuclear Overhauser Effect spectroscopy (2D-NOESY) in DMSO-d6. The polymer to

surfactant ratio for NMR is kept same as that of dissolution studies. For 2D-NOESY, the mixing time was set to 0.5 s and the experiment was performed with a 1.5 s relaxation delay and 0.32 s acquisition time.

6.2.9. Moisture sorption analysis and Stability studies

Moisture sorption analysis of the ASDs was carried out using dynamic vapor sorption (DVS)-1000 Advantage, Surface Measurement Systems, U.K. Amorphous drug samples (5-10 mg) were analysed using a double ramp method from 0-90-0% RH (2 cycles) in 10% increment ($\frac{dm}{dt} = 0.001$ at each step) at 40 °C. Solid dispersions were also stored at 40 °C/75% RH. The physical stability of all the samples was evaluated after 4 weeks.

6.3. Results and Discussion

The association of polymer-polymer or polymer-surfactant combinations in aqueous solution have attracted considerable fundamental and technological interest. The resultant properties of these combinations possess unique properties that are significantly different from those of the individual components. Consequently, they have important applications in biological and industrial processes.[37] For example, synthetic water soluble polymer-polymer combinations have been used in operations such as flocculation during mineral processing,[38] while polymer-surfactant combinations have been used for immobilization of enzymes in polyelectrolyte complexes,[39] rheology control,[40] improving the solubility of drugs with low aqueous solubility and to control the drug release rate.[13 25 41] Thus, polymer-polymer or polymer-surfactant combinations are highly relevant, since pharmaceutical formulations often contains both excipients types.[25 41 42] Formulations containing high-energy amorphous drugs can enhance drug dissolution by generating supersaturated solutions.[9] Polymers are frequently added to delay crystallization, and surfactants are typically employed to improve processing properties or dissolution profiles.[14]

In the past, several publications have investigated the association between polymer-polymer and polymer-surfactant mixtures in solution.[13 25 41 42] The presence of hydrophilic excipients, such as polymer **or** surfactant, in a formulation containing a polymeric matrix may help prevent amorphous drug crystallization and/or prevent agglomeration of a fine crystalline precipitate into larger aggregates.[9] However, there has been limited systematic investigation of the interplay between surfactant or polymeric additive combinations in terms of the impact on solid-state properties and dissolution behaviour, although such an interplay could be very influential on the performance of the dosage form. Excipients such as polymers

or surfactants are well-known to impact nucleation and crystal growth and may accelerate or inhibit crystallization depending on their effect on crystallizing solute and solution properties.[41 42] This is important in the context of formulation of dosage forms where the goal is to prevent crystallization of amorphous drug during the shelf-life or dissolution. It is thus crucial to probe into the effect of excipient combinations on the solid-state properties and dissolution profile of amorphous drugs within solid dispersions, since the interaction can result in change in dispersion properties which may result in favourable or adverse effect on the amorphous drug crystallization inhibition. In this study, we have investigated the effect of polymer-polymer and polymer-surfactant combinations on the physical stability and supersaturation behaviour during dissolution of poorly water-soluble model drugs.

6.3.1. Drug-polymer and drug-polymer-polymer miscibility

The first step towards developing a multi-component amorphous systems is to assess the miscibility of the drug within the polymer matrix. Drug-polymer miscibility is crucial requirement for the formulation of stable ASDs.[19] Solubility parameters (δ) are used widely to quickly and effectively determine the drug-polymer miscibility was screening different systems.[37] In Chapter 3, the δ values of DPM (28.57 $MPa^{1/2}$), CNZ (21.00 $MPa^{1/2}$) and PVP (26.28 $MPa^{1/2}$) has been reported.[19] The δ value of HPMC, calculated in this study, is 22.48 $MPa^{1/2}$. It has been reported that compounds with a Δδ of less than 7.0 $MPa^{1/2}$ are likely to be miscible because the energy released by the interaction between the components balances the enthalpy of mixing within the components.[25] On the other hand, compounds with Δδ greater than 10.0 $MPa^{1/2}$ are likely to be immiscible. Thus, both the model polymers were expected to be miscible with both drugs, as they exhibited a Δδ of less than 7.0 $MPa^{1/2}$.

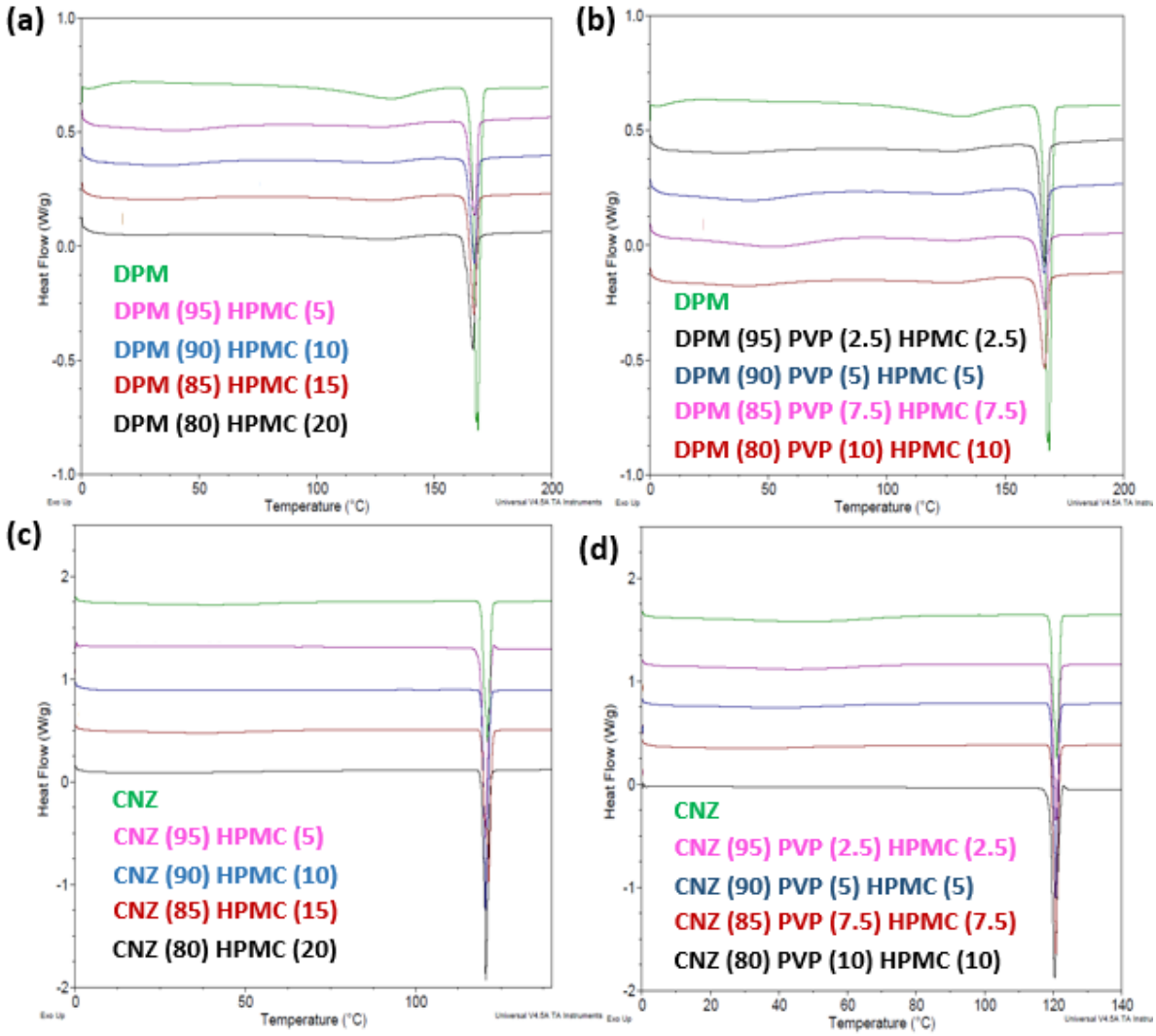

Figure 6.2. DSC thermograms of physical mixtures of model drugs and polymers at various drug loads; n = 3. Values in parentheses are % weight fractions.

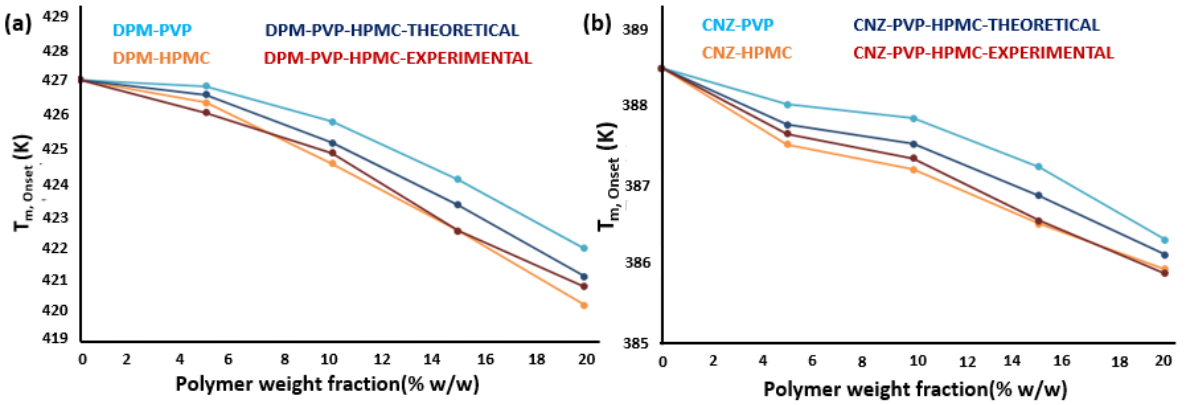

Figure 6.3. Experimental and theoretical depression in melting point of model drugs at various %w/w drug loading.

To further investigate the drug-polymer and drug-polymer-polymer interaction and the likelihood of the formation of a miscible system after spray drying, we employed melting

point depression (MPD) analysis. The chemical potential of a crystalline material becomes equal to the chemical potential of its molten material at its melting point. However, drug-polymer miscibility reduces the chemical potential of the drug in the solution (molten drug and polymer mixture), compared to the pure molten drug, which leads to a depression in melting point of the drug dissolved in the polymer.[44] Strong exothermic mixing of the drug and polymer produces a large depression in melting point of the drug, whereas weakly exothermic mixing or immiscible drug-polymer system should result in less significant MPD or no depression at all. This method has been previously used (chapter 3) to investigate drug-polymer mixing thermodynamics of DPM-PVP and CNZ-PVP systems, which showed clear evidence of a depression of the melting point of both drugs, indicating a significant degree of drug-polymer mixing at the melting temperature of the drug.[19] In this chapter, the DSC thermogram for physical mixtures of DPM and CNZ at different weight ratios with HPMC and PVP-HPMC combinations have been investigated. As shown in Figure 6.2 and 6.3, significant mixing of model drugs with HPMC and PVP-HPMC were observed. To compare the depression in melting point due to the individual polymers and their combination, theoretical depression values for the ternary mixtures were proposed based on the contribution of each polymer within the binary systems. Since the ternary mixture contains two polymers (each polymer in half proportion compared to binary system), the depression from both the polymers was averaged. If the experimental values showed a greater effect compared to this average value, then that would indicate a synergistic benefit. It was found that the depression in melting point of DPM and CNZ in the ternary systems (drug-PVP-HPMC) was higher than the average values from the binary PVP and HPMC systems suggesting synergism (Figure 6.3). This suggests that ternary ASDs may perform better than binary ASDs in increasing physical stability of amorphous drug within dispersions.

6.3.2. Solid State Characterization of freshly prepared Spray Dried dispersions

The spray dried binary, ternary and quaternary solid dispersions were prepared and examined using DSC and MDSC to determine amorphization, crystallization and glass transition. In a standard TGA ramp test, all the spray dried ASD systems showed a residual solvent content of $\leq$ 2% w/w.

6.3.2.1. Thermal analysis

PVP-based system: As shown in Figure 6.4 (a), all PVP based dispersions were found to be completely amorphous except for the CNZ-PVP-P188 system, where a crystalline CNZ

melting peak was observed. The DPM-PVP and CNZ-PVP dispersions displayed the highest T_g values (single T_g indicating molecular level mixing of the drug and polymer) when compared to other PVP-surfactant based dispersions (Table 6.2). The surfactant based PVP dispersions of DPM and CNZ displayed two T_g's (DPM-PVP-SDS, DPM-PVP-P188 and CNZ-PVP-SDS) or one T_g along with a melting peak (CNZ-PVP-P188). The ASDs displaying two T_g's represent amorphous system with phase separation leading to the formation of drug-rich (lower T_g region) and polymer-rich domains (higher T_g region). These results suggest that surfactants have a negative effect on the stability of PVP based DPM and CNZ spray dried ASDs.

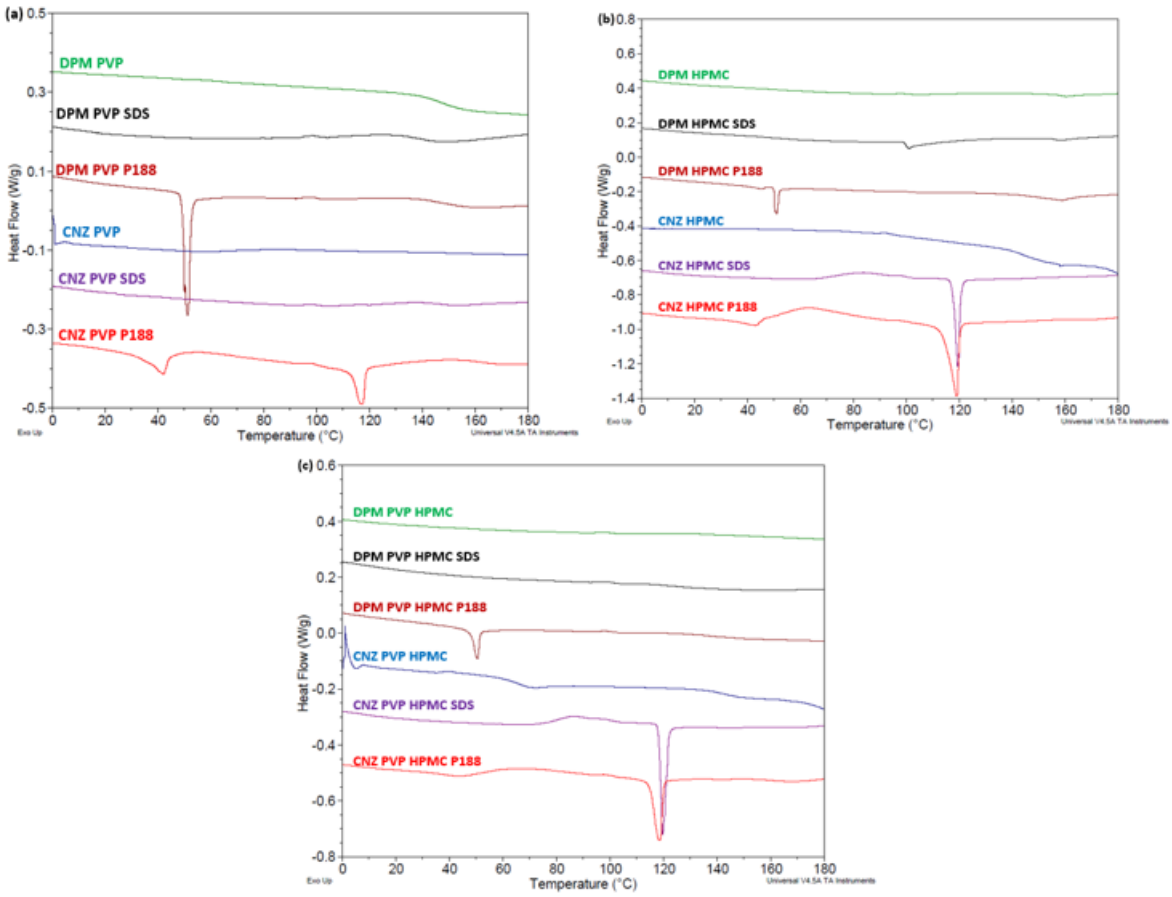

Figure 6.4. DSC thermograms of freshly prepared DPM and CNZ ASDs with PVP or group I (a), HPMC or group II (b) and PVP-HPMC or group III (c); n = 3

HPMC-based system: Binary ASDs of DPM and CNZ with HPMC remained completely amorphous as shown in Figure 6.4 (b). The dispersions displayed a single T_g (Table 6.2) indicating complete mixing and amorphization of the drug with HPMC. The T_g of the DPM-HPMC and CNZ-HPMC systems is higher than the T_g of their PVP counterparts, suggesting that HPMC has a greater antiplactization effect on the model drugs. On the other

hand, surfactants have negative effect on the stability of DPM-HPMC ASDs where drug melting peak was observed indicating the presence of crystalline drug. The negative effects of SDS and P188 were more pronounced in CNZ-HPMC based dispersions where a CNZ recrystallization peak was also present in addition to drug melting peak. These results indicate that, in the absence of surfactants, HPMC is a better antiplasticizing agent for DPM and CNZ dispersions compared to PVP whereas in the presence of surfactants PVP is a more effective stabilizer of amorphous DPM and CNZ. The presence of SDS and P188 in HPMC based dispersions of DPM or CNZ increased the molecular mobility of the amorphous drugs (lower T_g values compared to drug-polymer system without surfactant) leading to phase separation in DPM dispersions and crystallization in CNZ systems. Surfactants interfered more with the stabilizing efficiency (drug-polymer interaction and miscibility) of HPMC compared to PVP.

Table 6.2: Physicochemical properties of binary, ternary and quaternary ASDs

Formulations	Fresh		Aged		Solubility after 24 hr (µg/mL)	
	T_g (°C)	ΔH_m (J/g)	T_g (°C)	ΔH_m (J/g)	PM	SD
DPM-PVP	147.98	-	143.07	-	7.04	22.32
DPM-PVP-SDS	139.36/100.25	-	111.42	-	7.19	19.18
DPM-PVP-P188	145.94/99.24	-	137.60/98.62	-	6.04	17.18
CNZ-PVP	106.54	-	82.50	10.84	2.43	12.84
CNZ-PVP-SDS	100.10/148.23	-	88.27	12.29	2.51	12.20
CNZ-PVP-P188	100.22	2.84	21.73	11.02	2.89	12.53
DPM-HPMC	150.20	-	134.42	1.75	6.93	26.45
DPM-HPMC-SDS	99.99	0.29	98.82	6.95	6.31	18.94
DPM-HPMC-P188	99.35	2.54	98.36	3.43	6.04	21.12
CNZ-HPMC	145.66	-	64.22	2.49	2.38	13.24
CNZ-HPMC-SDS	65.76	6.45	98.40	9.35	2.34	13.23
CNZ-HPMC-P188	68.33	8.53	111.91	10.62	2.09	13.12
DPM-PVP-HPMC	157.70	-	148.61	-	6.66	29.76
DPM-PVP-HPMC-SDS	124.20	-	109.54	1.034	6.41	25.48
DPM-PVP-HPMC-P188	139.13	-	117.85	3.41	6.95	21.41
CNZ-PVP-HPMC	66.17/143.51	-	88.22	-	2.11	16.79
CNZ-PVP-HPMC-SDS	9.72	5.78	82.29	16.96	2.27	14.57
CNZ-PVP-HPMC-P188	10.93	5.27	67.91	16.34	2.09	13.49

PM and SD represents physical mixtures and solid dispersions, respectively.

PVP-HPMC based system: DPM-PVP-HPMC ternary dispersions were found to be amorphous with the T_g of the system significantly higher than the T_g of the binary DPM-PVP or DPM-HPMC based systems (Figure 6.4 (c)). This confirms the improved efficiency of the polymer combination in the formation of stable ternary DPM ASDs compared with binary dispersions. Adding surfactants to DPM-PVP-HPMC significantly reduced the T_g of the system. CNZ-PVP-HPMC dispersions displayed two T_g's suggesting the presence of two different amorphous domains. Based on our CNZ-PVP and CNZ-HPMC DSC results it is suggested that the higher T_g domain is amorphous CNZ in HPMC rich region and lower T_g phase corresponds to PVP rich region. In Chapter 3, it has been reported that CNZ exhibit no interaction with PVP and formed a solid solution with PVP such that the amorphous CNZ was kinetically frozen within the PVP matrix rather than being in a thermodynamic equilibrium.[19] Also, if the concentration of CNZ within PVP is increased then it will lead to self-association of CNZ molecules leading to phase separation and crystallization. Furthermore, as reported in previous section, HPMC has a greater stabilizing effect on amorphous CNZ due to strong drug-polymer interaction compared to PVP. Therefore, it could be generalized that the lower concentration of HPMC (40% w/w) in the CNZ ternary dispersion has led to the instability of the system. The two T_g's of in the CNZ-PVP-HPMC system is in accordance with these observations. Furthermore, the inclusion of surfactant has negatively affected the stability of the CNZ-PVP-HPMC system.

Based on the DSC results of freshly spray dried ASDs of DPM and CNZ, it was found that surfactant promotes the phase separation and crystallization of amorphous drugs within spray dried ASDs which may be due to the interference with the drug-polymer interaction or miscibility. Furthermore, a synergistic effect of the PVP-HPMC combination was observed to be stronger in the DPM dispersions than CNZ dispersions.

6.3.2.2. Spectroscopic Analysis

FTIR spectroscopy was used to assess the molecular interactions within the samples. The FTIR spectra of DPM, CNZ, PVP, HPMC and their solid dispersions are shown in Figure 6.5. The characteristic peaks of DPM are present at 1359 cm^{-1} (C – N bonds), 1533 cm^{-1} (C = N ring), 2851 cm^{-1} (symmetrical stretching of CH_2 group), 2923 cm^{-1} (asymmetrical stretching of CH_2 group) and 3303/3377 cm^{-1} (OH stretching vibration). The CNZ spectra displayed characteristic peaks at 963 cm^{-1} (aromatic out-of-plane), 1001 cm^{-1} (= C – H alkene), 1141 cm^{-1} (C – N stretching peak), 2956 cm^{-1} (aliphatic CH stretching peak), 3021 cm^{-1} (alkene CH stretching) and 3066 cm^{-1} (aromatic CH stretching). The spectra of the

physical mixtures of DPM and CNZ with PVP, HPMC and surfactants are not shown here as they did not show any apparent changes in the FTIR spectra.

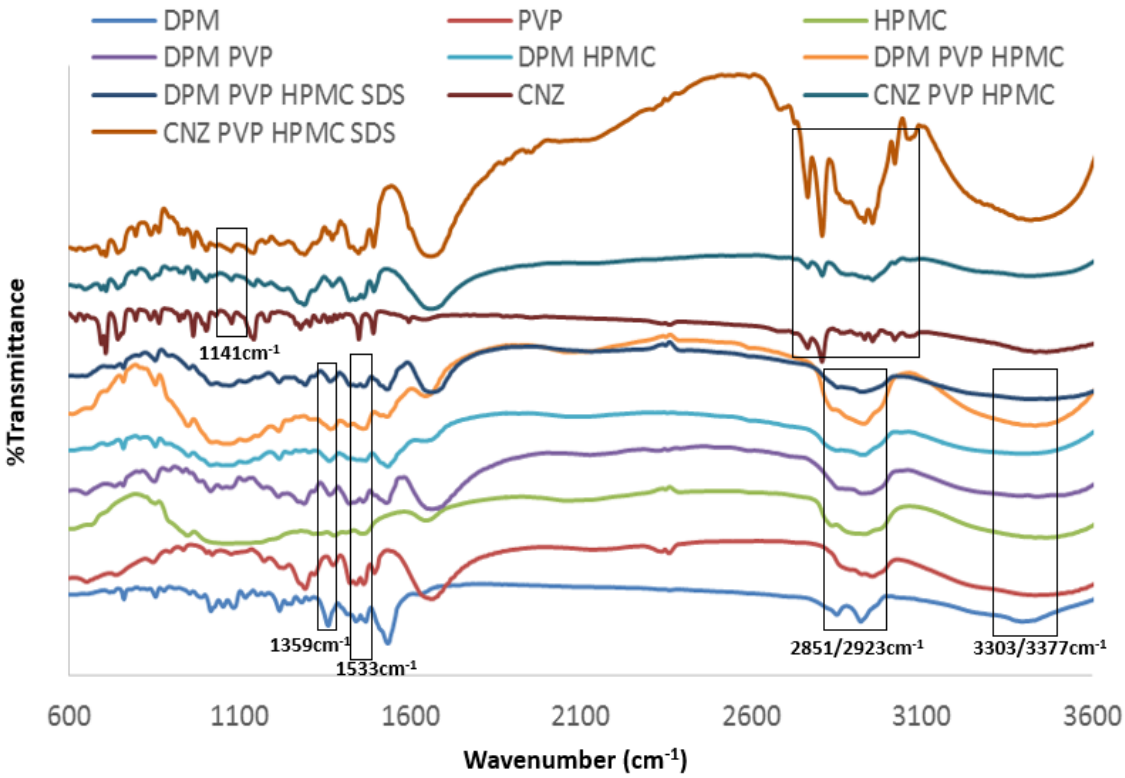

Figure 6.5. FTIR spectra of freshly prepared DPM and CNZ ASDs

The formation of DPM ASD with PVP, HPMC and PVP-HPMC resulted in the disappearance of DPM OH stretching vibration indicating the formation of hydrogen bonds with the polymers (Figure 6.5). Broadening (DPM-PVP, DPM-HPMC and DPM-PVP-HPMC) and shifting (DPM-PVP-HPMC) of symmetrical (2851 cm^{-1}) and asymmetrical (2923 cm^{-1}) stretching of DPM CH_2 group was also observed suggesting drug-polymer-polymer interaction was stronger compared to drug-polymer interaction. Shifts were also recorded for C = N and C-N bands at 1533 and 1359 cm^{-1} in DPM-PVP-HPMC system. CNZ, on the other hand, displayed no interaction with PVP but HPMC based CNZ dispersions demonstrated the presence of drug-polymer interaction (shifts in CNZ C – N peak). These shifts and broadening of peaks were observed in CNZ-PVP-HPMC dispersion which could be due to the synergistic interaction between CNZ and PVP-HPMC combination. This helps explain the better synergistic effect of PVP-HPMC on DPM compared to CNZ; both the PVP and the HPMC interact with DPM individually whereas only the HPMC interacts with the CNZ. This highlights the importance of the nature and strength of drug-polymer interactions while choosing a polymer combination for stabilizing

amorphous drug. Furthermore, on comparing drug-PVP-HPMC spectra of DPM and CNZ with drug-PVP-HPMC-SDS displayed significant differences with reference to peak broadening and shifts suggesting the presence of surfactant affects drug-polymer-polymer interactions (Figure 6.5). It is important to mention here that FTIR spectroscopic studies conducted here are only for qualitative purpose and do not provide any quantitative understanding of the molecular interactions. Nevertheless, when combined with the DSC results, they help build a better understanding of molecular interactions.

6.3.3. Supersaturation generation and maintenance

6.3.3.1. Equilibrium solubility

The effect of various compositions of physical mixtures (containing crystalline drug) and solid dispersions (containing amorphous drug) on the equilibrium solubility of DPM and CNZ in PBS 6.8 are reported in Table 6.2. For direct comparison, the composition of physical mixtures has been kept the same as that of respective solid dispersion. The physical mixtures of DPM and CNZ with polymers and/or surfactants did not result in a significant change in the equilibrium solubility of crystalline DPM and CNZ. The reported CMC of poloxamer 188 and SDS are 0.743 mg/mL and 0.29 mg/mL.[45 46] The presence of surfactants (P188 and SDS) in physical mixtures with concentration below their respective critical micelle concentration (CMC) in PBS 6.8 did not result in any significant rise in the solubility of crystalline DPM and CNZ. Moreover, PVP, HPMC and their combination also have no effect on the equilibrium solubility of the crystalline DPM and CNZ (Table 6.2). On the other hand, the equilibrium solubility of amorphous drugs in the solid dispersions after 24 hr was much higher than their physical mixture (crystalline drug) counterparts. Thus, the higher drug concentration during dissolution was not due to the solubilizing effect of polymers and surfactant on the crystalline drug. It is due to crystallization inhibition efficiency of the polymer in solution to maintain apparent higher solubility of amorphous drug. Furthermore, the maintenance of amorphous DPM and CNZ supersaturation in PBS 6.8 was due to the polymers rather than the surfactants. This was confirmed when the amorphous drug equilibrium solubility from surfactant based ASDs (higher amorphous drug solubility) was compared to their surfactant free counterpart (lower amorphous drug solubility). The maximum supersaturation concentration of DPM and CNZ was observed in drug-polymer-polymer combinations which again suggests a synergistic effect of this polymer-combination on drug supersaturation. By comparison, surfactants were found to have negative impact on the amorphous drug supersaturation maintenance (Table 6.2) with lower concentrations

observed after 24 hrs for ASDs containing surfactants. The difference in drug concentration was found to be significant for drug-polymer or drug-polymer-polymer systems compared to surfactant incorporated dispersions.

6.3.3.2. In-vitro dissolution studies

To further understand how the molecular interactions in the multi-component solid dispersions affect the DPM and CNZ release profile from spray dried ASDs upon exposure to water, *in-vitro* dissolution experiments were performed. Of particular interest was whether the synergistic effect of the polymer combinations and the incorporation of surfactants into the solid dispersions affected the supersaturation generation and maintenance of DPM and CNZ.

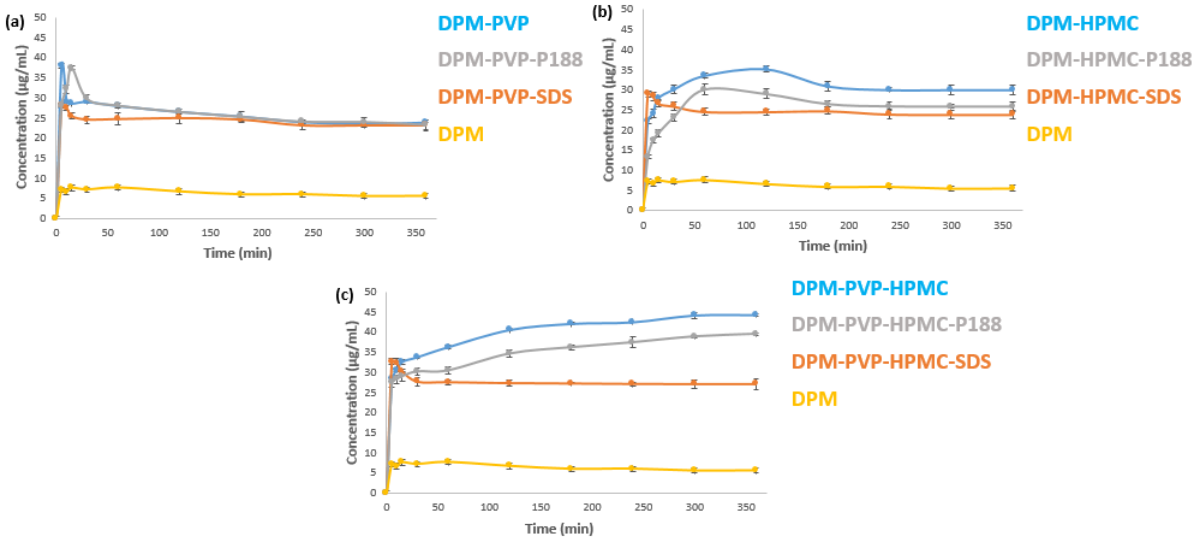

Figure 6.6. In-vitro dissolution profile of DPM ASDs in PBS 6.8 at 37°C with PVP (a), HPMC (b) and PVP-HPMC (c); samples equivalent to 25 mg of drug was added to PBS 6.8; Each point represents mean ± SD; n = 2

The dissolution profile of spray dried dispersions of DPM in PBS 6.8 (Figure 6.6) demonstrated that supersaturation was generated rapidly with a maximum concentration (C_{max}) achieved within 5 min. Then, a rapid drop in the free DPM concentration was observed, suggesting that water-mediated crystallization predominated in this stage. Once the concentration of DPM reached a plateau, the dissolution process was in equilibrium with the crystallization process. Significant differences were found between the C_{max} for different systems (PVP, HPMC and PVP-HPMC based dispersions). The descending order of C_{max} is DPM-PVP-HPMC > DPM-PVP > DPM-HPMC. Thus, it was found that PVP-HPMC combination has a synergistic effect on generating and maintaining DPM supersaturation. The presence of 5% w/w SDS or P188 in the formulations have variable effects on the

dissolution profile of DPM. SDS or P188 had a minimal effect on the dissolution profile of DPM in PVP based dispersions (Figure 6.6 (a)). This suggests that the surfactants did not have any significant influence on the DPM dissolution profile in PVP based dispersions. In DPM-HPMC systems, both SDS and P188 had a significant effect on the supersaturation level of DPM (Figure 6.6 (b)), adversely affecting the release of DPM as indicated by the lower C_{max} attained in the presence of SDS or P188. The level of supersaturation achieved and the duration of supersaturation maintained was found to be maximum for DPM-HPMC system followed by DPM-HPMC-P188 dispersion and the lowest for DPM-HPMC-SDS system. These results suggest that the presence of the surfactant did not inhibit DPM crystallization during dissolution to the same extent as their surfactant free counterparts in the HPMC-based dispersions. Similar results have been observed for DPM-PVP-HPMC based systems (Figure 6.6 (c)) where the dissolution profile of the DPM dispersions without SDS or P188 was significantly better than the dispersions with surfactants. The decreasing order of dissolution performance is as follows: DPM-PVP-HPMC > DPM-PVP-HPMC-P188 > DPM-PVP-HPMC-SDS.

The effect of binary, ternary and quaternary combinations of drug, polymer and surfactant on the dissolution profile of spray dried CNZ dispersions was also investigated. The dissolution profiles of CNZ solid dispersions in PBS 6.8 containing a combination of polymer and surfactants are illustrated in Figure 6.7. CNZ, in PVP and PVP-HPMC based formulations, achieved a C_{max} within 5 min followed by a decline in free CNZ concentration, indicating that CNZ crystallizes quickly in the presence of water. This could be due to strong plasticization effect of water on the amorphous drug. The CNZ-HPMC system, on the other hand, achieved a maximum concentration after 120 mins followed by decline in free drug concentration. The dissolution of ternary CNZ-PVP-HPMC resulted in significantly higher CNZ concentration in solution compared to CNZ-PVP and CNZ-HPMC binary dispersions. The effect of surfactants on CNZ dissolution is similar to that of DPM dispersions.

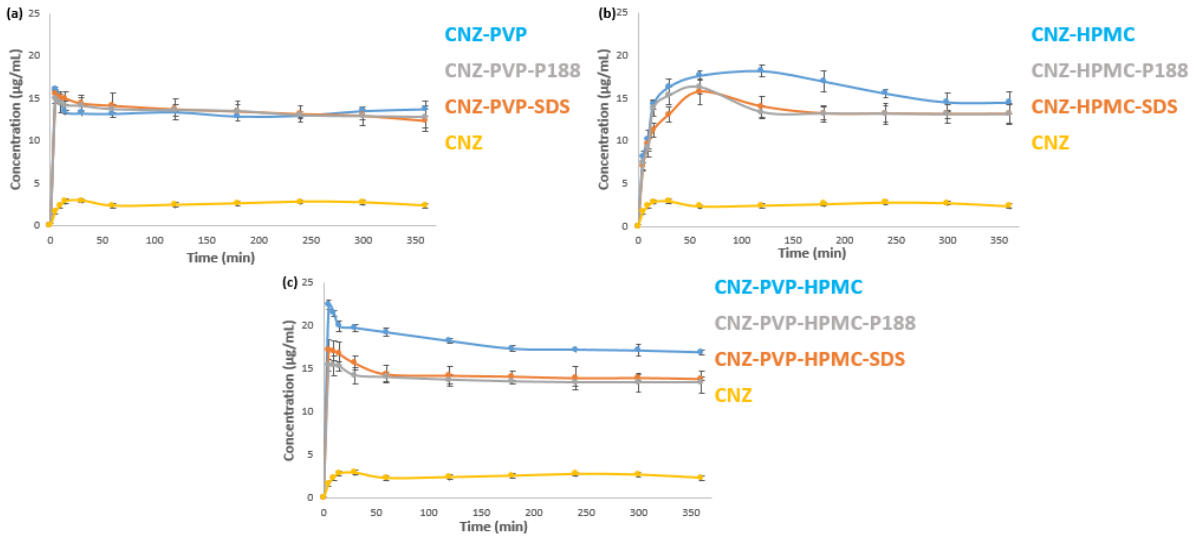

Figure 6.7. In-vitro dissolution profile of CNZ ASDs in PBS 6.8 at 37°C with PVP (a), HPMC (b) and PVP-HPMC (c); samples equivalent to 25 mg of drug was added to PBS 6.8; Each point represents mean ± SD; n = 2

The dissolution results suggests that the surfactants interfere with the crystallization inhibitory efficiency of the polymers. The effect of SDS and P188 on HPMC based dispersions of DPM and CNZ is more pronounced than in the PVP based systems. The effect is even more pronounced in PVP-HPMC based dispersions of DPM and CNZ. There are two possible explanations for the lower drug supersaturation in the presence of surfactants. The first possibility is that the surfactant and polymer molecules could be competing to interact with the drug molecules.[41] Due to the hydrophobic nature of DPM and CNZ, there was a higher tendency for the hydrophobic parts of SDS and P188 molecules to interact to DPM or CNZ molecules than for the hydrophilic HPMC or PVP-HPMC polymers. The adsorption of surfactant molecules on to the drug molecules would lead to a reduced interfacial tension which eventually reduces the nucleation activation energy, finally leading to a higher nucleation rate. [9, 20, 41] Another possible explanation for the reduced supersaturation level is that the polymer and surfactant molecules interact to form clusters and therefore the number of freely available polymer molecules to inhibit the crystallization of dissolved DPM and CNZ molecules is reduced.[47, 48] Thus, the use of surfactant to enhance the dissolution performance of solid dispersion formulations may be counterproductive.

6.3.3.3. Solution ^{1}H NMR studies

Solution ^{1}H NMR spectroscopic studies were performed to probe the molecular mechanism behind the improved supersaturation performance of ternary drug-polymer-polymer ASDs of DPM and CNZ. This study was performed on the best performing ASDs (generating and maintaining highest level of supersaturation) screened during the dissolution

studies and compared to the binary drug-polymer ASDs. This study was performed to study the site of interaction between the drug and polymer in solution to help explain the results obtained in the dissolution studies. The peak shifts in ^{1}H NMR spectra of DPM, CNZ and their binary and ternary ASDs (without surfactants) are shown in Figure 6.8 and 6.9.

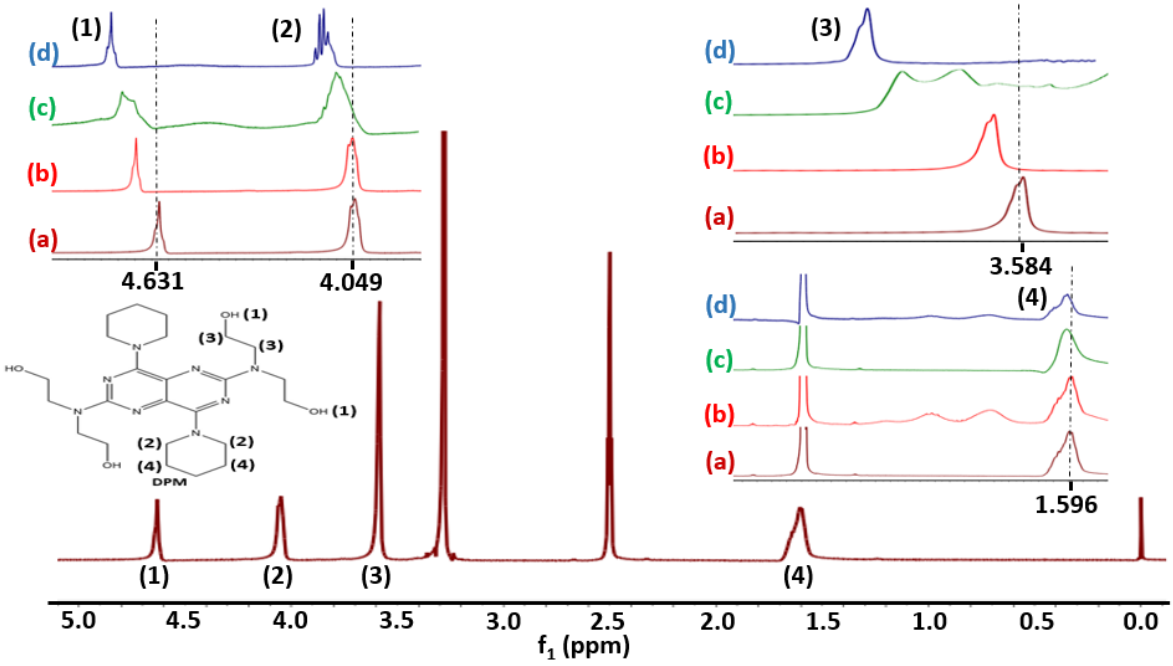

Figure 6.8. Solution ^{1}H NMR spectra of DPM (1000 µg/mL) in DMSO-d6. Figures in inset represent the chemical shift of DPM (a), DPM-PVP (b), DPM-HPMC (c) and DPM-PVP-HPMC (d). The numbers at top of each inset figure represent the peak number in DPM spectra. Assignments of DPM resonance is based on spectral database[49]. Numbers are assigned arbitrarily

As shown in Figure 6.8, the chemical shift of protons (1) and (3) shifted upfield to higher values in all the systems. This suggests the deshielding of the protons in the presence of polymers. A chemical shift for proton (2) and (4) was not observed in DPM-PVP system whereas a deshielding effect was observed in the DPM-HPMC and DPM-PVP-HPMC systems. In case of CNZ, the shifts were most pronounced for protons (1), (2), (6) and (7) of CNZ in PVP dispersions and for protons (1), (2), (3), (4), (5), (6) and (7) in HPMC and PVP-HPMC systems (Figure 6.9). The shifts shown in Figure 6.8 and 6.9 suggests DPM and CNZ interact with PVP, HPMC and PVP-HPMC systems in a different way which goes some way towards explaining the different polymeric effect, particularly in terms of inhibition of drug recrystallization during dissolution of DPM and CNZ ASDs. The larger peak shifts corresponds to the possibility of stronger drug-polymer interaction in ternary system compared to individual PVP and HPMC binary systems. The significantly higher shifts in ternary systems again suggests a synergistic effect of polymer on the drug-polymer

interaction in solution. The relative extent of shift, in the decreasing order, was drug-PVP-HPMC > drug-HPMC > drug-PVP (for both the drugs) which explains the dissolution results where the ternary drug-PVP-HPMC generated and maintained highest level of supersaturation compared to other systems studied. This also matches the rank order observed for MPD analysis.

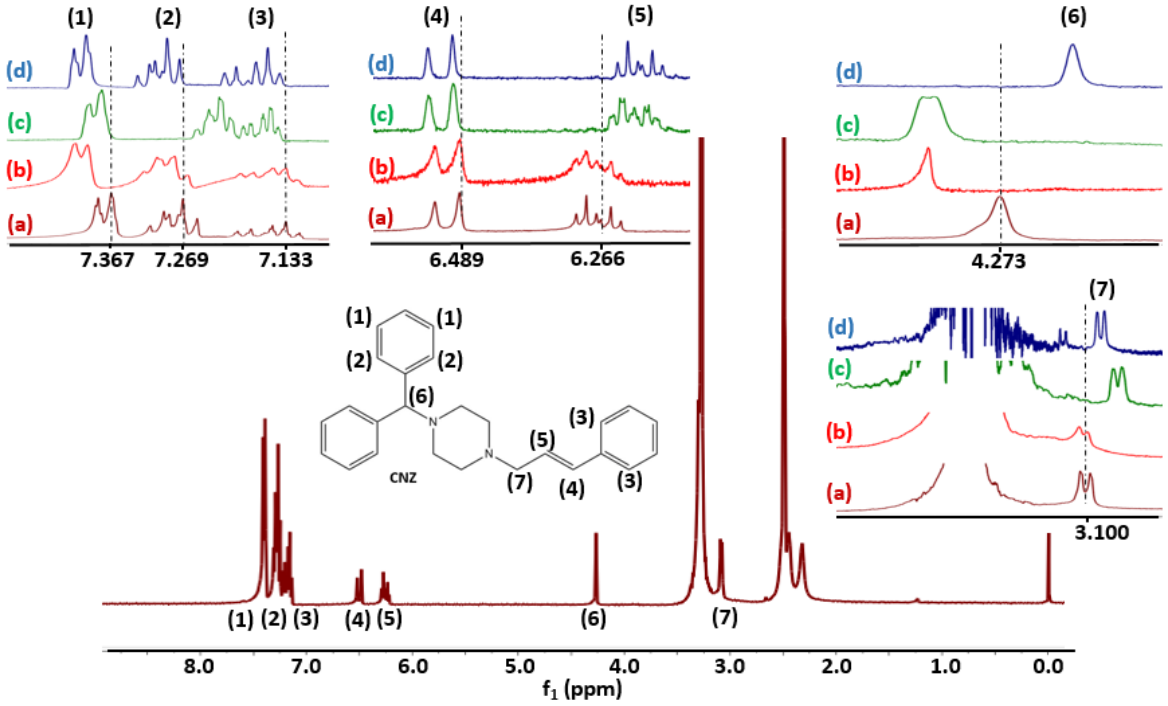

Figure 6.9. Solution ^{1}H NMR spectra of CNZ (1000 µg/mL) in DMSO-d6. Figures in inset represent the chemical shift of CNZ (a), CNZ-PVP (b), CNZ-HPMC (c) and CNZ-PVP-HPMC (d). The numbers at top of each inset figure represent the peak number in CNZ spectra. Assignments of CNZ resonance is based on Sassene *et al.*[50]. Numbers are assigned arbitrarily

It is interesting to observe that the thermal characterization results (Figure 6.4) have been negatively affected by the presence of SDS and P188. Also, as shown in Figure 6.6 and 6.7, the increased crystallization rate of amorphous drugs during dissolution incorporating surfactants could be attributed to their higher affinity for water that could act as plasticizer. The negative impact of surfactant is believed to be due to reduction in glass transition temperature (Table 6.2) and also may be due to molecular effects possibly promoting polymer chain entanglements and polymeric globule formation.[51] The globules formed in the spray drying solution seemed to be present in the solid state, and therefore, diffusion of the drug is reduced. This indicates the presence of a memory where incorporation of surfactant in the liquid state (spray drying solution) in polymer chain remained even after the solid particles have had formed. Towards this end, 2D-NOESY experiments have been conducted

to understand the surfactant-polymer interaction in the solution state (spray drying drug-polymer-surfactant solution and also during dissolution). It provides information on the distance between protons that are spatially close to each other.[52] This will help to probe into the mechanism of the impact of surfactant on amorphous drug crystallization inhibition efficiency of polymer in the spray dried particles and also during the dissolution of ASDs incorporation surfactant.

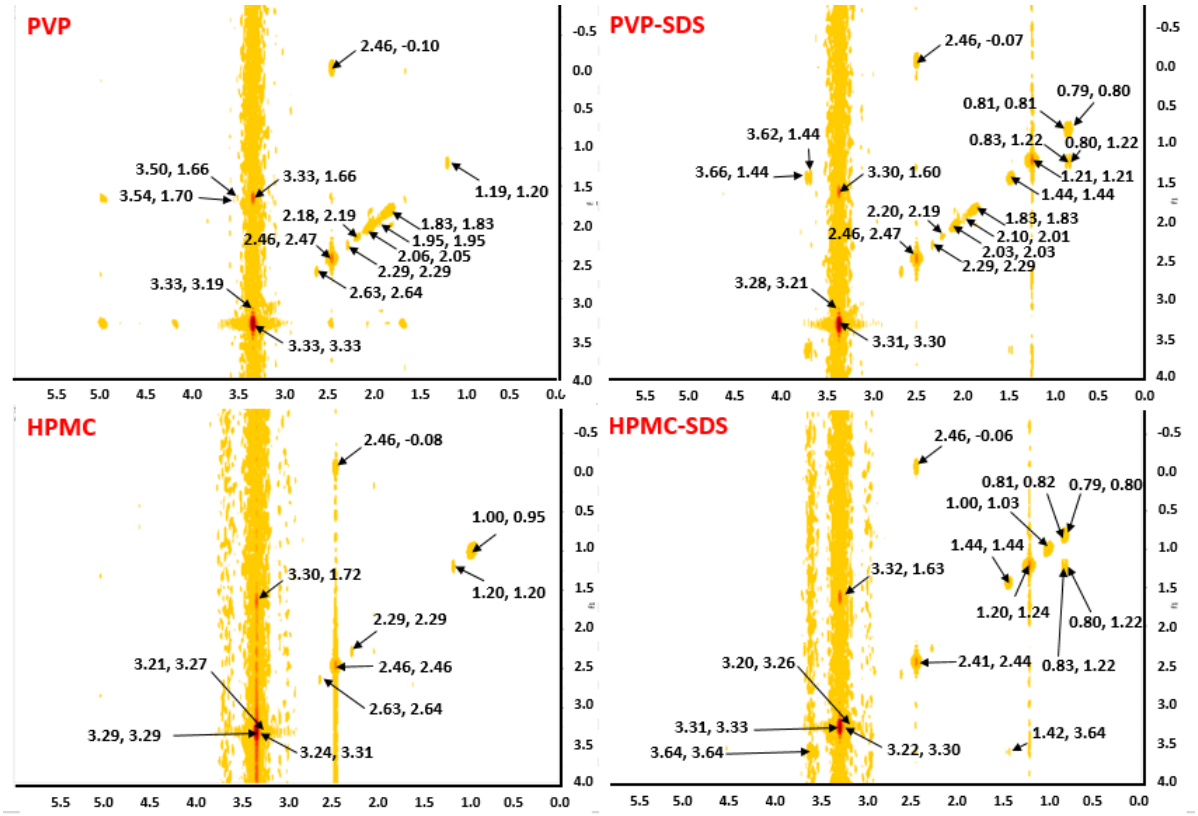

Figure 6.10. 2D -^{1}H NOESY spectra of PVP, PVP-SDS, HPMC, HPMC-SDS. The polymer concentration was maintained at 1000 µg/mL to which 5% w/w surfactant was added.

PVP, PVP-SDS, HPMC and HPMC-SDS are chosen as model systems and their 2D-NOESY spectra are shown in Figure 6.10. The peak of each proton of PVP and HPMC were assigned according to literature.[53 54] The investigations reported here suggest that surfactant-polymer interaction is due to synergistic electrostatic (pyrrolidone ring of PVP) and/or hydrophobic (ring methylene of PVP) interaction with the head-group and alkyl moiety of SDS, respectively. For the HPMC system, strong NOE interactions between the protons on the cellulose chain and on hydroxypropyl group of HPMC, and the protons on hydrophobic tails of SDS are observed. Similar effect of surfactant on PVP and HPMC have been reported previously.[52 53 54] Thus, it has been observed that NOE interactions between the protons of

polymer and surfactant, indicating close proximity of the polymer and surfactant in solution. As discussed earlier, the molecular interaction between polymer and drug serves to inhibit the crystallization of amorphous drug in the precipitates. The fact that the surfactant interacts with PVP and HPMC in a competitive manner may alter the interaction between DPM/CNZ and PVP/HPMC, thus jeopardizing the ability of polymer to inhibit DPM or CNZ crystallization. These considerations are in agreement with the results obtained from solid-state thermal analysis and in-vitro dissolution which suggests that surfactant is competing with the drug molecules for polymer functional groups and thereby reducing the crystallization inhibition efficiency of the polymer.

6.3.4. Moisture sorption analysis and Stability studies

To further understand the behaviour of multi-component (binary, ternary and quaternary) ASDs in the presence of moisture under stress conditions, the freshly prepared spray dried dispersions were exposed to DVS analysis using double ramp method from 0-90-0% RH (2 cycles) in 10% increments (dm/dt = 0.001 at each step) at 40 °C. As can be seen in Figure 6.11, the amount of water uptake was greater in PVP based dispersions compared to HPMC or PVP-HPMC based systems. This could be due to the more hydrophilic nature of PVP compared to HPMC. Furthermore, the effect of surfactants on the moisture sorption profile was greater in PVP based dispersions compared to HPMC or PVP-HPMC based systems (Figure 6.11). Also, the time required to complete the double sorption-desorption cycle varied significantly in different systems which suggests incorporating surfactant within the dispersion significantly affects the moisture sorption ability of drug-polymer or drug-polymer-polymer systems. This could be due to differences in the surface energy and relaxation of amorphous API at the surface.[55] It has been reported that structural relaxation at the surface can vary significantly from relaxation in the bulk of amorphous materials.[56] Surfactants get localised at the surface of the particles, affecting the relaxation energy and consequently the crystallization rate.[51] Furthermore, the T_g of the systems decreased when the surfactants were incorporated within the dispersions (freshly prepared) which could suggest a plasticization effect (supplementary information). Crystallization was evident (post DVS cycles, Figure 6.11) in DPM-PVP-SDS, DPM-HPMC, DPM-HPMC-SDS and DPM-HPMC-P188 dispersions signifying altered drug-polymer interaction due to moisture sorption and surfactant incorporation. Other dispersions showed no signs of crystallization. Similar results were observed for CNZ ASDs (data not shown). These observations are in accordance with the previous DSC analysis and dissolution results of freshly prepared dispersions.

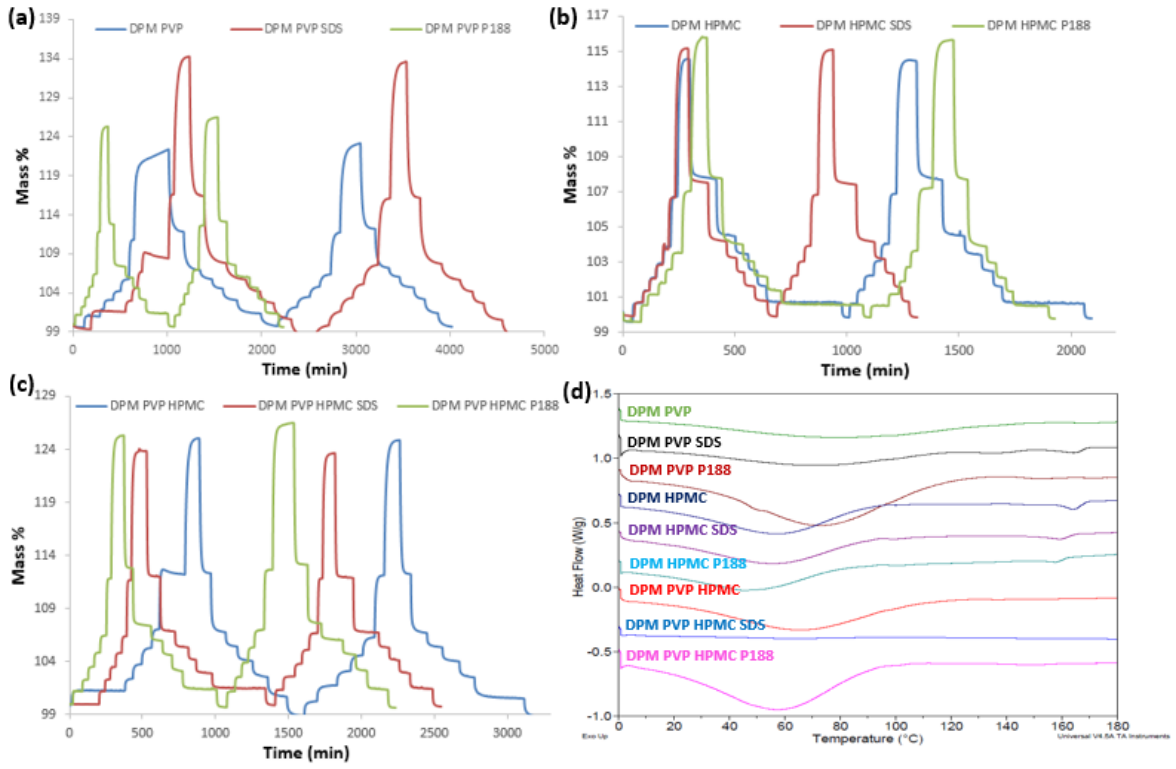

Figure 6.11. DVS analysis of freshly prepared DPM ASDs with PVP (a), HPMC (b) and PVP-HPMC (c) using double ramp method from 0-90-0% RH (2 cycles) in 10% increment ($\frac{dm}{dt} = 0.001$ at each step) at 40 °C; DSC thermograms (d) of DPM ASDs post DVS double cycle

It has been reported in chapter 2 and 3 that the amorphous forms of pure DPM and CNZ tend to recrystallize rapidly in the absence of stabilizing polymers.[11] It has also been shown that recrystallization of amorphous drug is delayed within ASDs.[19] In this study, the physical stability of multi-component ASDs was assessed under storage conditions of 40 °C/75% RH for 4 weeks (Figure 6.12). As shown in Figure 6.12, DPM-PVP systems were found to be completely amorphous after 4 weeks, both with and without surfactant. However, amorphous-amorphous phase separation was observed in DPM-PVP, DPM-PVP SDS and DPM-PVP-P188 systems (Table 6.2). All HPMC based DPM dispersions underwent crystallization suggesting PVP is better in maintaining solid-state stability of amorphous DPM compared to HPMC. The solid dispersions of ternary DPM-PVP-HPMC remained amorphous with significantly higher T_g values compared to binary dispersions (Table 6.2). This suggests a synergistic effect of polymer combination in improving the solid-state stability of amorphous DPM. Further evidence of the synergistic effect of PVP-HPMC was observed in case of CNZ dispersions where all CNZ systems showed crystallization after 4 weeks of storage at 40 °C/75 % RH except CNZ-PVP-HPMC dispersion (Figure 6.12 and Table 6.2).

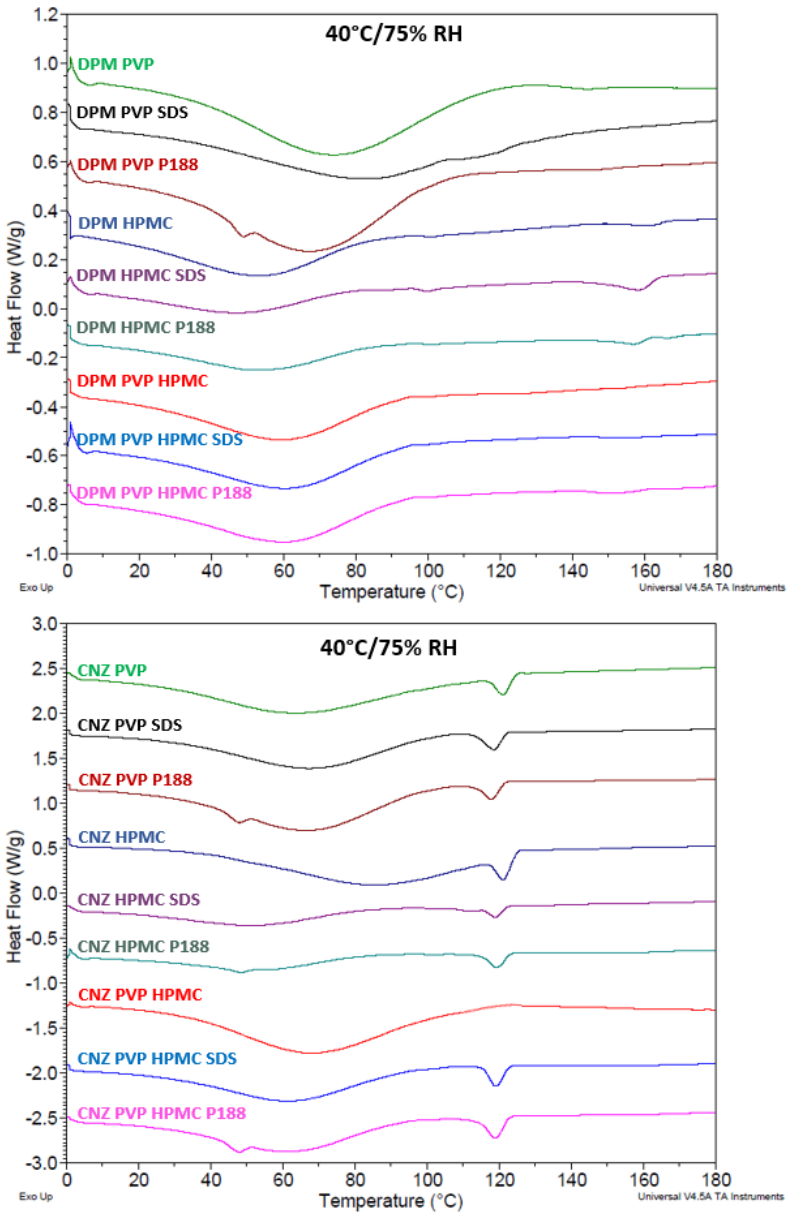

Figure 6.12. DSC thermogram of DPM (a) and CNZ (b) ASDs stored at 40 °C and 75% RH for 4 weeks

Similar observations have been made in the past where surfactants had a negative impact on the solid dispersion performance.[51] Difference in the physicochemical properties of SDS and P188 suggest that these events are controlled by the type of surfactant used. Thus, in this study, we observed surfactants (when they are incorporated within the dispersions) neither improved the solid state stability (Figure 6.4 and 6.12) nor increased the supersaturation level during dissolution (Figure 6.6 and 6.7). It has been found, in this case, that drug-excipient and excipient-excipient interaction could have considerable impact on the crystallization of amorphous API. Different systems behaved differently when observed under different conditions (DSC, dissolution, DVS or stability). Further investigations are

required to confirm the localization of surfactants within spray dried particles to have a better understanding of how surfactants affect drug-polymer interactions. Nevertheless, the use of surfactants (as solubilizing or wetting agents) in spray dried ASDs requires prudent consideration.

On the other hand, drug-polymer-polymer ternary ASDs showed higher stability and dissolution compared with binary ASDs. PVP K30 and HPMC K100 complemented each other to provide enhanced stability as well as improved drug supersaturation. The synergistic efficiency of these polymers when used in combination in ternary ASDs could be due to greater DPM and CNZ miscibility in the ternary systems compared with the binary system as confirmed by MPD analysis and also stronger drug-polymer interaction in the ternary dispersions, as confirmed by T_g measurements (Table 6.2) and FTIR results. In solution, the presence of molecular interactions between the drug and polymer is responsible for generating and maintaining drug supersaturation for a prolonged period of time (Figure 6.8 and 6.9). Similarly, crystallization of amorphous drug in solid state requires favorable orientation for the crystal nucleation. It has been confirmed that surface crystallization occurs at relatively faster rate compared to bulk crystallization.[25] In ternary systems, the presence of two polymers might increase overall entropy of the system by providing a barrier for crystallization in surface and bulk. This was confirmed by the stability studies of the CNZ-PVP-HPMC system (Figure 6.12) which showed it was stable after exposure to moisture for 4 weeks whereas all other CNZ system showed drug crystallization. Ternary dispersions are complicated systems where weak drug-polymer interactions are involved in the amorphous drug solubilisation and stabilization. Further molecular level investigations are required to obtain a mechanistic understanding of the synergistic effects reported in this study. Further work should investigate the interactions between additives and drug nuclei or crystal surfaces, which had previously been reported as a critical factor of crystallization inhibition or morphology modification.[41] Also, more studies are required to examine more drug-polymer combinations or the combinations of different additives including other surfactants at different concentrations for synergistic effects using advanced characterization techniques such as solid-state NMR, dielectric spectroscopy, inverse gas chromatography, nucleation induction studies in the presence of moisture or during dissolution, and others.

6.5. Conclusion

The incorporation of surfactants and polymer combinations seemed to have a significant effect on the properties of the resulting ASDs. Surfactants, when incorporated in

ASDs, resulted in altered dissolution rates, reduced stability and altered drug-polymer interactions. The combination of PVP K30 and HPMC K100, two polymers which displayed drug-polymer interaction, resulted in significant crystallization inhibition (both in solid-state and dissolution) of the poorly soluble drugs DPM and CNZ. This enhanced crystallization inhibition efficiency can be correlated to the synergistic effect of PVP K30 and HPMC K100. This study also highlights the importance of utilizing ternary drug-polymer-polymer interactions by combining polymers with different crystallization inhibition mechanisms for improved solid-state stability and dissolution enhancement of poorly soluble drugs.

6.6. References

1. Babu N.J, Nangia A. 2011. Solubility advantage of amorphous drugs and pharmaceutical cocrystals. Cryst Growth Des. 11: 2662-2679.

2. Jornada D.H, dos Santos Fernandes G.F, Chiba D.E, de Melo T.R, dos Santos J.L, Chung M.C. 2015. The prodrug approach: A successful tool for improving drug solubility. Molecules. 21: 1-31.

3. Liu Y, Wang L, Zhao Y, He M, Zhang X, Niu M, Feng N. 2014. Nanostructured lipid carriers versus microemulsions for delivery of the poorly water-soluble drug-luteolin. Int J Pharm. 476: 169-177.

4. Karashima M, Sano N, Yamamoto S, Arai Y, Yamamoto K, Amano N, Ikeda Y. 2017. Enhanced pulmonary absorption of poorly soluble itraconazole by micronized cocrystal dry powder formulation. Eur J Pharm Biopharm. 115: 65-72.

5. Buckley S.T, Frank K.J, Fricker G, Brandl M. 2013. Biopharmaceutical classification of poorly soluble drugs with respect to "enabling formulations". Eur J Pharm Sci. 50: 8-16.

6. Samie A, Desiraju G.R, Banik M. 2017. Salts and cocrystals of the antidiabetic drugs gliclazide tolbutamide and glipizide: Solubility enhancements through drug-coformer interactions. Cryst Growth Des. 17: 2406-2417.

7. Sun D.D, Lee P.I. 2015. Probing the mechanism of drug release from amorphous solid dispersions in medium-soluble and medium-insoluble carriers. J Control Release. 211: 85-93.

8. Shah T, Laaksonen T, Rades T, Aaltonen J, Peltonen L, Strachan C.J. 2013. Unravelling the relationship between degree of disorder and the dissolution behaviour of milled glibenclamide. Mol Pharm. 11: 234-242.

9. Baghel S, Cathcart H, O'Reilly N.J. 2016. Polymeric amorphous solid dispersions: A review of amorphization, crystallization, stabilization, solid-state characterization and aqueous solubilization of biopharmaceutical classification system class II drugs. 105: 2527-2544.

10. Brouwers J, Brewster M.E, Augustijns P. 2009. Supersaturating drug delivery systems: the answer to solubility-limited oral bioavailability? J Pharm Sci. 98: 2549-2572.

11. Baghel S, Cathcart H, Redington W, O'Reilly N.J. 2016. An investigation into the crystallization tendency/kinetics of amorphous active pharmaceutical ingredients: A case study with dipyridamole and cinnarizine. Eur J Pharm Biopharm. 104: 59-71.

12. Amstad E, Spaepen F, Weitz D.A. 2016. Stabilization of the amorphous structure of spray-dried drug nanoparticles. J Phys Chem B. 120: 9161-9165.

13. Xie T, Taylor L.S. 2016. Dissolution performance of high drug loading celecoxib amorphous solid dispersions formulated with polymer combinations. Pharm Res. 33: 739-750.
14. Baghel S, Cathcart H, O'Reilly N.J. 2018. Understanding the generation and maintenance of supersaturation during the dissolution of amorphous solid dispersions using modulated DSC and 1H NMR. Int. J. Pharm. Sci. 536: 414-425.
15 Murdande S.B, Pikal M.J, Shanker R.M, Bogner R.H. 2011. Solubility advantage of amorphous pharmaceuticals, Part 3: I maximum solubility advantage experimentally attainable and sustainable? J Pharm Sci. 100: 4349-4356.
16. Kalepu S, Nekkanti V. 2015. Insoluble drug delivery strategies: review of recent advances and business prospects. Acta Pharm Sin B. 5: 442-453.
17. Vasconcelos T, Marques S, das Neves J, Sarmento B. 2016. Amorphous solid dispersions: Rational selection of manufacturing process. Adv Drug Deliv Rev. 100: 85-101.
18. Vo C.L, Park C, Lee B.J. 2013. Current trends and future perspective of solid dispersions containing poorly water-soluble drugs. Eur J Pharm Biopharm. 85: 799-813.
19. Baghel S, Cathcart H, O'Reilly N.J. 2016. Theoretical and experimental investigation of drug-polymer interaction and miscibility and its impact on drug supersaturation in aqueous medium. Eur J Pharm Biopharm. 107: 16-31.
20. Yoo S, Krill S.L, Wang Z, Telang C. 2009. Miscibility/stability consideration in binary solid dispersion systems composed of functional excipients towards the design of multi-component amorphous systems. J Pharm Sci 98: 4711-4723.
21. van den Mooter G, Wuyts M, Blaton N, Busson R, Grobet P, Augustijns P, Kinget R. 2001. Physical stabilization of amorphous ketoconazole in solid dispersions with polyvinyl pyrrolidone K25. Eur J Pharm Sci. 12: 261-269.
22. Damian F, Blaton N, Kinget R, van de Mooter G. 2002. Physical stability of solid dispersions of the antiviral agent UC-781 with PEG 6000, Gelucire 44/14 and PVP K30. Int J Pharm. 244: 87-89.
23. Wang X, Michoel A, van den Mooter G. 2005. Solid state characteristics of ternary solid dispersions composed of PVP VA64, Myrj 52 and itraconazole. Int J Pharm. 303: 54-61.
24. Karavas E, Geogarakis E, Sigalas M.P, Avgoustakis K, Bikiaris D. 2007. Investigation of the release mechanism of a sparingly water-soluble drug from solid dispersions in hydrophilic carriers based on physical state of drug, particle size distribution and drug-polymer interactions. Eur J Pharm Biopharm. 66: 334-347.

25. Prasad D, Chauhan H, Atef E. 2014. Amorphous stabilization and dissolution enhancement of amorphous ternary solid dispersions: Combination of polymers showing drug-polymer interaction for synergistic effects. J Pharm Sci. 103: 3511-3523.
26. Ghebremeskel A.N, Vemavarapu C, Lodaya M. 2007. Use of surfactant as plasticizers in preparing solid dispersions of poorly soluble API: Selection of polymer-surfactant combinations using solubility parameters and testing the processability. Int J Pharm. 328: 119-129.
27. Ghebremeskel A.N, Vemavarapu C, Lodaya M. 2006. Use of surfactants as plasticizers in preparing solid dispersions of poorly soluble API: stability testing of selected solid dispersions. Pharm Res. 23: 1928-1936.
28. Jain S.K, Shukla M, Shrivastava V. 2010. Development and in vitro evaluation of ibuprofen mouth dissolving tablets using solid dispersion technique. Chem Pharm Bull. 58: 1037-1042.
29. Agarwal A.M, Dudhedia M.S, Zimmy E. 2016. Hot melt extrusion: Development of an amorphous solid dispersion for an insoluble drug from mini-scale to clinical scale. AAPS PharmSciTech. 17: 133-147.
30. Ghebremeskel A.N, Vemavarapu C, Lodaya M. 2007. Use of surfactants as plasticizers in preparing solid dispersions of poorly soluble API: Selection of polymer-surfactant combinations using solubility parameters and testing the processability. Int J Pharm. 328: 119-129.
31. Paudal A, Worku Z.A, Meeus J, Guns S, van der Mooter G. 2013. Manufacturing of solid dispersions of poorly water soluble drugs by spray drying: Formulation and process consideration. Int J Pharm. 453: 253-284.
32. Al-Obaidi H, Lawrence M.J, Buckton G. 2016. Atypical effects of incorporated surfactants on stability and dissolution properties of amorphous polymeric dispersions. J Pharm Pharmacol. 68: 1373-1383.
33. Rashid R, Kim D.W, ud Din F, Mostapha O, Yousaf A.M, Park J.H, Kim J.O, Yong C.S, Choi H.G. 2015. Effect of hydroxypropylcellulose and Tween80 on the physicochemical properties and bioavailability of ezetimibe-loaded solid dispersions. Carbohyd Polym. 130: 26-31.
34. Mah P.T, Peltonen L, Novakovic D, Rades T, Strachan C.J, Laaksonen T. 2016. The effect of surfactants on the dissolution behaviour of amorphous formulations. Eur J Pharm Biopharm. 103: 13-22.

35. Vora A, Patadia R, Mittal K, Mashru R. 2015. Preparation and characterization of dipyridamole solid dispersions for stabilization of supersaturation: effect of precipitation inhibitors type and molecular weight. Pharm Dev Technol. 3: 1-9.
36. http://www.drugbank.ca/drugs/DB00568
37. Dubin P.L, Li Y. 1994. Structure and flow in surfactant solutions: Polymer-surfactant complexes. ACS Symposium Series. 578: 320-336.
38. Yu X, Somasundaran P. 1996. Role of polymer conformation in interparticle-bridging dominated flocculation. J Coll Inter Sci. 177: 283-287.
39. Margolin A, Sherstyuk S.F, Izumdov V.A, Zexin A.B, Kabanov V.A. 1985. Enzymes in polyelectrolyte complexes. The effect of phase transition on thermal stability. Eur J Biochem. 146: 625-632.
40. Brackman J.C. 1991. Sodium dodecyl sulfate-induced enhancement of the viscosity and viscoelasticity of aqueous solutions of poly (ethylene oxide), A rheological study on polymer-micelle interaction. Langmuir. 7: 469-472.
41. Ileebare G.A, Liu H, Edgar K.J, Taylor L.S. 2012. Effect of binary additive combination on solution crystal growth of the poorly water-soluble drug, ritonavir. Cryst Growth. 12: 6050-6060.
42. Deshpande T.M, Shi H, Pietryka J, Hoag S.W, Medek A. 2018. Investigation of polymer-surfactant interactions and their impact on itraconazole solubility and precipitation kinetics for developing spray dried amorphous solid dispersions. Mol Pharm. doi: 10.1021/acs.molpharmaceut.7b00902
43. Zheng X, Yang R, Tang X, Zheng L. 2007. Part 1: Characterization of solid dispersions of nimodipine prepared by hot-melt extrusion. Drug Dev Indus Pharm. 33: 791-802.
44. Marsac P.J, Shamblin S.L, Taylor L.S. 2010. Theoretical and practical approaches for prediction of drug-polymer miscibility and solubility. Pharm Res. 23: 2417-2426.
45. Tian J, Zhao Y.Z, Jin Z, Lu C.T, Tang Q.Q, Xiang Q, Sun C.Z, Zhang L, Xu Y.Y, Gao H.S, Zhou Z.C, Li X.K, Zhang Y. 2010. Synthesis and characterization of poloxamer 188-grafted heparin copolymer. Drug Dev Ind Pharm. 36: 832-838.
46. Khan A.M, Shah S.S. 2008. Determination of critical micelle concentration (CMC) of sodium dodecyl sulfate (SDS) and the effect of low concentration of pyrene on its cmc using ORIGIN software. J Chem Soc Pak. 30: 186-191.
47. De Martins R, Da Silva C, Becker C, Samios D, Christoff M, Bica C.D. 2006. Interaction of (hydroxypropyl) cellulose with anionic surfactants in dilute regime. Colloid Polym Sci. 284: 1353-1361.

48. Wesley R.D, Cosgrove T, Thompson L, Armes S.P, Baines F.L. 2002. Structure of polymer/surfactant complexes formed by poly(2-(dimethylamino)ethyl methacrylate) and sodium dodecyl sulphate. Langmuir. 18: 5704-5707.

49. http://sdbs.db.aist.go.jp/sdbs/cgi-bin/cre_index.cgi

50. Sassene P.J, Mosgaard M.D, Loebmann K, Mu H, Larsen F.H, Rades T, Mullertz A. 2015. Elucidating the molecular interactions occurring during drug precipitation of weak bases from lipid based formulations – a case study with cinnarizine and a long chain self nano-emulsifying drug delivery system. Mol Phar. 12: 4067-4076.

51. Al-Obaidi H, Lawrence M.J, Buckton G. 2016. Atypical effects of incorporated surfactants on stability and dissolution properties of amorphous polymeric dispersions. J Pharm Pharmacol. 68: 1373-1383.

52. Chen Y, Wang S, Wang S, Liu C, Su C, Hageman M, Haskell R, Stefanski K, Qian F. 2016. Sodium lauryl sulphate competitively interacts with HPMC-AS and consequently reduces oral bioavailability of Posaconazole/HPMC-AS amorphous solid dispersion. Mol. Pharm. 13: 2787-2795.

53. Roscigno P, Asaro F, Pellizer G, Ortona O, Paduano L. 2003. Complex formation between poly(vinylpyrrolidone) and sodium dodecyl sulfate studied through NMR. *Langmuir*. 19: 9638-9644.

54. Hammarstrom A, Sundelof L.O. 1993. NMR study of polymer surfactant interaction in the system HPMC/SDS/water. Colloid. Polym. Sci. 271: 1129-1133.

55. Hasegawa S, Ke P, Buckton G. 2009. Determination of the structural relaxation at the surface of amorphous solid dispersions using inverse gas chromatography. J Pharm Sci. 98: 2133-2139.

56. Ke P, Hasegawa S, Al-Obaidi H, Buckton G. 2012. Investigation of preparation methods on surface/bulk structural relaxation and glass fragility of amorphous solid dispersions. Int J Pharm. 422: 170-178.

CHAPTER 7. CONCLUSIONS AND FUTURE WORK

The aim of this study was to investigate the solubility and stability of amorphous solid dispersion of BCS class II drugs. Dipyridamole (DPM) and cinnarizine (CNZ) have been selected as model compounds. Chapter 2 investigated the crystallization tendency/kinetics of these model drugs. Thermodynamic fragility (m_T) was measured from the heat capacity change at the glass transition temperature (T_g) whereas dynamic fragility (m_D) was evaluated using methods based on extrapolation of configurational entropy to zero ($m_{D_{CE}}$), and heating rate dependence of T_g ($m_{D_{Tg}}$). The mean relaxation time of the amorphous drugs was calculated from the Vogel-Tammann-Fulcher (VTF) equation. Moreover, the crystallization kinetics of the model drugs under isothermal conditions has been studied using Johnson-Mehl-Avrami (JMA) approach to determine the Avrami constant 'n' which provides an insight into the mechanism of crystallization. To further probe the crystallization mechanism, the non-isothermal crystallization kinetics of the model systems were also analyzed by statistically fitting the crystallization data to 15 different kinetic models and the relevance of model-free kinetic approach has been established. It has been found that CNZ has higher fragility and poor glass forming ability compared to DPM. The work is novel as for the first time a systematic preformulation study to understand the amorphous drug crystallization tendency has been performed to predict the crystallization behaviour of amorphous drug during downstream processing.

In the next phase (Chapter 3), a comprehensive investigation of various ASD systems of DPM and CNZ in polyvinyl pyrrolidone (PVP) and polyacrylic acid (PAA) at different drug loadings was carried out. Theoretical and experimental examinations related to drug-polymer interaction and miscibility were performed, including the solubility parameter approach, the melting point depression method, phase diagram, drug-polymer interaction in the presence of moisture, and the effect of drug loading on the interaction parameter. The application of ternary F-H theory using vapor sorption analysis to predict the drug-polymer-water interactions is relatively novel in the area. Using this theory it has been shown how the change in dynamics of these interactions will effect polymer efficiency as a drug crystallization inhibitor. The information obtained from this study was used to predict the stability of ASDs at different drug loadings and under different environmental conditions. The DPM-PAA system outperformed all other ASDs in various stability conditions (dry-state and in the presence of moisture), which was attributed to the strong DPM-PAA interaction and the robustness of this interaction at different thermal and moisture conditions.

In Chapter 4, the dissolution behaviour of DPM and CNZ spray-dried ASDs using PVP and PAA as a carrier matrix was evaluated and compared. To date, there have been limited investigations describing the drug-polymer interaction in a supersaturated solution although a large number of studies have been performed to examine the drug-polymer interaction in the solid state. This chapter attempts to broaden the overall understanding of dissolution mechanisms and the role of drug-polymer interaction in prolonging supersaturation. The drug concentrations achieved from the dissolution of PVP and PAA solid dispersions were significantly greater than the equilibrium solubility of crystalline DPM and CNZ in phosphate buffer pH 6.8 (PBS 6.8). The maximum drug concentration achieved by the dissolution of PVP and PAA solid dispersions did not exceed the theoretically calculated apparent solubility of amorphous DPM and CNZ. However, the degree of supersaturation of DPM and CNZ increased considerably as the polymer weight fraction within the solid dispersion increased. In addition, the supersaturation profile of DPM and CNZ were studied in the presence and absence of the polymers. PAA was found to maintain a higher level of supersaturation compared to PVP. The enhanced drug solution concentration following the dissolution of ASDs can be attributed to the reduced crystal growth rates of DPM and CNZ at an equivalent supersaturation which may be due to strong drug-polymer interaction in solution. It has been shown that, for drugs having high crystallization tendency and weak drug-polymer interactions, a feasible way to increase the dissolution might be to increase the polymer weight fraction in the ASD. Solution ^{1}H NMR spectra were used to understand the dissolution mechanism and to identify drug-polymer interactions. Changes in the electron densities around the proton attached to different groups in DPM and CNZ suggested drug-polymer interaction in solution. The relative intensities of the peak shift and the nature of interaction between drug and polymer in different systems are different. These different effects suggest that DPM and CNZ interact in a different way with PVP and PAA in solution. This goes some way towards explaining the different polymeric effect, particularly in terms of inhibition of drug recrystallization and dissolution of DPM and CNZ from ASDs. These results established that the different drug-polymer interactions in the solid state and in solution give rise to the variation in dissolution profile observed for different systems.

An investigation into the effect of temperature and relative humidity (RH) on the physical stability and dissolution of binary ASDs was carried out in Chapter 5. DPM and CNZ ASDs within PVP and PAA polymeric carrier matrices at three different drug loadings (20, 50 and 80% w/w) were prepared by spray drying and exposed to different stress

conditions: temperature (25, 40 and 60 °C) and RH (0 and 75%) for 4 weeks, and stored in a desiccator at room temperature for one year. The effectiveness of the model polymers (with different drug-polymer interaction and miscibility) in inhibiting the crystallization of model drugs exposed to different temperatures and RH was evaluated using modulated differential scanning calorimetry (MDSC), dynamic vapor sorption (DVS) and *in-vitro* dissolution testing. For samples stored at room temperature in a desiccator, non-linear physical aging was observed and the dissolution rate was also decreased. For samples stored under stress conditions, the results showed phase separation and/or crystallization of DPM and CNZ with a subsequent reduction in dissolution rate. Evidence of stress-induced amorphous-amorphous phase separation was observed in both PVP and PAA based dispersions. It was concluded that, when an ASD containing a hydrophobic drug and a hydrophilic polymer is subjected to stress conditions, drug crystallization can occur via one of the two mechanisms: crystallization from the plasticized one-phase solid dispersions, or crystallization from plasticized drug-rich amorphous phase in a two-phase solid dispersion. In the former case, drug and polymer are present in the same phase and the polymer can inhibit crystallization to a greater extent than the latter scenario, where the polymer concentration in the drug-rich phase is reduced as a result of amorphous-amorphous phase separation. Furthermore, it has also been observed that the strength of drug-polymer interactions appears to be important in influencing the phase behaviour. In this study, PAA performed better than PVP in raising the glass transition temperature (T_g) and providing better stabilization of amorphous DPM and CNZ against crystallization. The results also indicate that temperature and RH seemed to have comparable effects on the crystallization of DPM and CNZ ASDs. Furthermore, it was also concluded that the glass transition temperature in addition to recrystallization may also be a good indicator of the changes in dissolution behaviour of ASDs.

In the above mentioned chapters, it has been shown that the optimal design of oral ASD formulations includes the use of excipients to improve physical stability and maintain supersaturation in order to ensure adequate shelf-life stability and better absorption during intestinal transit, respectively. Combinations of excipients (polymers and surfactants) are often employed in pharmaceutical products to improve the delivery of poorly water-soluble drugs. However, additive interactions in multi-component ASD systems have not been extensively studied and may promote crystallization in an unpredictable manner, which in turn may affect physical stability and dissolution profile of the product. The main aim of the final chapter of this thesis was to understand the effect of different surfactant and polymer

combinations on the solid-state properties and dissolution behaviour of ternary spray dried solid dispersions of DPM and CNZ. The surfactants chosen for this study were sodium dodecyl sulphate and poloxamer 188 and the model polymers used were PVP and hydroxypropyl methylcellulose K100. The work is novel in presenting a molecular understanding of the role of polymer-surfactant and polymer-polymer combinations on the physical stability and dissolution profile spray dried binary (drug-polymer), ternary (drug-polymer-surfactant or drug-polymer-polymer) and quaternary (drug-polymer-polymer-surfactant) solid dispersions. The ASDs were characterized by differential scanning calorimetry (DSC), modulated DSC, Fourier-transform infrared (FTIR), in-vitro dissolution, ^{1}H nuclear magnetic resonance (NMR), NOESY and dynamic vapor sorption (DVS). The spray dried ternary dispersions were able to maintain higher supersaturation levels compared to either the crystalline drug equilibrium solubility or their respective physical mixtures. However, rapid and variable dissolution behaviour was observed for different formulations. The maximum supersaturation level was observed for drug-polymer-polymer ternary dispersions. On the other hand, incorporating the surfactant into binary (drug-polymer) and ternary (drug-polymer-polymer) ASDs adversely affected the physical stability and dissolution properties by promoting crystallization. Based on these observations, a thorough investigation into the impact of combinations of additives on amorphous drug crystallization during dissolution and stability studies is recommended in order to develop optimized formulations of supersaturating dosage forms. Thus, it is concluded that the design of multi-component amorphous formulations requires the appropriate selection of a combination of excipients. This study will add to the overall understanding of the use of excipients in ASDs and will help in future multi-component amorphous product development.

7.1. Future Work

7.1.1. Development of solid dispersion and process optimization

A comparative study of the effect of different processing techniques (spray drying, hot melt extrusion and supercritical fluid) on solid dispersion (binary and ternary) would be of interest to establish the best method for a particular drug-polymer combination. The resulting solid dispersions could be characterised by DSC, TGA, XRPD, FTIR, SEM and ssNMR to examine drug loading in polymer matrix, percentage yield efficiency, drug-polymer miscibility, phase separation, molecular mobility and stability of the dispersion. *In vitro* dissolution studies should also be carried out in simulated gastric and intestinal fluids and drug release kinetics should be examined. Furthermore, the solid dispersions should also

be assessed to see if additional surfactants or polymers are required to stabilise the supersaturated state.

7.2. Recrystallization kinetics, statistical analysis and stability study

The recrystallization kinetics of amorphous drugs in solid dispersions (binary and ternary) and the role of polymer in decreasing the rate of crystallization could be thoroughly studied. The amorphous solid dispersion should also be subjected to stability studies at different temperatures and relative humidity. Humidity-adjusted Arrhenius kinetics could be employed to model the recrystallization kinetics. While this has been used extensively in the study of drug degradation, it is relatively novel to apply this technique to recrystallization. The stability study should be able to show the effect of temperature and humidity on the solid dispersion and may help in determining and predicting the storage conditions and shelf life of the product. The different mechanism by which polymer stabilizes the amorphous drugs such as H-bond formation, anti-plasticization or reduction in molecular mobility could be examined by using instruments like DSC, FTIR, XRPD and NMR.

7.3. Formulation of tablets and capsules

Formulating solid dispersions into dosage forms and studying their characteristics is a logical progression of this work. Various combinations of different dispersion carriers and adsorbents (excipients) should be studied. The final dosage form should also be characterized for micromeritics properties, uniformity of weight and content, friability test and hardness test as per United State Pharmacopoeia (USP) guidelines. Further i*n-vitro* dissolution studies should be carried out using simulated gastric and intestinal fluid to determine the drug release profile. A long term stability study should be performed in order to study the stability of the preliminary dosage formulation as per ICH guidelines.